AERODYNAMIC AND FUEL DILUTION EFFECTS ON NON-PREMIXED GAS JET FLAMES

JAMES IKPEME ERETE

Submitted in accordance with the requirements for the degree of

Doctor of Philosophy

The University of Leeds

School of Chemical and Process Engineering

Faculty of Engineering

October, 2015

Intellectual Property and Publication Statements

The candidate confirms that the work submitted is his own, except where work which has formed part of jointly authored publications has been included. The contribution of the candidate and the other authors to this work has been explicitly indicated. The candidate confirms that appropriate credit has been given within the thesis where reference has been made to the work of others. The following publications have been derived from this thesis:

The work in Chapters 4 and 6 has appeared in publication as follows:
A.A. Aboje, J.I. Erete, K.J. Hughes, L. Ma, M. Pourkashanian, and A.Williams. (2015) An Investigation of Methane and Propane Vertical Flares, Journal of the Energy Institute.

The work in Chapter 5 has been submitted for review as follows:

J. I. Erete, K. J. Hughes, L. Ma, M. Fairweather, M. Pourkashanian and A.Williams. (2015) Effect of CO_2 Dilution on the Structure and Emissions from Methane / Air Jet Diffusion Flames, submitted to the Journal of the Energy Institute.

In the first publication, the second author was responsible for the generation, analyses and interpretation of the experimental data, while all the work in the second publication is directly attributable to the lead author and the contributions of the co-authors were in the interpretation of the results and in the editorial corrections.

Meetings and Journal Publications

Conference:

J.I. Erete, A.A. Aboje, K.J. Hughes, L. Ma, M. Pourkashanian, and A.Williams.

An Investigation of Methane and Propane Flares. 7th Biennial Joint Meeting of the British and Scandinavian-Nordic Sections of the Combustion Institute, Cambridge, UK, 27th - 28th March, 2014.

Parliamentary Group Meeting for Energy Studies (PGES), Portcullis House, The UK Parliament, London, 17th November, 2015.

Journal Publications:

A.A. Aboje, J.I. Erete, K.J. Hughes, L. Ma, M. Pourkashanian, and A.Williams. (2015) An Investigation of Methane and Propane Vertical Flares, Journal of the Energy Institute, 1-14.

J. I. Erete, K. J. Hughes, L. Ma, M. Fairweather, M. Pourkashanian and A.Williams. (2015) Effect of CO_2 Dilution on the Structure and Emissions from Methane / Air Jet Diffusion Flames, submitted to the Journal of the Energy Institute.

Acknowledgements

I am grateful to The Almighty God for ordering my steps rightly, and for His Grace, Mercy and Favour which sustained me throughout the period of my research.

Many thanks to Dr. (Mrs) Christiana Atako and the Niger Delta Development Commission's funding of this study. If it had not been for this financial support, this research would not have been possible.

I am indebted to my supervisors: Prof. Alan Williams and Prof. Michael Fairweather, my external supervisors in the University of Sheffield, UK: Prof. Mohamed Pourkashanian, Prof. Derek Ingham, Prof. Lin Ma, Prof. Bill Nimmo, and Dr. Kevin Hughes, for their continuous advice and guidance towards the successful investigation and writing of this thesis. The contributions of Paul Crosby, Gurdev Bhogal, and Stuart Micklethwaite are also acknowledged.

I remember my late twin brother, Mr. Emmanuel Ikpeme Erete and my late mother, Princess (Mrs) Okoho Ikpeme Erete who have gone to be with The Lord. Your painful demise has been my motivation to carry on. In addition, I appreciate the support and the encouragement of my dad, Engr. Ikpeme I. Erete, my uncle, Engr. Victor I. Erete, my siblings, Erete and Mary, and all my family members. I also acknowledge Kafesta Scott for always keeping me on my toes to meet the deadlines for the completion of this study and for being there for me.

Finally, I extend my appreciation to my friends and colleagues: Dr Alexander Black, Dr Alechenu Aboje, Dr Irina Flyagina, Dr Detlev Mielczarek, Eirini Karagianni, Armin Arfaie, Jujar Panesar, Davide Poggio, amongst others, for making my stay at Leeds more enjoyable and enlightening.

Abstract

This study examines the changes in the flame structure and emissions from laboratory-scale flares over a wide range of test conditions.

In the initial study, the experimental measurements examined the effect of varying the fuel jet velocity on the flame temperature, flame structure, and the in-flame and post-flame composition of species in methane flames. The test conditions involved laboratory-scale flares in the attached and lifted regimes under laminar, transitional and turbulent conditions. The results show that while an increase in the jet velocity leads to an increase in EINOx, this also leads to a decrease in EICO, and similarly, EICO decreases with decreasing flame luminosity and sooting propensity.

The second study examined the effect of CO_2 dilution on methane jet flames where CO_2, which was used as a diluent, was injected into the fuel-jet stream. The dilution-induced extinction was achieved by fixing the fuel flow rate, while varying the diluent mole fraction. The effect of the changes in the flame length, lift-off height, and in the emissions due to this dilution was studied. Amongst other findings, this study shows that CO_2 is effective in reducing the EINOx in the post-flame region of methane jet flames at Reynolds number ranging from 1584 to 14254, and that soot formation is suppressed at higher diluent concentrations in the jet flame.

The final study involved the characterisation and the comparison of the in-flame composition of major species and the post-flame soot and pollutant emissions generated from the combustion of methane and propane flames. The results show that the dilution of the fuel stream with CO_2 reduces the size of soot aggregates in propane flames and that the soot emission factor decreases at increased diluent concentrations. In addition, for the same test conditions utilised in this study, the EICO and EINOx are higher in methane flames than in propane flames.

TABLE OF CONTENTS

CHAPTER FOUR

COMPARISON OF ATTACHED AND LIFTED METHANE FLAMES

CHAPTER FIVE

EFFECT OF CO_2 DILUTION ON METHANE / AIR JET FLAMES

CHAPTER SIX

COMPARISON OF POLLUTANT EMISSIONS FROM METHANE AND PROPANE FLAMES AND THE EFFECT OF FUEL-STREAM DILUTION ON SOOT EMISSION IN PROPANE DIFFUSION FLAMES

Figures

Figure 6.34 Variation of the aggregate size as a function of the diluent mole fraction at y/d=188

Figure 6.35 Variation of the soot emission factor as a function of the diluent mole fraction at the post-flame location.

Tables

Nomenclature

Roman Letters

c Time dimension

c_a Specific heat of air

C_F Fuel concentration

C_{st} Fuel concentration in stoichiometric fuel-air mixture

c_t Specific heat of air

d Jet nozzle inner diameter at outlet

d_a Air tube diameter

d_b Burner source diameter

d_c Shroud diameter

d_{eff} Effective outlet diameter, $\left(d\sqrt{\rho}\right)$

d_f Dilution factor

d_o Jet nozzle outer diameter

d_s Stack diameter

d^* Momentum diameter, $d(\rho_0 / \rho_\infty)$

D Mean diffusion coefficient

Da Damköhler Number

Fr Froude Number

Fr_n Froude Number with combustion

FS Soot emission factor

g Magnitude of gravitational acceleration

G_o Momentum flux of jet at burner exit

h_f Flame height

h_l Lift-off height

K_F Fuel constant

Kp Geometric shape parameter dependent on flow

K_{st} Stoichiometric ratio by mass of oxygen to fuel

K_o Stoichiometric coefficient at exit conditions

K_t Timescale

M_{ca} Molar heat capacity of air

M_{st} Stoichiometric mixing ratio

MW_a Molecular weight of air

MW_f Molecular weight of fuel

MW_i Molecular weight of species s

M_F Rate of fuel supply at source

M_O Mean oxygen mass supply per unit area to mean flame surface

m_s Soot mass

NOx_{corr} NOx concentration corrected to a reference oxygen basis (ppmvd)

NOx_{meas} Actual concentration of NOx measured (ppmvd)

$O_{2oxidant}$ Concentration of oxygen in the oxidiser stream (given as 20.9, except in an oxygen-enriched flame, where $O_{2oxidant}$ varies, depending on the percentage of oxygen enrichment in the flame, Howard, 1998).

O_{2ref} Reference oxygen (Volume percentage on a dry basis, either 3%, 6% or 15%, depending on the fuel type)

O_{2meas} Measured concentration of oxygen in the flue gas (volume percentage on a dry basis)

P Measured pressure, mbar

Q Heat release

r Radial distance

R Ratio of cross wind speed to burner jet exit velocity

Re Reynolds Number

Re_T Reynolds ratio at the tip of the flame

Ri_F Flame zone Richardson ratio

R_{st} Stoichiometric fuel to air mass ratio

T Measured temperature, (K)

T_{ab} Ambient air temperature

T_{FA} Adiabatic flame temperature

T_t Temperature of jet fluid

T_w Temperature of the wire, (K)

U *G*as velocity at nozzle

U_a Air velocity

U_b Laminar burning velocity

U_t Jet velocity

U_∞ Crossflow velocity

u Velocity of the fluid passing through the thermocouple bead, (m/s)

v_a Volumetric flowrate of air via duct

v_b Volume of the gas burned

v_g Volumetric flowrate of post-flame product via sample line

V_F Volumetric flow rate of fuel

V_t Volumetric flow rate of jet

X_s Mole fraction of species, s

X_{st} Stoichiometric mole fraction

y Axial position measured from the jet nozzle when ξ_F is less than 20 and from the fuel starting plane when ξ_F is greater than 20.

$Y_{o,f}$ Initial mass fraction of fuel

$Y_{f,t}$ Mass fraction of fuel in jet fluid

Y_{st} Stoichiometric mass fraction

$\bar{Y}$ Mean fraction fraction

$\overline{Y_C}$ Mean fraction of carbon atoms in the fuel (0.75 for methane)

Greek Letters

α_{st} Moles of reactants / mole of product for stoichiometric fuel-air mixture

β Entrainment parameter

ΔH_c Heat of combustion, per mole of fuel

ΔT_{rad} Radiation correction (K)

σ Stefan-Boltzmann constant ($W/m^2 K^4$)

ε Emissivity of the thermocouple bead (where ε =0.16 for bare platinum wires, and 0.22 for coated platinum wires)

η Viscosity of the gases at the wire temperature (kg/m s),

λ Thermal conductivity of the gases at the wire temperature (J/ m s K)

μ Fuel-gas dynamic viscosity

μ_k Kinematic viscosity

ξ Richardson number

$\overline{\xi}$ Mean mixture fraction

ρ Density of fuel gas stream, (kg/m^3)

ρ_a Density of air

ρ_o Density at nozzle exit conditions

ρ_t Density of jet

ρ_∞ Density at reservoir conditions

$\overline{\rho}$ Density ratio of fluid to air

τ_M Time scale for molecular mixing

τ_C Time scale for chemical reaction

τ_x Time scale for extinction

ψ Non-dimensional flame length

Acronyms

AMAP	Arctic Monitoring Assessment Programme
API	American Petroleum Institute
BC	Black Carbon
BCF	Billion Cubic Feet
BCM	Billion cubic metres
CCC	Climate Change Committee
CMD	Count Median Diameter
DECC	Department of Energy and Climate Change
DEFRA	Department for Environment, Food and Rural Affairs
DMS	Differential Mobility Spectrometer
EI	Emission Index
EIA	Energy Information Administration
FESEM	Field Emission Scanning Electron Microscopy
GAINS	Greenhouse Gas – Air Pollution Interactions and Synergies
GGFR	Global Gas Flaring Reduction
GHG	Greenhouse Gas
GTA	Global Trade Atlas
GWP	Global Warming Potential
HFID	Heated Flame Ionization Detection
HMDSO	Hexamethyldisiloxane
IMF	International Monetary Fund
IPCC	Intergovernmental Panel on Climate Change
ISO	International Standards Organisation
LIF	Laser Induced Fluorescence
LII	Laser Induced Incandescence
MMD	Mean Number Diameter
MMT	Million Metric tons
NBZ	Near-burner zone
NOAA	National Oceanic and Atmospheric Administration
OECD	Organisation for Economic Co-operation and Development
OPEC	Organisation of Petroleum Exporting Countries
PAH	Polycyclic Aromatic Hydrocarbons
PM	Particulate Matter

SRES	Special Report on Emissions Scenarios
TCF	Trillion Cubic Feet
TPD	Thermocouple Particle Densitometry
UNFCCC	United Nations Framework Convention on Climate Change
VOC	Volatile Organic Compounds

Chapter 1
INTRODUCTION

1.1. REVIEW OF WORLD ENERGY

The BP Review of World Energy (2015) reports that as of the year 2014, there was an increase in the production of all fuel types except coal, and there was an increase in the consumption of all types of fuel with the exception of the nuclear energy, with China still having the highest share in the energy consumption globally. The country with the greatest increase in the production of oil in the world was the United States, which for the first time replaced Saudi Arabia in oil production, due to the growth in the shale oil extraction.

1.1.2 CRUDE OIL PRODUCTION AND CONSUMPTION

The consumption of oil in 2014 was 0.8 million bpd, which was lower than the 1.8 million bpd consumption in the previous year, with non-OECD countries accounting for the growth in consumption globally, while there was a decline of about 1.2% in the consumption amongst the OECD countries. Globally, the growth in the production was twice greater than the consumption, with a growth increase of about 2.1 million bpd, while amongst the non-OPEC countries, there was also a 2.1 million bpd growth in the production, and the US recorded the largest growth in production at about 1 million bpd. Also, the US became the largest producer of oil in the world, followed by Saudi Arabia. Other countries that recorded high production levels were Canada and Brazil which recorded production levels of 0.31 million bpd and 0.23 million bpd, respectively. Also, there was a $9.7 decline in the price of crude oil in 2014 compared to the year 2013 and a further decline in the oil price towards the end of the year 2014 because of the stall in the growth of oil production in non-OPEC countries.

1.1.3 NATURAL GAS PRODUCTION AND CONSUMPTION

Globally, there was a 1.6% growth in the production of natural gas in 2014 although this growth was below the average when compared with the average of about 2.5% which was observed about 10 years ago. With the exception of North

America, other regions recorded production levels which were below the average. In Russia, the decline in the production was about 4.3%, while in the EU, it was 9.8%, and about 18.7% in the Netherlands. However, the largest increase was recorded in the US which was about 6.1% and represented about 77% of the increase in the growth globally. In terms of the consumption, natural gas recorded about a 23.7% increment in the consumption of the primary energy. However, the growth was only about 0.4% in 2014 when compared with 10 years ago. The largest decline in the consumption was recorded by the EU, which was about 11.6%, while the European and the Eurasian countries recorded declines of about 4.8%. However, the largest increase in the growth was recorded by the US, Iran and China, and was 2.9%, 6.8%, and 8.6%, respectively.

1.1.4 COAL PRODUCTION AND CONSUMPTION

There was a 0.7% decline in the production of coal globally, with China and Ukraine recording the largest decline. Similarly, there was a 0.4% growth in the consumption of coal, although this was about 2.9% below the average recorded in 10 years. In terms of the share consumption of the primary energy sources, the share of coal declined by about 30%, with Ukraine and the UK recording the most significant decline, while India recorded the largest global increase in the consumption, and the consumption from OECD countries declined by about 1.5% and about 6.5% in the EU.

1.1.4 OTHER ENERGY SOURCES

Globally, there was a 1.8% increase in the nuclear output which was due to the increments in China, France and South Korea.

The output from the hydroelectric power recorded about 6.8% of the share in the primary energy consumption, while this global net output increased below an average of about 2%, with the output from China recording a growth of about 15.7%, and being the only country with the highest output globally.

The renewable energy sources recorded a 3% increase in the consumption of energy globally which is about a 0.9% increase in the consumption in the last ten years. In the generation of power, the energy from renewable sources recorded growths of about 6 % globally, with China recording the highest increase in the power generation from renewable enegy sources. The energy from wind accounted for an increment of about 10.2% in renewable energy, while solar energy recorded

growths of about 38.2% and the production of energy via biofuels accounted for about a 7.4% increment in the global energy production. From the discussions so far, it is observed that as of the year 2015, there is a still a significant demand for fossil fuels, and this demand leads to an increase in the production of fossil fuels globally. The CO_2 emission from the burning of natural gas is about 30 % less than that from oil and about 45 % less than that from coal burning (Mokhatab and Poe, 2012), implying that natural gas is the only fossil fuel that has the lowest CO_2 emission (USEIA, 2013). Table 1.1 lists the various fossil fuel sources and the CO_2 emissions that are generated from burning these fuels in descending order. In addition, Table 1.2 lists the amount of the pollutant emissions from fossil fuels.

Fuel	**Amount of CO_2 emitted (lb/MBtu) of Energy**
Anthracite coal	228.6
Lignite coal	215.4
Sub-bituminous coal	214.3
Bituminous coal	205.7
Diesel fuel and heating oil	161.3
Gasoline	157.2
Propane	139.0
Natural gas	117.0

Table 1.1 Amount of CO_2 emitted from the combustion of different fuels (US EIA, 2013).

Pollutant	**Natural Gas**	**Oil**	**Coal**
Carbon dioxide	117,000	164,000	208,000
Carbon monoxide	40	33	208
Nitrogen oxides	92	448	457
Sulphur dioxide	1	1,122	2591
Particulates	7	84	2744
Mercury	0	0.007	0.016
Formaldehyde	0.75	0.220	0.221

Table 1.2 Pollutant emissions from fossil fuels (lb / BBTU of energy) (EIA, 1998).

It is observed that the CO_2 emission from coal is about twice the CO_2 emitted from natural gas burning. Similarly, the emission levels of pollutants such as NOx and SO_2 are lower during the burning of natural gas, than during the burning of coal. In the year 2012, the CO_2 emitted from the global energy consumption per capita in 2012 was about 4.6 MMT (US EIA). Similarly, the CO_2 that was emitted from the consumption of energy was about 32,310 MMT. From these energy sources, the share of coal was about 43 % of the CO_2 emissions, petroleum accounted for about 36 % of the CO_2 emissions, while the CO_2 emissions from the consumption and the flaring of natural gas was about 21 %. Amongst the fossil fuels, coal emits the greatest amount of CO_2, and coal has the greatest share from the global energy source.

1.2 OVERVIEW OF FLARES

Flaring is used to get rid of the associated gases (Brzustowski, 1976) that do not have an economic value, either due to the small volume of the gas that is produced which may not be cost-effective to process, or the lack of the facilities to transport the gases to production plants for further processing (Dubnowski and Davies, 1983; Beychok, 2005). Figure 1.1 is a photograph of an onshore gas flare. Flaring is also used during emergencies and in non-emergency situations in process plants, when there is the need to reduce an excessive pressure-build-up in the plants, or when there is a leakage and it is necessary to purge the gas line, in order to reduce the risk of an explosion or fire (US EPA, 2012).

There are three types of flaring, which are the emergency flaring, process flaring and the production flaring (Brzustowski, 1976). Emergency flaring may be performed during fire out-breaks or when there is a pressure-build-up in the plant. Process flaring is performed at short time intervals and in small volumes during well-testing and during routine checks, when it is inevitable to do so. Production flaring is performed either to remove sour gases or when the gas volume to be flared is small and it is not advisable to further process the gas due to the cost implications.

	FLOW STATION									
	A	**B**	**C**	**D**	**E**	**F**	**G**	**H**	**I**	**J**
	MOLAR COMPOSITION (%)									
Methane	68.42	90.12	68.14	78.41	82.23	89.34	69.58	86.32	79.85	72.32
Ethane	7.65	6.94	14.22	5.68	2.38	5.25	0.25	5.28	11.54	2.41
Propane	11.27	2.09	10.27	0.23	4.24	1.58	12.54	4.25	2.25	6.24
N-butane	4.39	0.361	3.23	0.7	0.94	0.58	2.35	0.42	2.58	8.12
I-butane	4.42	0.41	2.38	4.12	5.12	0.18	5.12	1.24	0.14	5.12
N-Pentane	0.94	0.042	0.75	9.12	2.25	1.25	5.2	2.23	3.24	3.14
I-pentane	1.55	0.037	1.01	0.25	2.14	1.22	2.54	0.14	-	2.48
Hexane	0.18	-	-	0.23	0.25	0.52	1.97	0.12	0.14	0.15
Nitrogen	0.16	-	-	0.05	-	0.05	0.24	-	0.1	-
Carbon dioxide	1.02	-	-	1.21	0.45	-	0.21	-	0.16	-
Hydrogen sulphide						0.03				0.02

Table 1.3 Natural gas constituents from different reservoirs in the Niger Delta region of Nigeria (Sonibare and Akeredolu, 2004).

Figure 1.1 Photograph of a flare showing a sooty gas flare (Smoot *et al*., 2009).

An analysis of the composition of natural gas produced from crude oil and gas reservoirs show that other hydrocarbons which include ethane, propane, butane, pentane, and non-hydrocarbons, such as carbon dioxide, hydrogen sulphide, nitrogen, water vapour, etc., are constituents of natural gas (EIA, 1998). Although the composition of natural gas varies, however, methane is the major constituent of natural gas (US EIA, 1998). A typical example of the constituents of natural gas and their average molar compositions in different reservoirs in the Niger Delta region of Nigeria (Sonibare and Akeredolu, 2004) are presented in Table 1.3.

1.2.1 GAS FLARING STATISTICS

In the year 2010, The World Bank's estimate of the volume of the gas flared globally was about 138 bcm. In 2011, there was a 2 bcm increase in the volume, and this was due to the increase in the exploration, production and consumption of oil and gas worldwide and the development in unconventional gas sources. Table 1.4 lists the estimates of the volume of gas flared by country in a descending order of the volume of gas flared between 2007 and 2011. As of 2011, only about 20 countries were responsible for flaring about 86% of the gas flared worldwide, while the first five countries alone flared more than half of the total gas flared worldwide which was about 79.9 bcm (2.8 tcf) of associated gas, which represents 57 % of the gas flared worldwide.

VOLUME (Billion Cubic Metres)	2007	2008	2009	2010	2011	Change between 2010 and 2011
Russia	52.3	42.0	46.6	35.6	37.4	1.8
***Nigeria**	16.3	15.5	14.9	15.0	14.6	-0.3
Iran	10.7	10.8	10.9	11.3	11.4	0.0
Iraq	6.7	7.1	8.1	9.0	9.4	0.3
USA	2.2	2.4	3.3	4.6	7.1	2.5
Algeria	5.6	6.2	4.9	5.3	5.0	-0.3
Kazakhstan	5.5	5.4	5.0	3.8	4.7	0.9
Angola	3.5	3.5	3.4	4.1	4.1	0.0
Saudi Arabia	3.9	3.9	3.6	3.6	3.7	0.1
Venezuela	2.2	2.7	2.8	2.8	3.5	0.7
China	2.6	2.5	2.4	2.5	2.6	0.1
Canada	2.0	1.9	1.8	2.5	2.4	-0.1
Libya	3.8	4.0	3.5	3.8	2.2	-1.6
Indonesia	2.6	2.5	2.9	2.2	2.2	0.0
Mexico	2.7	3.6	3.0	2.8	2.1	-0.7
Qatar	2.4	2.3	2.2	1.8	1.7	-0.1
Uzbekistan	2.1	2.7	1.7	1.9	1.7	-0.2
Malaysia	1.8	1.9	1.9	1.5	1.6	0.2
Oman	2.0	2.0	1.9	1.6	1.6	0.0
Egypt	1.5	1.6	1.8	1.6	1.6	0.0
Total top 20	**132**	**124**	**127**	**118**	**121**	**3.1**
Rest of the world	22	22	20	20	19	(1.1)

Global flaring level	154	146	147	138	140	1.9

Table 1.4 Estimated flare volumes from satellite data by source (National Oceanic and Atmospheric Administration (NOAA) satellite data).

The projections by The World Bank show that if there is a steady reduction in the flaring of gas, then by 2017, the volume of the gas flared would have reduced by 30%. However, it is also projected that if stringent and revised legislations, and newer / improved technologies are not developed, there may be an increase in flaring in the future, due to the increased production and consumption and the developments in conventional and unconventional oil and gas sources, which may lead to increased flaring of larger gas flare volumes.

Pollutants (mg/m^3)	**Flow station 1**	**Flow station 2**
Carbon dioxide	**0.05925**	**0.06905**
Carbon monoxide	**0.055**	**0.0112**
Nitrogen dioxide	**0.0163**	**0.0373**
Sulphur dioxide	**0.00745**	**0.0242**
Particulates	**0.0008**	**0.00085**

Table 1.5 Mean composition of pollutants from different gas-gathering stations (flow stations) (Nwaichi and Uzazobona, 2011).

In Nigeria alone, the data from The World Bank show that the natural gas which was produced was about 28.3 bcm, of which about 14.6 bcm was flared in the year 2011 alone. This loss in the revenue due to flaring was estimated to be up to about US $2.5 billion per year. Similarly, the losses in the revenue in a 36-year period starting from 1970 to 2006 were estimated to be about $150 billion when averaged at a 1.2 tcf per year. This gas which is flared could adequately be used to generate about 12,000 megawatts of electricity (Ogiemwonyi, 2009). The flaring of gas also emits harmful pollutants to the atmosphere. Table 1.3 lists the varying constituents of natural gas from ten different flow stations in the Niger Delta region

of Nigeria, while Table 1.5 summarises the mean concentration of the pollutant species which are generated from two different flow stations in Nigeria.

Figure 1.2 Photograph of a ground flare (Lohuizen,2008).

In designing a flare burner, it is important to take into consideration the effect of fuel–air mixing on the flare burner, because the mixing affects the structure of the flame, the stability of the flame, completeness / in-completeness of combustion, and the pollutant emissions generated from the flame. Therefore, to enhance the efficiency of a flare system, the operating condition of the flare such as the wind speed, gas jet exit velocity, gas jet exit diameter, detailed measurement and analysis of the composition of the fuel, flare stack size, or flare tip design must be taken into consideration in the design of a flare system, since these factors affect the combustion efficiency of flare systems (Siegel, 1980; McDaniel, 1983; Pohl *et al*., 1986; Johnson and Kostiuk, 2000). The US EPA classifies flares under two main categories. The first is the mixing which depends on the flame's tip design, which also determines the amount of the soot, and the pollutants that are emitted, while the second is the height of the flare stack and the flame's height, which has consequences on radiation. The flare's height may be either elevated or ground flare, while the burner which controls the mixing of the fuel and the oxidiser at the flare's tip may be designed to be pressure-assisted, air-assisted, steam-assisted, or even un-assisted. Environmental, industrial and inter-agency legislations exist in different countries, which set standards to regulate, monitor and control the emissions that are

generated from the flaring of gas. The US EPA is one of such regulatory agencies, which set standards for the designing and the operation of gas flare systems for a greater efficiency. For instance, a combustion efficiency of about 98 % has been recommended (OAQPS, 2012). However, this high efficiency has hardly been achieved because of the several challenges which are listed as: the difficulties in collecting samples from the plume for the analysis of the plume compositions, the excessive steam or air that are being injected into the flame in an attempt to suppress the smoke in the flare, the effect of high cross-wind velocities which cause the flame to be wake-dominated, and the effect of the flame being stabilised above the nozzle's tip which affects the flame's stability and emissions.

1.3 MOTIVATION FOR THE STUDY

One of the consequences of gas flaring is the production of a significant amount of soot and other pollutant emissions (Arctic Council Task Force, 2011). Soot has been suggested as the main source of global warming right after CO_2 (Bond *et al*., 2013). This warmth is thought to be about twice the previous estimations that have been reported by the IPCC (2007). The soot emissions generated from flaring in oil and gas industries have been estimated to account for about three per cent of the emissions from anthropogenic sources reported in the global inventory (Stohl *et al*., 2013). Other anthropogenic sources of soot emissions include residential combustion, burning of agricultural wastes, biomass combustion, and other sources, which include the transportation industry, the energy sector (which excludes flaring in the oil and gas industry), etc. Table 1.6 is a summary of the contributions of soot from various sources in the global inventory, and the latitudinal variation of soot as recorded in the ECLIPSE database. The differences in the daily, monthly, and yearly variations of emissions have been reported, based on the available database, where it has been estimated that amongst the anthropogenic sources, depending on the time of the year, flaring alone constitutes up to about fifty-two per cent of the emissions modelled in the arctic (Stohl, 2006; Stohl *et al*., 2013).

A similar suggestion has been made by Jones *et al*. (2013) that climatic and atmospheric variations affect the temperature and the emissions generated from flaring in the environment. According to Bond *et al*. (2013) and Stohl *et al*. (2013), although the estimates of these emissions have been successfully modelled, however, these emissions have not been fully quantified. One of the reasons is

because the composition of soot emission and other pollutants from other sources present in the emission measurement sample makes it difficult to accurately measure the emissions, which in turn limits the amount of the available and reliable data generated from full-scale flares. Another consequence of flaring is as stated in the report by the Arctic Monitoring Assessment Programme (AMAP), that there has been a 30% increase in the acidity of the seas in the Arctic and in the Nordic regions, due to an increase in the carbon dioxide emissions, which has significantly increased the vulnerability of these seas to acidification, since absorption rates are greater in colder waters. This is due to the greater solubility of CO_2 in colder waters as in the arctic waters, than in warmer waters, which leads to a greater absorption of CO_2 in the arctic seas, leading to the reduction in the PH of the seas and the death of some organisms. The composition of natural gas is mainly methane, and CO_2 is one of the products of combustion during the flaring of natural gas. Other products are unburned hydrocarbons, soot, and pollutant emissions such as NOx and CO (McEwen and Johnson, 2012; US Environmental Protection Agency). Gas flaring is the burning of unwanted gases produced during the production or processing of crude oil. The CO_2 emitted from flaring accounts for over 350 million tonnes of CO_2 which is annually emitted into the atmosphere. However, there are options for the disposal of these unwanted / unmarketable associated gases. Flaring is one of such options. However, during flaring, CO_2 which is a greenhouse gas is released into the atmosphere. Another option is venting, which is the release of gas into the atmosphere without combustion. This option leads to the release of methane which is more potent than CO_2 into the atmosphere. Other options are: the injection of the gas into the reservoir to increase the volume of the oil to be recovered from the reservoir, liquefaction of the natural gas, utilization of the gas to provide power for the generating plants used to generate electricity, or the provision of power required in driving the compressors used in the production and processing sites. In laboratory-scale flares, several researchers (Kalghatgi, 1981; Choudhuri and Gollahalli, 2000; Majeski *et al*., 2004; El-Ghafour *et al*., 2010, etc.) have studied the effect of additives such as Ar, H_2, N_2, etc., on the combustion characteristics of hydrocarbons. Also, previous studies have highlighted the importance of utilizing CO_2 as inert additives in jet flames (Fells and Rutherford, 1969). These additives may be injected either into the fuel stream or oxidizer stream of the jet flames. Previous investigations have shown that these additives aid in the reduction of the

reactant species, which leads to a reduction in the flame temperature, hence, leading to a reduction in the thermal NOx formation, and a reduction in the soot volume fraction. For example, the investigations of Lock *et al*. (2007, 2008, 2009), Takahashi *et al*. (2008), Guo *et al*. (2010), Min and Baillot (2012), Oh and Noh (2014), etc., have highlighted the effect of the dilution of the oxidizer stream by CO_2. Similarly, previous researchers have investigated the effect of the CO_2 inert dilution on the fuel-stream: Gollahalli (1977) investigated the effects of diluents on the flame structure and radiation of propane flames; Kalghatgi (1981) studied the effect of CO_2 dilution on the blow-out stability of methane and propane diffusion flames; Berhan *et al*. (2001) investigated the effect of CO_2 dilution on flame temperature and radiation in ethylene flames in microgravity conditions; Briones *et al*. (2006) performed a numerical investigation of the effect of fuel dilution on the stability of non-premixed flames; Lock *et al*. (2007) investigated the lift-off and the extinction characteristics of fuel- and air-stream-diluted methane-air flames; Wu *et al*. (2009) investigated the stability limits of pure hydrogen and mixtures of hydrogen / hydrocarbon flames; Samanta *et al*. (2010) performed a numerical analysis on the effect of CO_2 dilution on the structure of the flame, and on NOx formation in methane /air diffusion flames, amongst others. However, to the best of the author's knowledge, there is no simultaneous study on the effect of the dilution of the methane fuel stream on the in-flame composition of major species, post-flame emissions, or on the structure of the flame over a broad range of Reynolds numbers, *Re*. It is important to investigate the changes in the flame structure at different flow regimes because turbulent diffusion flames are characterized by their non-linearity (Jeng *et al*., 1984), and in the turbulent fluctuations in the temperature, species concentration, etc., which these flames exhibit (Chen *et al*., 1992). Characterising these quantities provide a better understanding of the structural changes these flames exhibit with respect to the changes in the different diluent mole fractions at different Reynolds number. Hence, investigations on the effect of varying the diluent mole fraction over different Reynolds number, ranging from 1584-14254 on the EICO and EINOx are discussed in this thesis. This is the first time the Emission Indices (EI) of pollutant species has been measured by varying the diluent mole fraction over a very wide range of Reynolds number. The only other investigation that is closely related to the present investigation is the variation of the EI at a wide range of diluent mole fraction over a fixed Reynolds number by Gollahalli (1978).

Source	Global inventory		Latitudes greater than 40ºN		Latitudes greater than 50ºN		Latitudes greater than 60ºN		Latitudes greater than 66ºN	
	Emission (kt/year)	%	Emission (kt/year)	%	Emission (kt/year)	%	Emission (kt/year)	%	Emission (kt/year)	%
Flaring	228	2.85	83	6.4	69	12.8	52.2	32.8	26.4	65.5
Agricultural sector	341	4.27	73	5.6	29	5.4	0.2	0.1	0	0
Biomass combustion	2276	28.5	219	16.8	205	38.0	92.4	58.1	12.3	30.5
Residential sector	3055	38.3	472	36.2	93	17.3	6.2	3.9	0.6	1.5
Others	2088	26.1	458	35.1	143	26.5	8.0	5.0	1	2.5
Total	7988	100	1305	100	539	100	159	100	40.3	100

Table 1.6 Summary of the contributions of soot from various sources in the global inventory, and the latitudinal variation of soot as recorded in the ECLIPSE high-latitudinal emissions database for the year 2010 (Stohl *et al*., 2013).

Another motivation for this research is that in oil and gas industries alone, the main constraints in quantifying the emissions generated from gas flaring are that flare systems are not enclosed, and hence make measurements challenging, due to the differences in the flare stack designs and dimensions. For example, plumes from flares cannot be controlled, because of the effect of the changes in crosswind directions and velocities, and other meteorological variables, which vary significantly in unenclosed flare systems, thus driving the flare plumes at different directions, which presents challenges to making accurate measurements. This is where laboratory-scale or pilot-scale flares play an important role. It is clear from the discussions presented so far, that there is an enormous demand for cleaner energy and for an accurate quantification of the emissions generated during gas flaring. Therefore, the emissions generated from flare flames, and the role of stability due to strain rate and dilution effects in lifted flames, which is the focus of this research, will help in understanding how varying parameters such as the jet flame velocity and the effect of CO_2 dilution could affect flame stability and emissions, which is the motivation for this research.

1.4 OBJECTIVES OF THE STUDY

The main objective of this research is to examine the changes in the temperature, flame structure, composition of species, and in the emission indices of pollutant species (EICO, EINO and $EINO_2$) of laboratory-scale flares at various test conditions. This will be achieved by performing a comparative study on the effect of varying the fuel type, the fuel jet velocity, and the diluent mole fraction on methane jet diffusion flames over a wide range of operating conditions. In this regard, the objectives of this study are as follows:

i. Performing an extensive literature search and critically reviewing the experimental methods and the types of data generated by past and present authors in characterising the behaviour of soot, CO and NO, and NO_2 emissions in laboratory-scale methane diffusion flames.

ii. Investigating the effect of varying the test conditions such as the fuel jet velocity, and what influence the emission of NOx, CO and CO_2 has on both the attached and the lifted flow regimes in methane diffusion flames.

iii. Varying the mole fraction of CO_2 in the fuel, and what effect this variation has on flame stability, temperature and pollutant emissions in the flame.

iv. Examining how the emission indices of the pollutants vary with each jet flame.

v. Characterising the axial and radial profiles of these pollutants at different flow regimes.

vi. Performing an in-flame and post-flame investigation of all the pollutant species listed above.

1.5 SCOPE OF THE THESIS

From the aforementioned, it is clear that the continuous and more accurate investigation into emission reduction in the flaring industry is inevitable, added with the already-existing vast wealth of knowledge that is available, which is aiding in making informed decisions in the operation of gas flaring systems in energy conservation, and in the formulation of emission regulations. It is expected that the conclusions drawn from the results in this research will fill a knowledge gap, based on the various test conditions which will be employed, and in the results which will be collated and compared in this experimental investigation. In order to fully quantify emissions in the oil and gas industry at a laboratory scale, the experimental measurements would have to be carried out under different test conditions which includes, but not limited to using different fuels with different sooting propensities, different flow rates, different burner jet nozzle geometries and dimensions, different meteorological variables, such as temperature and the effect of wind in an unconfined space, amongst others. However, the scope of this study is limited by the facilities and the funding available for this research, and includes the following: varying the fuel jet velocity, varying the diluent mole fraction of CO_2 to characterise the temperature and the emissions generated in the combustion of methane / air flames, estimating the soot emission factor using fuels with different sooting propensities, characterising the morphology of the soot particles and the soot particle size of post-flame combustion products. In addition, measurements of the flame temperature, concentration of major gas species such as NOx, CO, CO_2, O_2 and unburned hydrocarbons at both the attached and the lifted flow regimes, and at different diluent concentrations at different stream-wise locations, and comparing

the emission indices of NOx, NO, NO_2 and CO at different operating conditions will be performed. Thereafter, the experimental results will be compared with the literature, and conclusions will be drawn from the present study.

1.6 OUTLINE OF THE THESIS

In order to accomplish the set objectives, this thesis is organised into seven chapters and a brief description of each chapter is as follows:

Chapter 1 The chapter outlines the current global energy production and consumption trends. From there, a comparison of the level of emission from different energy sources is presented, where the level of emission in fossil fuels from each pollutant is presented. In addition, the problem statement is formulated where the motivation for this research is discussed, together with an outline of the set objectives, and a defined scope of this research.

Chapter 2 is composed of a review of the statistics on global gas flaring and gas flaring reduction methods, alternatives to gas flaring, different types of flare systems, reviews of flame length, and lift-off height correlations, a review of soot measurements in laminar and turbulent flow regimes of methane flames at different pressures, a critical review of measurements on both unconfined and confined turbulent methane-air flames.

Chapter 3 presents a detailed description of the experiment conducted, including the instruments used for the measurements, the experimental set-up, and the techniques used for the measurements.

Chapter 4 The results generated from the experimental investigation on attached and lifted flames is discussed. This is comprised of comparisons and discussions on the visualisation of the flame, the in-flame measurement of the flame temperature, the variation of species at different stream-wise locations in the jet flames, plots of the mixture fraction space showing the distribution of the major species on the fuel-lean and fuel-rich regions of the jet diffusion flames, and a comparison of the post-flame pollutant species at various jet velocities.

Chapter 5 The combustion characteristics of CH_4+CO_2 / air jet diffusion flames are presented in this chapter, where the effect of varying the diluent mole fraction of CO_2 on methane fuels are examined. A side-by-side comparison of the visualisation of the flame, flame length, and the lift-off distance will also be presented, added

with comparisons of the flame temperature, in-flame and post-flame composition of major species, and the emission indices of the post-flame products at different diluent levels.

Chapter 6 focuses on the results on the comparison of the combustion characteristics of methane and propane flares, with emphasis on the flame temperature, composition of species, post-flame emission indices of pollutants and the effect of fuel-stream dilution on the soot particle size of the laboratory-scale propane flares.

Chapter 7 presents the key findings from this investigation and an outline of the suggestions for future investigations.

Chapter 2
LITERATURE REVIEW

2.1 INTRODUCTION

The combustion of a fuel issuing from an orifice which is not mixed with an oxidiser requires diffusion of an oxidiser into the stream of the fuel containing the unburned fuel, and this is the origin of the name “diffusion flames” (Thomas *et al*., 1961). Diffusion flames have been investigated extensively by several authors. For example, Burke and Schumann (1928) investigated confined laminar flames using a cylindrical burner, by using a theoretical model to describe laminar diffusion flames; Yagi (1943); Hottel and Hawthorne (1949); Wohl *et al*. (1949) and Yagi and Saji (1953) investigated unconfined laminar diffusion flames using the diffusion theory; while Hawthorne *et al*. (1949); Wohl *et al*. (1949); Yagi (1943); and Yagi and Saji (1953) investigated the flame length of turbulent flames. Gaseous flames may be classified under two combustion systems, due to the type of mixing of the fuel and the oxidiser, which could be either premixed, or non-premixed flames (Warnatz *et al*. 2006). If there is an intimate mixing of the fuel and the oxidiser before combustion takes place, then such as system is referred to, as a premixed system. If the reactants (fuel and the oxidiser) are introduced independently into the flow domain, where mixing occurs, then such a system is referred to, as a non-premixed system. Combustion occurs in the reaction zone at a location where there is an optimal mixing of the reactants in the flow field (Peters and Göttgens, 1991).

In non-premixed combustion, the rate of the chemical reaction is very fast, and is a consequence of fast mixing rates (Puri, 1993). The occurrence of a chemical reaction is resultant of the reaction of the reacting species at high temperatures. A schematic of a non-premixed system showing the fuel and the oxidizer streams are shown in figure 2.1, where in mixture fraction space, this varies between 0 and 1, where 0 denotes that the flame is fuel-lean and air-rich, and 1 which is a pure fuel stream, and denotes that the flame is fuel-rich or air-lean. The mixing is in two ways: either by molecular mixing or by eddy diffusion (Hottel and Hawthorne, 1949). In molecular mixing, the rate of mixing is slower than in eddy diffusion, where the mixing is faster, as a result of the turbulent interaction of the fluid’s

micro-particles (Hottel, 1953). Non-premixed flames, which are also known as diffusion flames (Bilger, 1989), are further classified as either laminar or turbulent flames, depending on the conditions in the combustion zone (Takahashi *et al*., 1982).

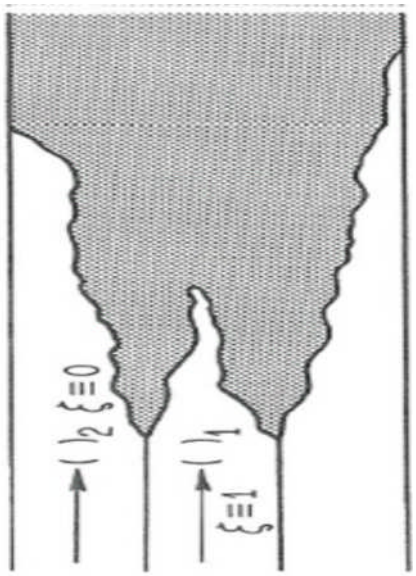

Figure 2.1 Schematic of a non-premixed flame showing the fuel and the oxidiser streams (Libby and Williams, 1994).

In non-premixed flames issuing from a fuel jet tubing into the surrounding, at lower velocities, the flow is laminar. As the fuel jet velocity is increased, visible eddies are observed at the far-burner downstream locations in the flame. A further increase in the velocity causes the eddies to move upstream, where the flame becomes transient and at much higher velocities, the flame becomes turbulent and may get detached from the tip of the fuel jet rim. The turbulence of the flame causes an increase in the rate of entrainment of air into the flame at the same rate as the velocity of the fuel jet. The entrainment occurs mainly in the upstream location in the near-burner zone (Dahm and Dibble, 1988). The increase in the fuel jet velocity leads to an increase in the height of the flame up to a stage where there is no longer any significant increase in the height of the flame, where the height of the flame is no longer proportional to the jet velocity. The evidence of an increase in the jet velocity is the propagation of the flame from the laminar regime to the turbulent regime. This leads to an increase in the mixing rate of the fuel and oxidiser, and is characterised by a change in the flame's geometry, radiation, emissions, etc. Flares in real-life are largely turbulent and non-premixed (McEwen and Johnson, 2013).

However, it is possible to observe a degree of partial pre-mixing in a flame (RØkke *et al*., 1994), although the non-premixed combustion is the dominant mixing mode that is evident in a flame (Gollahalli and Nanjundappa, 1995). Turbulent non-premixed flames also play a role in industrial furnaces and burners because of their reliability, simplicity and efficiency (Gerstein, 1991). Non-premixed systems are also more cost-effective and safer than premixed flames, because the need for the mixing of the fuel and the oxidiser prior to combustion is eliminated (Howard, 1998), thereby reducing the risk of premixing large volumes of the reactant, which if not controlled, can cause a huge accidental explosion (Warnatz *et al*. 2006).

According to Burke and Schumann (1928), in non-premixed flames firing vertically upwards from a fuel tubing, the amount of time required for the mixing of the fuel and the oxidant is dependent on the height and the in-flow velocity of the flame. A detailed mathematical expression of this relationship will be discussed later. In non-premixed flames, the characteristic luminescence of the flame, which is as a result of the glowing of the particles of soot, is an indication of the chemical reactions occurring in the fuel-rich region of the flame (Warnatz *et al*., 2006).

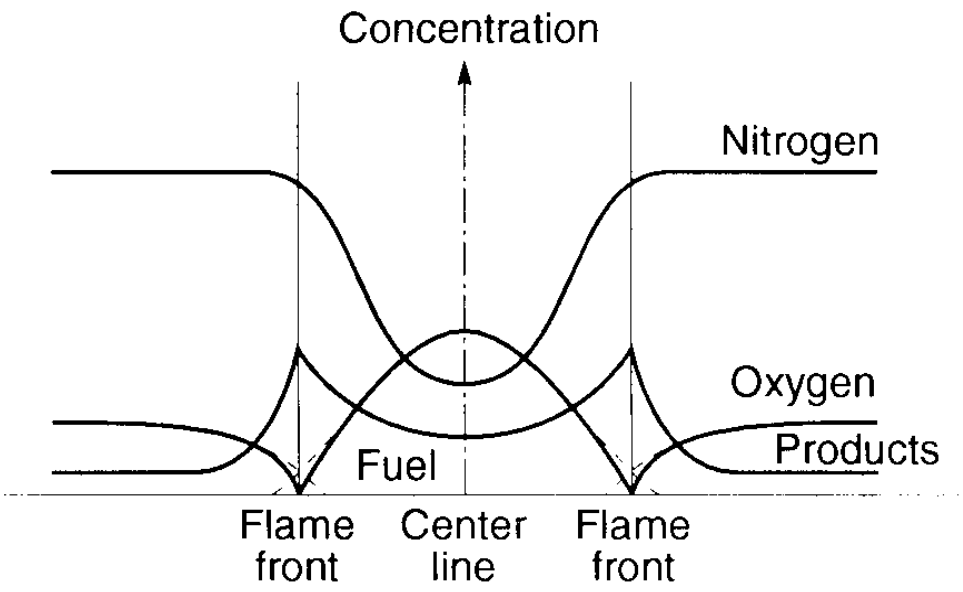

Figure 2.2 Schematic of variation of species in a laminar concentric gaseous diffusion flame (Hottel and Hawthorne, 1949).

Similarly, in non-premixed flames, there is a diffusion of the fuel and the oxidiser to the flame-front as a result of the gradient encountered via a chemical

reaction, and the highest concentration of the product is at the flame front, while the fuel and oxidiser disappear at the flame front. (Hawthorne, 1939). A schematic showing the variation of species in a gaseous diffusion flame is shown in figure 2.2.

In diffusion flames generally, the fuel micro-particles diffuse towards the flame front, while the oxidiser diffuses towards the flame front, causing reactions to take place, where the reactants are in stoichiometric proportions. In laminar diffusion flames, there is a mixing of the fuel and oxidiser by the molecular mixing mechanism, at the flame front (reaction zone), see figure 2.2, which leads to a uniform flow as a result of the smooth sliding layers of fluid, enabling scalars such as the concentration of species and temperature to have definite values and smooth contours.

2.1.1 TURBULENT DIFFUSION FLAMES

Turbulent diffusion flames are characterised by the irregularity of the properties they exhibit, which is marked by fluctuations, and a sharp gradient in properties such as temperature, composition, density, velocity, etc. (Howard, 1998). The fluctuation in velocity is caused by the vortices, which are generated by shear in the flow, causing the vortices to compete between the non-linear generation and destruction processes via viscous dissipation (Warnatz *et al*., 2006). The propagation of the flame occurs when the generation term exceeds the viscous damping term (Howard, 1998). Similarly, when a critical value of the Reynolds number is surpassed, a transition from the laminar regime to the turbulent regime takes place. Below this critical value, a smooth flow of fluid is observed, where the layers of fluid slide past each other uniformly. Beyond this critical value, there is a change in the characteristics of the flame, such as noise, visual appearance, stability, etc., which are indications of turbulence.

Turbulent flows could be characterised by either mean or fluctuating quantities (Howard, 1998). Mean values of a quantity are derived by taking the time average of that quantity over a large time interval. Since the flame exhibits turbulence, the larger the dataset sets which are gathered and averaged, the more representative the mean value is. Similarly, the fluctuating quantities are the difference between the instantaneous value and the mean value. The results of the mean and fluctuating temperature values of the different flames investigated will be discussed in the

fourth chapter of this thesis. In turbulent flames, eddies exist in sizes which are known as length scales, which depends on the flow condition. The different length scales are: Kolmogorov microscale, Taylor microscale, Integral scale (Taylor macroscale), and the characteristic width of flow (macroscale). The Kolmogorov microscale is the smallest length scale, and it represents the scale where there is a dissipation of the turbulent kinetic energy to the internal energy of the fluid. The characteristic width of flow, also called the macroscale accounts for the largest possible eddies. In practice, for example, in a pipe flow, the largest possible eddy would be the equal to the diameter of the pipe. The Taylor microscale and the Taylor macroscale are intermediate lengths found between the characteristic width and the Kolmogorov scales. The vorticity which is used in characterising turbulent flows have large range of length scales and times scales and may lie in close range with one another (Baukal, 2003). According to Verseeg and Malalasekera (1995), when turbulent flows are visualised, they reveal swirling flow structures, which are also known as turbulent eddies, at different length scales, which implies that in turbulent flows, microparticles which were separated by a large distance could be brought together by the interaction of eddies to enhance mixing. Turbulence is sustained when the largest turbulent eddies are in constant interaction with smaller eddies, thereby stretching the smaller eddies in a process called “vortex stretching”.

During this process, there is an increase in the rate of rotation of the larger eddies and a reduction in the radius of the cross-section of the larger eddies, thereby creating motions at smaller length scales where the vortex-stretching work which is done by the average flow on the larger turbulent eddies provide the energy which sustains the turbulence (Dearden, 1996). When the jet velocity increases, the kinetic energy of the microparticle also increases, and the interaction between these particles causes a transfer of energy, mass and momentum, which in turn causes an enhanced turbulent mixing. There is a significant effect of turbulence on combustion. If the turbulence is in a small scale, and the size of the turbulence eddies do not exceed the thickness of the flame front, then there is an increase in the heat and mass transport in the flame, causing an enhanced combustion. However, if the turbulence is on a large scale, a distortion (wrinkled flame) of the flame front is observed, (Damköhler, 1940), causing an increased burning rate because of the increase in the surface area.

Turbulent combustion could be investigated based on the dimensionless quantities that represent length or time scales, which could either be Reynolds Number, *Re*; Froude Number, *Fr*; or Damköhler Number, *Da* (Williams, 1985).

The Reynolds number is a parameter used to determine the level of turbulence, and is the ratio of the destabilising momentum (inertial forces) and the stabilising (damping) viscous forces. It is mathematically expressed as:

$$\mathrm{Re} = \frac{(\rho U d)}{\mu} \tag{2.1}$$

The Froude number is the ratio of the inertial forces to the gravitational forces, and is mathematically expressed as:

$$Fr = \frac{U^2}{gd} \tag{2.2}$$

The Damköhler number, Da, is an expression of the timescale for molecular mixing to the timescale of the chemical reactions and is mathematically expressed as:

$$Da = \frac{\tau_M}{\tau_C} \tag{2.3}$$

The regions of turbulent combustion are either identified in terms of either the "fast" or "slow" (finite) chemistry. If the region of combustion corresponds to conditions of equilibrium (fast chemistry), where the Damköhler number, *Da*, is greater than unity, then molecular mixing dominates in those regions. However, if the combustion region corresponds to conditions away from equilibrium, where the *Da,* is less than unity, then the slow (finite) chemistry dominates. In a fuel-jet firing vertically upwards, the friction that exists between the combustion products' streams and the still air leads to the formation of the eddies, thereby causing the combustion products' vortices to shroud the jet stream of the fuel from ambient air. This reduces the diffusion of the oxidiser and the fuel, resulting in an increased length of the flame. However, the breaking of these eddies create an enhanced diffusion of oxygen into the reaction zone, thereby shortening the length of the flame. Transitions from laminar to turbulent conditions in diffusion flames are marked by changes in the structure of the flame, with significant differences in the length and

shape of the flame, with increasing fuel jet velocity, as shown in figure 2.3.

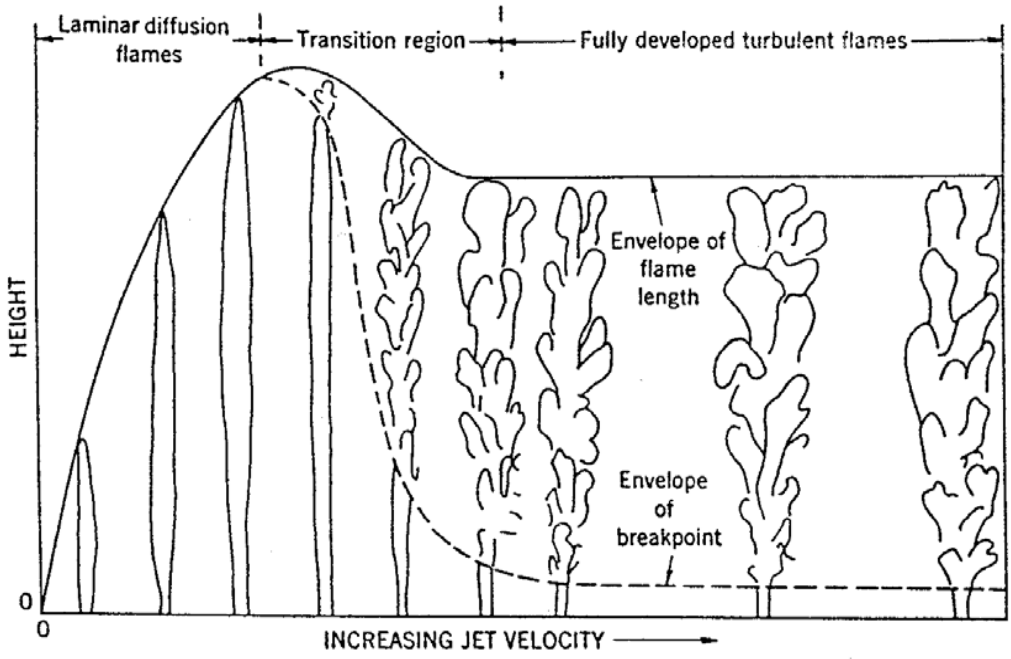

Figure 2.3 Schematic of the variation in the flame height as a function of the jet's velocity (Hottel and Hawthorne, 1949).

In the laminar regime, the flame length varies directly with the jet velocity up to a critical value, where the tip of the flame begins to flicker. Below the critical value, the mixing of the fuel and the oxidiser is by molecular diffusion. Beyond this critical value, the flame becomes turbulent, where a further increase in the fuel jet velocity does not lead to an increase in the length of the flame, and the flame begins to lift off and stabilise at a location downstream of the flame axis, where at a higher velocity of the fuel jet causes the flame to blow out entirely (Dahm and Mayman, 1990). Before the flame lifts off, the mixing in this region is by eddy diffusion along the flame front (Hawthorne *et al*., 1949). The widening of the flame volume, the shortening of the flame length, and an increased noise, marks the turbulence in this region. Numerous studies on diffusion flames have been performed in the past, some of which have focused on characterising the flame structure, temperature, and composition of species in diffusion flames. A review of these investigations is presented in the next section.

2.2 REVIEW OF FLAME LENGTH CORRELATIONS

The characteristics of a flare may be affected by parameters such as the flame's geometry (length and the shape of the flame), thermal properties (radiation and temperature) (Peters and Göttgens, 1991), the composition of the gaseous fuel, the flow-rate of the fuel stream, and the crosswind velocity of the flare (Baukal, 2011). It is useful to characterise the behaviour of a flame in order to estimate the radiative properties and efficiency of the flame (Leahey and Schroeder, 1987). In order to assess the risks associated with jet flames, analysis may be conducted to assess the risks involved in installing flare stacks close to other process plants. The information on the flame length, the trajectory of the flame, the transfer of heat to the process plant, etc., will aid in the decision to install the flare stack at an optimal distance away from other process plants, in order to reduce the risk of fire (Cumber and Pearpoint, 2006). Appreciable work has been performed on both the experimental and the theoretical estimation, correlation and prediction of flame lengths of buoyancy-dominated and momentum-dominated diffusion flames firing both vertically into still air, and in crosswind. These investigations have been performed by Burke and Schumann (1928); Hawthorne *et al*. (1949); Wohl *et al*. (1949); Blinov and Khudakov (1957); Thomas *et al*. (1961); Thomas (1963); Putnam and Speic (1963), Vieneau (1964); Putnam and Gringerg (1965), Kosdon *et al*. (1969); Steward (1970), Brzustowski (1973, 1975, 1984); Gollahalli *et al*. (1975), Gollahalli (1977); Becker and Liang (1978); Beychok (1979); Kalghatgi (1983, 1984); SØnju and Hustad (1984); Leahey and Schroeder (1987); Peters and Göttgens (1991); Blake and McDonald (1993); Majeski *et al*. (2004), amongst others.

Different definitions of flame length have been proposed by various investigators. In a correlation of turbulent buoyant diffusion flames, Steward (1970) defined flame length as the sum of two lengths – the length of the stoichiometric air, and the length of the excess air required for entrainment into the fuel. His predictions, which were validated against experimental measurements, estimated that about four hundred percent of excess air is entrained at the tip of the flame. This percentage of excess air entrainment had also been established by Hawthorne *et al*. (1949). In addition, Steward (1970) and Brzustowski (1973) establish that the visible flame length is subject to errors, which may differ, based on the observer's ability to

spot the exact point above the flame's tip or base, where the indicator is. The measurement may also be affected by the lighting used in the location of the investigation and the luminosity (soot incandescence) of the flame. Brzustowski (1977) presented another definition of the flame's length as the downstream distance between the port of the jet nozzle where the fuel issues and the location where the CO is not traceable in the flame. Similarly, in their investigation of the visible length of turbulent diffusion flames, Becker and Liang (1978) defined the flame tip as the farthest extent in the downstream location of a flame where the visible flame could be visualised. Becker and Liang (1978) employed a time-averaged measurement of the tip of the flame over a short exposure time mode in the camera in their investigation. Ibrahim and El-Mahallawy (1985) distinguished between the visible, thermal and chemical flame lengths, and proposed mathematical expressions for the flame length of a butane flame. They defined the thermal flame height as the location of the maximum temperature measured in the centreline of the flame. The chemical flame height was defined as the location where the concentration of CO_2 was maximum, and the visible flame height was determined by taking an average of a series of photographs and visually observing the flame height against a scale placed near the flame and reading off the height of the flame. A number of flame length correlations have been suggested, based on the buoyancy and the momentum of the flame, which is defined by the Froude number. According to Peters and Göttgens (1991), if the Froude number, $Fr \leq 10^5$, then the flame is a buoyancy-dominated flame, and if the Froude number, $Fr \geq 10^5$, then the flame is a momentum-dominated flame. The influence of buoyancy and momentum in diffusion flames have been investigated by Becker and Liang (1978), where they suggested that momentum-dominated flames are longer than buoyant flames (Heskestad, 1999; Molkov and Saffers, 2012). The effect of buoyancy in flames is obvious when there is a difference in density, at axial locations between the fuel jet's nozzle outlet, and the downstream location of the flame, creating more buoyancy in the flame during combustion (Peters and Göttgens, 1991).

In their investigation, Burke and Schumann (1928) concluded that the length of a flame is proportional to the flow of the fuel. Burke and Schumann's (1928), experimental prediction was supported by the experimental investigations performed by Goudie and Taylor (1951), who showed that the length of city gas flames is

proportional to the fuel flow, for flame lengths which are up to about 90 cm. City gas flames have been found to have compositions that are similar to methane (Thomas, 1963; Brzustowksi, 1973), which implies that it is likely that Goudie and Taylor's (1951), flames are similar to methane flames. However, Lewis and Von Elbe (1951) are of the opinion that this prediction does not apply to all burners with larger jet diameters. Barr (1949, 1953) also shares a similar view with Lewis and Von Elbe (1951) and concludes that this prediction does not apply to every fuel. According to Barr (1953), there have also been theories by Hottel and Hawthorne (1949) and Wohl *et al*. (1949) supporting Burke and Schumann's (1928) flame length estimation. These theories have been proposed based on the assumption that the radial distribution of the air velocity from the jet to the surrounding is even, and that the air velocity is the same as the mean velocity of the fuel, but these assumptions are disputed (Barr, 1953).

A simple correlation of the length of a flame was suggested by Hawthorne *et al*. (1949), which established a relationship between the flame length, jet diameter, and the flow issuing from a jet diffusion flame as follows:

$$h_f \approx \frac{d^2 U}{D} \tag{2.4}$$

In flames that are in the laminar regime, where the mode of the mixing is via molecular diffusion, the diffusion coefficient, *D*, does not depend on the exit diameter and the velocity of the jet. However, according to Lewis and Von Elbe (1987), the flame height is dependent on the volumetric flow rate, $\left(d^2 U\right)$. In turbulent flames, *D*, is the eddy diffusivity, which is the turbulent mixing coefficient, and is a product of the scale and intensity of turbulence, with the same unit as the molecular diffusivity (m^2/s). It is independent of the molecules of the particles of the fluid, but depends on the motion of the microscopic fluid particles. Since the eddy diffusivity scales with the product of the jet exit diameter and the jet's velocity, then a mathematical expression for the height of a turbulent flame may be written as:

$$h_f \approx \frac{d^2 U}{DU} \approx d \tag{2.5}$$

The difference between equation 2.4 and equation 2.5 is that the former is the expression for estimating the flame height in laminar flames, while the latter predicts the flame height in turbulent flames. In addition, the former establishes a relationship between the flame's height and the jet velocity, while the latter establishes a relationship between the flame height and the jet exit diameter.

In a comparison of the formula for estimating the flame length of buoyant flames, Brzustowski (1973) compared his expression of flame length with Putnam and Speich (1963) and established a similarity. The estimated flame length of buoyancy-controlled flames is expressed as:

$$\frac{h_f}{d} = 26\left(\frac{U^2}{gd}\right)^{0.2} \tag{2.6}$$

According to Brzustowski (1973), in a turbulent diffusion flame issuing into still air, the length of a flame may be estimated from this expression:

$$\frac{h_f}{d} = \frac{5.3}{C_{st}}\left\{\frac{T_{FA}}{\alpha_{st} T_t}\left[C_{st} + (1 - C_{st})\frac{MW_a}{MW_f}\right]\right\}^{0.5} \tag{2.7}$$

where in equation 2.7, the constant, 5.3 represents the ratio of the visible flame length to the flame width at the location of stoichiometric entrainment (Hawthorne *et al*., 1949). The value of the constant, which is 5.3 has been proven by Ibrahim and El-Mahallawy (1985), while Gunther (1966) reports it as 5.2, and Baron (1954) reports it as 5.13. For hydrocarbon gases, equation 2.7 may be reduced to Brzustowski (1973):

$$\frac{h_f}{d} \cong \frac{15}{C_{st}}\left(\frac{MW_a}{MW_f}\right)^{0.5} \tag{2.8}$$

For momentum-dominated flames, where the Froude number is very high, the flame height may be expressed as (Brzustowski, 1973):

$$\frac{h_f}{d} = \frac{Y_{f,t}}{0.32}\left(\frac{\rho}{\rho_a}\right)^{0.5}\left[1 + \frac{MW_a}{MW_f}\left(\frac{1}{0.297 C_F} - 1\right)\right] \tag{2.9}$$

while in buoyancy-dominated flames, taking into account the Froude number, Fr_n with combustion, the flame length may be expressed as:

$$\frac{h_f}{d} = 2.96\left(\frac{\rho}{\rho_a}\right)^{0.5} Fr_n{}^{0.2} Y_{f,t}{}^{0.6} \times \left[1 + \frac{MW_a}{MW_f}\left(\frac{1}{0.297C_F} - 1\right)\right]^{0.6} \tag{2.10}$$

where

$$Fr_n = \frac{U^2}{gd}\left(\frac{\rho_a}{\rho}\right)^{0.5} \frac{c_a T_{ab}}{Y_{f,t}\Delta h + c_t(T_t - T_{ab})} \tag{2.11}$$

According to Brzustowsi (1973), for hydrocarbons at conditions where the fuel gas is at ambient temperature, with no diluents or primary air, and C_F is approximately 0.04, then equations 2.9 and equation 2.10 respectively become:

$$\frac{h_f}{d} = \frac{10.5}{C_F}\left(\frac{MW_a}{MW_f}\right)^{0.5} \tag{2.12}$$

and

$$\frac{h_f}{d} = 6.1\left(\frac{U^2}{gd}\right)^{0.2}\left(\frac{1}{C_F}\right)^{0.6}\left(\frac{M_{ca}T_{ab}}{\Delta H_c}\right)^{0.2} \tag{2.13}$$

For full scale flares used in the oil and gas industry, the flame length correlation suggested by Brzustowsi and Sommer (1973,) is widely accepted. It has been quoted in the American Petroleum Institute (API) Standard 521 (2014) pressure-relieving and depressurising systems' publication. This flame length correlation estimates the flame height from the heat release, where the heat release is a product of the fuel flow rate and the low heating value (LHV) of the fuel. The heat release is then correlated on a curve shown in appendix C, to estimate the flame height. However, the flame height correlation does not estimate the lift-off height separately from the flame height, but both the flame height and the lift-off height are estimated as the height of the flare flame. Shore (2006) has performed a regression analysis on the data used in fitting the curve shown in appendix C for the estimation of the flame length and this is expressed as:

$$h_f = \frac{Q^{0.467}}{135} \tag{2.14}$$

The visible flame length of non-premixed turbulent flames has been investigated by Becker and Liang (1978). In their investigation on flame heights, they defined the flame height as the distance between the location of the existence of the visible jet flame and the visible tip of the flame. They established that for jets with a high

Reynolds ratio, this origin is about thrice the effective diameter of the jet in the downstream location of the burner exit. In addition, they suggested a correlation for determining the flame length using the Richardson ratio. The Richardson ratio, like the Reynolds ratio and the Mach ratio are aerodynamic parameters used in determining the rate of entrainment in a jet (Becker and Liang, 1978). This ratio is an expression of the buoyancy of the flame's jet to the jet momentum flux at the jet exit, and is expressed as:

$$Ri_F = \frac{\prod g\rho_a d^3}{4G_o} \tag{2.15}$$

Equation 2.15, which is derived from the expression on entrainment and momentum growth (Becker and Yamazaki, 1977), may be represented non-dimensionally as follows:

$$\xi = \left(\frac{\Pi g\rho_a}{4G_0}\right)^{0.33}.y \tag{2.17}$$

and the non-dimensional flame length correlation becomes:

$$\psi = 0.18 + 0.022\xi \qquad (1 \le \xi \le 20) \text{ and } (\mathrm{Re}_T \ge 8000) \tag{2.18}$$

Becker and Liang (1978) established that buoyancy may be reduced by increasing the Reynolds number, and that buoyancy effects on flame characteristics are of no effect when the non-dimensional parameter, ξ, is less than unity. Becker and Liang (1978) have established a similarity in their expressions for estimating the flame length in the forced convection limit between Hawthorne *et al* (1949) and Gunther (1966). However, Idicheria *et al*. (2004) questioned both the use of the dimensionless parameter by Becker and Liang (1978), and if it is either the unimportance of buoyancy, or an increase in Reynolds number that are the main factors used in characterising the effect of buoyancy in flames. Idicheria *et al*. (2004) observed that there are limitations in the investigations by Becker and Liang (1978), because their investigations were not conducted over broader test conditions, such as for momentum-dominated flames, and that conclusions may only be drawn when these investigations are conducted over broader test conditions, including micro-gravity and normal-gravity conditions.

Similarly, according to Peters and Göttgens (1991), the correlation by Becker and Liang (1978) in equation 2.18 does not capture the flame length for momentum-dominated flames. In this regard, Peters and Göttgens (1991) proposed an expression for the Richardson ratio and the non-dimensional flame length respectively, as follows:

$$\xi = \frac{h_f}{d}\left(\frac{\rho_a}{\rho} Fr\right)^{-0.33} \tag{2.19}$$

and

$$\psi = \left[\frac{46.67\left(\sqrt{\frac{\rho}{\rho_a}}\right)^{0.5}}{\frac{h_f}{d}}\right]^{0.67} \tag{2.20}$$

In addition, although Kalghatgi's investigation of the correlation of the non-dimensional flame length follows closely with Hawthrone *et al*. (1949), Gunther (1966), Becker and Liang (1978), as shown in equation 2.18, however, using different fuels such as hydrogen, methane, propane and ethylene, and different burner diameters, Kalghatgi (1984) proposed another non-dimensional flame length correlation as follows:

$$\psi = 0.2 + 0.024\xi \qquad (2 \le \xi \le 11) \tag{2.21}$$

Kalghatgi (1984) concluded that irrespective of the gaseous fuel used, it is possible to plot the non-dimensional flame length curve for any gaseous fuel on a single curve, according to the correlations expressed by Becker and Liang (1978), for vertically oriented jets issuing into a fluid with uniform density.

For jets in crosswind, from the experimental results of Kalghatgi (1983), he performed a regression analysis on the data he generated, and concluded that the flame length and the angle between the axis of the jet and the direction of the wind are dependent on the ratio of the cross-flow velocity to the jet velocity, and that this may be expressed by a correlation. Therefore, he proposed an empirical correlation for the flame length as:

$$\frac{h_f}{d_s} = \left(\frac{MW_a}{MW_f}\right)^{0.5}\left(6 + \frac{2.35}{R} + 20R\right) \tag{2.22}$$

and the expression for the normalised flame length as:

$$d_b = \left(\frac{MW_a}{MW_f} \right)^{0.5} .d_s \tag{2.23}$$

However, Leahey and Schroeder (1990) and Damiano (1990) observed that the typographical errors reported in equations 2.22 and 2.23 of Kalghatgi's (1983) paper, affected the results of the predictions made by Leahey and Schroeder (1987). Damiano suggested that equations 2.22 and 2.23 be rewritten respectively as expressed in equations 2.24 and 2.25 as follows:

$$\frac{h_f}{d_s} = \left(\frac{MW_f}{MW_a} \right)^{0.5} \left(6 + \frac{2.35}{R} + 20R \right) \tag{2.24}$$

and the correct expression for the normalised flame length as:

$$d_b = \left(\frac{MW_f}{MW_a} \right)^{0.5} .d_s \tag{2.25}$$

In the light of these corrections, Leahey and Schroeder (1987) developed a mathematical expression to predict the flame height of a diffusion jet flame above the jet rim in a crosswind, and compared their experimental results with that of Kalghatgi (1983). Equation 2.26 is developed with the assumption that diffusion flames are momentum-dominated only. The expression developed by Leahey and Schroeder (1987) is as follows:

$$\frac{h_f}{d_s} = \frac{5}{\beta} \left(\frac{1}{RM_{st}} \right)^{0.5} \tag{2.26}$$

where the entrainment parameter, β , is related to R , according to the expression:

$$\beta = 0.4 + 1.2R \tag{2.27}$$

The results of Leahey and Damiano (1987) compare with the expression by Beychok (1979) as shown in equation 2.28. Beychock (1979) generated data from tests conducted on large-scale flares. From his empirical correlations, he performed a regression analysis on his data and estimated the flame length as:

$$h_f = 0.006\, Q^{0.478} \tag{2.28}$$

Equation 2.26 has been found to be applicable to large-scale flares, and is comparable with the estimations predicted using equation 2.28 (Beychok, 1987).

In addition to the correlations proposed by Brzustowksi (1976) and Kalghatgi (1983), their correlations were successful in predicting the flame length for flares with very high jet to crosswind ratios, where the momentum flux ratio, R, is much greater than one. However, according to Majeski *et al*. (2004), full-scale flares in the oil and gas industry operate at momentum flux ratios which are less than, or equal to one. In their investigation of diffusion flames in crosswind with low momentum flux ratio using propane fuel in their investigation, Majeski *et al*. (2004) derived an empirical expression for the length of a flame as:

$$\frac{h_f}{C_F{}^{0.5}} = K_F\left(\rho_t U_t\right)^{0.5}.d + K_t U_\infty \tag{2.29}$$

where:

$$C_F = \frac{\rho V_F}{\rho_t V_t} \tag{2.30}$$

$$K_F = \left(\frac{K_{st}}{4K_p M_o}\right)^{0.5} \tag{2.31}$$

$$K_t = \frac{\partial h_f}{\partial U_\infty} \tag{2.32}$$

$$K_{st} = \frac{M_o}{M_F} \tag{2.33}$$

and K_F is dependent on the gaseous fuel.

Chen and Driscoll (1990) had established that the rate of entrainment and mixing of air affects both the length of a flame and the volume of the flame's reaction zone. Similarly, the length of a flame may be optimised either by increasing or decreasing the fuel jet diameter, regulating the non-premixed coaxial air to the fuel jet, or by regulating the premixed air or inerts fed into the fuel stream (Driscoll, *et al*., 1992), depending on the results to be achieved. When coaxial air is added to the flame, the amount of ambient air originally required to be entrained downstream to dilute the fuel to a stoichiometric ratio is reduced, causing a reduction in the length of the flame (Feikema *et al.*, 1991; US EPA, 2012). A correlation showing

the relationship between the flame length and coaxial air is as follows (Chen and Driscoll, 1990):

$$\frac{h_f}{d} = \frac{\left[15\left(1+R_{st}^{-1}\right)\left(\frac{\rho}{\rho_a}\right)^{0.5}\right]}{\left[1+\frac{\rho_a U_a{}^2\left(d_a{}^2-d_o{}^2\right)}{\rho U^2 d^2}\right]^{0.5}} \tag{2.34}$$

where the numerator of equation 2.34 represents the normalised flame length of a jet flame, which has a value of 200 for methane / air flames (Dahm and Mayman, 1990).

2.3 REVIEW OF FLAME LIFT-OFF

For any given air velocity, there is an optimal fuel velocity required to keep a flame stable. Increasing the air / fuel jet velocity, or adding diluents to the air or fuel stream beyond this optimal value, causes the flame to become unstable and lift-off or blow out. A flame lift-off occurs when a flame detaches from its initially attached issuing jet stream and becomes suspended above the issuing jet nozzle. In some cases, the flame lifts and becomes suspended independently without any physical medium aiding the suspension, while in other cases, the flame lifts and stabilises with the aid of a medium, e.g., flame holder, fuel jet rim, etc. Beyond an optimal condition, the flame lifts and even blows out. The lifting of the flame above the burner port causes the flame to stabilise at a downstream location above this burner port. An interaction between the shear zone and the flame zone leads to an intermittency in the flame's behaviour (Chen *et al*., 1992), which may be due to the thermochemical properties of the fuel and the co-flowing oxidiser, and occurs at the flame base, at radial locations where combustion occurs (Pitts, 1988). Some of the factors responsible for lift-off are an increase in the fuel jet velocity, an increase in the co-axial air, an increase in co-flow air, size of issuing jet diameter, Froude number, the mole fraction of diluents injected into the fuel or air stream, or a combination of these factors (Palacios *et al*., 2009). Although the flame lift-off may lead to an extinguishment of the flame (US OAQPS, 2012), flame lift-off aids in preserving the flare tip, by minimising or avoiding the contact of the flame with the nozzle, in order to reduce the damage to the flare tip. The difference between a blow-off and a blow-out is that a blow-off occurs when an increase in the inlet

velocity of the fuel causes the extinguishing of the flame before lift-off occurs, while a blow-out occurs when a further increase in the velocity of a lifted flame causes the flame to be extinguished The theory of lift-off has been investigated by several researchers over the decades, namely: Scholefield and Garside (1949); Wohl *et al*. (1949); Philips (1965); Vanquickenborne and Van Tiggelen (1966); Peters (1983); Peters and Williams (1983); Broadwell *et al*. (1984); Eickhoff *et al*. (1984); Kalghatgi (1984); Gollahalli *et al*. (1986); Miake-Lye and Hammer (1988); Pitts (1988); Coats (1996); Dold (1988); Dahm and Mayman (1990); Veynante *et al*. (1994); Ruetsch *et al*. (1995); Buckmaster (1996); Buckmaster (2002); Boulanger *et al*. (2003); Upatniek *et al*. (2004); Iyogun and Birouk (2008); amongst others. Most of these investigators studied flame lift-off from jets issuing from cylindrical (axisymmetric) burner nozzles, while few of these investigators studied the effect of lift-off from jet flames issuing from non-cylindrical (asymmetric) burner nozzles. It was concluded that the geometry of the nozzle affects the degree of mixing and the flame stability (Iyogun and Birouk, 2008). Different theories have been suggested which have attempted to explain the concept of a flame lift-off. Based on suggestions by various investigators, these theories are summarised:

The premixed flame theory, which was proposed by Wohl *et al*. (1949), and then adopted by VanQuickenborne and Van Tiggelen (1966), and Eickhoff *et al*. (1984). These investigators argue that the flame base of a lifted flame is a form of a pre-mixed flame, This is because the stabilisation ring observed in a flame which is stabilised above the jet exit is at a region in the flame where the entrained air is enhanced, in order to support premixing, and flame stabilization is attained at a location of complete premixing of fuel and air. Similarly, the premixing at the flame base is due to the lift-off which leads to mixing at the upstream location of the flame which leads to a partial-premixing at the base of the flame (Lock, 2007). However, this theory is applicable mostly in premixed flames, because it does not capture the turbulence observed in large-scale diffusion flames.

The laminar flamelet model, according to Peters (1983), and Peters and Williams (1983), suggest that flame stabilisation does not occur at any upstream location in the combustion zone where there is a significant molecular premixing of fuel and air. They concluded that the lift-off height of a flame may be predicted using the flamelet description, and that flame extinction best describes the theory of

lift-off, which they later modified by the introduction of the partially-premixed laminar flamelets concept. However, at that same location, a significant amount of mixing of fuel and air has been reported (Eickhoff *et al*., 1985; Sobiesiak and Brzustowski, 1984; 1986). Similarly, it has also been argued (Pitts, 1988) that theories based on laminar flamelet are inadequate in describing flame stability and that this model does not account for the partial-pre-mixing of the fuel and the oxidiser at an upstream location of the flame.

Byggstoyl and Magnussen (1983) also proposed that lift-off is determined by the premixed flame characteristics of the jet which is caused by extinction due to a stretch in the smallest vortices of the flow. Their small-scale and large-scale experimental data are in agreement with the investigations of McCaffrey and Evans (1986) and Pitts (1988).

The triple-flame concept (Phillips, 1965), also called the edge-flame concept, which assumes that at the edge (Lyons *et al*., 2005) of the base of a flame stabilised above the burner nozzle, three flame types may be observed, which are the lean-premixed, and the rich-premixed flame front, and a diffusion flame (Buckmaster and Weber, 1996; Buckmaster, 2002), implying that the base of a flame which is stabilised above the burner port could be described as being partially-premixed. Other theories are the theory on the flame's turbulence intensity which was put forward by Kalghatgi (1984), which suggests that the propagation of the flame at the reaction zone is mainly impacted by the turbulent burning velocity of the flame. Using different fuels and nozzle dimensions, Kalghatgi (1984) concluded that there was no effect of the fuel jet diameter of the nozzle outlet on the lift-off height of a flame, but that the height of the flame which is stabilised above the burner nozzle scales directly with the fuel's jet velocity, and scales inversely with the square of the laminar burning-velocity. However, RØkke *et al.* (1994) show an enhanced flame lift-off height for jet nozzles with smaller outlet diameters, at the same velocity, which disagrees with the conclusion of Kalghatgi (1984) on the independence of the fuel jet outlet diameter on flame lift-off. Similarly, a large-scale structural-mixing theory has been proposed by Broadwell *et al*. (1984), and Miake-Lye and Hammer (1989), which suggests that it is the presence of large eddies at the "leading-edge" of a flame which is stabilised above the jet nozzle that causes the flame to be suspended at the reaction zone. Despite the fact that investigations on the theory of

lift-off has been carried out both theoretically and experimentally, however, disagreements still exist on which theory best describes the physical process of flame stabilisation. These may be caused by the differences in the definition of where a flame lift-off starts (Chen and Goss, 1991), or the different test conditions utilised in the previous investigations, such as the investigations, which are made in small-scale flames being used to draw conclusions on large-scale flames. Similarly, the geometry of a nozzle has been known to affect flame stability, where for example, it has been established that asymmetric nozzles, especially elliptic nozzles (Gollahalli, 1998) enhance the entrainment of air into a flame, which causes a more uniform mixing and stability (Iyogun and Bioruk, 2008). These differences cause a limitation in the characterisation of the mechanism of flame lifting. Based on the theories of flame lift-off, different investigators have proposed different experimental and theoretical expressions for estimating flame lift-off.

Kalghatgi (1984) proposed a non-dimensional relationship between the lift-off height and fuel jet velocity. He suggested that for a pure fuel discharging from a jet nozzle, the lift-off height of the flame is proportional to the jet velocity, when the lift-off height is about $10d$ and it may be expressed as:

$$\frac{h_l}{d^*} = \tau_C \frac{U_t}{d^*} \tag{2.35}$$

When there are smaller dilutions of fuel, where $Y_{o,f} \approx 1$, then according to Miake-Lye and Hammer (1989):

$$\frac{h_l}{U_t} \alpha \frac{1}{Y_{o,f}} \tag{2.36}$$

Hence, equation 2.35 may be re-written as:

$$\frac{h_l}{d^*} = \tau_C \frac{U_t}{d^*} \frac{Y_{st}}{Y_{o,f}} \tag{2.37}$$

The experiments performed by SØnju and Hustad (1984), with methane and propane flames indicate that for subsonic conditions, the normalised flame lift-off height may be expressed in terms of the outlet velocity of the fuel jet and the jet exit diameter and is expressed as:

$$\frac{h_l}{d} = c \frac{U_t}{d} \tag{2.38}$$

Equation 2.38 is in agreement with the experiments performed by Peters and Wiliams (1983). SØnju and Hustad (1984) concluded that the lift-off height is independent of the nozzle diameter. This has been supported by the investigations performed by Santos and Costa (2005), and Kiran and Mishra (2007). However, RØkke *et al.* (1994), and several other researchers (Broadwell *et al*., 1984; Lee *et al*., 1994; etc.) concluded that the lift-off height is dependent on the fuel jet exit diameter. Based on these investigations, Palacios *et al*. (2009) developed a relationship between the lift-off height and the jet exit Reynolds number for propane flames in sonic and sub-sonic flows and is expressed as:

$$h_l = 6 \times 10^{-4} . \mathrm{Re}^{0.5} \tag{2.39}$$

A linear relationship between the liftoff height and the jet velocity of methane and propane flames, respectively, has been established by Chen *et al*. (1992), and is given by:

$$h_l = 2.61 U_t - 28.45 \tag{2.40}$$

and $$h_l = 2.5 U_t - 21.74 \tag{2.41}$$

where h_l is the flame height in mm, and U_t is the jet velocity, in m/s.

As an extension of previous investigations on the development of correlations for the prediction of lift-off heights, RØkke *et al.* (1994) proposed a correlation for the flame lift-off height for partially-premixed unconfined propane flames. This correlation was tested with experimental data and found to be in agreement with the investigations of Donnerhack and Peters (1984), and is expressed as follows:

$$\frac{h_l}{d} = 1.2 \times 10^{-2} U_t d_{eff}^{\ -0.7} \left(\frac{1}{Y_{f,t}} \right)^{0.5} \tag{2.42}$$

The investigations performed by Cha and Chung (1996) on the lift-off height of non-premixed propane flames indicate that there is a difference between the lift-off behaviour of confined and unconfined jet flames. They concluded that the lift-off height of confined jet flames vary linearly with the jet nozzle diameter and jet velocity, while the lift-off height of free jet flames does not depend on the dimension of the fuel jet nozzle's exit. They proposed correlations for estimating the lift-off of jet flames for both confined and unconfined, cases, respectively, as follows:

$$\frac{h_l}{d} = U_t\left(1.02 + \frac{0.0976}{d_c}\right) \tag{2.43}$$

and for the unconfined case:

$$h_l = 0.002245U_t - 0.01663 \tag{2.44}$$

In their investigation of flame lift-off in Liquefied Petroleum Gas (LPG) jet diffusion flames, Kiran and Mishra concluded that there is a linear relationship which exists between the flame's lift-off height and the jet velocity, and that a relationship also exists between the normalised lift-off height and the global strain-rate, which agrees with the predictions of Santos and Costa (2005), and is expressed as:

$$\frac{h_l}{d} = 1.8\times10^{-3}\left(\frac{U_t}{d}\right) \tag{2.45}$$

In summary, based on the theories of flame lift-off discussed by different investigators, the expression of the flame lift-off is tabulated in Table 2.1 as follows (RØkke *et al.*,1994):

Investigators	**Lift-off Estimation**
Peters and Williams (1983)	$\frac{h_l}{d} = 3.6\times10^{-3}.\left(\frac{U_t}{d}\right)$
Byggstoyl (1984)	$U_t = \left[\frac{0.35K_o}{\left(\frac{d_{eff}}{h_l}\right)^3 \frac{\tau_x{}^2}{h_l}\left(\frac{h_l X_{st}}{d_{eff}}\right)^{2.85} \ln\left(\frac{4.54d_{eff}}{X_{st}h_l}\right)}\right]^{0.33}$
Kalghatgi (1984)	$h_l = 50\frac{\mu_k}{U_b{}^2}(\bar{\rho})^{1.5}U_t$
Miake-Lye and Hammer (1988)	$h_l = 14\frac{k}{U_b{}^2}\frac{\bar{\xi}_{st}}{\bar{Y}_f}U_t$

Table 2.1 Comparison of the prediction of flame lift-off from the theories of lift-off.

Hammer (1990) made a comparison of the theories of lift-off, where the lift-off height, and the blow-out predictions for different fuels were examined. It was concluded that these stability theories accurately predict the experimentally-

observed dependence of the time-averaged lift-off height on the jet exit velocity, and that it is difficult to tell which of these theories is more reliable over the other. Pohl and Soelberg (1986) have identified several factors affecting flame stability, which amongst others are the fuel jet exit velocity, the fuel heating value, the fuel composition, the amount of air or steam used to suppress soot in smoky flares, etc. Similarly, a relationship between flame stability and flare efficiency had been established by Pohl *et al*. (1986), who, in their investigation of pilot-scale flares concluded that a combustion efficiency of about, or greater than 98 % may be achieved in stable flames, and that even a slight change in the stability of a flame may affect a flame's combustion efficiency and emissions. A discussion of pollutant emissions will be discussed in the next section.

2.4 COMBUSTION-GENERATED POLLUTANTS

In the combustion of fossil fuels, pollutant species are emitted. The type of species emitted and their emission levels depend on the condition of the combustion process taking place in the combustion device (US EPA). These pollutants which may / may not be formed as an intrinsic part of the combustion process are particulates, which include aerosols, organic compounds, which include partially-burned and unburned hydrocarbons, sulphur oxides, nitrogen oxides, carbon monoxide, and soot. Some of these pollutants are discussed briefly as follows:

2.4.1 CARBON MONOXIDE AND CARBON DIOXIDE

Carbon monoxide (CO) is an intermediate product pollutant species formed due to an incomplete combustion of carbon-containing fuels. The quenching of oxidation reaction of hydrocarbons by dilution air may cause in-complete combustion. High levels of CO in a combustion process are an indication of a loss in the operating efficiency of the combustion system (Amato *et al*., 2011), which leads to a higher fuel and energy cost for the same output of energy. However, with favourable conditions of temperature and mixing, CO reacts with O_2 to yield CO_2, and in the oxidation of methane at high temperature, the following rapid reactions lead to the formation of CO (Bowman, 1975):

$$CH_3 + O \rightarrow HCHO + H \qquad \text{(R2.4.1.1)}$$

$$HCHO + M \rightarrow CHO + H \qquad \text{(R2.4.1.2)}$$

$$HCHO + OH \rightarrow CHO + H_2O \quad \text{(R2.4.1.3)}$$

$$CHO + M \rightarrow CO + H \quad \text{(R2.4.1.4)}$$

$$CHO + OH \rightarrow CO + H_2O \quad \text{(R2.4.1.5)}$$

Lower levels of CO have been recorded in the exhaust and in the post-flame regions of flames than those measured in-flame. This is because of the rate of conversion of CO to CO_2, which is due to the reaction between CO and OH to yield CO_2, and is thought to be the primary reaction in hydro-carbon flames, thus:

$$CO + OH \leftrightarrow CO_2 + H \quad \text{(R2.4.1.6)}$$

The rate of reaction in R2.4.1.6 is independent of temperature below 1000K, but at temperatures up to, and exceeding 1500K, the rate of reaction significantly depends on temperature (Bowman, 1975). The oxidation of CO to CO_2 may also occur via the following reactions:

$$CO + HO_2 \leftrightarrow CO_2 + OH \quad \text{(R2.4.1.7)}$$

$$CO + O_2 \rightarrow CO_2 + O \quad \text{(R2.4.1.8)}$$

However, the oxidation of CO in reaction R2.4.1.7 has been reported to be significant at temperatures exceeding 1600K, while reaction R2.4.1.8 has been found to be very slow in comparison with reactions R2.4.1.6 and R2.4.1.7, and may not be a significant reaction route in hydrocarbon flames, which have been known to have a large amount of OH radical concentrations (Bowman, 1975).

2.4.2 NITROGEN OXIDES

Nitrogen oxides are compounds, which are formed from the reaction of nitrogen and oxygen. In environmental applications, the commonest oxides of nitrogen considered are nitric oxide (NO) and nitrogen dioxide (NO_2), which are most-acceptably referred to as NOx ($NO+NO_2$). Nitrous oxides (N_2O) also exist, but are not the focus of this investigation. In hydrocarbon jet flames, the contribution of NO in NOx is about 80% and above, while the remaining is NO_2 (Namazian *et al*., 1994), whereas in gas turbine power plants, the fraction of NOx that is NO_2 is higher than that which is NO- contributing about 80% (Hayhurst and Vince, 1980; Bowman, 1992). Similarly, in the post-flame region, the percentage of NOx that is NO_2 ranges from about 7% - 40% (Turns and Lovett, 1989), and the peak

concentration of NO_2 has been found to be at the downstream regions of the flame, and at post-flame locations where rapid cooling or dilution occurs, which coincide with the locations where the radicals which are formed in the peak-temperature region of the flame are rapidly cooled (Gollahalli, 1977; Homma And Chen, 2000). NO_2 has often been neglected in combustion processes (Zhuang and Leuckel, 1998) because of its relatively low concentrations which are found in traceable quantities in hydrocarbon flames (Liu *et al*., 2001), yet NO_2 is more toxic than NO (Homma and Chen, 2000), and NO is ultimately converted to NO_2 in the atmosphere (Driscoll, *et al*., 1992; Turns *et al*., 1993), which is why as a convention, the emission index of NOx is usually calculated using the molecular weight of NO_2, and NOx emission regulations are reported as NO_2 equivalent.

NO_2 formation occurs mainly via the oxidation of NO with HO_2 radical in the flame zone at short residence times via the reaction (Merryman and Levy, 1974; Hori, 1986):

$$NO + HO_2 \rightarrow NO_2 + OH \qquad \text{(R2.4.2.1)}$$

NO_2 may also be formed via the reaction of NO with other radicals such as O_2, O, and OH in the flame zone in a combustion system (Glarborg and Hadvig, 1991; Hanson and Salimian, 1998). The NO-NO_2 conversion is most effective at low temperatures, and are promoted by the type of fuel which could easily be decomposed to yield high HO_2 radical species, with propane being the most effective of the C_1-C_3 hydrocarbons at a low temperature ranging from 700K and above, ethylene – 800K and above, while in methane flames, the effectiveness is from 1000K and above (Marinov *et al*., 1998).

NOx may be produced either by natural mechanisms, which involve the action of bacteria in the soil, volcanic eruptions, etc., or by human activities, which involve combustion. In combustion processes, the predominant oxide of nitrogen is NO (Bowman, 1975), and its formation is via three primary routes, namely: thermal NO, prompt NO, and fuel NO. A brief discussion of these routes are presented as follows:

2.4.2.1 THERMAL NO MECHANISM

The thermal NO formation route via the extended Zeldovich mechanism which is mostly predominant during the combustion of natural gas, is formed via the

oxidation of the atmospheric nitrogen at high temperatures. The NO formation rate is highly dependent on the flame temperature and on the residence time of nitrogen at that peak temperature. This high temperature dependence on the rate of formation of NO is due to the large activation energy required to break the nitrogen bond, and is effective at temperatures above 1800^{o}C, where the molecular nitrogen and the oxygen that are present in the combustion air dissociate and react with each other to form NO. This reaction may occur via the following routes:

$$N_2 + O \leftrightarrow NO + N \qquad \text{(R2.4.2.2)}$$

$$N + O_2 \leftrightarrow NO + O \qquad \text{(R2.4.2.3)}$$

$$N + OH \leftrightarrow NO + H \qquad \text{(R2.4.2.4)}$$

Reaction (R2.4.2.2) has been found to be the rate-controlling step in the formation of NO in post-flame gases, because of its high activation energy. However, the activation energy required for the oxidative action on nitrogen atoms in reaction (R2.4.2.3) is minimal, which leads to a very weak dependence on the oxygen concentration. This implies that in a fuel-lean (oxygen-rich) flame, the formation rate of the free nitrogen atoms equals the rate of consumption, assuming a quasi-steady-state concentration of the nitrogen atom. Similarly, the reaction of atomic nitrogen with the OH radical in fuel-rich mixtures, when $OH>>H>O$, is another route for the formation of thermal NO as shown in reaction R2.4.2.4. The Zeldovich mechanism is dependent on the peak flame temperature, but independent on the fuel-type (Pourkashanian *et al*., 1990).

2.4.2.2 PROMPT NO MECHANISM

The formation of the NO via the prompt mechanism involves the reaction of atmospheric nitrogen with radical species, such as C, CH, CH_2, C_2, C_2H, etc., which are derived from the fuel at regions of low temperature in the flame, and at shorter residence times (Hayhurst and Vince, 1980). These radicals must contain carbon in order to form the prompt NO (Baukal, 2001), and the total prompt NO present in the fuel is approximately equal to the number of the carbon atoms present in each molecule of the hydrocarbon fuel (Pourkashanian *et al*., 1990). The CH and CH_2 radicals are the major contributors which react to form the prompt NO according to the following reactions:

$$CH + N_2 \leftrightarrow HCN + N \quad \text{(R2.4.2.5)}$$

$$CH_2 + N_2 \leftrightarrow HCN + NH \quad \text{(R2.4.2.6)}$$

The products of these reactions yield amine- and cyano-compounds, which may further undergo an oxidation reaction to form NO (Hayhurst and McClean, 1974) via the route:

$$HCN \rightarrow CN \rightarrow NH \rightarrow N \rightarrow NO \quad \text{(R2.4.2.7)}$$

Prompt NO are more prominent in fuel-rich than in fuel-lean flames, and are weakly dependent on the flame temperature (Hayhurst and Vince, 1980).

2.4.2.3 FUEL NO MECHANISM

Fuel NO are formed when chemically-bound organic compounds containing nitrogen are oxidised. In the combustion process, the nitrogen that is present in the fuel is released as a free radical-species which is finally then converted to NO. The conversion of nitrogen to NO are higher in fuel-lean flames, and are dependent on the combustion environment i.e. flame temperature and stoichiometry (Bowman, 1992). Methane flames do not contain a significant fuel-bound nitrogen (Annamalai and Puri, 2007), and hence, it is not significant in this study.

2.5 SOOT EMISSION

Soot which is comprised of Black Carbon (BC) and Organic Carbon (OC) is a pollutant that absorbs the light that is emitted when an in-complete combustion occurs in automobiles, such as in diesel engines. This incomplete combustion may also occur during gas flaring, and when fuels such as bio-fuels, bio-mass, fossil fuels, etc., are burned (US EPA, 2012). Soot may either be termed “elemental”, “graphitic” or “black carbon”, and its composition consist of organic compounds. Elemental carbon is used to denote the thermal and wet chemical properties, while graphitic carbon consists of “micro-crystalline structures” which have the form of graphites, as has been suggested by Rosen and Novakov (1977). BC denotes both the graphitic and the elemental components of soot (Novakov, 1984; Arctic Council Task Force, 2011; and Bond *et al*. 2013). The composition of soot is mainly carbon and about 10% hydrogen (Santos *et al*., 2011), and a molecular formula of C_8H has been proposed for soot (Palmer and Cullis, 1965). Other than CO_2, soot has been suggested as the main source of global warming (Bond *et al*., 2013). This warmth is

thought to be about twice the previous estimations that have been reported by the IPCC (2007). Rissler *et al*. (2012) suggest that because of the small size of the particles which are produced from diesel engines, more than about 50% of the particles of soot are inhaled and are accumulated in the lungs, which leads to health challenges and death (Miller *et al*., 2007). In flares, the sooting propensity depends on the composition of the fuel (Seinfeld and Pandis, 2006), and on the amount and distribution of air in the combustion zone. The characteristics of the fuel which influences the formation of soot are the carbon-to-hydrogen ratio, and the molecular structure of the fuel to be combusted, with the branched-chain paraffins having a higher sooting propensity than the normal isomers. This implies that the greater the branches in the chain, the higher the sooting propensity (USEPA). In flares, primary and secondary air is supplied to the flame to aid combustion. The primary air is premixed with the flame, while the secondary air is entrained into the flame (USEPA). If the air supply to the flame is insufficient, then the gas supply to the flame base becomes preheated by the combustion zone, causing larger hydrocarbonsto crack and form unsaturated hydrocarbons, hydrogen and carbon particles. If these particles escape further combustion, they cool down and form soot, which escapes at downstream locations of the flame (Bento *et al*., 2006), while the unsaturated hydrocarbons polymerise to former larger molecules, which may also crack and form carbon particles, and the process continues.

Figure 2.4 Photograph of an automobile emitting soot (US EPA, 2008).

The luminous orange colour which is observed in flames during gas flaring and the black plumes which are observed in the exhaust of diesel engines are an indication of soot in those combustion systems. BC is the greatest light-absorbing constituent of particle matter (PM) that is emitted in the atmosphere to produce the $PM_{2.5}$ particles, and accounts for about half of the warming recorded in arctic regions. The dark colour of soot is caused by the dark colour of the BC (Arctic Council Task Force, 2011), and these absorbing properties are accountable for absorbing the visible light (Yasa *et al*., 1979; Rosen *et al*., 1980). The action of BC in the atmosphere is due to the interaction of BC with the cloud where the BC absorbs the radiation from the sun, and emits it in the form of heat, where the heat then leads to a reduction in the reflectivity of the snow and the ice due to the absorption of the BC by the snow and the ice (USEPA, 2012; IGSD, 2012). The Arctic Council Task Force (2011) reports that the flaring of gas yields a significant amount of soot, with a high degree of uncertainty in quantifying these emissions. This uncertainty is because the composition of soot and other pollutants from other sources that are present in the emission measurement sample makes it difficult to measure soot emissions accurately, thereby limiting and / or compromising the integrity of any reliable data that is generated from the emissions-monitoring locations. Secondly, this difficulty is also due to the fact that flare plumes cannot be controlled, because of the effect of the changes in crosswind directions, crosswind velocities, and other meteorological variables which vary significantly in unenclosed flare systems, thus driving the flare plumes at different directions, thereby making measurements difficult to make. Bond *et al*. (2007) suggest that if the estimates of the volume of the gas flared is about 139 bcm, and that if an emission factor of about 0.5 kilogramme of soot per 103 cubic meter is used to estimate the soot emission from the flaring of gas, then the soot that is emitted from the flaring of gas is about 71 Gg, which represents about 1.6% of BC emissions from energy-related sources of combustion, globally. This implies that the reduction of BC emissions is about the best strategy in the reduction of global-warming.

2.6 REVIEW OF SOOT

Several authors (Dobbins and Subramaniasivam, 1994; Köylü *et al*., 1995; Richter and Howard, 2000; and Stanmore *et al*., 2000) suggest that the primary particles of soot are of various sizes which range from about 10 nm - 50 nm or

larger (Palmer and Cullis, 1965; Dobbins and Subramaniasivam, 1994) due to the fuel-type (Glassman, 1988; Mansurov 2005; Shaddix and Smyth, 1996; Dombrovsky, 2010), or due to the processes taking place in the combustor. Harris and Maricq (2011) suggest that the particles of soot are distinctive from other aerosols, and even the size of the particles of soot produced from the burning of biomass is different from those produced from other fuels (Bond *et al*., 2013). For instance, the size of the primary particles of soot emitted from diesel engines varies between 10 nm and 70 nm (Gimenes, 2006), while the size of the primary particles in a pre-mixed methane flame varies between 3 nm and 10 nm. Also, the particulates in methane flames are the least in comparison with other gaseous fuels, when compared under similar test conditions in the flame (D'Anna *et al*., 2008). Similarly, the particles' morphology are different under conditions of microgravity and in normal gravity (Manzello and Choi, 2002). Also, Bohm *et al*. (1988) suggest that the soot particles which are formed in the high-temperature regions of the flame are different from those formed in low temperature flames, which is opposed to the consensus that soot is formed in high flame temperatures only. This has been confirmed by Clague *et al*. (1999) who suggest that the particles formed in a flame are different from those formed in gas-exhaust systems, and it is due to both the physical and the chemical properties of the soot particle (D'Alessio *et al*., 2005). Figure 2.5 shows the TEM image of soot from a diffusion flame.

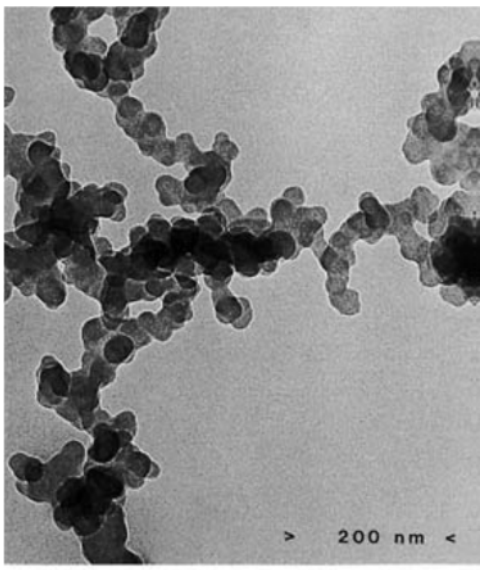

Figure 2.5 Photograph of soot particles from a non-premixed flame (Dobbins and Subramaniasivam, 1994).

In characterising soot particles, several parameters are investigated which include: the number density of the soot particle, soot volume fraction, particle size distribution, surface area of the aggregate, and the composition of the particle, the KL factor and the flame temperature (Gimenes, 2006; Smallwood, 2008). However, Karatas and Gülder (2012) suggest that the major parameters to be investigated include the volume fraction of the particle, and the morphology of the particles, which consist of the particle diameter of the primary particle, the aggregate size, mobility diameter, the aerodynamic diameter, the Feret diameter, etc. This is because these parameters assist in developing and accurately predicting radiation models. However, the particle size is considered to be of the utmost importance to be investigated, because of its health consequences, although most of the emissions regulations pay more attention to the soot volume fraction (Gimenes, 2006).

2.7 REVIEW OF SOOT FORMATION AND OXIDATION

From the extensive studies on the processes of the formation of soot to its oxidation, it has been agreed that there are challenges in fully understanding soot formation processes (Leung *et al*., 1991; Santos *et al*., 2011). This is caused by the quick steps involved in soot formation, which limits the feasibility of observing this formation at each step in detail, as it occurs. Even in turbulent diffusion flames, there is no clear-marked distinction between each of these steps (Puri, 1993; Stasio, 2001). This is due to the very short residence times (usually a few milliseconds) involved in the formation of soot, and also due to the flame's intermittency (Bento *et al*., 2006). This is because the turbulence in the flame increases the intermittency of the soot field in the flame (Lee *et al*., 2009), and this intermittency leads to an increase in the random spatial distribution of the precursors of soot and their particles, thereby limiting an accurate step-wise observation of soot formation processes. Nevertheless, the consensus is that the formation of soot starts with the formation of soot precursors (Wagner, 1979), which are acetylene and Polycyclic Aromatic Hydrocarbons (PAHs). Other precursors which include: coronene (Bockhorn *et al*., 1983), polyynes, fullerenes, pyrene (Colket and Seery, 1994; Mukherjee *et al*., 1994; Schuetz and Frenklach, 2002; Skjøth-Rasmusses *et al*., 2004), etc., have been suggested. The schematic of the process of soot formation is shown in figure 2.6 The fluorescence in flames have been suggested to be due to the PAHs that are present in the flame (Zhang *et al*., 1992), and these PAHs are a

"bridge" between the fuel species and the soot (Karatas and Gülder, 2012), and the PAHs have a chemical structure that is almost as identical as soot (Shukla *et al*., 2007).

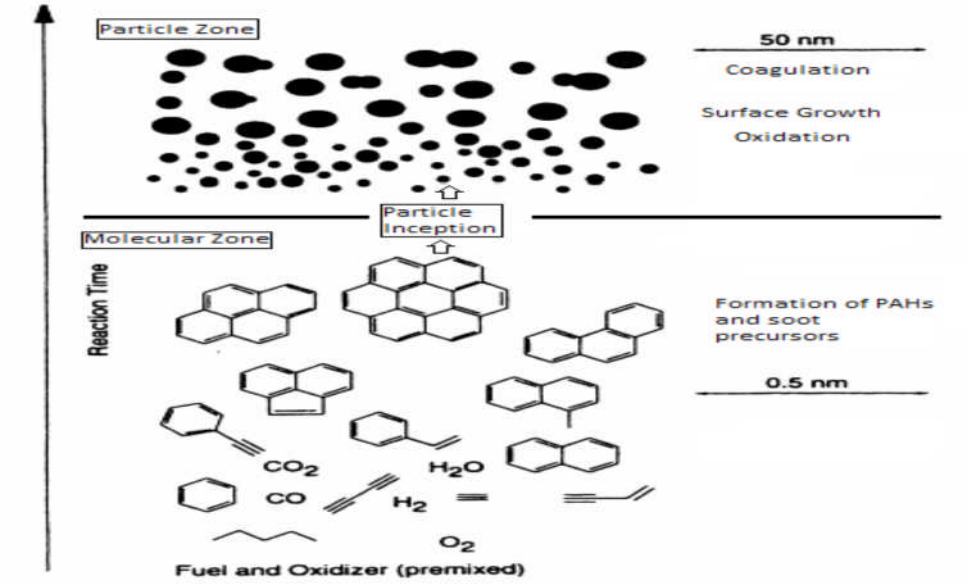

Figure 2.6 Schematic of the soot formation in a premixed flame (Bockhorn, 1994).

In addition, it has been suggested that these PAHs are formed mainly under fuel-rich conditions and regions in the flame (Mansurov, 2005; Dombrovsky, 2010). Soot formation begins with the formation of the precursor species, soot inception, soot surface growth and coagulation, and oxidation (Townend,1927; Rummel and Veh, 1941; Thomas,1962; Haynes and Wagner,1981; Wagner, 1979; Howard and Longwell, 1983; Howard and Bittner, 1983; Homann,1984; Glassman,1988; Fairweather *et al*., 1992; Turns, 1996; Wen *et al*., 2003). The schematic of the processes of soot formation to soot oxidation is shown in figure 2.7. During soot particle inception, there is a formation of particle-like structures when the fuel undergoes a thermal decomposition (pyrolysis), where the molecules of the fuel are conglomerated (Haynes and Wagner, 1981) during combustion, thereafter leading to the formation of the precursor species, which coagulate and lead to the formation of the PAH species (Shukla, 2007). A further growth of these PAH species lead to coagulation and the formation of primary particles. As the primary particles grow, they coagulate and form large aggregates which are called the soot particle. The soot particle has been suggested to contribute up to about 75% of the weight of the primary particle (Richter *et al*., 2004). During surface growth, the size of the primary particle increases when there is an heterogeneous chemical reaction with the gaseous species, which occurs at the particle's surface (Harris and Weiner,

1983), where about 95% of the soot is formed (Harris *et al*., 1986a; Mauss *et al*., 1994a).

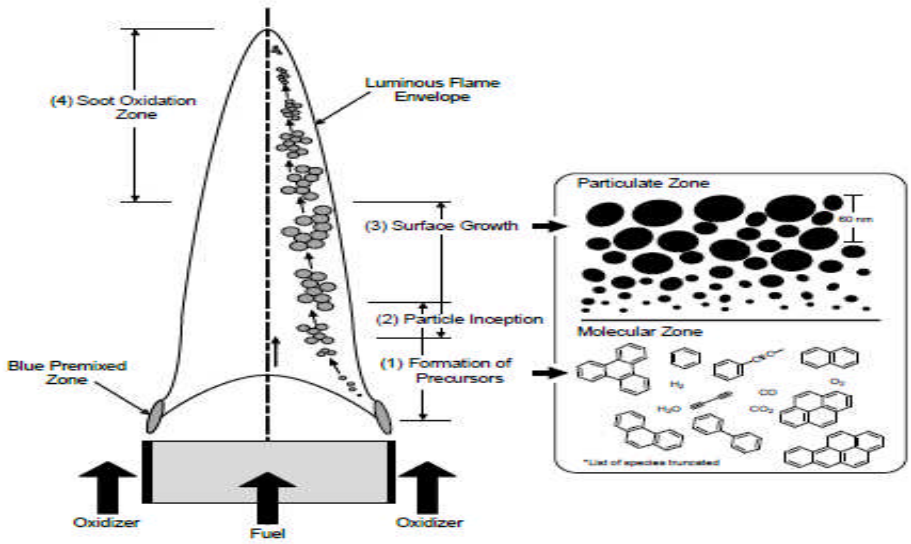

Figure 2.7 Schematic of the mechanism of soot formation and oxidation (Intasopa, 2011).

Also, the surface growth mechanism is responsible for the amount of the mass of the soot particle in the flame (Macadam *et al*., 1996). During growth by coagulation, the smaller particles collide and merge into larger-sized particles (Mansurov, 2005), and form spherical or near-spherical structures, and chain-like aggregates (Frenklach, 2002), where the aggregates consist of about 30 primary particles (Megaridis and Dobbins, 1988). Similarly, the number density of the particle reduces during the aggregation process, which leads to the increase in the size of the particle. The formation of soot is promoted at regions of high flame temperature that is within the range of between about 1200 K and about 1800 K (Coppalle and Joyeux, 1994; Lee *et al*., 2009). These high temperatures promote the reactivity and the collision of the particles, which promote growth by coalescence. However, not all particle collisions yield coalescence (Kellerer *et al*., 2000), and this may be due to non-optimal flame conditions (Bohm *et al*., 1988), such as lower flame temperatures due to the effect of dilution of the fuel stream, which leads to lesser collision and reactivity and hence lesser particle coalescence. Although these high temperatures promote coalescence due to collision and reactivity, these high temperatures also promote the oxidation of the soot particles at the oxidation zone. When the temperature is less than about 1300K, the rate of oxidation of the soot particles becomes too slow to oxidise the mature soot particles, and thus smoke will

be emitted (Kent and Wagner, 1984). This oxidation rate depends not only on the flame temperature, but also on the soot's surface area, which is susceptible to the attack of the oxidative radical species, and on the radical species themselves, such as the O atoms (Fenimore and Jones, 1967), CO_2 (Garo *et al*., 1990), O_2, and OH radicals (Warnatz, 2006), H_2O and NO_2, (Stanmore *et al*., 2001), etc. However, the main radical species that are responsible for the soot oxidation are the O_2 and OH radicals (Lee *et al*, 1962; Walls and Strickland-Constable, 1964; Fenimore and Jones, 1967; Neoh *et al*., 1984).

2.8 LIMITATIONS IN THE INVESTIGATION OF SOOT AND POLLUTANT EMISSIONS IN TURBULENT METHANE / AIR FLAMES

Investigations of soot in laminar and turbulent diffusion flames is documented for propane fuels (Vandsburger, *et al*., 1984; Shaddix and Smyth, 1996; Decroix and Roberts, 2000; Bento *et al*., 2006;), ethane fuels (Glassman and Yacarino, 1981; Intasopa, 2011; Mandatori and Gülder, 2011), and ethylene fuels (Harris and Weiner, 1983; Santoro *et al*., 1987; Flower and Bowman, 1988;Shaddix and Smyth, 1996;Xu *et al*., 1997; Decroix and Roberts, 2000; Lee and Na, 2000; McCrain and Roberts, 2005; D'Anna *et al*., 2007; Joo and Gülder, 2011), etc. Similarly, investigations on partially-mixed methane flames (Saito *et al*., 1986; Gülder, 1995; McEnally and Pfeffrele, 1999; Mungekar and Atreya, 2006), oxygen-enhanced combustion of natural gas flames (Saito, 1986; Gülder, 1995; Zelepouga *et al*., 2000; Beltrame *et al*., 2001; Santos *et al*., 2011), and in methane flames in cross-winds (Fairweather *et al*., 1992) are also documented. Methane, like other low or non-sooting flames have a very low tendency of soot formation at normal pressures, but at increased pressures, the sooting tendency increases (Brookes and Moss, 1999; Bento *et al*., 2006; Karatas and Gülder, 2012). This limits the soot investigations performed using methane flames, except at high pressures. Nevertheless, in gas flaring, irrespective of the field or the reservoir where the natural gas is produced, the main composition of natural gas is methane, although this composition varies (Ismail and Umukoro, 2014). However, because of the relevance of methane in gas flaring (Canteenwalla *et al*., 2007), a summary of the experimental investigations of soot in methane flames under different test conditions is presented in appendix D.

Jeng *et al*. (1984) examined the changes in the average flame temperature, the radiation and the concentration of species of confined methane - air flames, but the effect of the soot morphology was not investigated. Similarly, the concentration of

the gas species, the temperature and the velocity profiles of turbulent methane flames has been investigated by Smyth *et al*. (1985), however, one fuel flow-rate was investigated. Also, measurements of the mean flame temperature, the soot volume-fraction, and the radiation intensity of the turbulent methane-air jet flames at both the atmospheric pressure and at higher pressures in confined flames have been investigated by Brookes and Moss (1999). However, in their measurements, the jet flames which are stabilised above the jet nozzle were not investigated because of the challenges in setting the boundary-conditions in modelling flames that are stabilised above the burner. Wang *et al*. (2002) investigated the effect of radiation and the EINOx and EICO on soot, but they did not characterise the soot morphology of the different fuels they investigated. Qamar *et al*. (2009) investigated the distribution of the soot volume fraction of natural gas fuels, but they did not examine this distribution over a wide range of test conditions. There is a limited investigation of soot in methane - air flames at different jet velocities in the laminar, transitional and turbulent regimes, and very little has been done in investigating the soot emissions generated from flares. Characterising the emissions generated from flares aid in the control of soot emissions (Yang and Seitzman, 2003).

While some investigations were focused on the characterisation of soot emission of pure gaseous fuels, such as methane, ethane, ethylene, (Becker and Liang, 1982; Sivathanu and Faeth, 1990), propane (Becker and Yamazaki, 1978; Becker and Liang, 1982; Sivathanu and Faeth,1990); propylene (McDaniel,1983), acetylene (Dalzell *et al*., 1970; Magnussen, 1975; Becker and Liang, 1982; Sivathanu and Faeth, 1990), etc., other investigators proposed the soot emission factors of associated gas fuels made up of different gas compositions (McEwen and Johnson, 2012). Due to the inhomogeneity of the composition of flared gases, accurate characterisation of the efficiency of associated gases is still a challenge in the oil and gas industry, both in laboratory-scale, pilot-scale vertically-oriented flares (Pohl *et al*., 1986), and flares in crosswinds (Poudenx, 2000; Howell, 2004). This is because the various compositions of those gases may reduce the combustion efficiency of the flare, and may generate undesirable emissions as combustion products (Strosher, 2000). The differences in the emission factors proposed by previous investigators lends credence to the test conditions used in the investigations, which include fuel composition, fuel jet velocity, fuel jet diameter,

etc. Soot emission factors have been proposed by the USEPA (1995, 2009), for landfill gases. Also, the CAPP guide (2007) presented the soot emission factors for associated gases, but the effect of varying the velocity of the crosswind, fuel composition, etc., were not reported. More recently, in the laboratory-scale investigation carried out by McEwen and Johnson (2012), they proposed the soot emission factor of associated gases, using gases with different compositions, representative of the composition of associate gases flared in real life. However, no simultaneous characterisation of the soot emission factor, emission indices of pollutant species, and unburned hydrocarbons were reported.

To the best of the author's knowledge, prior to this study, there has been no previous study on the effect of varying the concentration of the inert diluent on the fuel-stream on the post-flame soot emission factor and on the EI of pollutant species. In addition, there is no study in the literature that shows both the in-flame and the post-flame variation of the composition of the major species in methane flames in turbulent conditions. Even the most recent study by Oh and Noh (2014), where the diluent was injected on the oxidiser side does not have results of the simultaneous measurements of the composition of the species. The other studies that report the effect of dilution on the fuel stream are the works of Lock *et al*. (2007), who studied the effect of dilution on the flame stability, Gollahalli (1978) on NOx emissions, where he reported the effect of fuel-stream dilution in propane flames in coflow and crosswinds at different CO_2 concentrations, but they did not vary the fuel flowrate. Gollahalli and Zadeh (1985) reported the effect of dilution of propane flames, but they used Nitrogen and not Carbon dioxide as the diluent, and they did not vary the mole fraction of the diluent, neither did they report the effect of dilution on NO_2 emissions. However, in this study, the effect of the dilution of the fuel-stream on turbulent unconfined co-flowing methane jet flames at different diluent mole fractions is investigated, where CO_2 is used as the diluent, and where the in-flame composition of species, including the in-flame concentration of NO_2, and the EINOx at different diluent concentrations are reported. The dilution of the fuel stream with an inert has been known to reduce the soot volume fraction, but the effect of this dilution at various diluent mole fractions on the soot emission factor has never been investigated. In addition, soot emissions are not the only source of emissions in flares. Even in the emissions-monitoring stations where soot emissions have been

characterised, it has been reported that pollutants from other sources, which are present in the emissions sample makes it difficult to accurately measure the emissions generated from flares. This presents a constraint and a challenge in the amount of the available and the reliable data for the accurate characterisation of the soot emissions generated from flares (Stohl *et al*., 2013). In this regard, it is insufficient to report only the soot emission factors of fuels alone, but to also report the emission indices of the post-flame species and products of combustion, to gain a better understanding of, and to generate a comprehensive database of the emissions generated by gas flaring in order to make a direct attribution of the emissions generated from flares, which is what this study will address.

2.9 PRESENT STUDY

From the limitations discussed in the previous section, it is obvious that more data needs to be added to the already-existing database of the soot and the pollutant emissions from laboratory-scale flares, which will be aimed at improving and validating the models used in the prediction of emissions. As a result, the present study will examine the consequences of varying different test conditions, such as the jet velocity and the effect of the dilution of the fuel stream on the in-flame and the post-flame temperature and species concentration in non-premixed, co-flowing, unconfined methane-air jet flames at atmospheric pressure. The measurement of the average visible flame height, average lift-off height, axial and radial measurements of the mean and fluctuating temperature, concentration of the major species, will be performed over a wide range of test conditions of different fuel jet velocities in the laminar, transitional and turbulent flows in the attached and in the lifted flow regimes. Similarly, the effect of CO_2 dilution on soot and other pollutant emissions will be examined, where the emission indices of EICO, EINOx, and the soot emission factor will be estimated, in addition to the comparison of the post-flame emissions generated from methane and propane flames. The results which are derived from laboratory measurements, which include measurements of the flame's temperature, species compositions, etc., may be used to estimate the soot emission factor, the emission indices of the pollutant species, etc., which are generated from gas flares.

2.10 EMISSION INDICES

The EI of a pollutant species is an indication of the mass of the pollutant species which is emitted (in grammes) per mass of the fuel which is burned (in kilogramme). According to Pourkashanian *et al*. (1994), the emission indices may be expressed as:

$$EIX_s(g/kg) = \frac{nX_s}{X_{CO_2}} \times \frac{MW_s}{MW_f} \times 1000 \tag{2.46}$$

Where *n* is the number of carbon atoms in an alkane (Turns and Lovett, 1989; Meunier *et al*., 1998; Rokke *et al*., 1994). When the concentration of the NO_2 in the flame is significant, and if it is assumed that all the carbon that is present in the fuel is finally oxidised to CO_2, in the post-flame region and in exhaust gases (Al-Fawaz *et al*., 1994), then the EINOx is written as: (Driscoll, *et al*., 1992; Turns *et al*., 1993):

$$EINO_x = \frac{\left(X_{NO} MW_{NO_2}\right) + \left(X_{NO_2} MW_{NO_2}\right)}{X_{CO_2} MW_{CH_4}} \times 1000 \tag{2.47}$$

However, in practice, the emission of NOx in fossil fuels is in the form of NO which is oxidised to NO_2 in the atmosphere and in exhaust systems (Pourkashanian *et al*., 1998), therefore, as a convention, the emission index of NOx is reported as the equivalent of NO_2, where the molecular weight of NO_2 is used in computing the EINOx (Driscoll, *et al*., 1992; Turns *et al*., 1993).

Chapter 3

EXPERIMENTAL METHOD

This chapter describes the instruments and the experimental methods used in this study. The investigation compromised of the axial and radial measurements of the mean and fluctuating temperature, the in-flame and the post-flame measurements of the composition of gas species, and the visualisation of the flame length and the flame's lift-off height of methane and propane flames at various test conditions. This spans from the laminar to the turbulent cases in the attached and lifted flow regimes, with and without the injection of the diluent into the fuel stream at different diluent mole fractions.

3.1 BURNER DESCRIPTION

Figure 3.1 Photograph of the Sandia burner

The co-flow burner utilised in this study was a Sandia burner. It is designed for the combustion of gaseous fuels, firing vertically upwards, with a configuration for co-flowing and co-axial oxidant flow streams, and an interchangeable fuel tube, for different investigations. This burner has been used at the Sandia National Laboratory, Livermore, and the BOC Technical Centre, USA. Several researchers have used it also, including Dearden (1996), Howard (1998), Yap *et al*. (1998), Erete (2012, 2015), etc., and has been adapted to meet the objective of the present investigation.

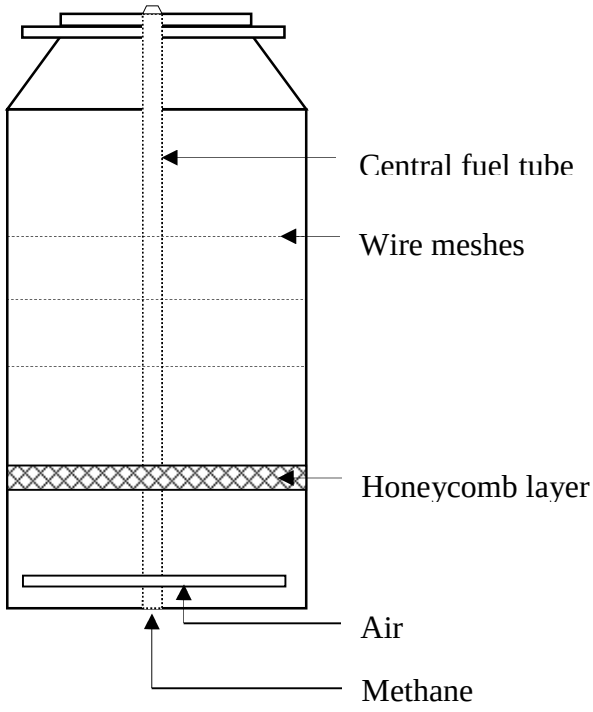

Figure 3.2 Schematic of the burner showing the main burner components.

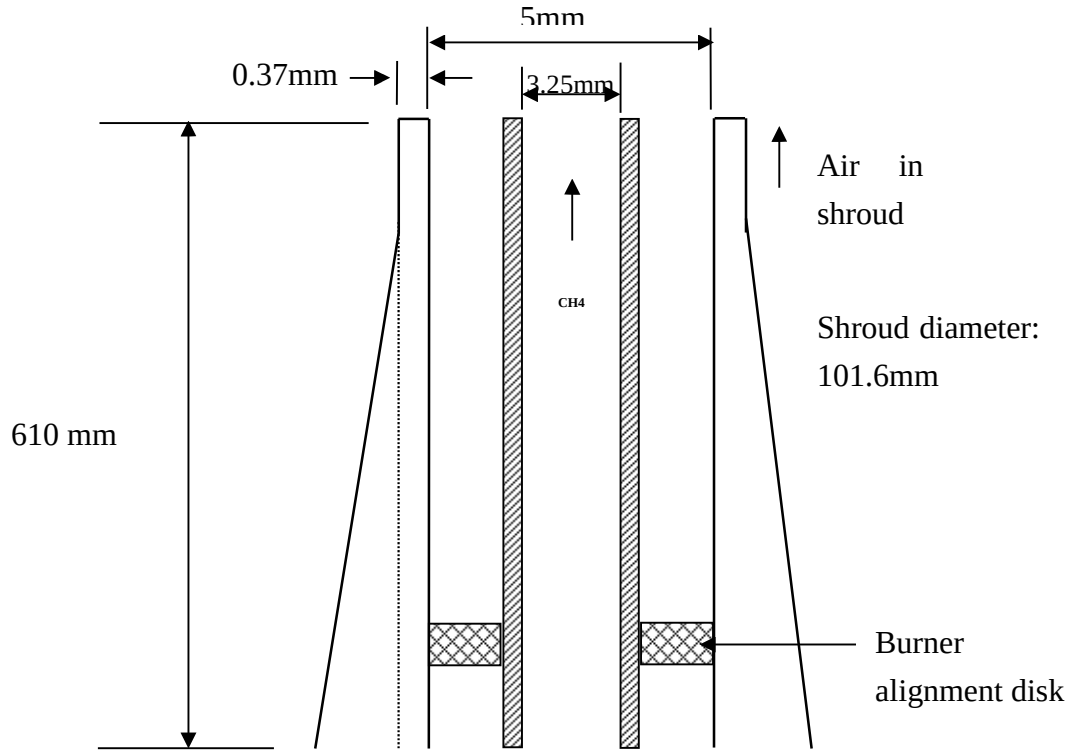

Figure 3.3 Schematic of the burner nozzle showing the nozzle dimensions.

The specification of the burner is as follows: fuel tubing inner diameter 3.25 mm, fuel tubing thickness 1.57 mm, fuel tubing outer diameter 6.21 mm, co-flow air inner tubing diameter 101.7 mm and co-flow air tubing thickness 6.08 mm. The

photograph of the Sandia burner and a schematic showing its components are shown in figures 3.1 and 3.2, respectively. Compressed air was connected to the burner which was the supply of the co-flow air. The co-flow air velocity which was used in all the investigations in this study was 0.3 m/s. The co-flow air aided in the reduction of the distortion due to the motion in the room, which, if not controlled, may lead to the flame's high sensitivity to the room drafts. In order to facilitate a smooth flow, the burner was equipped with a honeycomb flow straightener and wire mesh. The Sandia burner was attached vertically on an ISEL® traverse mechanism which allowed the movement of the burner in any desired direction, where the movement of the burner was controlled via a computer programme. The traverse mechanism has an accuracy of ± 1 mm in each of the axes.

3.2 FLAME SAMPLING PROBE AND ASSOCIATED MEASUREMENT ERRORS

The gas samples were obtained by using an uncooled quartz probe, which was designed by Drake *et al*. (1987), and has been used by other researchers (Namazian *et al*., 1994).

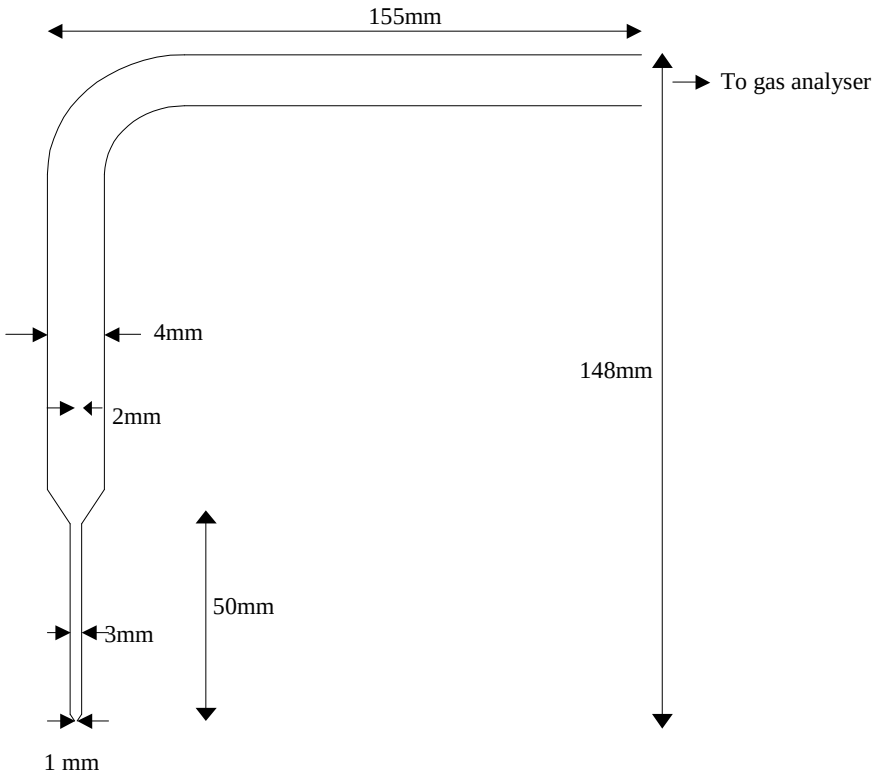

Figure 3.4 The probe used in this investigation.

Quartz is generally a good material for the design of a probe because they can withstand high flame temperatures and catalytic activities may be reduced (Bowman, 1977). The errors associated with the sampling probe may be mainly due to the flame's perturbation, or the chemical reactions due to an NO - NO_2 conversion within the probe, which might lead to false measurements and readings (Bilger and Beck, 1975; Matthews *et al*., 1977; Drake *et al*., 1987). Therefore, the probe should be designed to reduce the perturbation of the flame such that the measurements made at any location in the flame is representative of the unperturbed flow at the orifice of the probe and in the flame. Also, measurement errors may be minimised if the probe is designed to quench any chemical reaction which may occur in the probe. The probe was designed to minimize these errors such that there was a sudden expansion of the sample at the sampling orifice, rapidly cooling the sample, which was quenched via the "choked" flow principle (Colket *et al*., 1982), hence, minimizing any chemical reaction that could take place in the probe. The inner diameter of the probe's tip was 1 mm. The gas samples were conveyed through this orifice and via the heated sampling line to the gas conditioning system (VS-3000), and finally to the on-line gas analysis system (VA-3000), where the readings were shown. The VA-3000 was also connected to the data-logging system which was connected to the personal computer, where the measurements which were made were captured and stored. To avoid the clogging of the probe over time, the sample line was piped such that it was possible to perform a flushing of the probe and the sample line with a stream of air, without losing the probing position while taking measurements.

3.3 INSTRUMENT CALIBRATION

The calibration of the instrument for the measurements of the major species were performed using the span gases of known concentration which are listed in table 3.1. The nominal concentrations of the gases to be measured are known or pre-determined, because this aids the gas vendor in supplying a certified gas concentration, which is an estimate of the nominal value of the gas concentration. The multi-component gas analyser is fitted with different sensors for the measurement of the gas species simultaneously (Iwata, 2006). The NO and the NOx were measured directly, while the NO_2 was determined by taking the difference

between the NO and the NO_2, as has been performed by other investigators (Turns and Lovett, 1989; Hori *et al*., 1992).

SPAN GAS	SPECIES	NOMINAL CONCENTRATION	CERTIFIED VALUE
Span 1	*NO*	50 ppm in N_2 (Total NOx> 0.001ppm)	52 ppm
Span 2	Ambient air	21 %	21%
Span 3	CO_2	6% in N_2	6.25 %
Span 4	*CO*	8% in N_2	8.02%
MEXA-1170HFID SPECIFICATION			
Span Gas	C_3H_8	50 ppm in N_2	52.6 ppm
Fuel gas	H_2	40 % in Helium	38.78%
Zero gas		**Burner gas**	**Purge gas**
N_2		Refined air	Compressed air

Table 3.1 Span gases used for the calibration of the gas analyser and the FID.

The calibration of the instrument was performed after every twelve hours of measurements to reduce the drift of the instrument, as explained in the instrument's instruction manual. Nitrogen was used as the carrier gas due to its cost effectiveness, although gases such as helium or argon are also good alternatives due to their un-reactiveness and stability. Carrier gases aid in driving gas samples in the gas analyser, thereby facilitating the elution of the components which are in the sample with the carrier-gas. In taking measurements, the sample gas flows through the heated sample line which is connected to the quartz probe at one and to the VS-3000 gas conditioning unit at the other end. After the conditioning of the gas sample, this sample is conveyed into the VA-3000, where the measurement of the gas sample's concentration is made.

Figure 3.5 The photograph of the rack-mounted HFID, VA-3000 and the VS-3000 systems.

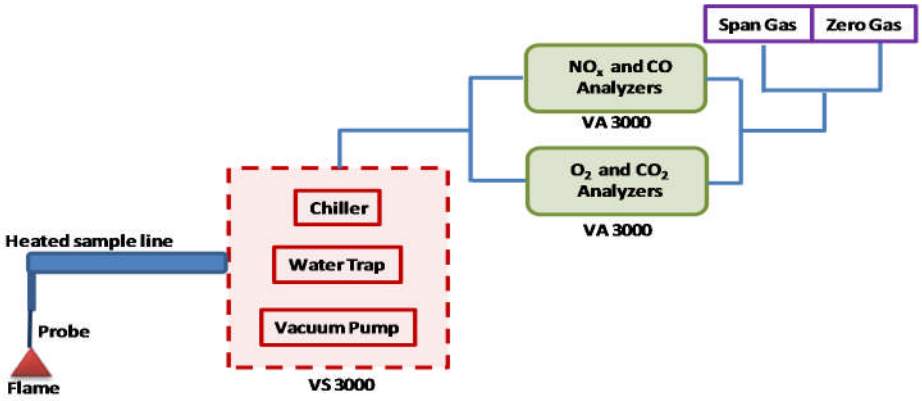

Figure 3.6 The gas analysis system.

Gas conditioning involves the removal of the moisture and the residue from the sample before the sample is conveyed to the gas analyser for measurements on a dry basis. In the conditioning system shown in figure 3.6, the gas sample which is drawn from the sample line by a vacuum pump, is conditioned as it passes through a water-trap, before the sample is conveyed into the analyser . The errors in the use of the gas analyser may be due to instrument drift, which may lead to inaccurate readings on the VA-3000. This error may be avoided by regular calibrations using

the span gases listed in Table 3.1. The discussions of the operation of the analysers are presented in the subsequent subsections.

3.3.1 CHEMILUMINESCENT NOx ANALYSER

The Horiba model VA-3000 chemiluminescent NOx analyser was used to measure the concentrations of NO and NOx. The accuracy of the analyser is $\pm 0.5\%$ of full scale. In the NOx analyser, NO reacts with O_3, yielding NO_2 and O_2, according to the reaction:

$$NO + O_3 \leftrightarrow NO_2 + O_2 + \mu u \qquad \text{(R3.1)}$$

The light intensity, ηu ,which is emitted is proportional to the rate of the mass of the NO_2 which flows into the chamber where the reaction takes place (Matthews *et al*., 1977). When light is emitted, there is a reduced energy loss by the NO_2 molecules, while the greater losses which occur are due to the collision of the molecules, as they interact with one another. A greater emission of the light intensity is achieved at lower pressures at the chamber where the reaction occurs, which is due to the lesser collisions which occur at a low pressure. The chemiluminescence reaction (R3.1) is NO-specific. However, the NOx may be determined when the NO_2 reaction occurs thus:

$$2NO_2 + (heat) \leftrightarrow 2NO + O_2 \qquad \text{(R3.2)}$$

$$NO_2 + C \leftrightarrow NO + CO \qquad \text{(R3.3)}$$

$$2NO_2 + C \leftrightarrow 2NO + CO_2 \qquad \text{(R3.4)}$$

The errors during the measurement were minimised by heating the sampling line, and the gas conditioning systems were heated above the dew point to prevent condensation due to moisture (H_2O) in the sample. If the sampling system is not heated properly, this moisture, which is a third-body quenching radical (Matthews *et al*., 1977) may cause the removal of NO_2, due to its high affinity to be dissolved in H_2O, thereby giving false readings.

3.3.2 INFRARED CO AND CO_2 ANALYSER

The CO and the CO_2 concentrations were measured using the Horiba VA model 3000 infrared analyser. The accuracy of this unit is $\pm 0.5\%$ on a full scale deflection, as reported by the manufacturers. The principle of the operation of this analyser is based on infra-red (IR) absorption. This instrument displays different readings for each of the measured CO and CO_2 gas species due to the signal it receives from these species at different wavelengths. In the analyser, the sample which is about to

be analysed is conveyed via an optical cell which is in-between the source of the IR radiation and a detection unit. The level of the absorption of the IR radiation by the sample depends on the concentration of the species to be sampled. This absorption then reduces the energy signal before the sample reaches the unit where the detection of the sample occurs. The energy-loss differs based on the concentration of the species to be measured. While the sample of the species is conveyed to the measurement-cell, the beamed IR energy is conveyed via the sample to the IR detecting unit. The sample to be measured then absorbs the IR energy thereby leading to a reduction in the energy which reaches the IR detecting unit. This leads to a build-up of the gas pressure in the first chamber which causes the gas sample to be conveyed to the adjacent chamber. The sample gas is then conveyed to a sensor which exists between these chambers and which decreases the resistance of the sensor-element. Since this resistance had already been calibrated for a particular sample concentration, the measurement of this resistance is now performed and shown as the concentration of the gas which has been sampled.

3.3.3 PARAMAGNETIC O_2 ANALYSER

This analyser was used to measure the concentration of O_2. The accuracy of this analyser is $\pm$ 0.1% on a full scale deflection. The measurement principle of this analyser is based on the utilization of the magnetic property of O_2. There is a greater affinity of O_2 molecules to magnetic fields than other species which leads to a generation of a magnetic field around the O_2 molecules, and leads to an increased sensitivity of O_2 to magnetic force fields.

In practice, two glass-shaped spheres which contain N_2 are set up on a device mechanism which are rotated around magnets, and which produce a magnetic force field (1 and 2), as shown in figure 3.7. A mirror is fitted to reflect the beam of the lights coming from an externally-installed light source which is positioned on two photocells (3). The sampled O_2 gas is drawn to the location where the nitrogen-containing spheres are placed. The signal of the motion generated via this affinity is picked up by these photocells and are then transmitted to another device, which causes a generation of current on the wire which is installed on the rotating unit (4). This induced current is proportional to the O_2 concentration in the gas sample which is output as an O_2 concentration reading in the paramagnetic analyser.

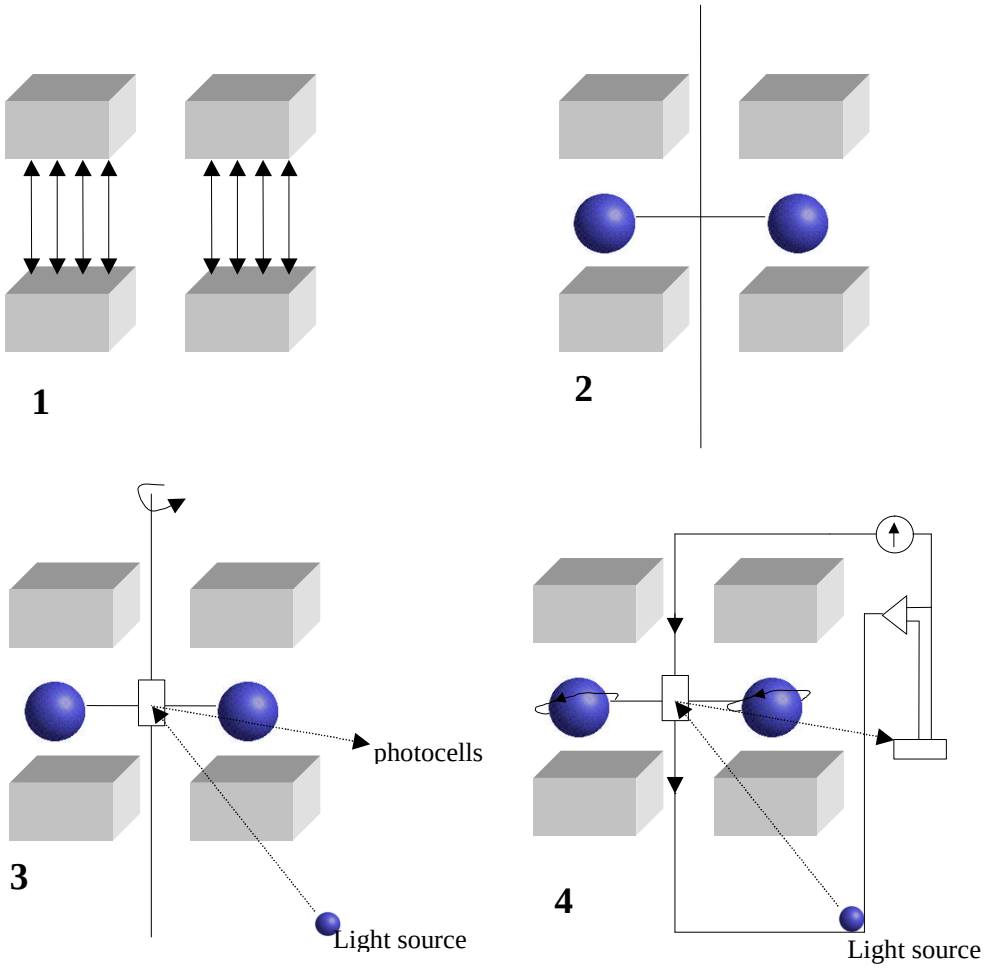

Figure 3.7 The schematic of the operation of an Oxygen Paramagnetic Analyser.

3.4 FLAME IONISATION DETECTOR (FID)

The FID is used in measuring the total hydrocarbon (THC) concentration of hydrocarbons in a gas sample. In principle, the sample gas to be measured is introduced into a hydrogen flame which is inside the FID, creating an increasing amount of ions as the hydrocarbon is combusted. A high DC polarising voltage repels the ions towards the tubular electrodes, called collector plates. When these ions hit these plates, a current-inducing signal is produced, and an electrometer receives this signal from the current generated. This current is proportional to the combusted sample, which is converted to a digital form as an output of the reading. The quoted accuracy for this instrument according to the manufacturers is within 3% on a full-scale deflection.

3.5 TEMPERATURE MEASUREMENTS

The measurement of the temperature was performed using the “R”-type thermocouple (Platinum Rhodium -13% / Platinum) due to the temperature range

and its tolerance limit in high-temperature applications. The bead of the thermocouple was made by welding two wires, with a wire diameter of 0.075mm. The bead diameter was measured before and after the coating of the thermocouple and their sizes were $160 \pm 0.003\mu m$ and $216 \pm 0.002\ \mu m$, respectively.

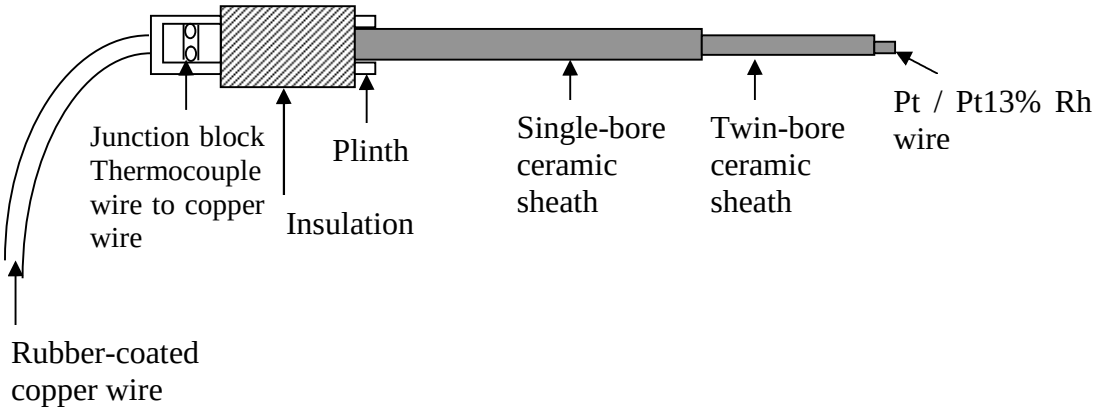

Figure 3.8 Schematic of the Pt 13% Rh fine wire thermocouple.

The measurements of the bead sizes were made using a Nikon Profile Projector Model V-16D. The coating of the bead of the thermocouple was performed using Hexamethyldisiloxane (HMDSO). The coating is done to reduce the catalytic reactions that may likely take place on the bead's surface, and which may affect the readings measured using the thermocouple. During coating, a layer of silicon dioxide (SiO_2) is attached to the bead, due to the oxidation of the HMDSO on the thermocouple bead.

In combustion applications, there has been widespread use of fine wire thermocouples due to their cost-effectiveness and their ease of fabrication. However, there are errors that are associated with these thermocouples, namely: flame perturbations due to aerodynamic upsets, catalytic effects and wire contamination, and due to conduction, convection and radiation heat transfer. In a flow field, the perturbation of the probe may have an effect on the mixing of the streams, where the flow field may be altered or interrupted. Similarly, this perturbation may cause the flame to be stabilised on the probe, or cause the thermocouple to act as a bluff-body, thereby creating flame recirculation, which may lead to increased reaction rates and higher temperature measurements in the flame. In addition, unreliable measurements may occur due to the thermocouple absorbing the heat from the flame. These upsets may be minimised by using thermocouples with small beads. Chemical reactions may occur due to radical recombination on the surface of the wires, which might

contaminate the wire. However, these errors may be minimised by the coating of the thermocouple wires with materials that are non-catalytic, although this might lead to an increase in the thickness of the wire, which might reduce the sensitivity of the thermocouple, depending on how thick the coating is (Heitor and Moreira, 1993).

The source of measurement errors may also be due to the different modes of heat transfer which occur between the hot gas, the thermocouple and the surrounding. The relationship between the measurement errors from the different modes of heat transfer is that heat may be transferred to / from the bead of the thermocouple to the wire via conduction, while there is also an exchange of heat between the bead and the surrounding hot gas via convection, and heat gain by the bead either through the flame, the hot surface or the hot gas, via radiation. Also, heat convection from the gas could either be conducted to the thermocouple or radiated from the thermocouple to the surrounding. The error due to convection may occur if there is a transfer of heat between the hot gas and the surface area of the thermocouple bead, leading to heat gain by the thermocouple from the flame. This is because thermocouples measure the temperature of the bead, and not the temperature of the gas (Apte, 2006). This error may be reduced by decreasing the surface area of the bead, thereby minimising the area of the bead that is exposed to heat transfer from the hot gas. The temperature gradient in the bead may be ignored because of the small size of the thermocouple bead. Therefore, the effect of the convection heat transfer on the bead is negligible, when the bead size is approximately 1 mm (Apte, 2006). This is because the bead size of the thermocouple used in this study was less than 1 mm. The error due to conduction may occur if there is a transfer of heat between the bead and the thermocouple wire, which means that a greater amount of energy would be required to keep the bead heated to the gas temperature. However, this error is usually minimised if the diameter of the thermocouple wire is small. Conduction may also be minimised by positioning the bead at an optimal distance away from the ceramic sheath. The error due to radiation may occur when the thermocouple is at a proximal distance to the flame, causing the flame to radiate energy to the bead which leads to heat gain by the thermocouple bead and hence a greater radiation of the thermocouple to the surrounding. Radiation error is the main source of error in this study. This error may be compensated for, by applying the mathematical expression by Kaskan (1957),

which is a correction for the radiative heat-loss to the surrounding, as shown in equation (3.2):

$$\Delta T_{rad} = \frac{1.25\varepsilon\sigma T_w^4 D^{0.75}}{\lambda}\left(\frac{\eta}{\rho u}\right)^{0.25} \tag{3.2}$$

This correction is done as a compensation for the loss of heat from the thermocouple as a result of the radiative effects which exist between the thermocouple and the surrounding. The heat-loss is prominent at temperatures above about 1200^{o}C, and a compensation may be made to account for these temperature losses. Radiation errors may also be reduced if the material of construction of the thermocouple have a low emissivity and conductivity (Mishra, 2014), and if the probe of the thermocouple is shrouded with a radiation shield which aids in the transfer of radiation back to the probe, in order to attain equilibrium in the rate of the radiation heat transfer (Lee, 2008). Equation (3.2) was used to correct the temperature data obtained from the thermocouple and the radiation-corrected temperature data are reported in Chapters 4 to 6.

3.6 EXPERIMENTAL SET-UP

The major component of this setup are the Sandia burner, fuel and co-flow air supply, metering systems, temperature and gas composition measurement and probing systems. The burner described in section 3.1 was mounted on a traversing mechanism as shown in figure 3.9. The exhaust hood was installed directly over the burner such that the products of combustion were removed from the laboratory by a suction system as shown in figure 3.10. The burner was placed vertically on a system to allow its movement in any specified direction. This movement was controlled by a computer programme which aided in the axial and radial positioning of the burner, relative to the probing system, as desired.

Above the burner was the exhaust hood, made of mild steel, at a height of 0.59 m above the floor of the laboratory, where the combustion products were removed by a forced-draft exhaust. The exhaust system was mounted at a downstream location above the visible flame, where the burner was aligned at a vertical symmetry to the duct, to ensure that the combustion products were discharged via suction, with a suction velocity of 6.6 m/s. This suction air velocity was sufficient to reduce the deposition of soot on the duct, and to avoid the contamination of the post-

combustion products. The in-flame gas samples were withdrawn using a heated Teflon sample line connected to an uncooled quartz probe which was positioned at a desired location in the flame. After each measurement , the probe was cleaned using an ultrasonic bath to remove traces of particles which are embedded in the walls of the probe which may contaminate the sample.The soot samples which were collected on filter papers were examined using the Hitachi model SU8230 Field Emission Scanning Electron Microscope (FESEM) at magnifications ranging from 5000 to 500000 for each sample.

The moisture from the filter paper was removed by placing the filter paper in an oven for a known period of time and then weighing the filter paper before and after the deposition of soot to determine the mass of the soot particle. The filter papers were placed in a filter holder and the soot was deposited on the filter paper using a vacuum pump which drew the samples into the filter paper via the gravimetric method. This has also been used by McEwen and Johnson (2012). Using an image processing software (ImageJ), the images were first converted from pixel size to a nanometer scale, and then digitised, then the software was used to measure the particle diameter, while the count of the primary particles was done by visual observation.

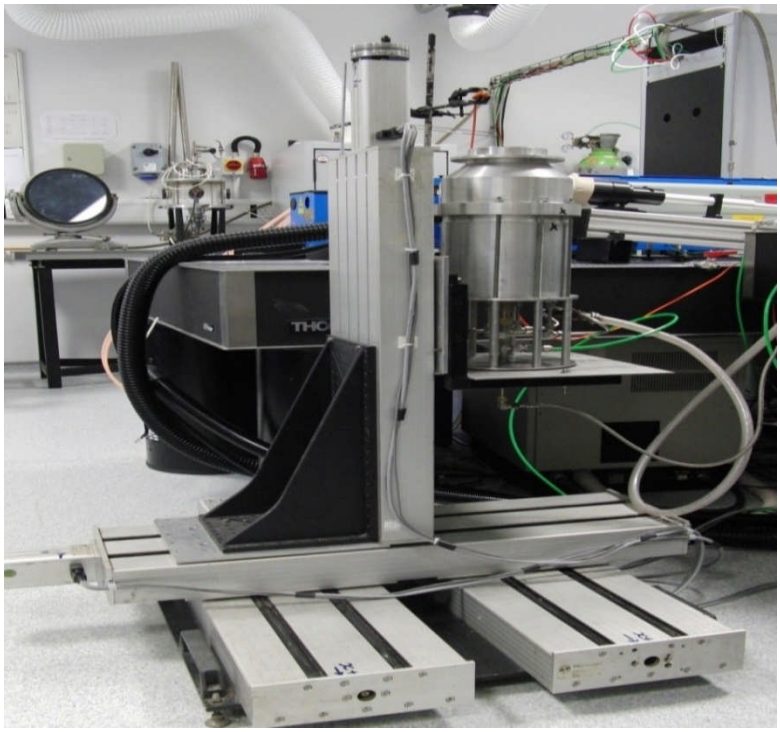

Figure 3.9 Photograph of the burner and the traversing mechanism.

Results from the use of this software in different applications have been published in several journals (Abramoff *et al.*, 2004). An image processing software is useful in quickly analysing large samples of particles (Koylu *et al*., 1997). The fuel which was commercial-grade methane (CP-Grade 99.5%), was metered via a calibrated rotameter, before being piped into the burner. A flashback arrestor was installed in the fuel line for safety reasons. In order to ascertain the readings generated from the adjustments of the rotameter, the flow rate readings generated from the calibration of the rotameter were corrected, to account for the changes in the room temperature and pressure as the experiment was performed.

The calibration curve for the rotameter calibration which shows the corrected volumetric flow rate as a function of the rotameter reading is shown in appendix A. The rotameters were calibrated before being used and the volumetric flow rate which was measured was corrected and converted to the conditions of STP (273.15 K and 101.325 mbar), by assuming that the gases are ideal gases, and that they obey the perfect gas equation (Atkins, 1997), thus:

$$Corrected flow rate = \left[(measured flow rate) \left(\frac{273.15}{T} \right) \left(\frac{P}{1013.25} \right) \right] \tag{3.3}$$

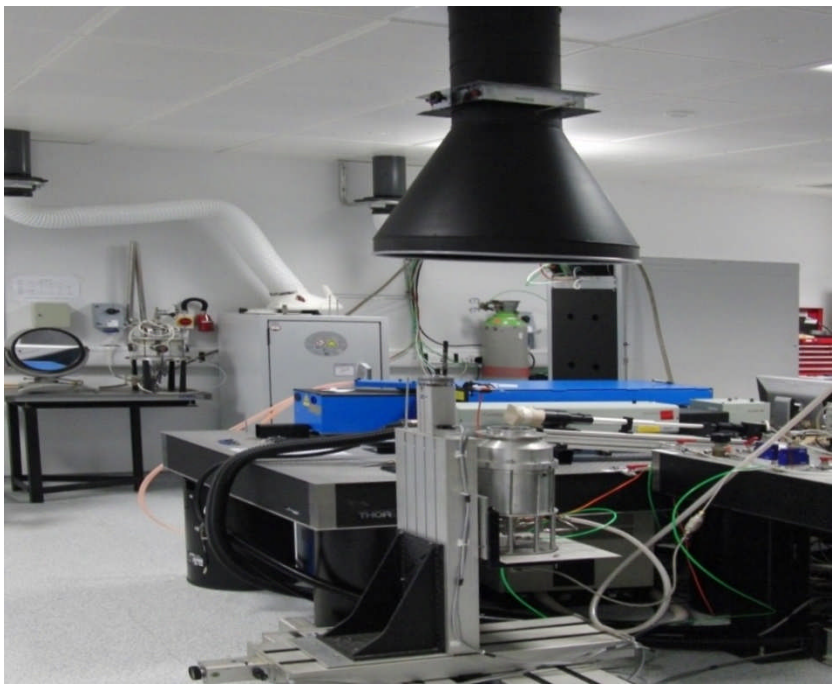

Figure 3.10 Photograph of the burner, traversing mechanism and the exhaust hood.

The co-flowing air, which was compressed air, was also metered with a calibrated rotameter before being piped into the co-flow air stream in the burner. To ensure uniformity of the air flow, the co-flow air velocity was measured using a hot-wire anemometer, which was placed over the burner port, and the reading was constant. The co-flow velocity was 0.3 m/s, which is sufficient to provide the desired shrouded air needed to minimise the flame from flickering due to disturbances in the room, such as movements. This co-flow air velocity was kept constant in all the conditions that were investigated. In addition, the co-flow air velocity was kept at less than 3% of the fuel jet velocity to avoid the influence of the coflow air on the length of the flame, flame's lift-off height, and on EINOx levels. This has previously been discussed by Driscoll *et al*. (1992). The flame temperature was measured using the type "R" thermocouple. The thermocouple was mounted at a known fixed position with a retort stand, while the mechanism where the burner sat on, was used in moving the burner to any desired position, relative to the thermocouple or the gas probe, depending on what experiments were performed at that time.

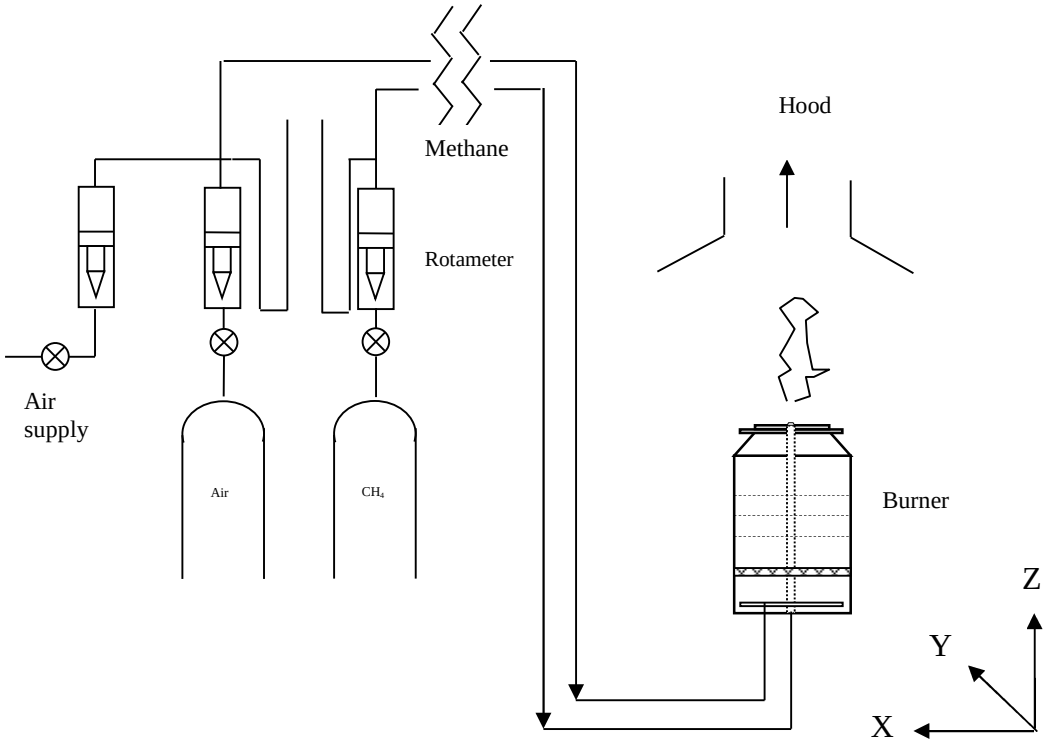

Figure 3.11 Schematic of the straight jet rig.

The thermocouple was connected to a data logger (MultiScan 1200 Data Acquisition System), which was connected to a high-speed computer. The instantaneous data was captured for each run, using windows-based software (Chartview®), at each

specified position, and stored in a spreadsheet programme, which was then processed to show the profile of both the mean and the fluctuating temperature readings. The samples were withdrawn at six axial locations in each flame. At each location, 300 readings which were made for each of the temperature and species concentration measurements, were averaged to give the mean value at each location. The sensitivity analyses conducted, indicated that 300 readings was the optimal number of readings to be made in order to ascertain the mean values at each position. The temperature correction for radiation heat losses was made using the expression by Kaskan (1957). The concentration of the major species was measured using the multi-component gas analyser (Horiba VA-3000) with a sample gas conditioning system (VS-3000), where measurements of NOx, NO, CO, CO_2, and O_2 were performed. The total hydrocarbon was measured using the Flame Ionisation Detector (MEXA 1170 HFID). The in-flame gas samples were drawn from an uncooled quartz probe. The orifice diameter of the probe was 1 mm. The gas samples were then conveyed via the heated sample line into the gas conditioning system, where traces of moisture were removed before the sample was analysed on a dry basis. The minimum sampling time which was required to obtain a steady gas concentration measurement at each position for each reading was 180 s. In order to ascertain accuracy and repeatability, each experimental investigation was repeated three times at each location, and the data were found to be consistent. In addition, the trends of the flame length, temperature and species composition of the lifted methane / air jet flame measured, have been modelled and simulated numerically (Erete *et al*., 2015), using the partially-premixed combustion model implemented in the ANSYS FLUENT version 14.5 numerical code.

The visualisation of the flame height and the lift-off height were determined experimentally by capturing these images using a digital camera, over a long exposure time. This procedure was repeated several times, and averaged to give the mean visible flame length and the mean lift-off distance. A measuring tape which was placed vertically side by side with the flame and the images, was used to capture the respective heights of the flame. In order to ensure that the burner and the measuring tape were fixed uprightly without tilting, a measuring plumb was used to ascertain this. The visible flame length for an attached flame used in this study was defined as the downstream distance between the jet nozzle exit port rim and the farthest downstream location where the tip of the flame is no longer visible to the

human eye. Similarly, for the lifted flame, the lift-off distance was defined as the downstream distance between the centreline of the jet nozzle exit port rim and the downstream plane where the flame just becomes visible i.e., the base of the flame where the flame stabilises independently above the burner jet rim. The light was turned off before the images were captured to ensure accuracy of the flame's visualisation. The probing systems were connected to a data-logger and to a computer and the results of the measurements were displayed on the computer in real-time, where these data were saved in a spreadsheet.

Chapter 4

COMPARISON OF ATTACHED AND LIFTED METHANE /FLAMES

4.1 INTRODUCTION

A discussion of the results generated from the use of the instruments described in chapter 3 under the test conditions listed in Table 4.1 is reported in this chapter.

Fuel	CH_4		
Jet Flame	A	B	C
Flow regime	Attached	Lifted	Lifted
Froude number	1731	22597	140608
Reynolds number	1584	5702	14254
Fuel velocity (m/s)	7.5	27.1	67.6
Heat release rate (kW)	2.2	8	20
Measurement locations	In-flame and post-flame		
Mixing	Non-premixed and unconfined		
Co-flow air velocity (m/s)	0.3		
In-flame and post-flame measurements	Temperature, gas composition, total unburned hydrocarbons, emission indices of pollutant species, mean mixture fraction, average visible flame length, average lift-off distance, and flame visualisation.		

Table 4.1 Experimental conditions used in the study.

Three test conditions were investigated at different Reynolds numbers as shown in figure 4.1 and a comparative analysis of the three test conditions were carried out. The measurements were comprised of both an in-flame and a post-flame measurement of the temperature and gas composition of major species for each of the flames. All the figures were plotted on the same scale for ease of comparison. The results generated from the test conditions are discussed in the following subsections.

4.2 VISIBLE FLAME APPEARANCE

The photograph of the jet flames are shown in figure 4.1. These images were taken using a digital camera and the images show the flames' luminosity and the stability of the flame. Each flame shows a distinctive colour at increased fuel jet velocities.

A: *Re* = 1584 B: *Re* = 5702 C: *Re* =14254

Figure 4.1 Photographs of the flames showing the burner rim-attached case and the flames which are stabilised above the burner port at increasing *Re*.

In the first flame photograph, the flame is very luminous with an orange-yellow colour at locations just above the burner port, and this extends all the way to the tip of the visible flame length, with a pale-blue colour upstream of the flame, at the flame base, indicating a degree of partial premixing of ambient air and fuel at that location. The luminous orange-yellow colour of the flame caused by the incandescence of carbon particles in the flame indicates the presence of soot, while the non-luminous bluish colour of the flame is an indication of CO (Giovaneti *et al*. 1980; Choudhuri and Gollahalli, 2000). Increasing the flow-rate of the fuel causes the jet flame to transit from the laminar condition to the turbulent condition, and this

increase in the flow-rate causes the flame to be stabilised above the jet's nozzle. At the transitional stage shown in the second photograph, the bluish colour of the flame begins to extend downstream, almost half-way through the length of the visible flame, and the orange-yellow colour of the flame is observed to be half-way through the length of the visible flame. Hereafter, a pale-blue colour change was observed in the third photograph. At this high jet velocity, just before the flame blows out, the flame becomes very unstable, with even a slight increase in the jet velocity or the co-flow air velocity leading to a blow-out. The partial premixing observed at the plane of the base of the lifted flame is expected because this region lies in a location between the burner port and the flame base, where air entrainment is promoted. This is in line with the observations of Chen and Goss (1989). Similarly, the higher concentration of soot in flame A than in flames B and C is due to the entrainment of air into the flame in the lifted cases at the flame base location of the flame, which leads to higher OH radical formation, thus suppressing soot formation, and impeding the formation of carbon, and this is consistent with the observations of Gollahalli and Zadeh (1985). Also, it was observed that an increase in the jet velocity led to an increase in the flame's lift-off height and in the broadening of the reaction zone. The broadening of the reaction zone suggests an increase in the turbulence as a result of the broadening of the OH profile, which scales with the flame width at higher Reynolds numbers. This has also been reported by Namazian *et al*. (1988), Chen *et al*. (1992), and Kelman and Masri (1997). The shape of the flame was distinctive in each of the jet flames; initially being slender when the flame is laminar, and becoming wider, with a wider flame base, as the flowrate is increased. Increasing the fuel flowrate further, leads to a vigorous oscillation of the base of the flame and also causes the flame to be further stabilised above the burner while there is no significant change in the height of the flame, and this is consistent with the observations of Peters and Williams (1983).

4.3 VISUALISATION OF THE FLAME HEIGHT AND LIFT-OFF HEIGHT

The average visible flame height and the lift-off distance of the three jet flames investigated are listed in Table 4.2, while the schematic of the changes in the flame's stability at increasing velocities is shown in figure 4.2. In each case investigated, the length of the visible flame and the flame's lift-off distance were measured by

averaging the luminous stream-wise length and the lift-off distance of the flame. In the attached case, the flame height was defined as the stream-wise distance which is between the plane of the fuel jet nozzle exit of the visible flame, where the flame was attached to the burner rim, and the tip of the visible flame. The attached flame was not forced-stabilised, and therefore there was no need to correct for the contribution of NOx from pilot flames or external stabilisers, which have been known to account for a significant NOx emission (Turns and Myhr, 1991; Bowman, 1992; Meunier *et al*., 1998). Similarly, the vertical distance between the plane of the visible flame, where the flame was suspended above the burner port, and the tip of the visible flame was taken as the visible flame height of the lifted flame, while the lift-off height was taken as the vertical distance between the fuel jet exit plane and the plane of the visible flame where the visible flame stabilised above the burner port. These images were captured over a series of instantaneous shots with an exposure time of 60 s. The increase in the length of the flame is caused by the vortices of the products of combustion which shroud the fuel stream from the ambient air, slowing down the diffusion of oxygen into the flame. Thus the flame extends to a height where the total flux of the air that is entrained into the flame would be sufficient for complete combustion, thereby causing an increase in the flame length.

Flame	**Fuel Jet velocity (m/s)**	**Reynolds Number**	**Measured flame length (cm)**	**Calculated flame length (cm)**	**Measured lift-off height (cm)**	**Calculated lift-off height (cm)**
A	7.5	1584	49.8±3	45.4	-	-
B	27.1	5702	51.3±5	50.7	8.5±4	8
C	67.6	14254	50.8±3	53.2	14.5±4	13.6

Table 4.2 Mean visible stream-wise length and lift-off distance for the jet flames.

These vortices are formed when there is friction between the stream of the products of combustion and the stagnant air, when the fuel jet discharges into still air. Increasing the flowrate of the fuel beyond the first test case showed a remarkable change in both the stability and in the luminosity of the flame, up to a stage where any further increase in the flowrate of the fuel did not lead to a remarkable change in

the flame's length for the fully turbulent case. In the second case, where the flame is transient, the flame height keeps increasing until a critical velocity is attained where the tip of the flame flickers. Increasing the fuel flowrate further, causes an increase in the visible length of the flame while causing the luminosity of the flame to decrease and the flame becomes stabilised intermittently at a downstream location further away from the burner port. The intermittency in the flame behaviour is caused by an interaction between the shear zone and the flame zone (Chen *et al*., 1992), which may either be due to the influence of the nozzle geometry, the properties of the fuel, or the co-flowing oxidiser at the flame base, at radial locations where combustion occurs (Pitts, 1988). In flame A, where the flame is laminar, the fuel jet discharges vertically upwards into quiescent air at a velocity which is lower than the critical velocity, and the mixing at this stage is by molecular diffusion, which is due to the mixing-rate existing between the fuel and the air, which leads to an increased stream-wise length of the flame until there is no remarkable change in the flame's length.

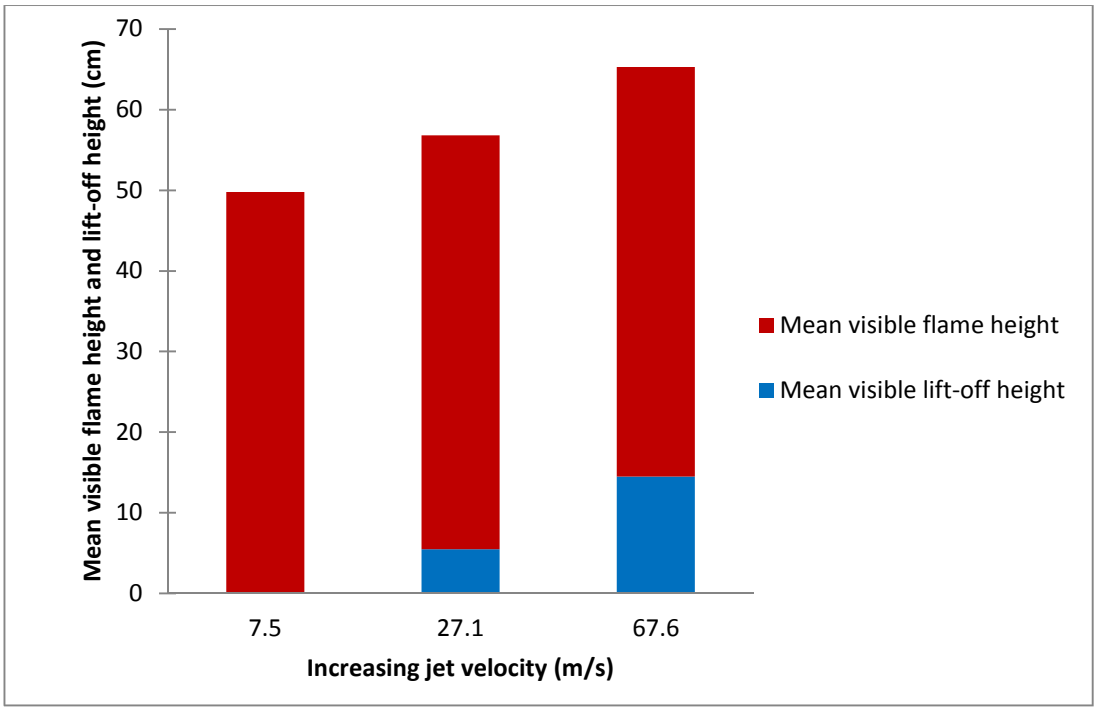

Figure 4.2 Changes in the visualisation of the mean visible flame height and lift-off height with an increase in the fuel jet velocity.

A further increase in the jet velocity decreases the stream-wise length of the flame, due to the break-up of the eddies by the entrainment of air into the flame, while an evidential increase in the flame's lift-off distance exists (Hottel and Hawthorne,

1949). This increase in the jet velocity has been known to scale linearly with the width of the flame, as suggested by Hottel and Hawthorne (1949). Similarly, a linear relationship between the fuel jet velocity and the lift-off height has been established (Kalghatgi, 1984; Chen *et al*., 1992; Cha and Chung, 1996; and Kiran and Mishra, 2007), and the measured lengths compare with the experimental correlation by Chen *et al*., (1992), as expressed in equation (2.40). The calculated flame lengths and the lift-off heights are within the range of the measured flame length and the lift-off height, and are listed in Table 4.2. The lift-off height is defined here as the axial distance between the plane of the rim of the fuel jet nozzle and the plane of the flame base of the visible flame which is stabilised above the burner nozzle. The flames stabilised above the burner are observed to be wider than the attached flame which is slender. This is as a result of the entrained air into the lifted flames which broadens their reaction zone and an increase in the jet velocity leads to a greater air requirement for the combustion of the fuel. In conclusion, the combustion of large amount of fuels result in large flames, because of the entrainment requirement of air into large flames than into smaller flames, resulting in a greater dissipation of heat into larger flames, thereby increasing the combustion efficiency of the flame (Strosher, 2000). The information on flame stability and flame height are useful in estimating the volume of the combustion zone, determining the level of the exposure of heat from a flame source to a location of interest, determining the efficiency of a flare, etc. In this regard, a comparison of the temperature profile of the three jet flames will be discussed in the next section.

4.4 TEMPERATURE PROFILE

The temperature data that was generated was corrected for the radiative heat loss from the bead of the thermocouple according to the expression by Kaskan (1957) shown in equation (3.2). The maximum difference between the measured and the corrected temperature reading was approximately 40 K. Birch *et al*. (1989) estimated a maximum difference of about 90 K, while Brookes and Moss (1999) measured and reported a difference of 50 K. In figure 4.4, the radial mean temperature profile for each flame is presented, at each axial location. The peak mean temperature of the jet flames were 1843 K, 1926 K, and 1953 K, at normalised axial locations of y/d=32.3, y/d=32.3, and y/d=38.5, respectively.

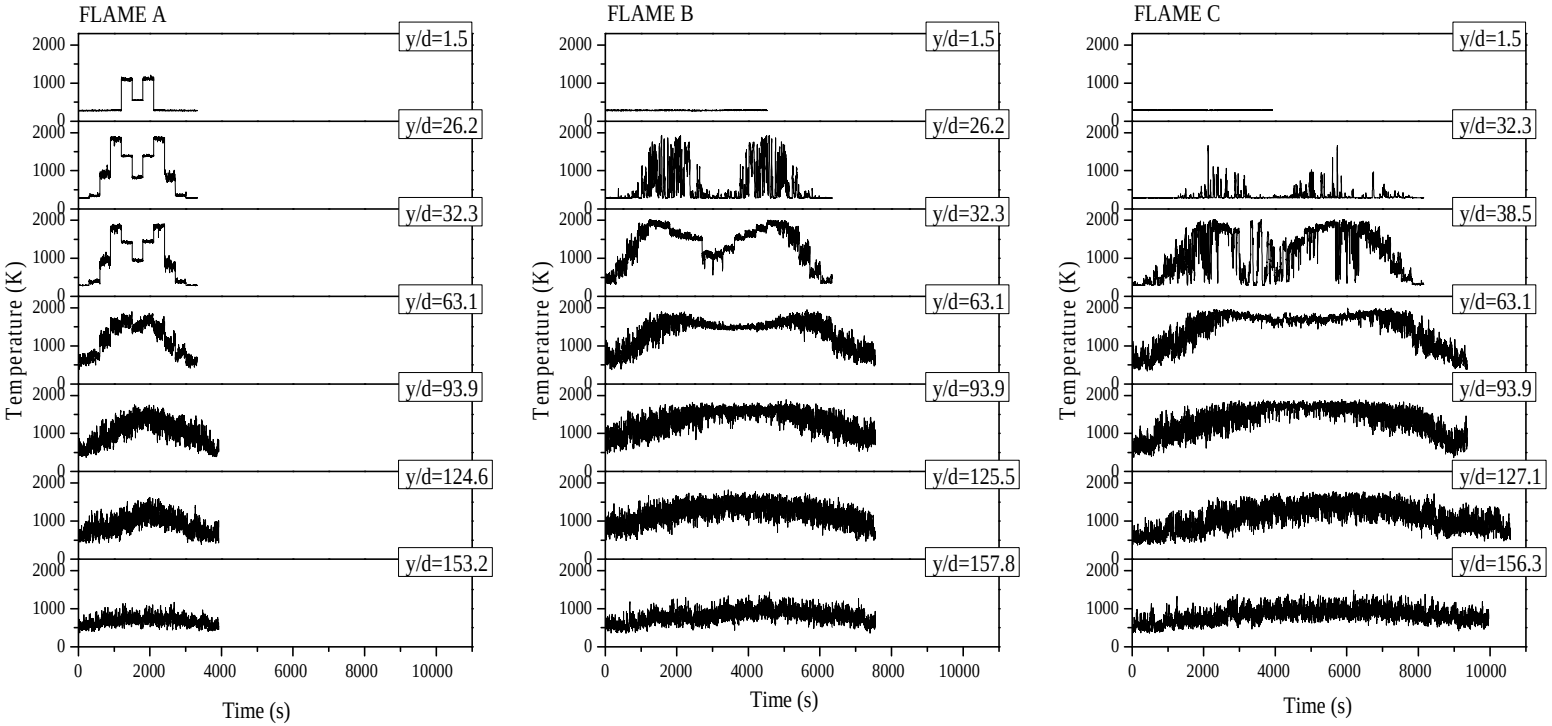

Figure 4.3 (a) Plots of the experimental data of the temperature for the three jet flames investigated.

The increase in the jet velocity leads to an increase in the flame temperature in all the cases investigated. The increase in the temperature at higher lift-off heights is due to the stabilisation of the flame above the jet rim, which leads to a greater mixing of the reactants, leading to greater homogeneous gas-phase reaction rates and hence higher temperatures (Gollahalli, 1977). The zero value at the abscissa is the centreline of the jet where the fuel issues, while the negative and positive values are an indication of the radial distances away from the centre of the jet, while traversing and measuring the temperature readings symmetrically. It is observed that the temperature of these jet flames exhibit a symmetrical profile, with the highest peak mean temperature observed mid-flame, due to the high heat-release rates leading to higher temperatures at that location. In addition, it was observed that the profile exhibited “humps” which were steepest mid-flame, as a result of the lower level of air entrainment into the flame at that region, which led to lesser air dilutions at that location than at the far-nozzle location. This is evidenced in the difference in the temperature at the near-nozzle region as a result of the dominance of the homogeneous gas phase reactions which leads to a quick development of a shear layer leading to reduced reaction rate, forcing the reactant species into the mid-flame location, thereby increasing the flame temperature at that location which is consistent with the observations of Gollahalli (1998).

The profiles of the experimental data of the temperature plot of the jet flames are shown in figure 4.3(a), while in figure 4.3 (b), the plot of the root mean square (RMS) temperature versus the radial distance is shown. These profiles aid in visualising the symmetry of the temperature fluctuations, and the level of turbulence in a diffusion flame. Figure 4.3 (a) shows how the fluctuations in the temperature develops from the near-burner location to the downstream region of the jet flame. In turbulent flames, hot and cold eddies are generated. The thermocouple captures the signal of these eddies and records the signal as the temperature of the flame at that location. Depending on the instantaneous signal received at a particular location, the recorded flame temperature may be higher or lower at that location. In addition, fluctuations in the temperature may be caused by the differences in the local concentration of the gas, which leads to fluctuations in the reaction rate. This implies that the thermocouple records temperature signals which coincide with the differences in the reaction rate, which means that as the reaction rate fluctuates, the thermocouple captures this fluctuating temperature reading at that location.

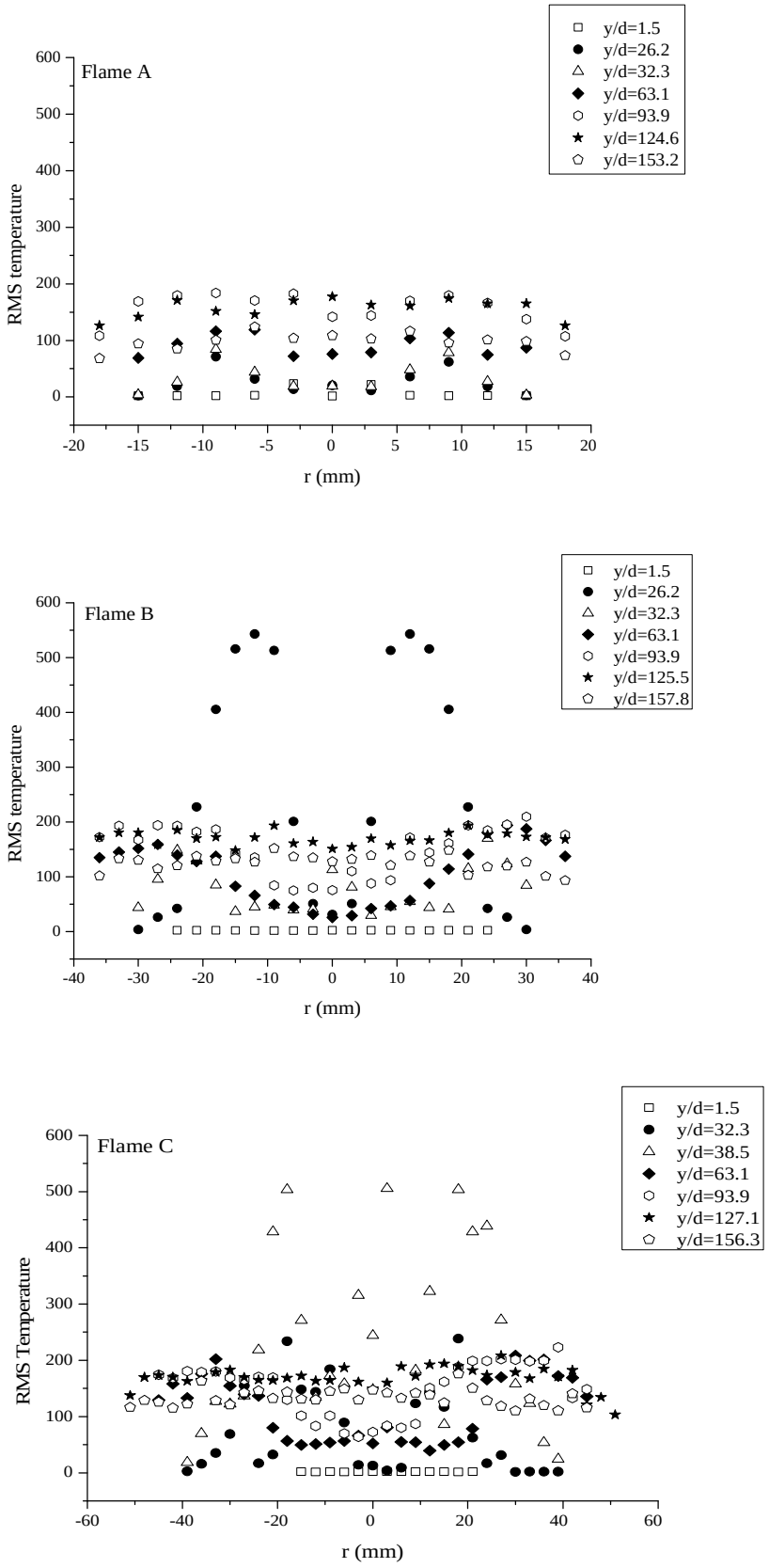

Figure 4.3 (b) Plots of the RMS temperature fluctuations as a function of the radial distance for the three jet flames investigated.

The degree of turbulence in a flame determines the degree of the temperature fluctuations at a particular location (Lenz and Günther, 1980). It is noteworthy to state that the straight lines observed at y/d=1.5 does not mean that there are no fluctuations at those locations; it only shows that in relation to other downstream locations, the level of the fluctuations is very small. In flames A to C, at axial locations above y/d=1.5, turbulence is seen to be developing, where the level of the fluctuations appear to be smaller. The fluctuation in flame A is observed to be progressing gradually from the flame base, where the flame is attached to the jet nozzle, and increases downstream to the tip of the flame.

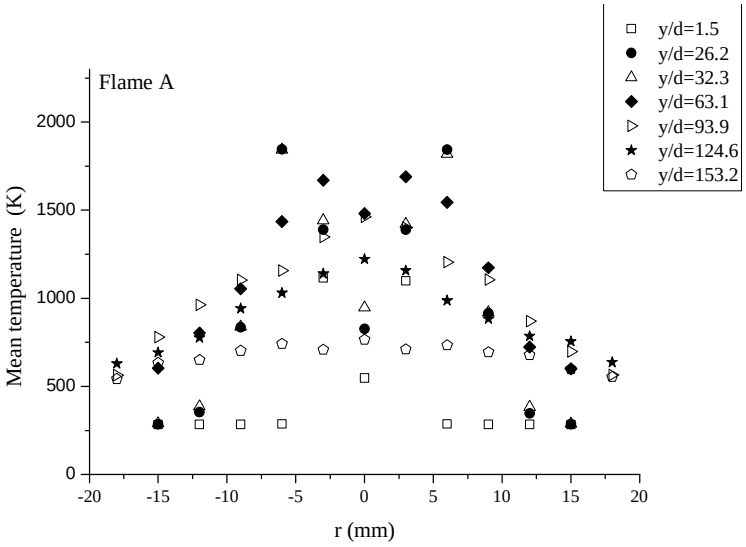

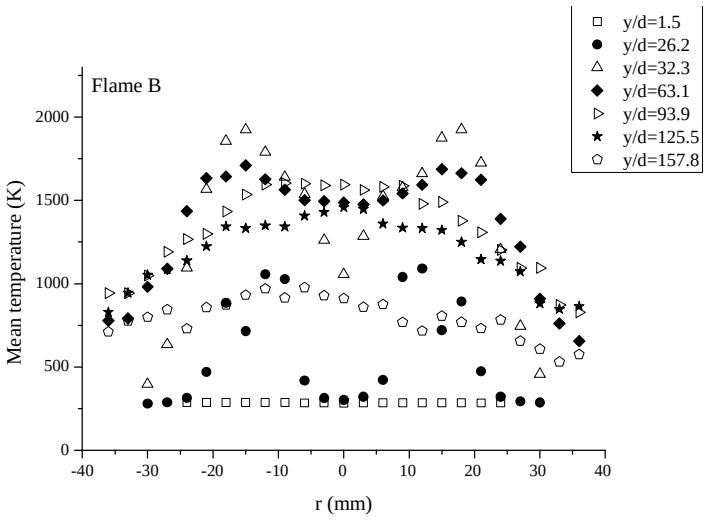

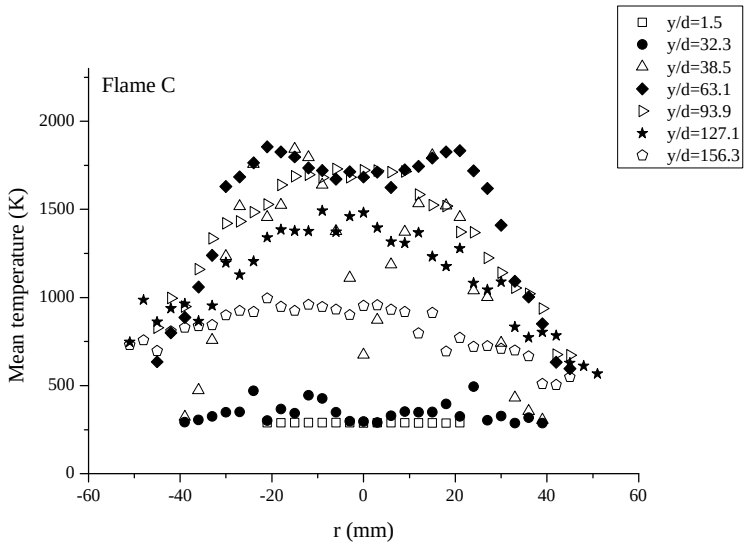

Figure 4.4 Mean flame temperature of flames A, B, and C.

The differences in the shape of the temperature profile of the flames at different axial locations are an indication of the level of air entrainment into the flame at those locations (Gollahalli, 1998), with higher dilutions observed in far-nozzle locations of high air entrainment. In flames B and C, which are the lifted flames, it is observed that the profile of the temperature fluctuations appear to be the same, at some locations, and vary at other locations. In flames B and C, at y/d=1.5, the mean temperature at these un-reacting locations is ambient temperature. The fluctuations are very small and this is because there is no visible flame at these locations, and this is because at these locations, the fuel has just issued from the burner nozzle, and the flame's base lies further downstream from the fuel jet nozzle, where the flame stabilises. In figure 4.3 (a), the major difference between the temperature profiles of flames B and flame C is at y/d= 26.2 and y/d=32.3 for flame B, and at y/d=32.3 and y/d=38.5 for flame C. At downstream locations above the locations of the major differences in the flame temperature fluctuations, the symmetry of the fluctuating temperature profile are not remarkably different between flames B and C, despite the large differences in the jet velocity, and hence the Reynolds number of both flames. The difference in the level of the temperature fluctuations in flames B and C are an indication of the degree of the oscillations observed at the flame base of both flames, where the oscillations in flame C is a reflection of the level of the turbulence in that jet flame. In figure 4.3 (b), for flame B, the highest fluctuation in temperature is at y/d=26.2, while for flame C, the highest fluctuation is at y/d=38.5. The difference in the axial location of these flames where the fluctuations occur is due to

the difference in the lift-off distance, which scales proportionally with the fuel jet velocity, as observed by Kalghatgi (1984). The temperature measurements were performed for each of the flames B and C at the plane of the visible flame's stabilisation location where the lift-off of the visible flame was clear, and at 20 mm above the plane of the visible flame. The choice of this additional small step-sized axial location of the flame base was an attempt to accurately characterise and record the level of the fluctuations in the temperature at those locations.

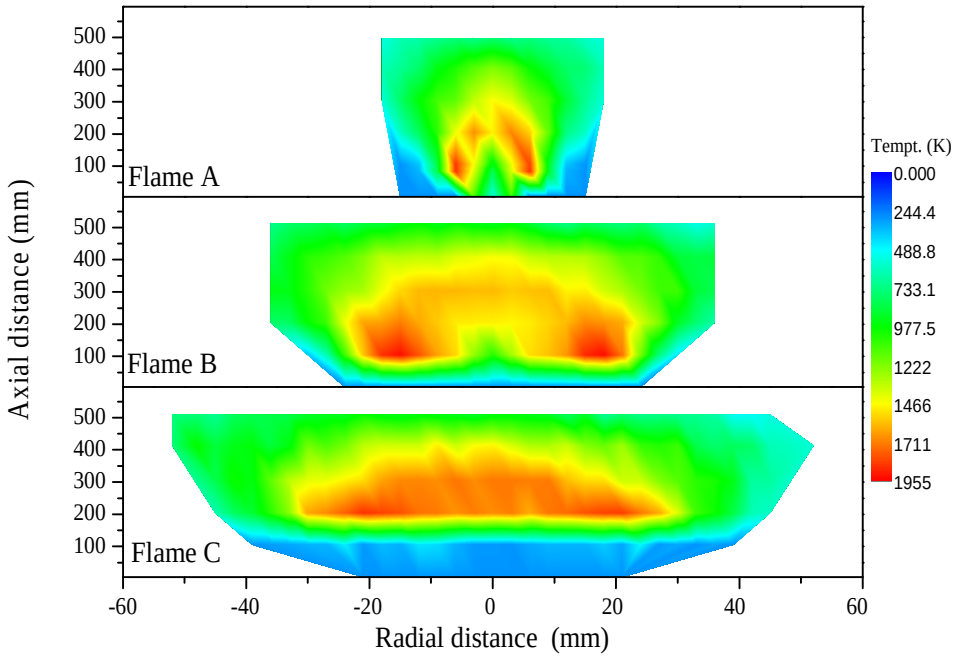

Figure 4.5 (a) Contour plots of the three jet flames showing one axial temperature measurement at the stabilisation zone for the two lifted cases.

The fluctuations in temperature is a consequence of the large oscillations observed at these locations, due to an increase in the fuel flow rate, the entrainment of ambient air, and the degree of partial-premixing, leading to turbulence at these locations. The air entrainment observed at this location is expected because the flame lies between the plane of the base of the lifted flame and the burner port. Of interest are the changes observed at the location in the lifted flames where the flame stabilises downstream of the flame base, as shown in figures 4.5 (a) and 4.5 (b).

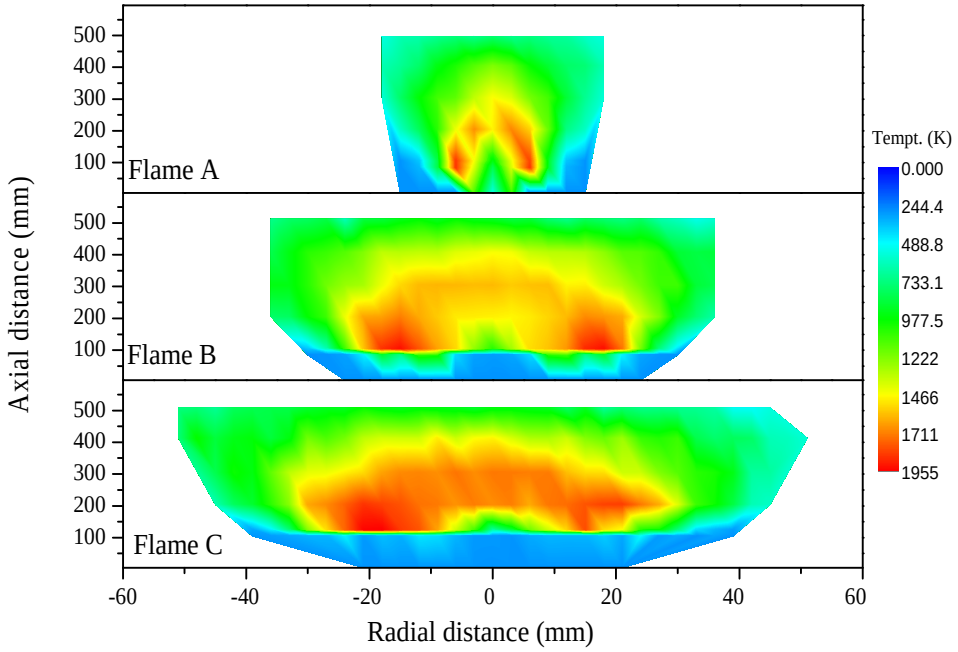

Figure 4.5 (b) Contour plots of the three jet flames showing two axial temperature measurements at the stabilisation zone for the two lifted cases.

In figure 4.5 (a), one axial temperature measurement was performed in the stabilisation zone for each of the lifted flames, B and C, while two temperature measurements were made in the stabilisation zone for each of the lifted flames, B and C, as shown in figure 4.5 (b).It was observed that the extra axial temperature measurements made for each of the flames, B and C, in figure 4.5 (b), at y/d=26.2, and at y/d=32.3, respectively, showed a different trend in the contour plot shown in figure 4.5 (b), as against figure 4.5 (a). The contour plots were made using OriginPro 8.6 from the experimental data which was generated. A comparison of the contour plot of flame B in figures 4.5 (a) and 4.5 (b) show that the fluctuation in figure 4.5 (b) is captured because of an additional measurement made at y/d=26.2, which is just 20 mm downstream of the flame next to y/d=32.3. Similarly, a comparison of the contour plot of flame C, which is shown in figures 4.5 (a) and 4.5 (b), captures both the hollow shape of the flame found in the upstream location of the flame in figure 4.5 (b), which is not captured in figure 4.5 (a), and an overlapping of the trends of the flame temperature, found in figure 4.5 (b), which is also not captured in figure 4.5 (a), indicating that at y/d=32.3, there is not a substantial difference in the mean temperature profile (see figure 4.4, Flame C) of that flame, but an inclusion of the RMS temperature profile in figure 4.3 (b) shows a

very large fluctuation in the temperature at that location. In fact, the fluctuation is so large that at the flame base, the temperature fluctuation in the lifted cases – flames B and C, at y/d =26.2 and y/d=38.5, respectively, is about 550K, which is an indication of turbulence, which is in line with the observations of Chen *et al*. (1992). This confirms that the mean measurements of quantities such as temperature, species concentration, velocities, etc., are not totally representative of the conditions taking place in turbulent flames, since the dynamics of the turbulence needs to be accounted for. However, because of time constraints, available resources, and the vast amount of data to be generated, most investigators report the mean values of quantities. Nevertheless, these mean values provide a picture of the basic features of the profiles of the quantities to be investigated, where conclusions may be made (Birch *et al*., 1989). The composition of species will be discussed in the next section.

4.5 SPECIES COMPOSITION

The in-flame and the post-flame axial and radial variation of the concentration of each of the major species will be discussed in subsequent sections.

4.5.1 O_2 CONCENTRATION PROFILE

The mole fraction of O_2 for the three jet flames are shown in figure 4.6, and the contour plots of these flames are shown in figure 4.7. In all three jet flames, the mole fraction of O_2 depletes from the ambient surrounding towards the centreline of the flame. For the attached case, the minimum mole fraction of O_2 is zero at the flame centreline, and increases radially outwards away from the flame, and axially at downstream regions above the fuel jet nozzle. At y/d=1.5, which is the near-nozzle location, the lowest O_2 concentration there coincides with the highest fuel concentration, indicating that the fuel has just issued and there is no combustion at that location. At downstream locations, the O_2 mole fraction is seen to be increasing up to the flame tip, due to the entrainment of air into the flame. At y/d=153, which is the tip of the flame, there is no significant difference in the concentration of O_2, which is due to the indifference in the entrainment of air at that location and a “hump” structure does not exist . However, moving radially towards the flame, at other downstream locations from the ambient surrounding, the O_2 concentration is observed to be increasing outside the flame, while depleting in the flame, thus indicating a mixing of the fuel and air at a molecular level at those locations,which is typical of diffusion flames.

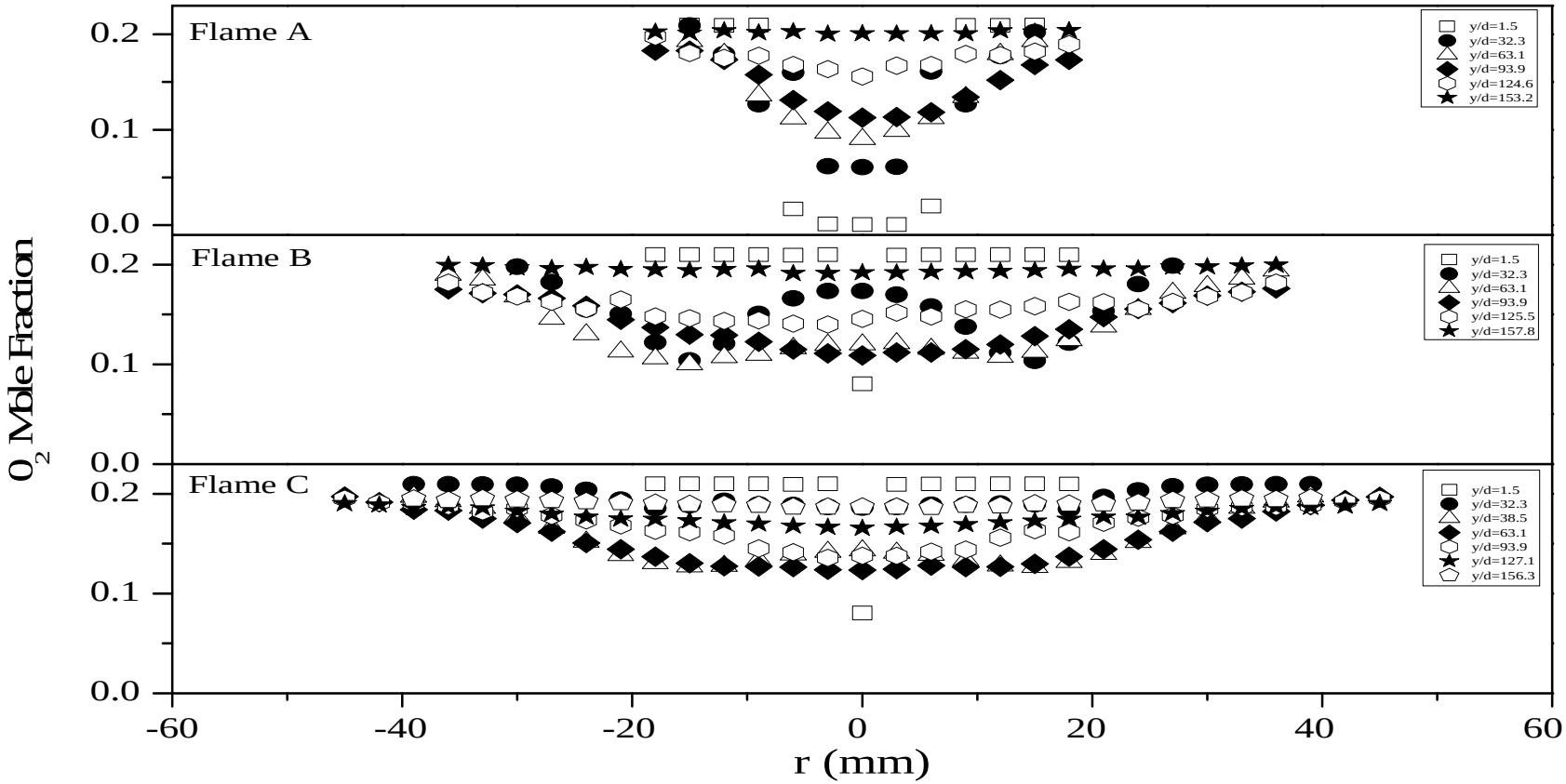

Figure 4.6 The O_2 mole fraction as a function of the radial distance at various stream-wise locations for the three jet flames.

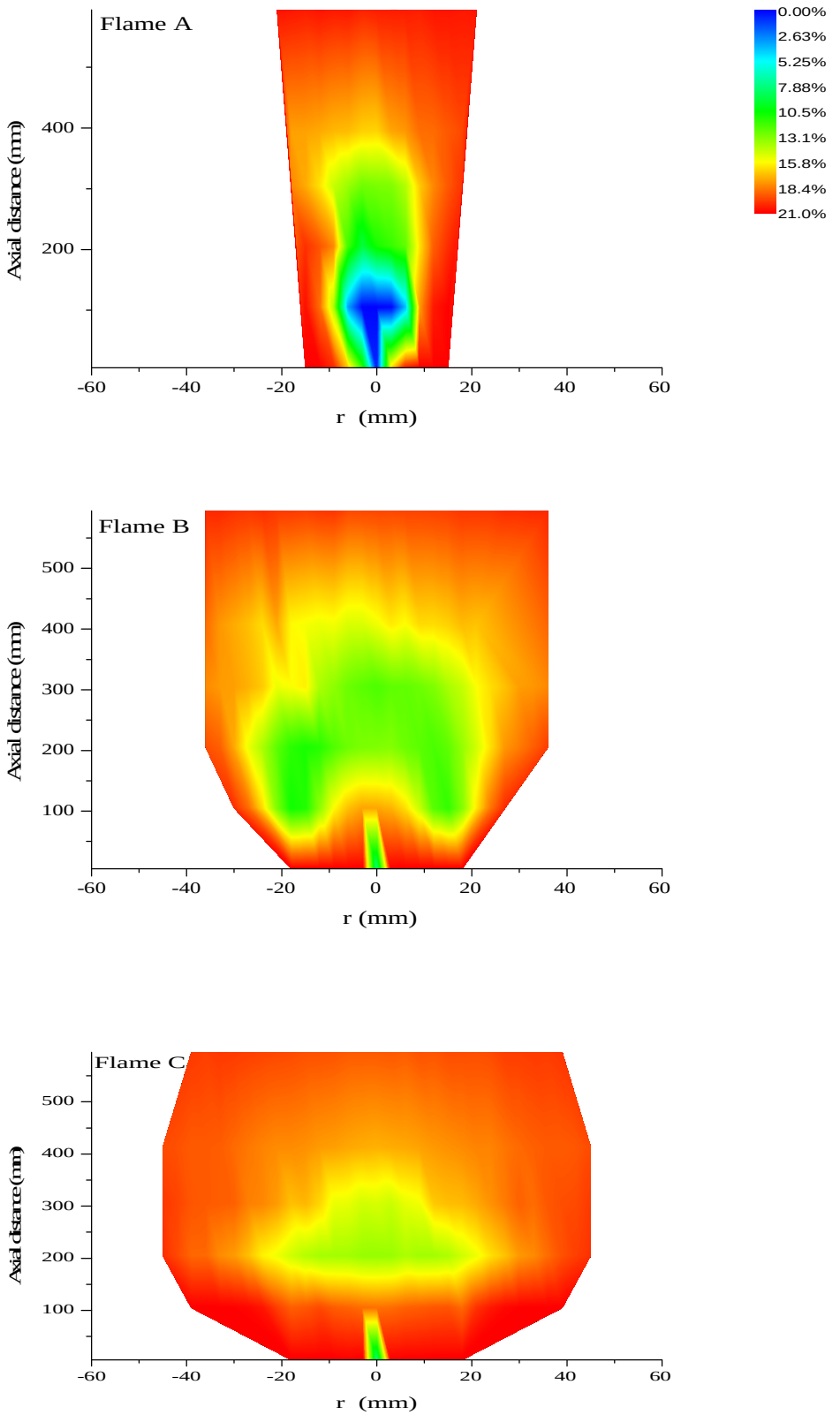

Figure 4.7 Contour plots of O_2 concentration for the three jet flames.

For the lifted cases, a significant concentration of O_2 was observed at the centreline of the flame because the flame had just lifted, creating room for the entrainment of air from the surrounding, and a mixing of the fuel with the entrained

air, thus suggesting the premixing of air and fuel at that location. The high entrainment of air in the lifted cases promote the oxidation of soot precursors in the flame, leading to a reduction in the soot concentration at higher flow rates in the lifted flame and this is consistent with the observations of Gollahalli and Zadeh (1985).

4.5.2 CO CONCENTRATION PROFILE

The profile of CO is presented in figure 4.8, while the contour plots of the jet flames are presented in figure 4.9. It is observed that the flame was symmetrical, which is evident in the mole fraction profile shown in figure 4.8 and in the contour plot. CO is an indicator of the degree of incomplete combustion (Gollahalli, 1998), and in flares, it indicates the level of the combustion efficiency of the flare (Strosher, 2000). In all the three cases investigated, incomplete combustion occurred when there was insufficient O_2 which was required to oxidise CO to CO_2.

In addition, in all the three jet flames, the concentration of CO was lower at the near-burner and the far-burner regions of the flame than mid-flame. This is because of the entrainment of oxygen downstream of the flame, which causes a rapid oxidation of CO at that far-burner location, as expected (Choudhuri *et al*., 1998). A view of the CO profile of these flames in figure 4.8 show that the peak CO concentration is recorded at radial locations near the flame-front. This region also coincides with the location of high CO_2 since CO can easily be converted to CO_2 when there is sufficient air, temperature and mixing (Bussman and Baukal, 2009).

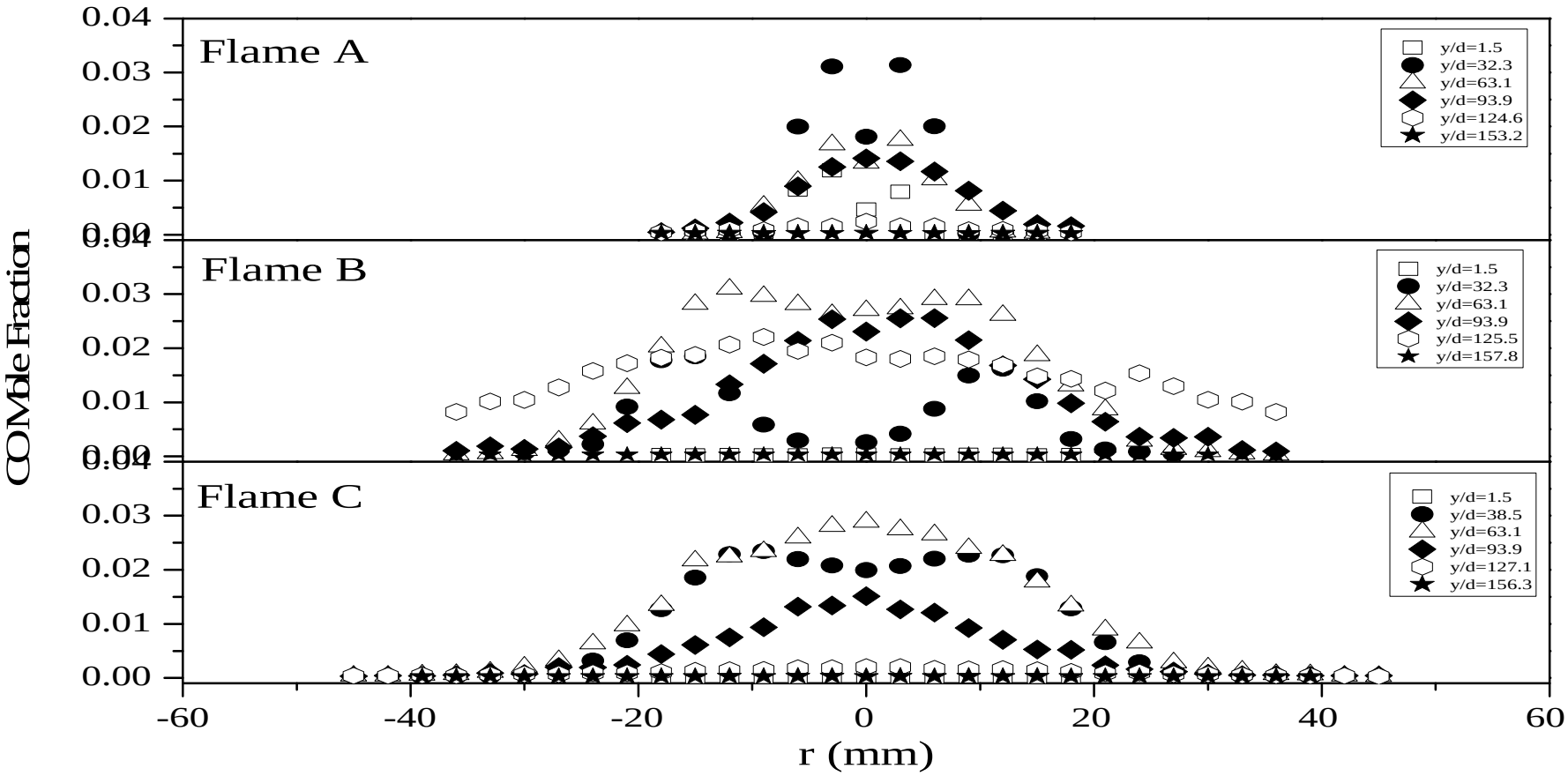

Figure 4.8 The CO mole fraction as a function of the radial distance at various stream-wise locations for the three jet flames.

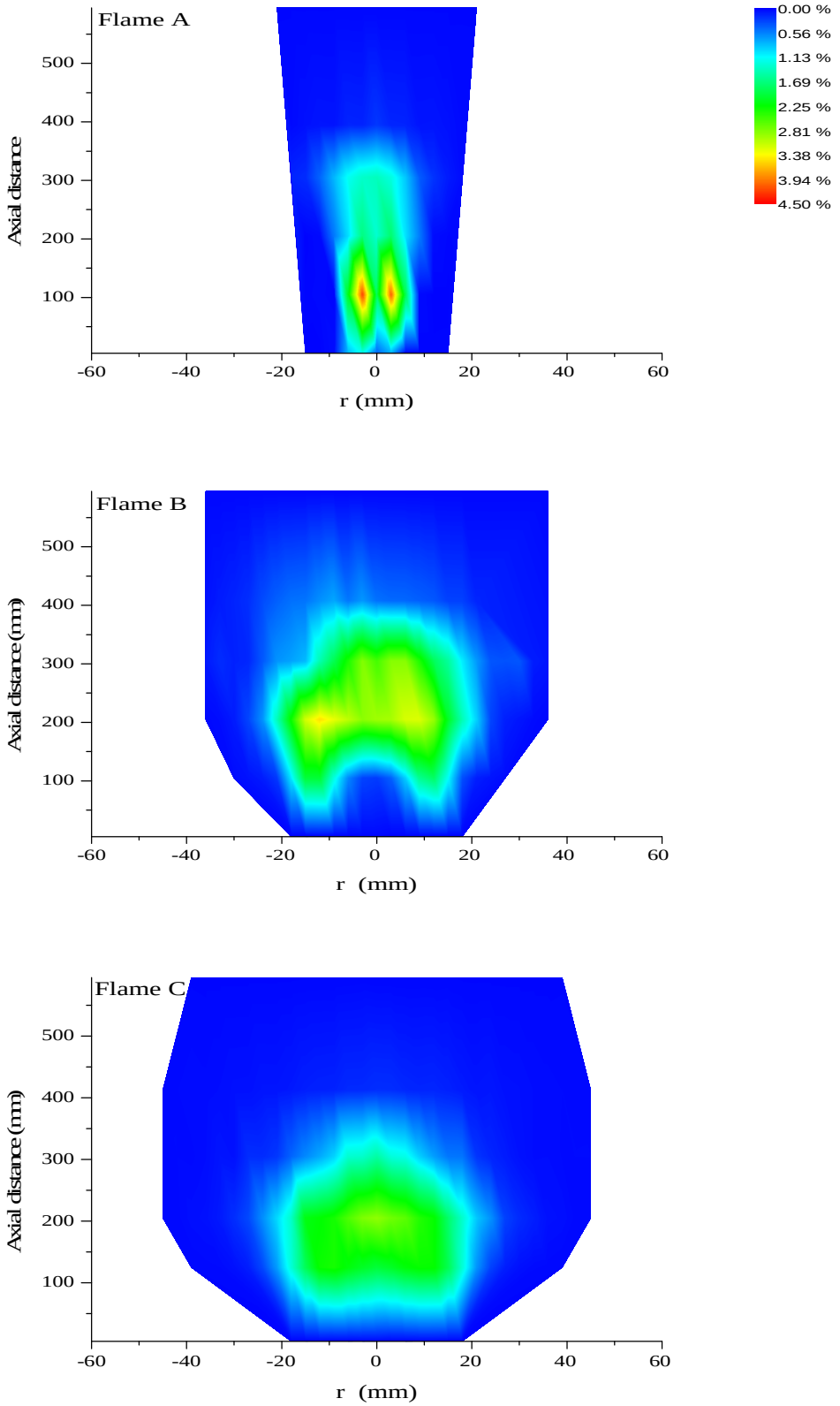

Figure 4.9 Contour plots of CO concentration for the three jet flames.

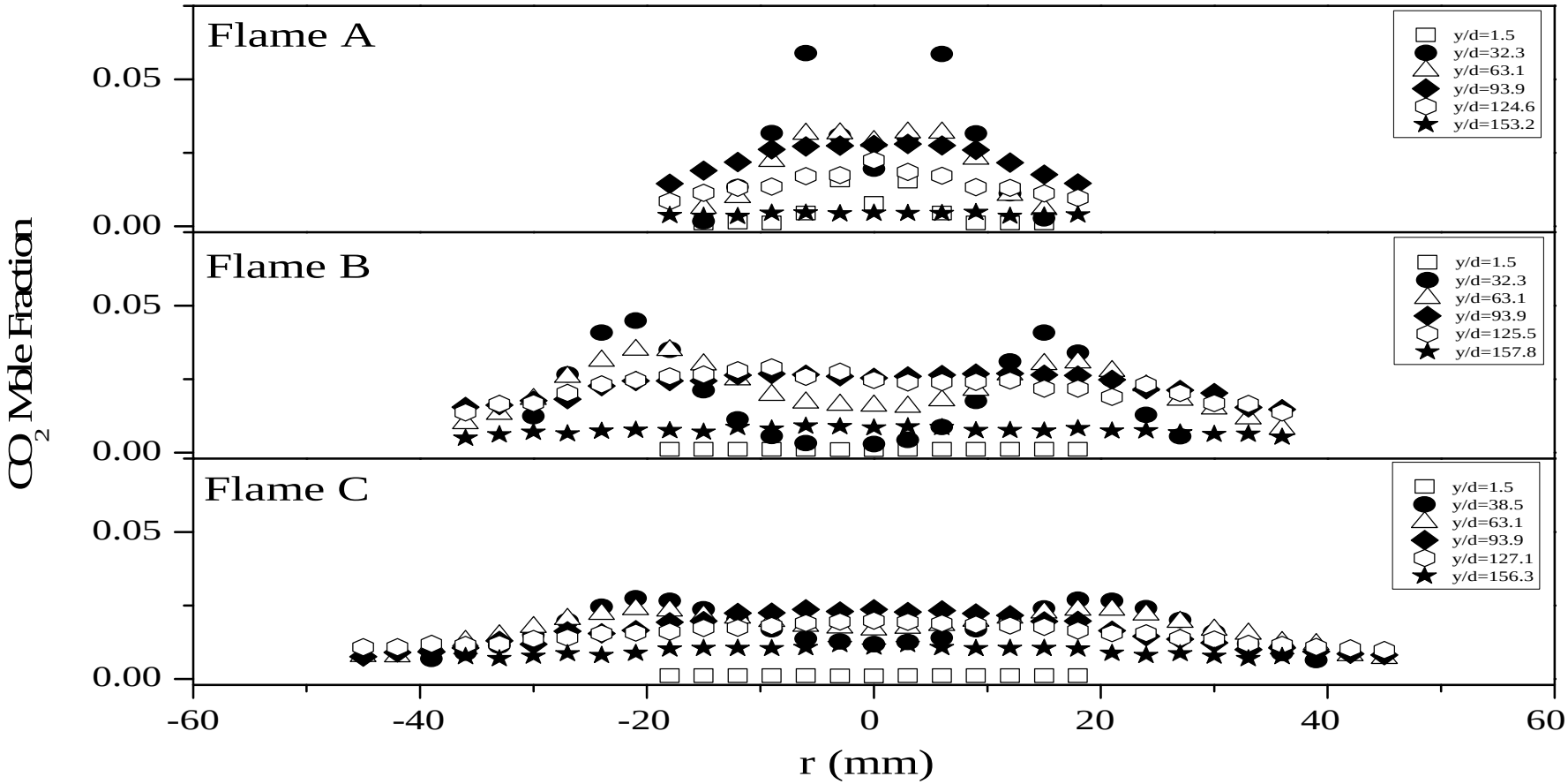

Figure 4.10 The CO_2 mole fraction as a function of the radial distance at various stream-wise locations for the three jet flames.

4.5.3 CO_2 CONCENTRATION PROFILE

The concentration profile of CO_2 is shown in figure 4.10. CO_2 is an indicator of the completeness of combustion. In each of the jet flames, the maximum concentration of CO_2 was recorded at the flame front, which coincides with the location of the highest temperature in the flame, and the location where the fuel and air were sufficient for combustion to take place, yielding CO_2 and H_2O as the products of complete combustion. A comparison of the CO_2 profile and the temperature profile for the three jet flames show a similarity in their trend. This is due to the effect of the stoichiometry and the flame temperature on the formation rate of CO_2, as expected (Choudhuri and Gollahalli, 2000). CO_2 can also be formed when CO reacts with sufficient O_2.

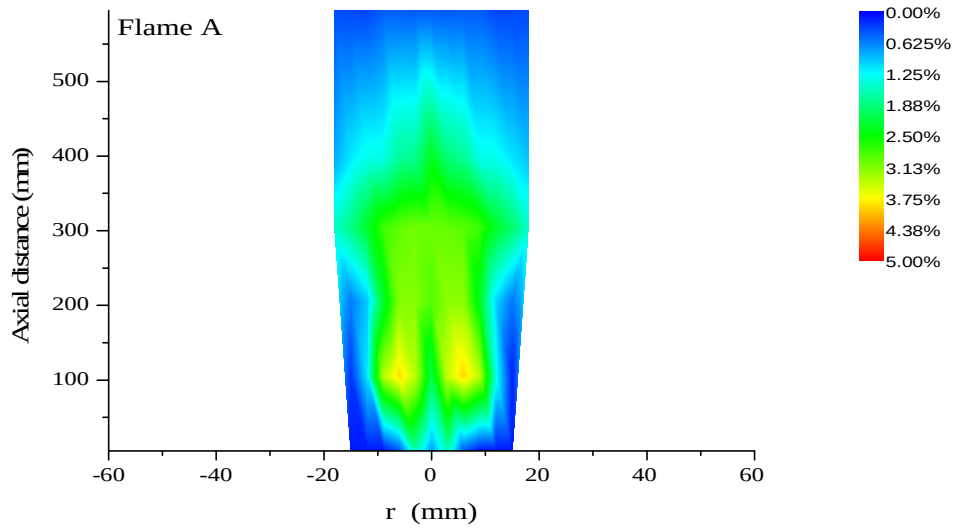

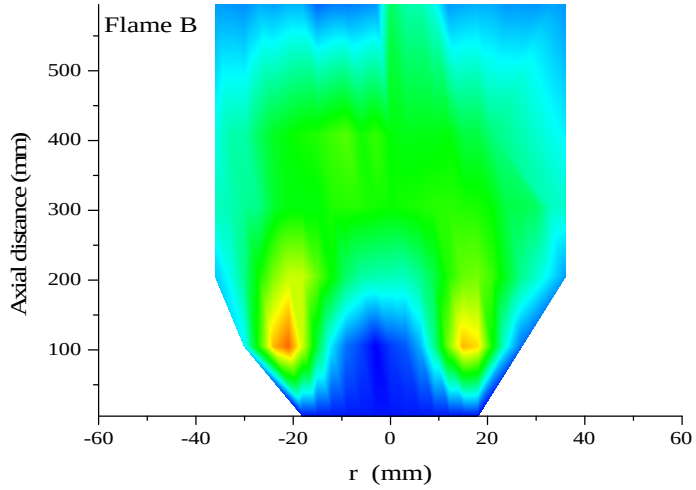

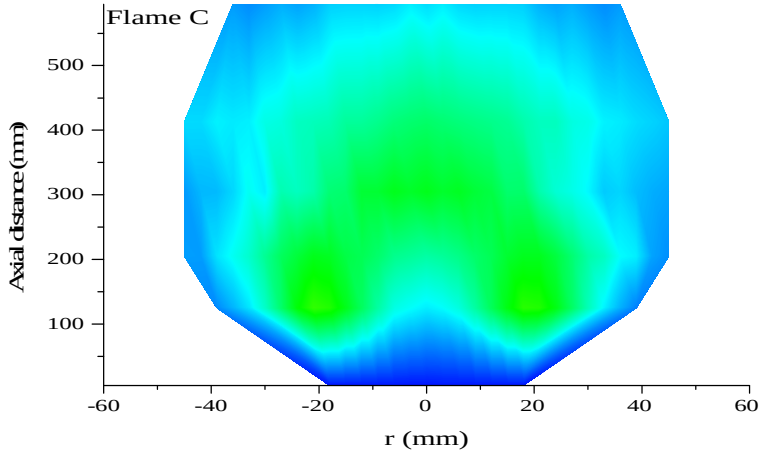

Figure 4.11 Contour plots of CO_2 concentration for the three jet flames.

This is also evident in the jet flames where the locations of high O_2 coincides with regions of CO, where CO_2 was formed. Similarly, the attached flame exhibited a "hump" structure which was very steep at the near-nozzle region and became less steep downstream, and eventually flattened out at the tip of the flame, indicating the level of mixing at those locations, which is marked by the concentration of the fuel and the oxidant at that location. An off-axis peak in the CO_2 concentration was recorded at all locations in the jet flame, which is an indication of the location of combustion at the flame front, except at the far-burner location, in the attached flame and at the near-burner location of the lifted flame. This is expected because combustion had not occurred in the near-nozzle region, therefore high levels of combustion would not be expected, with the low temperature at that location.

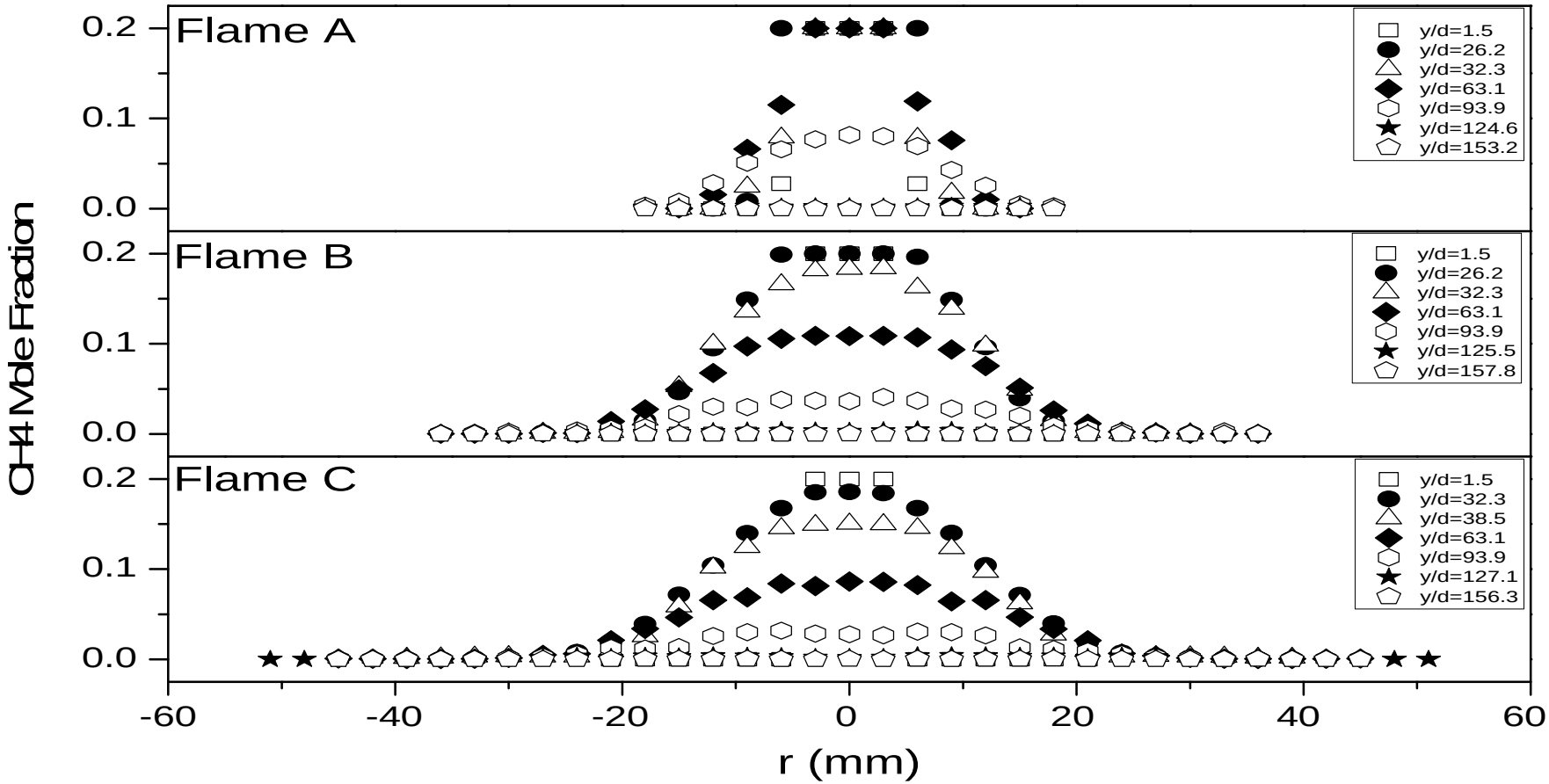

Figure 4.12 The CH_4 mole fraction as a function of the radial distance at various stream-wise locations for the three jet flames.

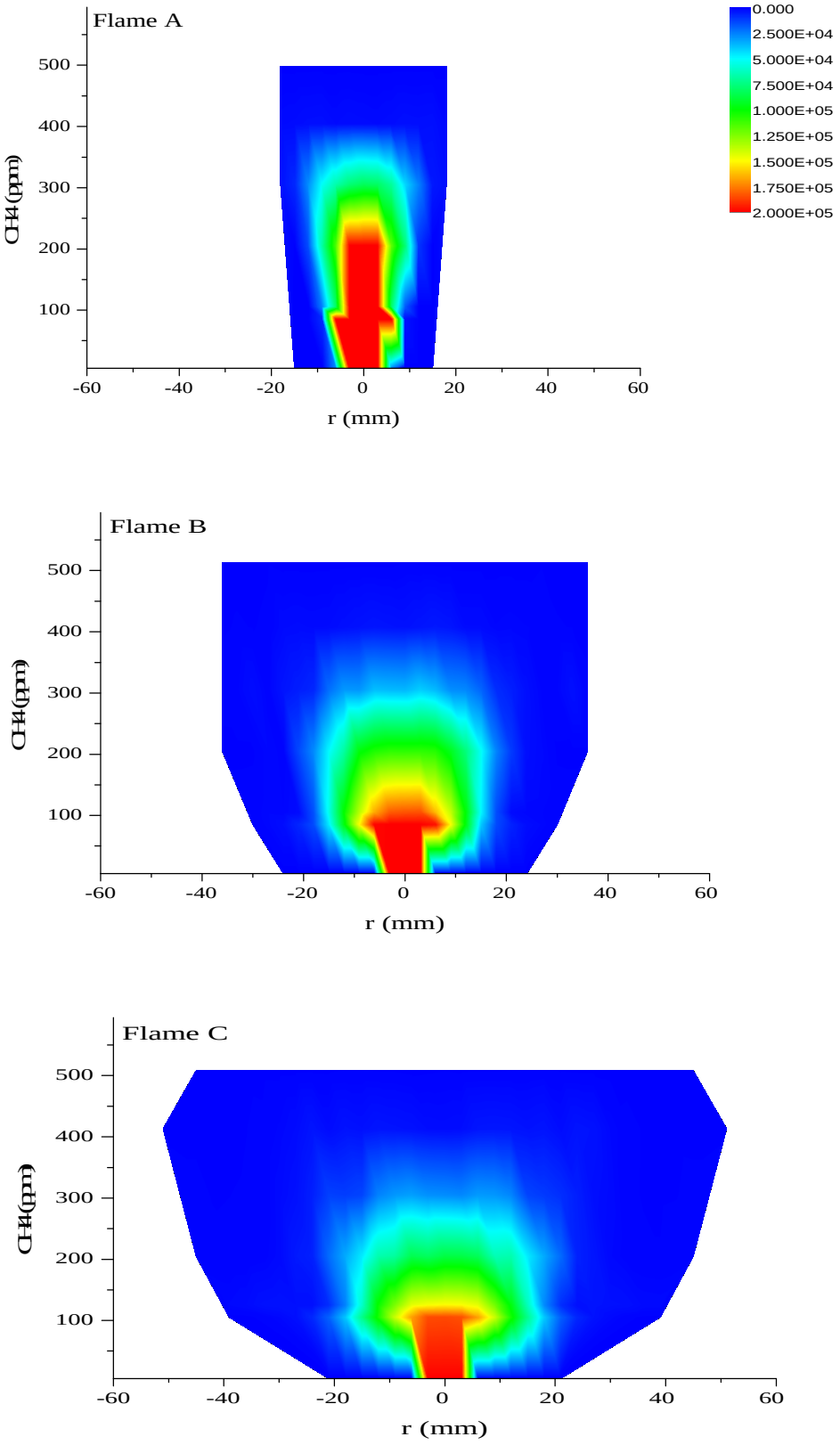

Figure 4.13 Contour plots of CH_4 concentration for the three jet flames.

4.5.4 CH_4 CONCENTRATION PROFILE

The concentration profile of the fuel is shown in figure 4.12. In the three jet flames, the highest concentration of the fuel was at the jet centreline, in the near-nozzle region of the jet. This is a characteristic of diffusion flames where the peak mole fraction is observed on the jet centreline and at the near-nozzle location, and this is because it is the closest upstream location where the fuel issues. A contour plot of this fuel distribution is shown in figure 4.13. A reduction in the mole fraction is observed at locations downstream of the three jet flames, with the highest mole fraction recorded at the jet centreline, while depleting radially towards the flame front, suggesting that the mixing and the combustion occurs at these downstream locations. The difference in the mole fraction on the centreline of both the attached and the lifted flames is that at locations above the near-nozzle location, the mole fraction in the former is greater than the latter. This is because mixing is more enhanced in the latter than in the former, due to turbulence, thereby leading to a faster rate of consumption of the fuel, and combustion occurring at the flame front, where there is sufficient air and fuel.

4.5.5 H_2O CONCENTRATION PROFILE

H_2O, like CO_2 is a product of combustion, and hence have a similar concentration profile, as seen in figure 4.14. In the attached and lifted cases, the maximum molar concentration of H_2O were observed mid-flame, at the flame front, as expected. This location coincides with the location of the product formation, and exhibits similarities with CO_2. In full-scale flares, H_2O in the form of steam is used to suppress smoke, by injecting steam into the flame at high velocities (Manning and Thompson, 1995). Similarly, it has been reported that H_2O in the form of moisture which is present in the combustion air may be used to reduce NOx, and this is because H_2O reduces the flame temperature by absorbing the heat from the flame, thereby reducing the thermal NOx emissions. However, care must be taken to avoid the reduction of the thermal efficiency of the flare by optimising the flare to achieve smoke suppression and NOx reduction. The effect of the humidity on the NOx formation on low- and high-NOx burners has been investigated (Bussman and Baukal, 2009). However, this is beyond the scope of the present investigation.

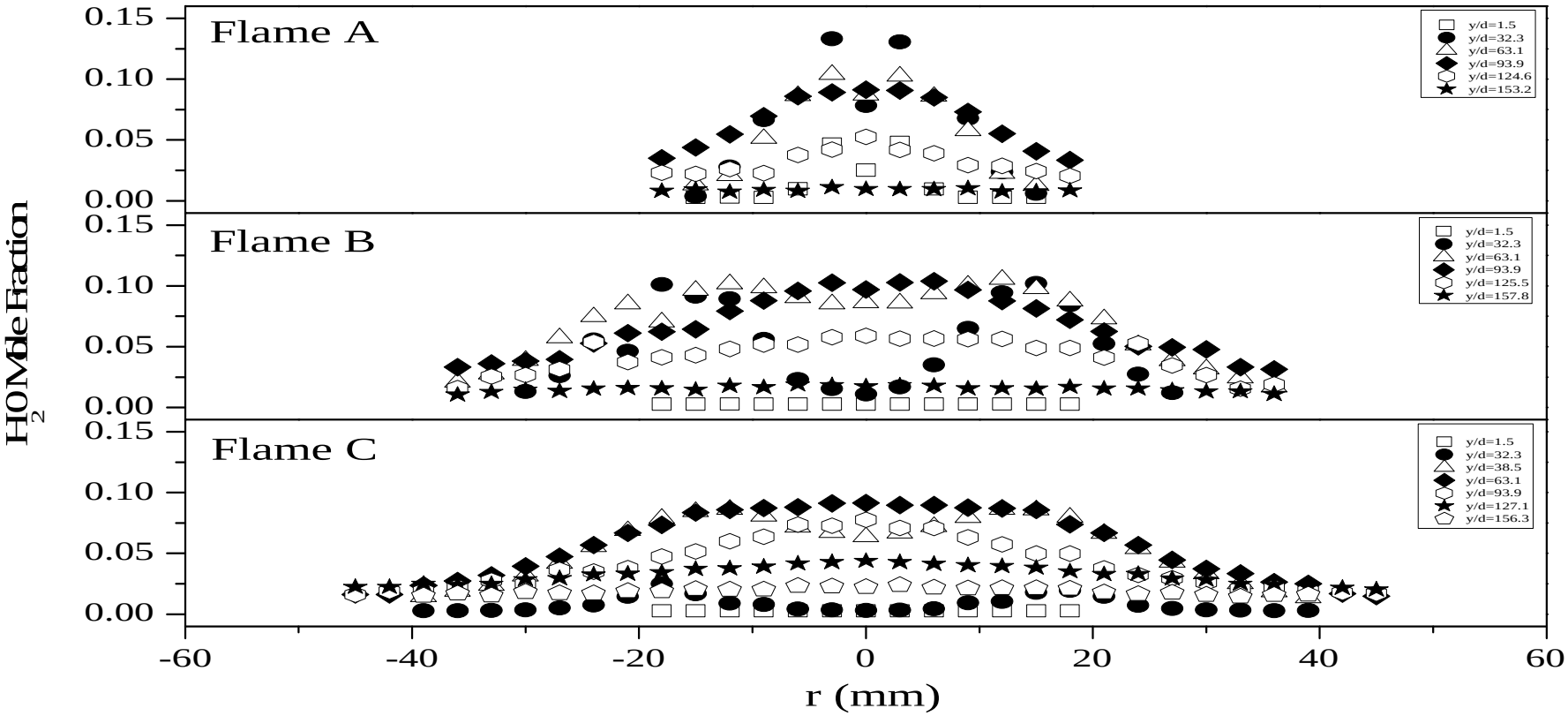

Figure 4.14 The H_2O mole fraction as a function of the radial distance at various stream-wise locations for the three jet flames.

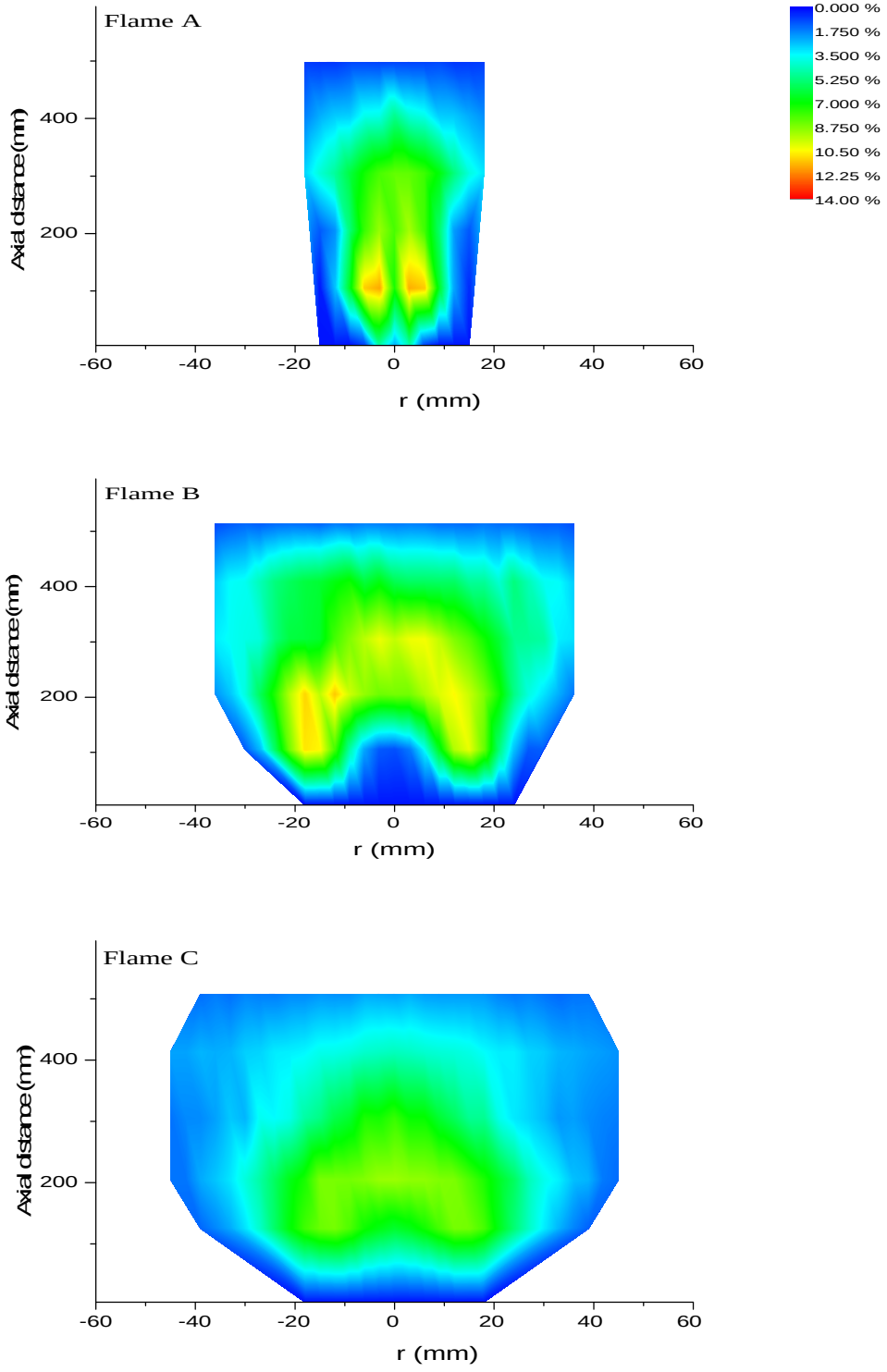

Figure 4.15 Contour plots of H_2O concentration for the three jet flames.

4.6 SPECIES MIXTURE FRACTION

Diffusion flames are usually described by a mixture fraction space. It is not sufficient to report the molar concentration of the species alone. In order to gain an

understanding of the fuel-rich and the fuel-lean regions, and the region of stoichiometry in the flame, Masri and Bilger (1986) proposed an expression for the plot of the mixture fraction space which is given by:

$$\bar{\xi} = \frac{\left(\frac{12}{16.032}\bar{Y}_{CH_4}\right)+\left(\frac{12}{28}\bar{Y}_{CO}\right)+\left(\frac{12}{44}\bar{Y}_{CO_2}\right)}{\bar{Y}_C} \qquad (4.1)$$

Where the mean mixture fraction, $\bar{\xi}$, is a measure of the mass fraction of the atoms in a jet mixture in a flame and it may be calculated by a carbon atom balance based on the experimental data generated for the fuel, CO, and CO_2. Plots of the mole fraction versus the mixture fraction of CH_4, O_2, N_2, CO, CO_2, and H_2O, NOx, NO, NO_2 and temperature for the attached and the lifted flames are shown in figures 4.16 to 4.21, and figures 4.24 to 4.27 where the vertical dotted lines indicate the stoichiometric mixture fraction, which has a value of 0.055 for a methane - air jet flame (Bilger *et al*., 1990). For the fuel mean mixture fraction profile, the fuel-rich location is on the right hand side of the stoichiometric line, while the fuel-lean location is on the left hand side of the stoichiometric line.

In figures 4.16 (a) to (c), the plots of the mole fraction of the fuel versus the mean mixture fraction is presented for the three methane / air jet flames. In the attached case, it was observed that the highest molar concentration of the fuel was recorded at the near-nozzle location, which corresponds to the fuel-rich side of the stoichiometry, as expected. This is because the fuel has just issued and there is no oxygen present at that upstream near-nozzle location. Similarly, at the far-nozzle location of the attached case, there was a very little concentration of the fuel on the fuel lean side of the flame, with a molar concentration of 0.00013, compared with the 0.2 molar concentration recorded at the fuel rich side of the stoichiometry, indicating that most of the fuel had been consumed at the downstream locations of the flame. A similar trend was observed in the lifted cases.

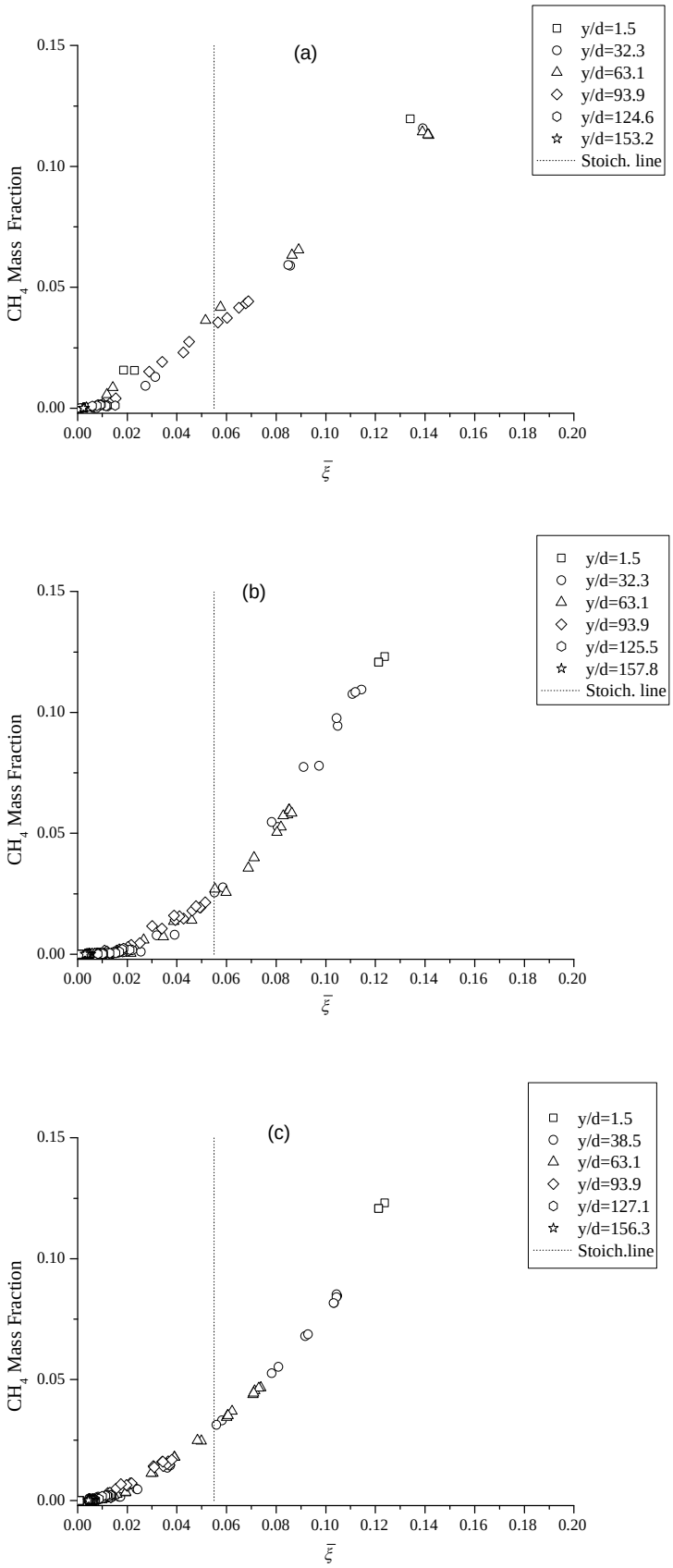

Figure 4.16 The CH_4 mass fraction as a function of the attached flame (a) A, and the lifted flames (b) B, and (c) C, respectively, at various downstream locations.

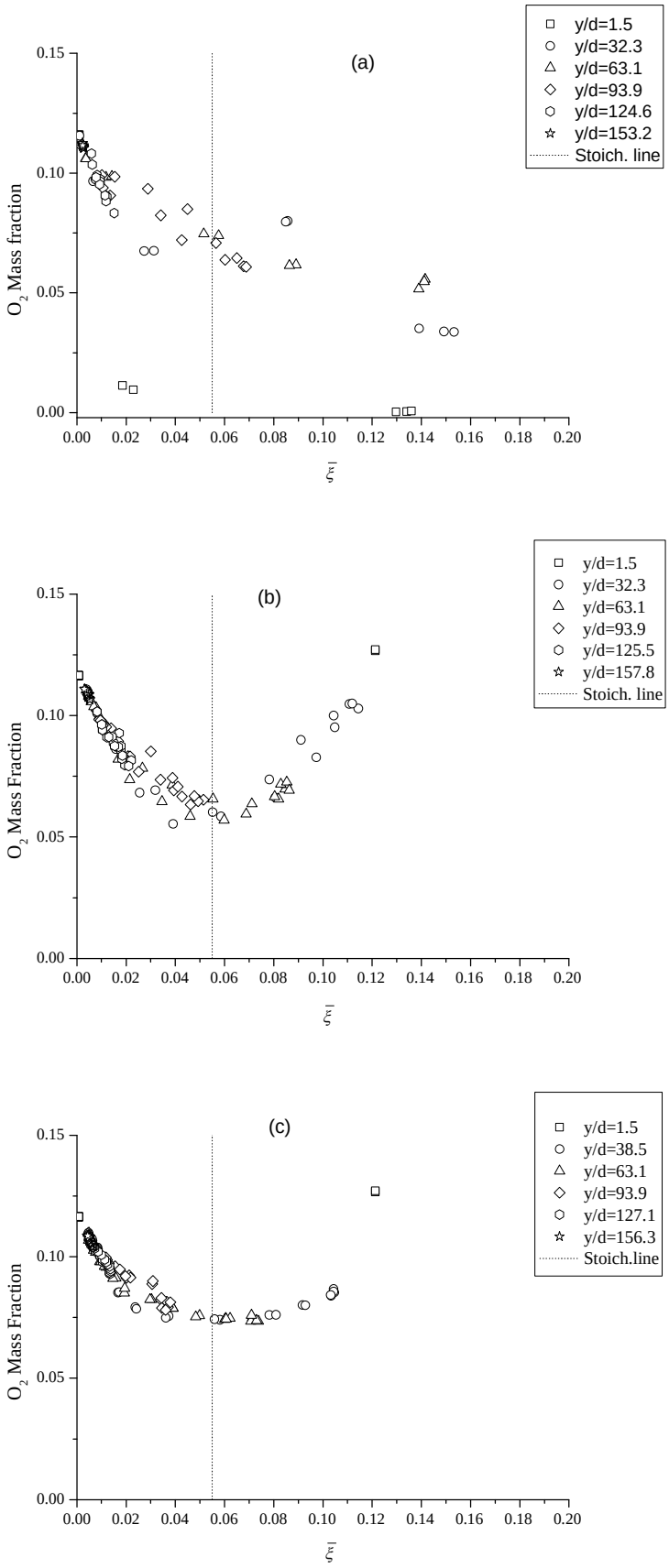

Figure 4.17 The O_2 mass fraction as a function of the attached flame (a) A, and the lifted flames (b) B, and (c) C, respectively, at various downstream locations.

In figure 4.17 (a) to (c), the mean mixture fraction profile of oxygen is shown. For the attached flame, there was no O_2 concentration on the jet centreline in the near-nozzle location, but moving radially away from the fuel jet centreline, the O_2 concentration was observed to be gradually increasing, as expected. This is because at the near-nozzle location, no O_2 is expected at the jet centreline, and this is because the fuel has just issued, but moving radially away from the jet, and therefore O_2 appears to be diffusing into the flame. However, a significant concentration of O_2 was observed at the downstream locations of the attached flame. In addition, a significant concentration of O_2 was present on the jet centreline of the lifted flames. This was due to the partial pre-mixing of the methane and the air in that near-nozzle upstream location. Similarly, at the near-nozzle location of the attached case, the O_2 profile had an "L-Shape" with the base of the "L" lying parallel to, and attached to, the abscissa of the mixture fraction plot, which indicates that the attached diffusion flame may be described by the mixture fraction space, as expected. However, the lifted cases exhibited a different trend in the mean mixture fraction profile. It was observed that the lifted flames were actually lifted above the abscissa of the mean mixture fraction coordinate, showing that the flames are lifted flames, as shown in figure 4.1. Even a physical inspection of the base of the profiles of the lifted flames show a higher lift-off of flame C than flame B, as also pictured in the photograph of figure 4.1, which shows that a plot of the O_2 molar concentration versus the mean mixture fraction may be used as a quick check of the flame regime (be it lifted or attached) of a diffusion flame. A similar trend has been observed by Howard (1998). The profile of the mean mixture fraction of N_2 is presented in figure 4.18 (a) to (c).

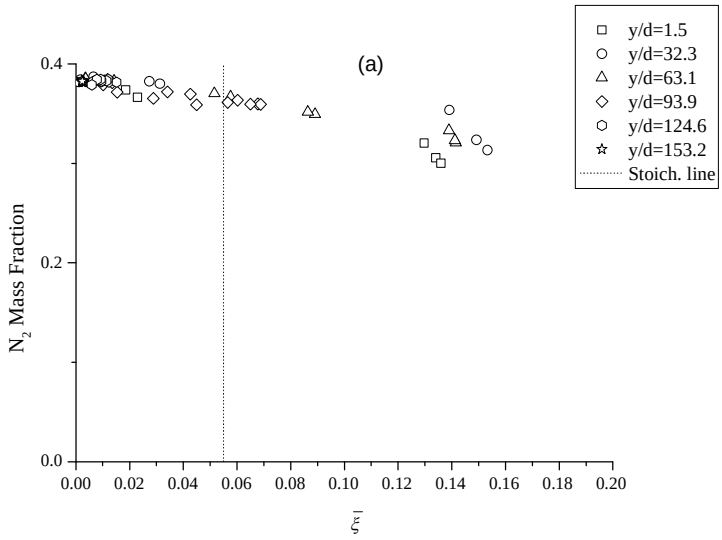

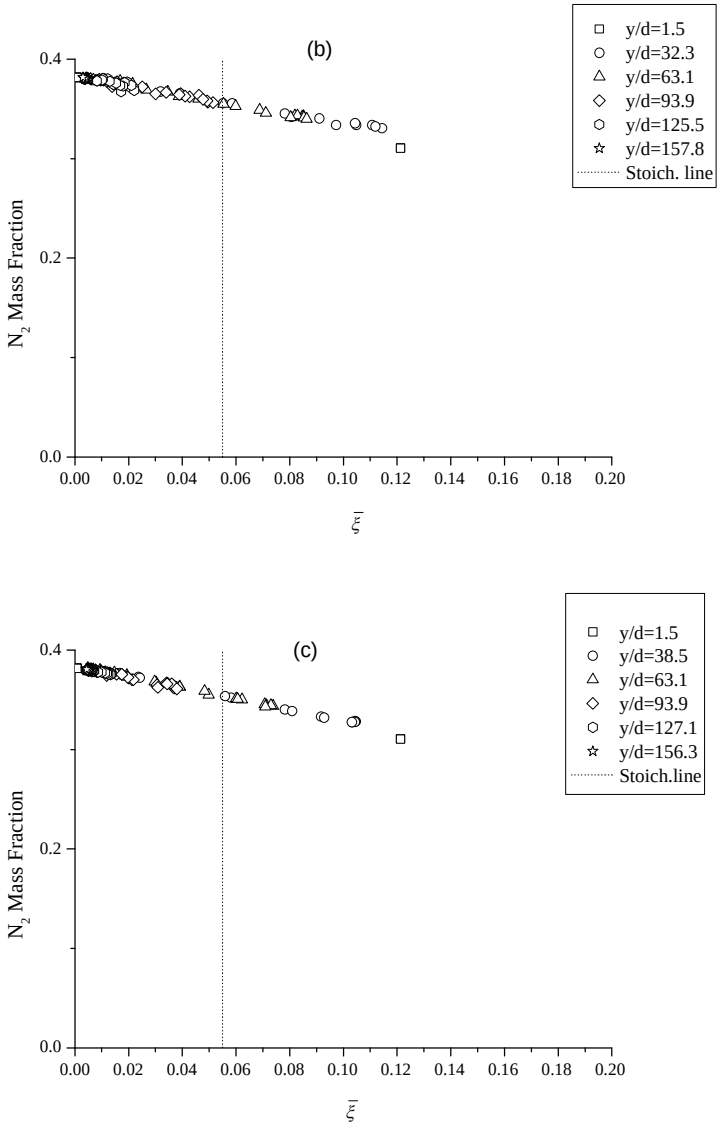

Figure 4.18 The N_2 mass fraction as a function of the attached flame (a) A, and the lifted flames (b) B, and (c) C, respectively, at various downstream locations.

In the cases investigated, the minimum concentration of N_2 in the flame was at the near-nozzle location of the flame, and at the centreline of the jet, (as it was also observed in the concentration of O_2), while the maximum concentration of N_2 was recorded at the far-burner locations of the flames. This is expected because in CH_4 / air combustion, both O_2 and N_2 are the major reactants, and the significant concentration of N_2 in the centreline of the jets at downstream locations far from the burner nozzle in the lifted flames support partial premixing, which contributes to the formation of NO at these locations, as will be discussed in section 4.7.

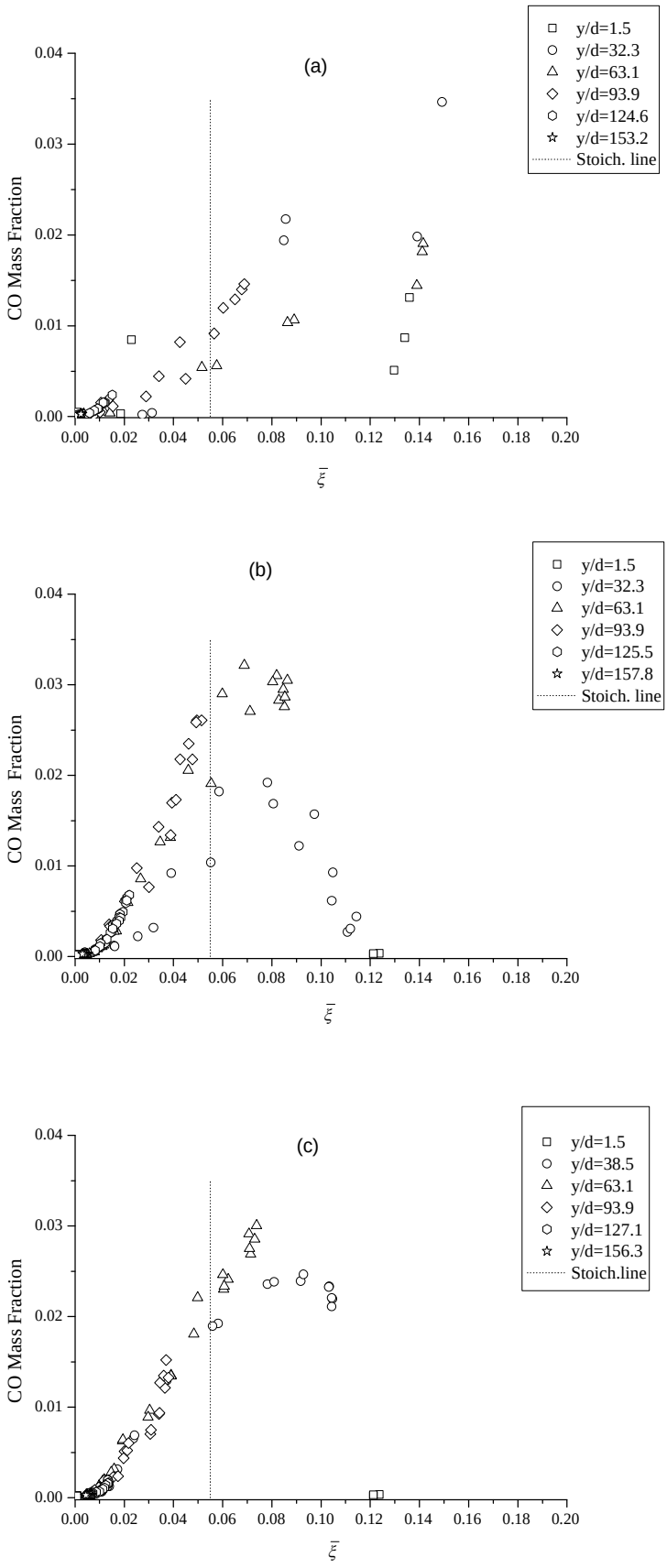

Figure 4.19 The CO mass fraction as a function of the attached flame (a) A, and the lifted flames (b) B, and (c) C, respectively, at various downstream locations.

The variation of the CO in a mixture fraction space for the attached and the lifted flames are shown in figure 4.19 (a) to (c). In all the cases investigated, the maximum molar concentration of CO was recorded at the fuel-rich side of the stoichiometric – an indication of incomplete combustion resulting from insufficient oxygen needed for combustion at those axial locations. However, the CO molar concentration was higher in the attached case than in the lifted cases. This is attributed to the insufficient oxygen entrained into the flame in the attached case compared to the lifted cases where the flame lift-off contributes to an additional entrainment of oxygen into the flame. In addition, it was observed that flame C had the least molar concentration of CO, followed by flame B, and then flame A. This is anticipated, because increased fuel flowrates lead to a higher air requirement for a complete combustion, and vice-versa. This explains the reason why in the CO mixture fraction plot, there is a greater concentration of CO on the fuel rich side of the attached flame, while in the lifted cases, the CO molar concentration is relatively lower than in the attached case, thus indicating a higher diffusion of O_2 into the lifted flames, and hence a lower molar concentration of CO. However, it is possible for CO to be converted to CO_2 when there is sufficient O_2, mixing, and temperature. The flame temperature and stoichiometry have been known to affect the rate of formation of CO_2 (Choudhuri and Gollahalli, 2000). Lower temperatures lead to a reduction in the emission of NOx. Similarly, lower temperatures also enhance the emission of CO (Bowman, 1992).

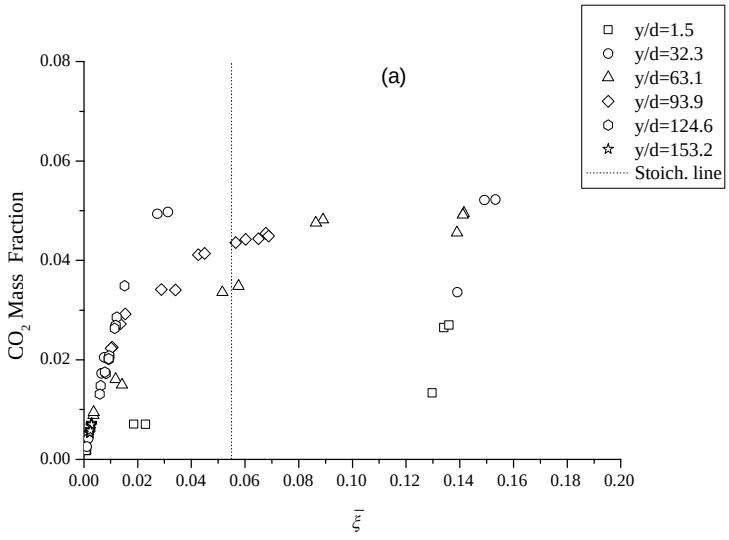

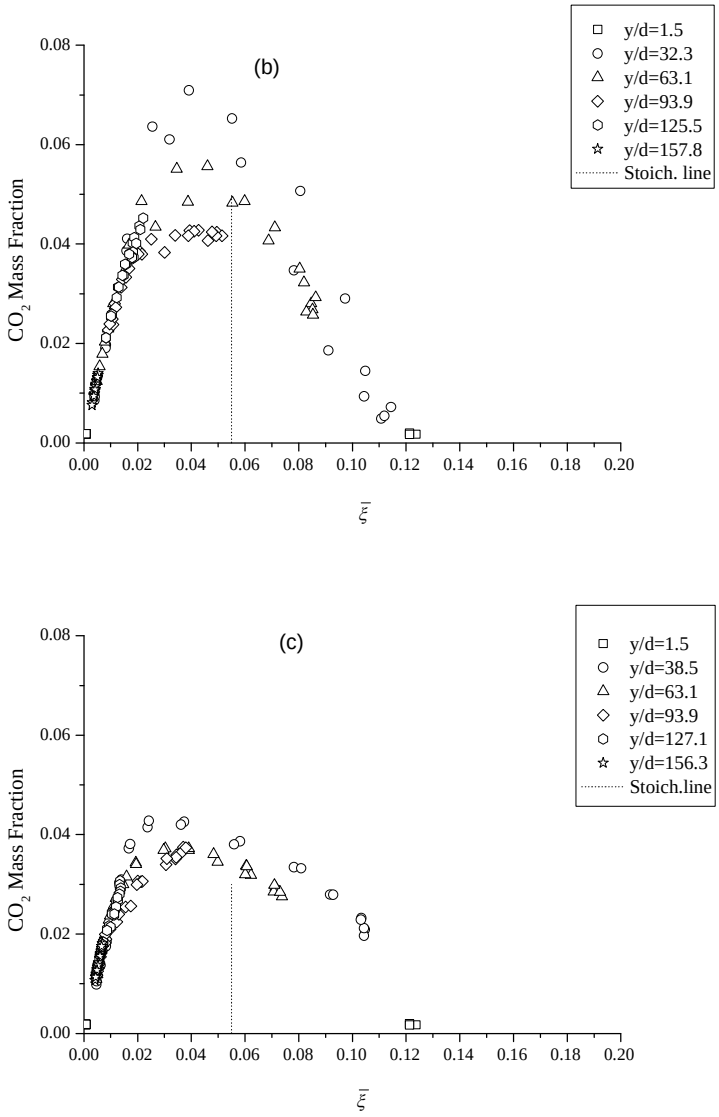

Figure 4.20 The CO_2 mass fraction versus mixture fraction for the attached flame (a) A, and the lifted flames (b) B, and (c) C, respectively, at various downstream locations.

Figure 4.20 shows the mixture fraction plot of CO_2 for both the attached and the lifted cases. The difference between these flames is that the mass fraction of the CO_2 was greater in the lifted cases than in the attached case, as expected, and also occurred at different sides of the stoichiometric in the flames. In the attached case, the peak molar concentration of CO_2 was observed at the fuel rich side of the flame, while in the lifted cases, the peak molar concentration of CO_2 was in the fuel lean side of the flame. This is because in the attached case, the molar concentration of CO is higher, as a result of an insufficient amount of O_2 needed to react with the CO to yield CO_2, thereby leading to a lower CO_2 molar concentration. In contrast, in the lifted cases, in the fuel-lean region, the lower molar concentration of CO reacts with

O_2 to yield a higher molar concentration of CO_2. Also, according to Bowman (1975), CO_2 may be formed either via the reaction between CO and OH, CO and HO_2, or CO and O_2, with the reaction between CO and HO_2 being significant in flames (Westenberg and deHaas, 1972), while the reaction between CO and OH is the principal reaction in hydrocarbon flames, which is also a likely reaction path for the formation of CO_2 in the flames investigated. A quick check of the concentration profiles reveal that the radial profile of O_2 is an inverse of the radial profile of CO_2. Similarly, the temperature of the flame follows the same trend as the CO_2 profile, and since CO_2 and H_2O are products of combustion, they follow a similar trend in the mixture fraction plot as shown in figures 4.20 (a) to (c) and figure 4.21 (a) to (c), respectively, and this is consistent with the observations of Choudhuri and Gollahalli (1998).

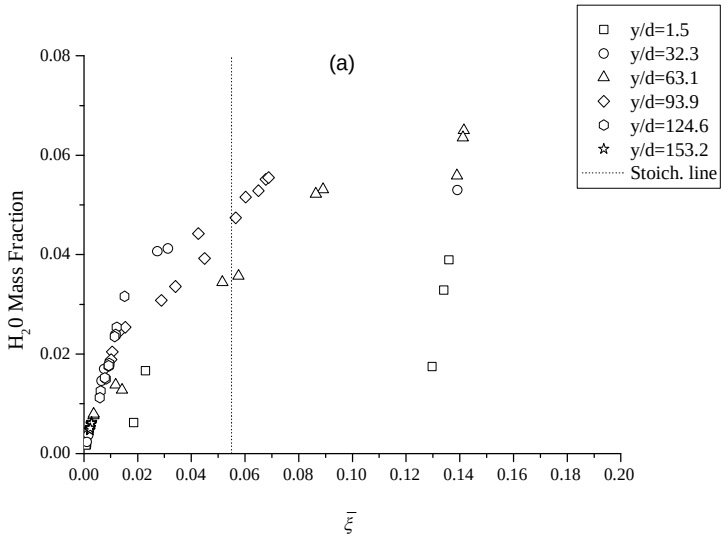

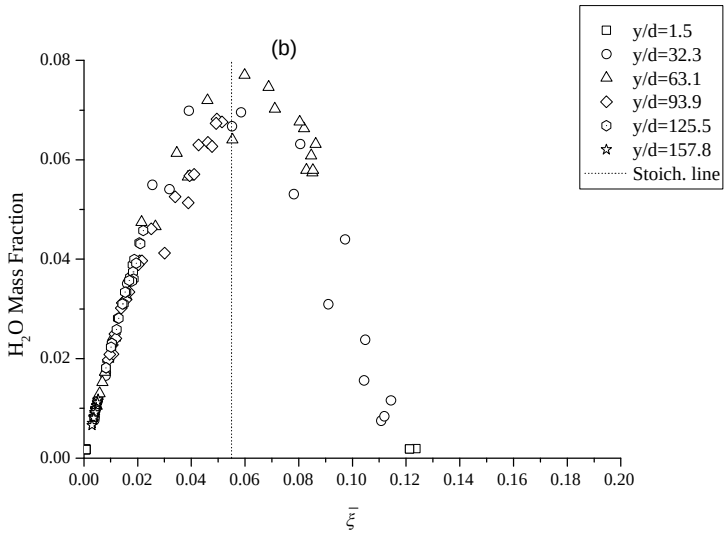

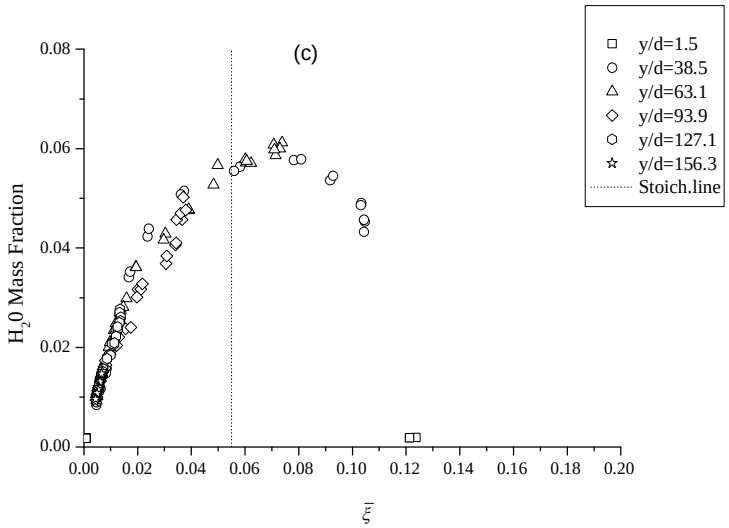

Figure 4.21 The H_2O mass fraction as a function of the mixture fraction for the attached flame (a) A, and the lifted flames (b) B, and (c) C, respectively.

4.7 NOx CONCENTRATION PROFILE

In figures 4.22 and 4.23, the molar concentration of NOx as a function of the radial distance, and the contour plots of the three jet flames are presented, respectively. In the attached case, the NOx concentration was higher than in the lifted cases, however, in the lifted cases, the NOx concentration was higher in flame C than flame B. This is as anticipated due to the increase in the jet velocity (strain rate), leading to increased flame temperatures, and hence a higher thermal NOx formation, as expected. In all the cases investigated, the downstream location where the highest concentration of NOx was observed, coincided with the downstream location with the highest mean temperature, as expected. This suggests that the formation of NOx was via the Zeldovich mechanism. This is expected because thermal NOx is formed at locations where the atmospheric Nitrogen and oxygen react at locations of high temperature in the flame, thus causing the nitrogen molecules in the air to be separated and to be combined with oxygen at high temperatures to yield NOx. This is consistent with the observations of Turns (1995), who suggested that the thermal NOx formation is more prominent at locations in the flame where temperatures of about 1800 K or higher are recorded. Similarly, the mean mixture fraction profile of NOx for the jet flames in the attached and lifted regimes are shown in figure 4.24.

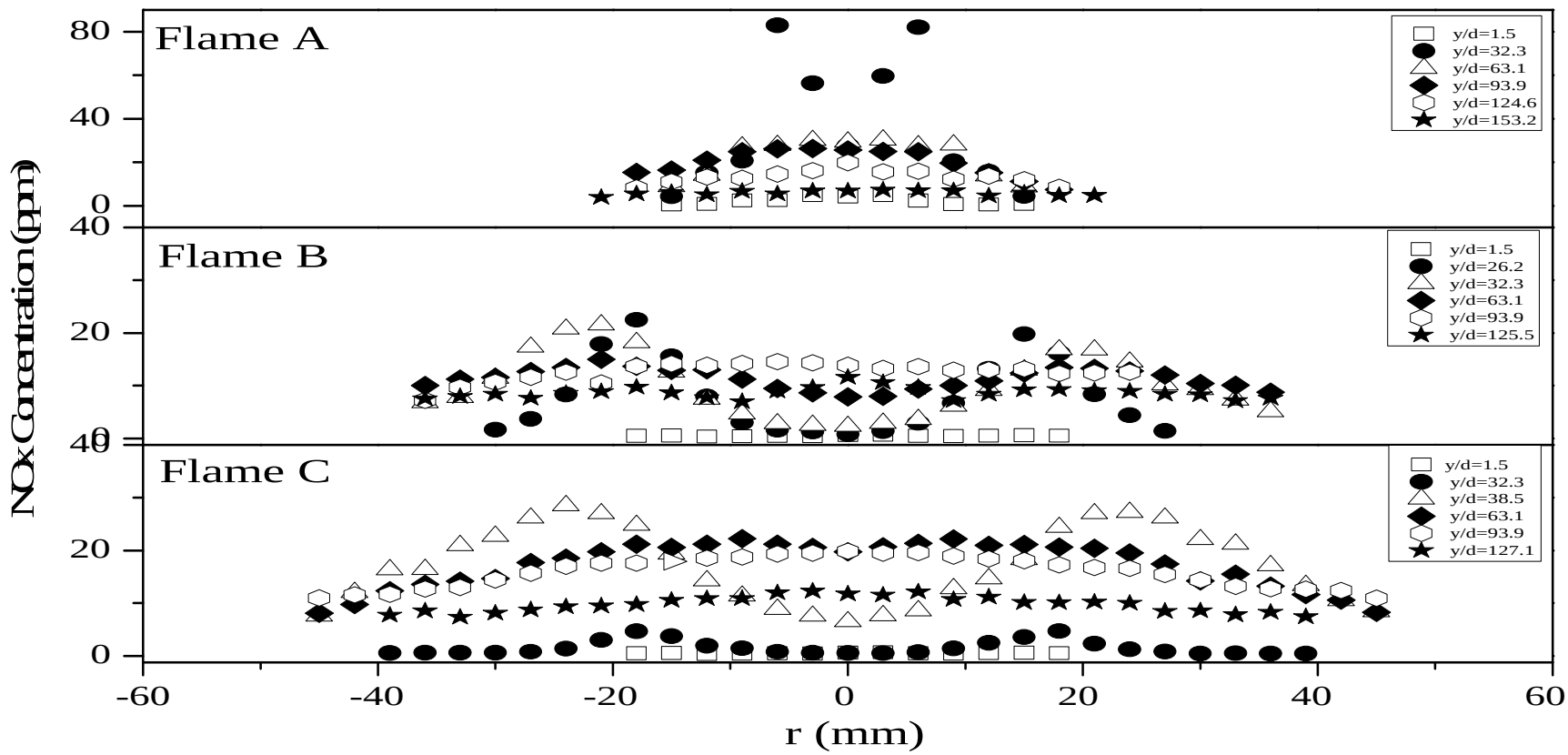

Figure 4.22 The NOx Mole Fraction as a function of the radial distance at various stream-wise locations for the three jet flames.

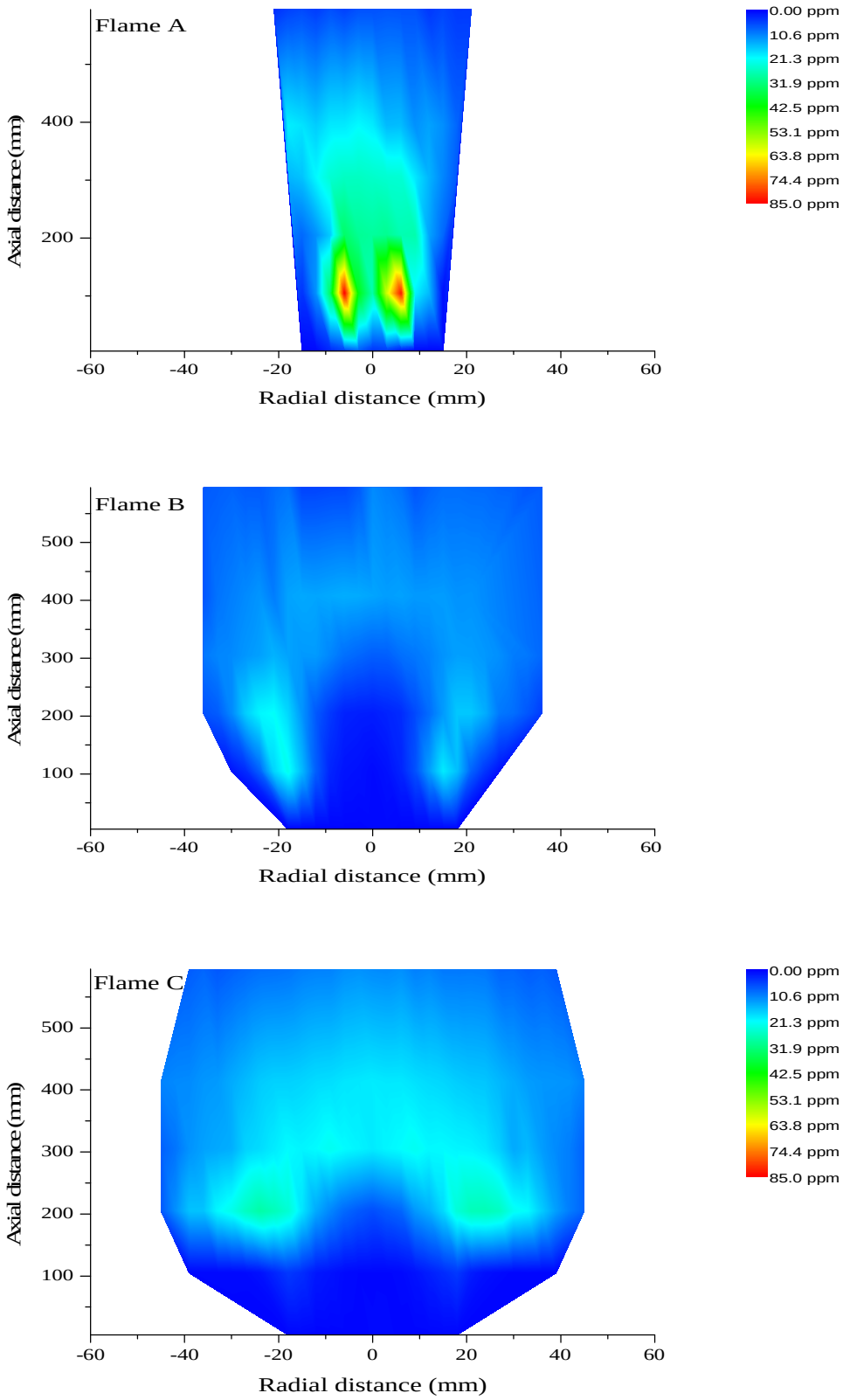

Figure 4.23 Contour plots of the NOx concentration for the three jet flames.

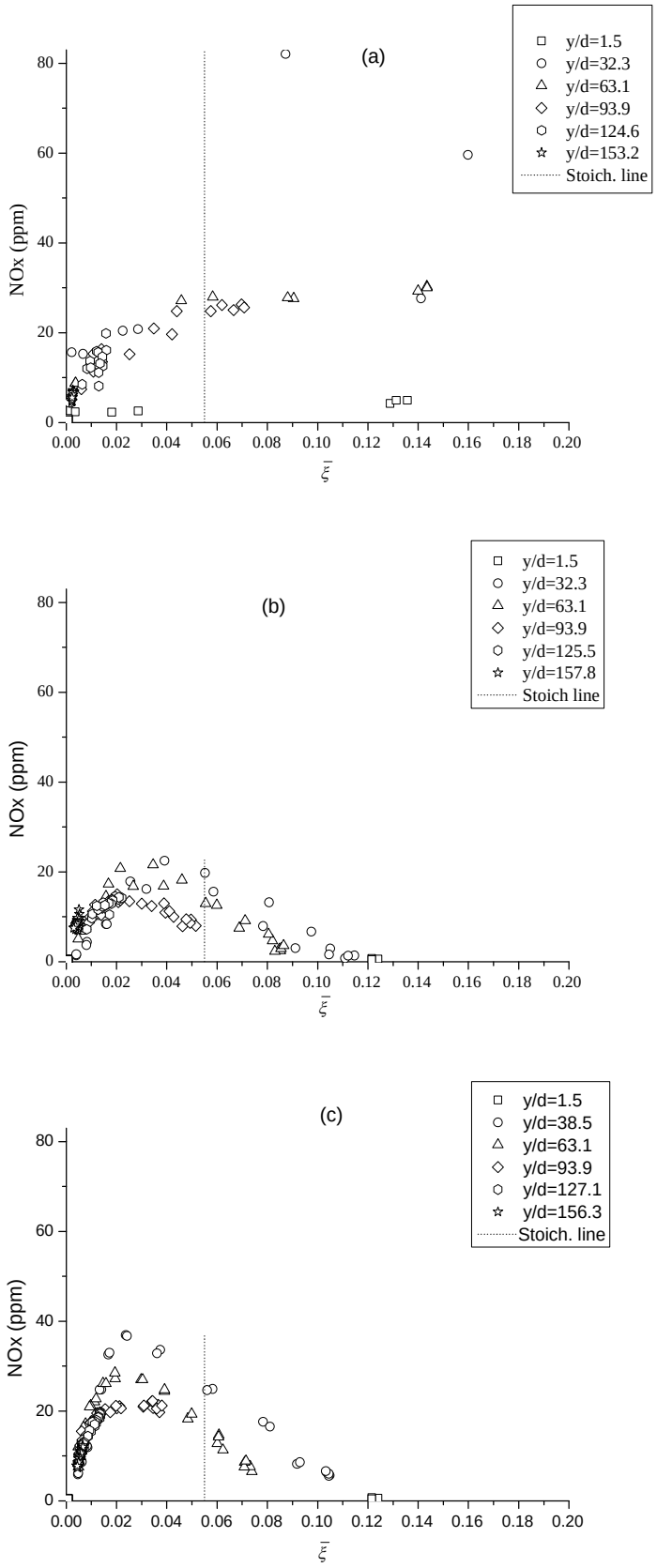

Figure 4.24 The NOx concentration as a function of the mixture fraction for the attached flame (a) A, and the lifted flames (b) B, and (c) C, respectively, at various downstream locations.

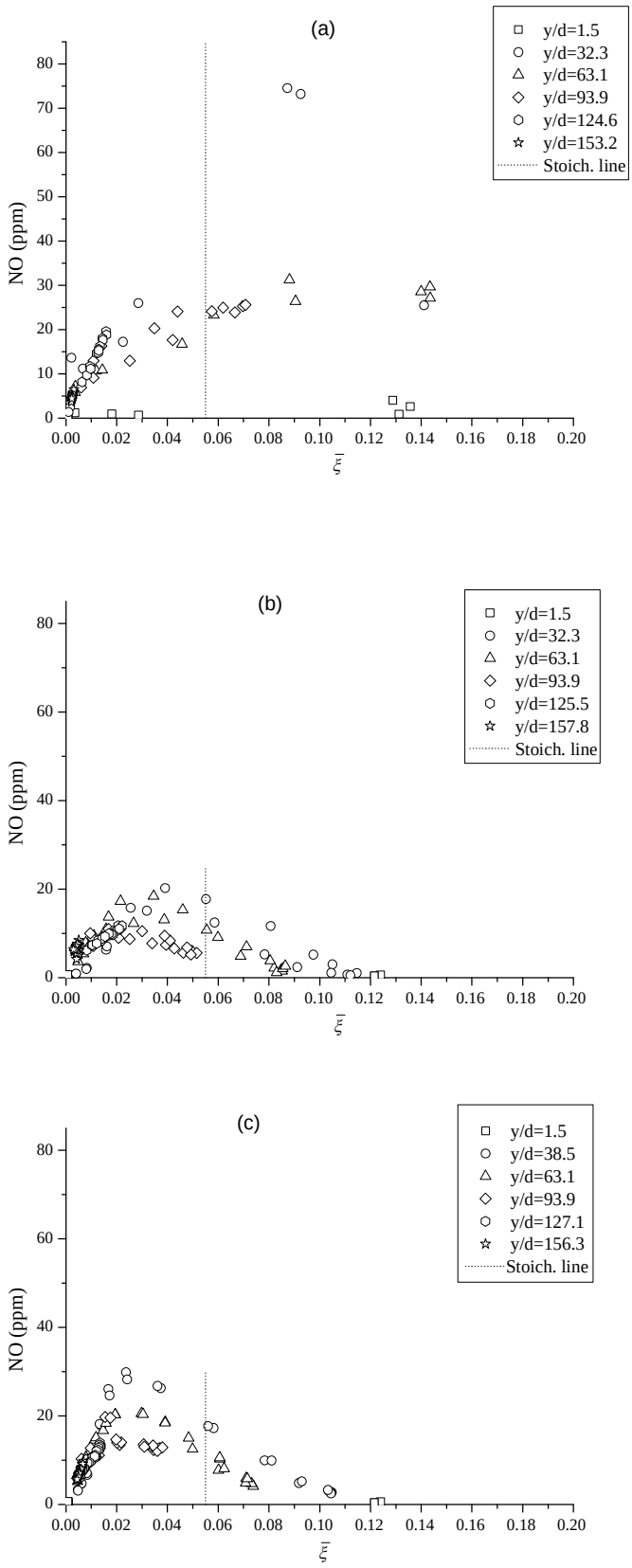

Figure 4.25 The NO concentration as a function of the mixture fraction for the attached flame (a) A, and the lifted flames (b) B, and (c) C, respectively, at various downstream locations.

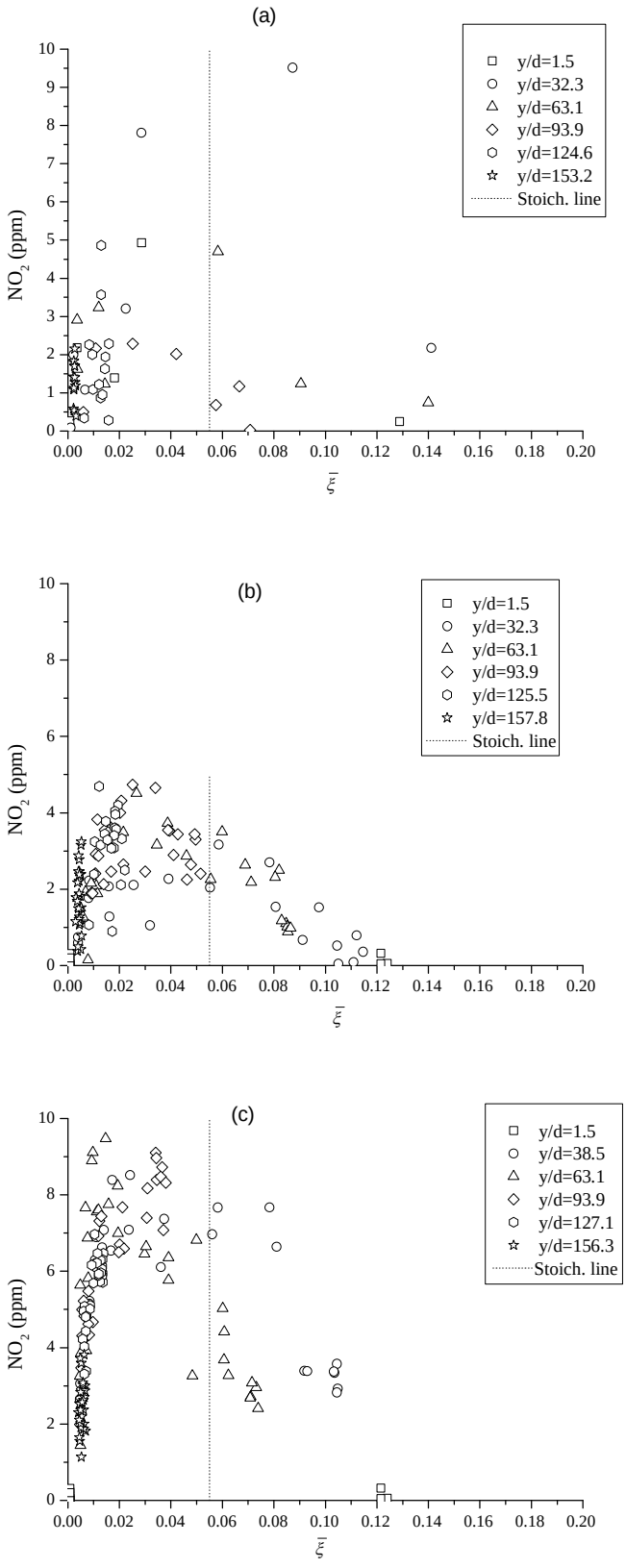

Figure 4.26 The NO_2 concentration as a function of the mixture fraction for the attached flame (a) A, and the lifted flames (b) B, and (c) C, respectively, at various downstream locations.

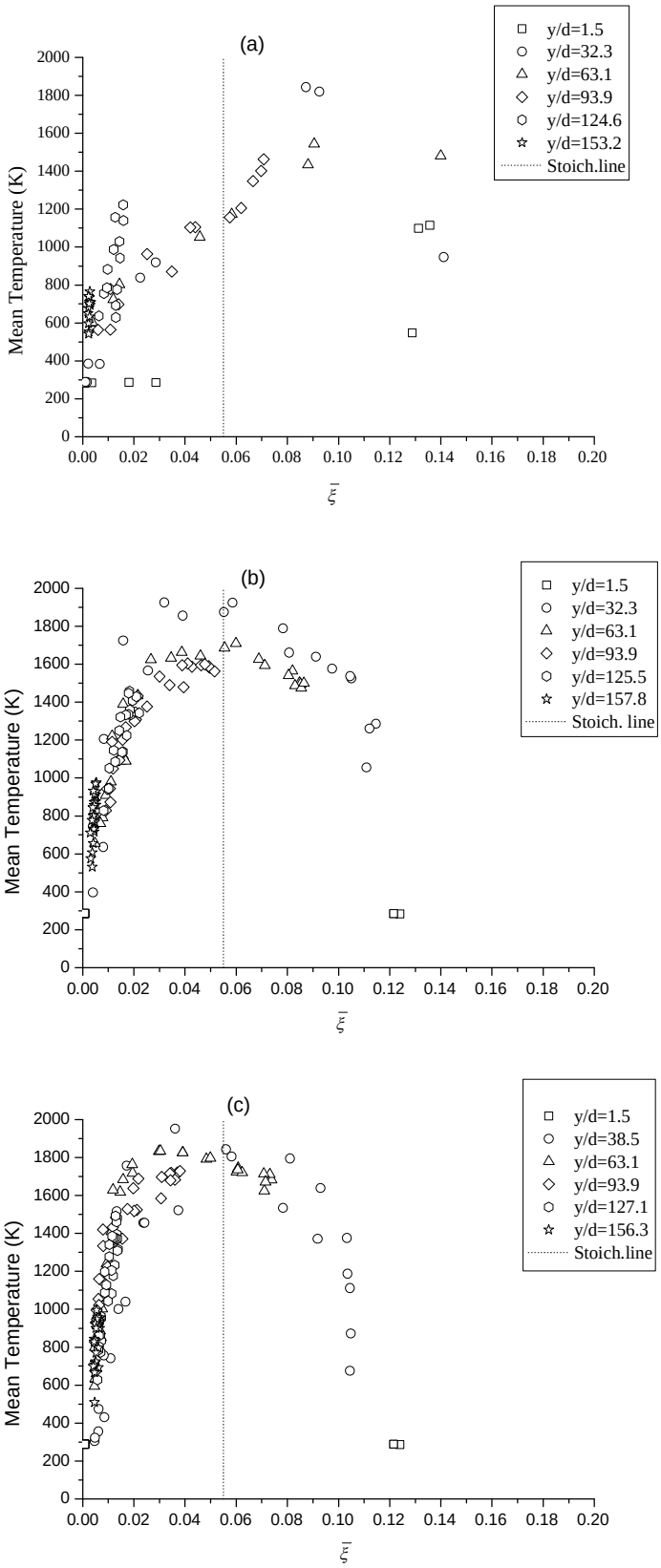

Figure 4.27 The temperature as a function of the mixture fraction for the attached flame (a) A, and the lifted flames (b) B, and (c) C, respectively, at various downstream locations.

In the attached flame, the maximum concentration of NOx was observed at the fuel-rich side of the stoichiometric, suggesting the prompt NO formation mechanism because of their prominence on the fuel-rich side of stoichiometric, while in the lifted jet flames, the maximum concentration of NOx was observed at the lean side of the stoichiometric. The same trend was observed in the plot of the mean temperature as a function of the mean mixture fraction plots, as shown in figure 4.27, thus suggesting that the highest concentration of NOx is recorded at locations with the highest flame temperature. Similarly, the mixture fraction profile of NO and NO_2 are shown in figures 4.25 and 4.26, respectively, with the maximum concentration of these species in the attached flame recorded at the fuel-rich side of the stoichiometric, while the maximum concentration of these species in the lifted cases were observed at the lean side of the stoichiometric. The trend of the NOx profile was similar to the trend of NO in the three jet flames investigated, as shown in figure 4.25. This is expected because in jet flames, NOx consists of about 90% NO, while NO_2 consists of about 10% of NOx (Bowman, 1992; Namazian *et al*., 1994). The small amount of NO_2 in the flames is because of the high flame temperature and the low reactive radical concentrations. The NO_2 radical-forming species are effective at low temperatures (Liu *et al*., 2001). This high temperature does not promote the formation of HO_2 radicals which aids in the conversion of NO to NO_2, and this conversion is more prominent at post-flame regions where rapid cooling occurs (Homma and Chen, 2000).

4.8 EMISSION INDICES OF SPECIES

One of the objectives of this investigation is to compare the emissions generated from the three jet flames investigated at different velocities and in different regimes. In the previous sub-sections, the in-flame composition of species were presented, in order to characterise and compare the composition of the major species in the jet flames at different jet velocities. This was aimed at understanding the basics of mixing in laminar and turbulent diffusion flames, before extending this comparison to the post-flame emissions generated from these jet flames. The relationship between the in-flame and the post-flame measurements made in this study is that it is the pollutants which are generated from the combustion of the fuel that is the source of pollutants measured in the post-flame. The best way to compare post-flame emissions is by reporting the EI of the species, instead of reporting only the concentration of the species. As discussed in Section 2.10, the EI of a species

estimates the mass of pollutant generated (grams) for a given mass of fuel burned (kilograms), which is a better method of estimating the post-flame emissions generated in flares.

	Flame A	**Flame B**	**Flame C**
EICO (g/kg)	109	57	42
EINOx (g/kg)	0.84	1.49	1.97

Table 4.3 Comparison of the post-flame emissions generated from the jet flames investigated.

The post-flame samples which were used in calculating the emission indices were taken at an axial location where there was a sufficient and uniform dilution along the location of the post-flame measurement. The expression for the EI shown in equation (2.46) was used in calculating the emission indices of the species. A summary of the EI of the species for each of these jet flames is presented in Table 4.3. EINOx was found to be increasing with increasing jet velocity. This is because increased strain rates lead to decreased residence times, decreased radiant fraction and higher temperatures, and hence higher EINOx (Turns and Lovett, 1989; Turns and Myhr, 1991). Similarly, EICO increased with increased sooting propensity and luminosity, while EICO also decreased with increasing jet velocity (Turns and Bandaru, 1993). This is because the stabilisation of the flame above the burner leads to a higher air entrainment into the flame, and hence a higher OH. Increasing the jet velocity (strain rate) decreases the sooting propensity because of the greater availability of the OH radical due to the air which is entrained into the flame, and which oxidises soot. This increased strain rate leads to a higher OH availability due to air entrainment, and this OH oxidises CO to CO_2, hence lesser EICO as the jet velocity is increased. In addition to comparing the differences between the EICO and EINOx for the three jet flames investigated in this study, the variation of the EICO and EINOx over a wide range of test conditions (*Re* =1584 to 14254), ranging from the laminar to the turbulent regimes, and at Froude numbers ranging from the buoyancy-dominated to the momentum-dominated flames on EICO and EINOx, are shown in figures 4.28 and 4.29, respectively. To the best of the author's knowledge, this is the first time the EI has been measured by varying the fuel jet velocity over a very wide range of Reynolds number. The only other investigation that is closely

related to the present investigation is the variation of the EI at a wide range of diluent mole fraction over a fixed Reynolds number by Gollahalli (1978).

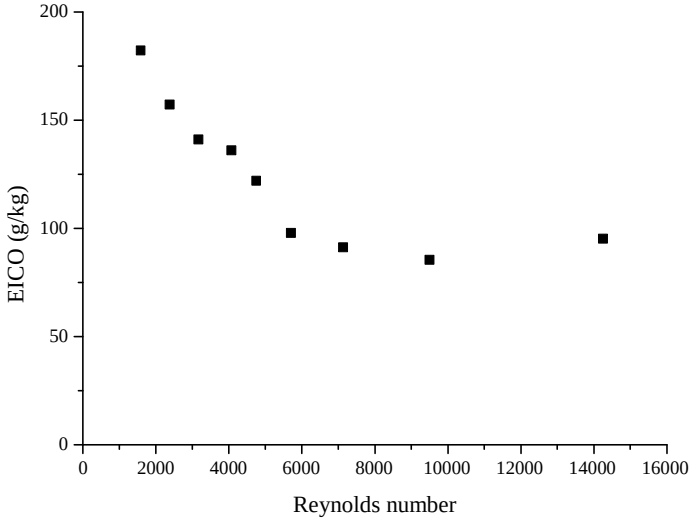

Figure 4.28 Variation of EICO on Reynolds number at the duct.

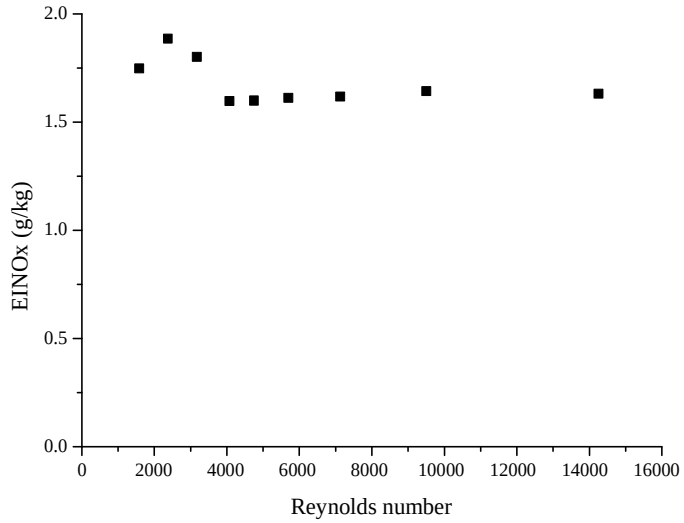

Figure 4.29 Variation of EINOx on Reynolds number at the duct.

The strain rate dependence on the EICO shows that EICO was highest in the laminar case, where the flame was also in the attached regime, while the EICO decreased as the jet velocity increased, and as the flame was stabilised above the burner. Similarly, the EINOx was found to increase first before decreasing, which was due to increased partial-premixing (Lyle *et al.*, 1999), and becoming constant from the transitional regime (Re=4073), up to the turbulent regime (Re=14254), before flame blow-out, thus indicating a weak dependence of EINOx at higher strain rates (Turns

et al.,1993). The initial increase in EINOx is because the increase in the strain rate leads to a decrease in the residence times (Turns and Lovett, 1989), decreased radiant fraction and higher temperatures, and hence higher EINOx (Turns and Lovett, 1989; Turns and Myhr, 1991). However, the reduction in the EINOx is due to the higher strain rates, which lead to shorter residence times of the products of the reactions in the flame zone, and also, since the flame is stabilised above the burner, there is greater mixing, and a greater air dilution. This dilution leads to lesser concentration of reactive species, shorter flame length, and lower flame temperatures, which leads to a reduction in the thermal NOx, hence lower EINOx, and is in line with the investigations of Meunier *et al*. (1998). Summarily, in this chapter, the consequence of varying the fuel jet velocity on the in-flame concentration of the species and on the post-flame emissions from methane flames has been investigated. In the next chapter, the consequence of diluting the fuel stream at a fixed fuel jet velocity while varying the diluent mole fraction on the in-flame concentration of the species, and the post-flame emissions over a wide range of Reynolds Number will be investigated.

Chapter 5

EFFECT OF CO_2 DILUTION ON METHANE / AIR JET FLAMES

5.1 INTRODUCTION

In the previous chapter, pure methane / air jet diffusion flames were investigated at different fuel jet exit velocities in the attached and the lifted regimes where both the in-flame and the post-flame composition of the species were examined. Prior to this study, several studies have focused on either the in-flame or the post-flame characteristics of jet flames. To the best of my knowledge, there is no investigation where the consequence of varying the jet velocity on both the in-flame composition of species and on the post-flame emissions from methane/air jet flames in the attached and lifted regimes have been reported. It is essential to examine how the flame temperature, composition of species and pollutant emissions vary both in the in-flame and post-flame regions of the flame in order to make an informed decision on how to optimise the combustion process for lesser pollutant emissions from a particular flame. The previous chapter addressed this gap.

Fuel	CH_4			
Diluent	CO_2			
Co-flow air velocity m/s	0.3			
Jet Flame	A	B	C	D
Velocity (m/s)	27.1	28.2	29.5	29.8
Reynolds number	5702	6989	7311	7385
Heat release rate (kW)	8	9	10.1	10.5
Fuel concentration (Vol. %)	100	90	80	78
Diluent Concentration(Vol. %)	0	10	20	22

Table 5.1 Test conditions for the present study.

In this chapter, the effect of the dilution of the fuel stream with CO_2 is investigated. Previous studies (see Section 1.3) have focused on the combustion characteristics of fuels blended with different inert diluents, where either the inert was added to the co-flowing or coaxial oxidiser stream, or the inert was diluted with the fuel. However, those previous studies were limited to the examination of the

effect of this dilution on either the in-flame or the post-flame regions of the flame. In this chapter, the effect of CO_2 dilution on the fuel jet stream of methane / air jet flames is investigated. The choice of CO_2 was because CO_2 is one of the components of the associated petroleum gases, which are found in reservoirs, and CO_2 is also emitted during gas flaring, as listed in Table 1.3 and Table 1.5, respectively. Similarly, the dilution of the fuel stream with CO_2 leads to a reduction in the flame temperature, leading to a reduction in the thermal NOx formation, and a reduction in the soot volume fraction. Therefore, this chapter examines the effect of varying the concentration of CO_2 on the flame structure, temperature, pollutant emissions, and the in-flame and post-flame composition of species in the flame. The test conditions used in this investigation are listed in Table 5.1, followed by the discussions on the effect of the dilution of the fuel-stream with CO_2 on CH_4 / air jet flames.

5.2 FLAME VISUALISATION

Figure 5.1 is a visualisation of the flame height, lift-off height, and the luminosity of the methane jet flames at increasing diluent mole fractions. Flame A in Table 5.1 is the same as flame B in Table 4.1 in chapter 4. The flames were wider at the base as the concentration of the diluent in the fuel-stream was increased. The broadening of the base of the flame was caused by the mixing of the air and the jet (Namazian *et al.*, 1988) at the upstream region where the entrainment of air into the lifted flame was favourable. It is observed that an increase in the concentration of the diluent led to a decrease in the luminosity of the flame. This luminosity is due to the chemiluminescence from the hot radicals in the reaction zone, where the effects of dilution reduces the flame temperature and the reactive species, and hence lowers flame luminosity. In flame A, the flame is mainly bluish, with a yellowish-orange colour at the far-burner region. The yellowish-orange colour is due to the incandescence caused by particles of carbon in the flame, and is an indicator of soot in the flame, while the bluish colour of the flame is due to the chemiluminescence of the CH and the C_2 radicals. (Choudhuri and Gollahalli, 2000). The soot is reduced at the region nearest to the burner due to the entrainment of air into the lifted flame and due to the increased diluent concentration, which lowers the flame temperature and soot nucleation rates, and hence suppresses the formation of soot at that location (Chen and Goss, 1989; Lock *et al.*, 2007).

A: 0% CO_2 B: 10% CO_2 C: 20% CO_2 D: 22% CO_2

Figure 5.1. Photographs of methane jet flames showing the effect of CO_2 dilution on the flames for flames A, B, C, and D respectively.

5.3 VISUAL OBSERVATION OF FLAME LENGTH AND LIFT-OFF HEIGHT

In table 5.2, the mean visible flame height and the mean lift-off height is listed, while in figure 5.2, the changes in the flame height and the lift-off height at different diluent mole fractions is shown. This investigation reveals that at increased diluent concentrations, the length of the flame decreases, while the flame's lift-off height increases. The linear relationship between the flame's average lift-off height and the jet velocity by Kalghatgi (1984), which has been verified by Chen *et al*. (1992) as shown in equation 2.40, has also been confirmed to match this experimental data. The calculated flame lengths and the lift-off heights are within the range of the measured flame length and the lift-off height, and are listed in Table 5.2. In flame A, the increase in the flame height is due to the buoyancy of the flame which is due to upward acceleration of the flow in the high-temperature region of the flame which supports a greater entrainment of air into the flame. This enhances a greater entrainment of air into the flame, thereby moving the flame zone to a downstream location of the flame's axis. The stabilisation of the flame above the burner port also

leads to enhanced mixing at an upstream location in the flame where partial-premixing is observed. Similarly, the shorter length of flames B to D is due to the effect of dilution on the flame.

Flame	Measured Flame height (cm)	Calculated Flame height (cm)	Measured lift-off distance (cm)	Calculated lift-off distance (cm)
A	51.3±5	50.7	8.5±4	8.3
B	39.8.3±4	42.2	11.4±3	9.6
C	29.6±4	25.6	15.8±3	13
D	11.8±7	14	19.2±4	15.1

Table 5.2. Average visible flame height and lift-off distance for flames A to D.

This dilution leads to the reduction in the combustible component of the flame, a decrease in the flame residence time, and a reduction in the temperature of the flame. This decrease in the flame temperature leads to a reduced rate of reaction, and a reduction in the time scale which is required for the mixing and the burning of the fuel (Majeski *et al*., 2004), thereby decreasing the turbulent flame's speed, and causing the fuel to travel a shorter distance before combusting.

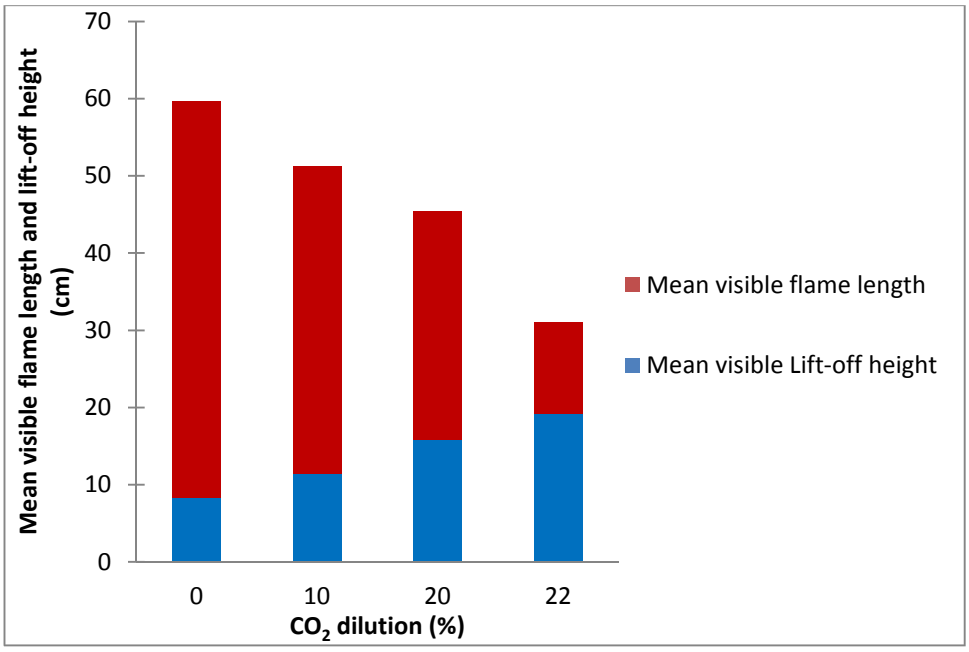

Distance

Figure 5.2. Changes in the visual observation of the flame height and lift-off height as a function of the fuel jet velocity.

A further increase in the diluent mole fraction leads to a further shortening of the residence time until the flame extinguishes, which explains the reason for the longer flame length of the undiluted case – flame A, in comparison with the CO_2-diluted jets of flames B to D, and is consistent with the observations of Choudhuri and Gollahalli (2003). Similarly, it should be noted that the concentration of CO_2 in flame C is 20 vol. %, while the concentration of CO_2 in flame D is 22 vol. %. Although the difference between the diluent concentration of flames C and D is small, this difference (2 vol. %) in the diluent concentration leads to a significantly greater flame length in flame C, and a greater lift-off height in flame D. This is reported in the investigations of Lock *et al*. (2007), where they showed that the inert dilution of the fuel-jet stream causes an initial slow flame lift-off in diffusion flames, followed by a quicker and a higher lift-off height that is more sensitive at higher diluent concentrations near the flame blow-out conditions, which ultimately leads to flame extinction. This was the reason why the temperature of the flame and the species composition were not measured in flame D, due to the fluctuations which were observed at the base of the flame, causing a continuous flame blow-out, thereby making reliable measurements difficult to perform.

In addition, the effect of the diluent concentration, the co-flow air velocity (Dahm and Dibble, 1988; Muniz and Mungal, 1997), the aerodynamics of the jet flame (Gollahalli and Zadeh, 1985), etc., has been known to affect the flame lift-off in a diluted jet. This is due to the influence of the lift-off on the fuel and the oxidiser jet velocities (Wyzgolik and Baillot, 2007; Min and Baillot, 2012), where there is a competition between these effects to alter the stabilization point of the lifted flame. However, this study suggests that when a fuel jet stream is diluted with CO_2, the increase in the flame's lift-off height is due mainly to the addition of the diluent in the flames that were investigated. This is because in spite of the jet and the co-flow velocities remaining unchanged across the jet flames that were considered, the lift-off height in the diluted case, flame B, was higher than in flame A, and a further increase in the diluent mole fraction led to a greater lift-off height in flames C and D, in comparison with the undiluted case –flame A. This may be explained by the dilution of the fuel with CO_2, which reduces both the concentration of the reactant and the length of the heat-release zone. This dilution leads to a reduction in the reaction-rate at the leading-edge of the flame (Gollahalli, 1977). This changes the propagation speed of the flame (Min *et al*., 2009), and leads to the flame being

stabilised at further downstream locations in the flame where a better mixing of the reactants exist until the flame blows out at increased diluent mole fractions, and is consistent with the observations of Briones *et al*. (2006) and Lock *et al*. (2008).

5.4 TEMPERATURE PROFILES

The contour plots of the mean temperature and the spatial plots of the peak mean temperature of the jet flames are presented in figures 5.3 and 5.4, respectively. The peak mean temperatures which were recorded in the jet flames were 1925 K, 1890 K, and 1858 K, corresponding to 0, 0.1, 0.2 diluent mole fractions, respectively, at a globalised downstream location of y/d=32.3. This location indicates the flame front along the axis of the flame where combustion occurs. The largest peak was observed at the near-burner reactive zone in flame A, which reduced at higher diluent concentrations, as shown in the temperature contour plots and in the spatial plots of the temperature profiles in figures 5.3 and 5.4, respectively. Similarly, the dilution of the jet stream with a 0.1 mole fraction of CO_2 led to a 35 K decrease in the flame temperature, while the dilution of the jet stream with a 0.2 mole fraction of CO_2 led to a 67 K decrease in the flame temperature, suggesting that increasing the diluent mole fraction in the fuel-stream leads to a decreased flame temperatures. The reduction in the maximum flame temperature in flames B and C is due to the effect of the increase in the diluent mole fraction, which reduces the concentration of the reactive species in these flames, and the higher lift-off height in these flames which promote the air entrained into the jet flame.

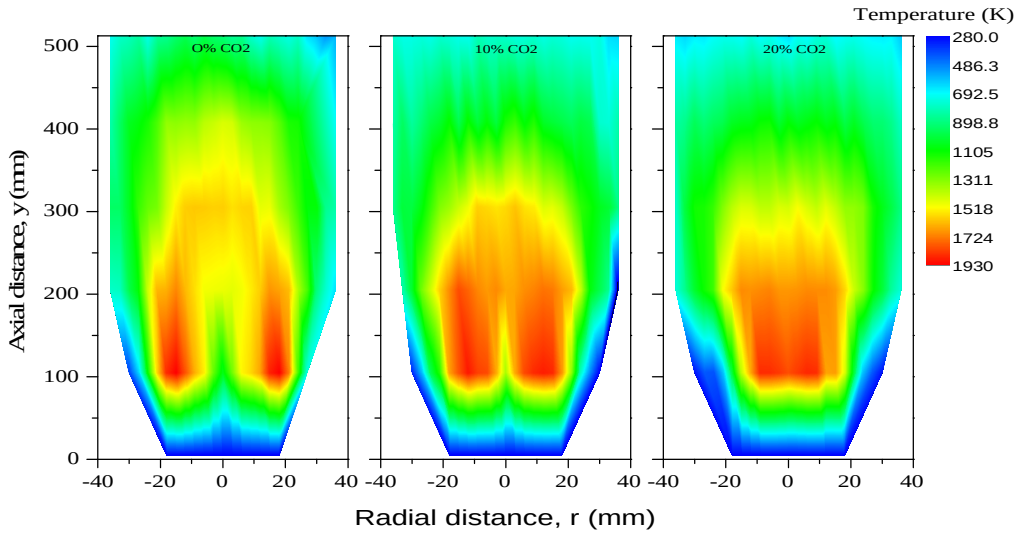

Figure 5.3. A contour plot showing the distribution of the mean temperature at various CO_2 mole fractions in the fuel stream of the jet flame.

As observed, increasing the concentration of the diluent leads to a decreased peak mean temperature. This is because the effect of dilution reduces the concentration of the radical species in the flame, thereby reducing the combustion intensity of the flame since the reaction rate is reduced due to lower flame temperatures, which is caused by the effect of dilution on the jet stream.

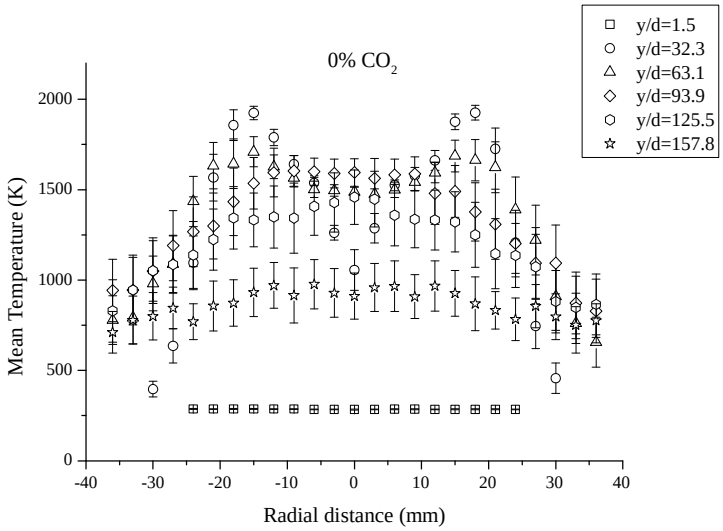

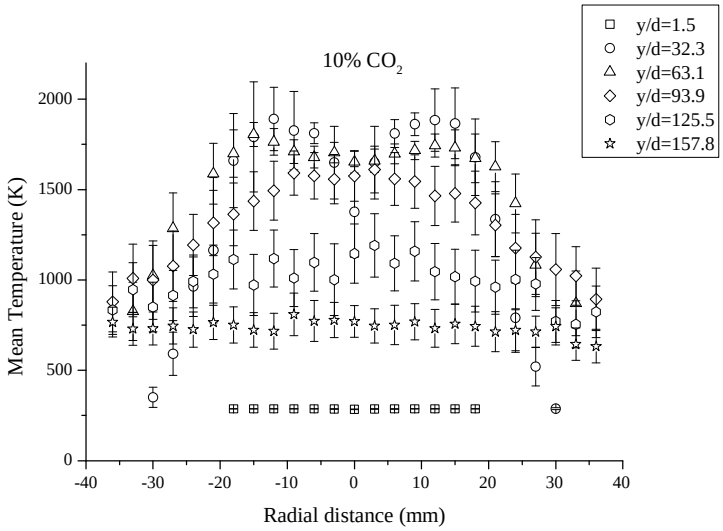

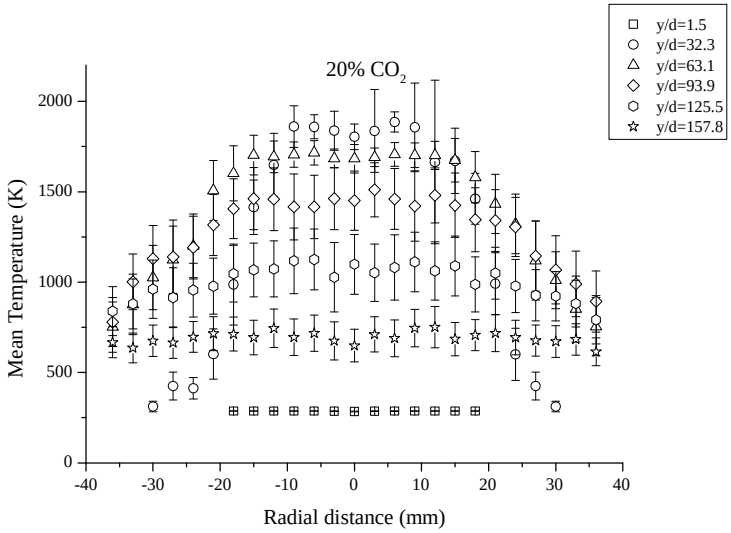

Figure 5.4. Mean temperature of the three jet flames investigated.

Similarly, via a thermal effect, the diluent, CO_2, has a high specific heat which provides an additional mass which absorbs the heat generated during combustion, hence, reducing the flame temperature via the thermal cooling of the flame. This suggests that increasing the concentration of the diluent in the jet stream or diluting the jet stream with diluents with higher specific heat capacities reduce the flame temperature., and is consistent with the observations of Gollahalli (1978), Puri (1992), Lock *et al*. (2008), amongst others. A practical significance of the effect of fuel-stream dilution in a laboratory-scale flame and in a full-scale flame stabilised above the burner is that the lower temperature of the flame aids in the preservation of the burner nozzle and the flare tip, respectively.

5.5 COMPOSITION PROFILES OF CH_4, O_2, N_2, CO_2, H_2O AND CO

The plots of the concentration of the species as a function of the radial distance at different downstream regions in the jet flame are shown in figures 5.5 to 5.11. These profiles visualise the spatial and the structural differences in the flame at different diluent mole fractions. In this section, the spatial variation of the species is discussed briefly, while in Section 5.5.1, detailed discussions of the effect of dilution on the species is presented.

In Figure 5.5, the concentration of the total hydrocarbons in the fuel is presented. In all the cases investigated, the peak mean concentration of the total hydrocarbons was 200,000 ppm which was at y/d=1.5, which is the normalised axial location closest to the burner. Axially, the maximum concentration of the fuel is expected at the centre of the measurement location where the jet fuel issues, while

the concentration of the fuel reduces downstream, and radially away from the centre of the jet, as combustion occurs. However, at increased diluent concentrations, the flame's reaction zone becomes stabilised further downstream of the flame, and the concentration of the reactive species reduces due to the effect of the dilution on the jet stream, thereby reducing the concentration of the fuel at the downstream locations as observed in the diluted cases in figure 5.5.

In figure 5.6, the spatial profile of the O_2 concentration is presented. The flames exhibit a symmetrical profile in all the cases investigated. At y/d=1.5, the concentration of O_2 is lowest at the jet centreline, while increasing radially away from the jet centreline line as expected. The high concentration of O_2 in the centreline at the near-burner region of the jet flames is due to the stabilisation of the flame above the jet nozzle, which promotes air entrainment into the flame, and also promotes the mixing of the air with the fuel. Also, this location corresponds with the location of the highest fuel concentration and the lowest O_2 concentration, which indicates that there is an occurrence of partial premixing in the flame. However, at increased diluent concentrations, the concentration of O_2 decreases because of the dilution effect of the inert diluent which leads to a reduction in the O_2 concentration that is mixed with the fuel, and hence, a reduction in the level of partial premixing in the diluted jets.

Figure 5.7 shows the radial profiles of CO_2 at different stream-wise locations in the undiluted and the diluted cases. These flames exhibit a symmetrical profile with a maximum concentration of CO_2 recorded at y/d=1.5 in the diluted cases and at y/d=32.3 in the undiluted case. The peak concentration of CO_2 in the diluted cases at y/d=1.5 is because this is the closest upstream location to the jet nozzle where the diluent which is added to the fuel stream issues, and this location of the peak CO concentration also coincides with the location of the peak fuel concentration in the diluted cases. However, further downstream, between y/d=32.3 and y/d=157.8, the peak concentration of CO_2 is recorded at the same non-dimensional axial location in the three jet flames investigated. This location coincides with the location of the highest temperature in the flame, which is the flame front, and suggests the location where combustion occurs. Since CO_2 is a product of combustion, it is expected that the location of the maximum product formation should coincide with the location of the peak flame temperature, where combustion occurs. Similarly, although the dilution of the fuel-stream with CO_2 reduces the flame temperature due to the high

heat capacity of CO_2, however, at higher CO_2 diluent concentrations, the peak CO_2 concentration in the flame actually increases because of the extra CO_2 content in the jet flame, which causes a further reduction in the flame temperature, and a slower oxidation of CO to CO_2, and hence higher CO concentrations, and lower thermal NO concentrations. The radial profiles of CO in both the undiluted flame and the diluted flames are shown in figure 5.8. The maximum concentration of CO in the 0%, 10% and 20% CO_2 diluted flames are 3.42%, 3.65%, and 3.67%, respectively, and occurs at y/d=63.1 in all the cases investigated. It is observed that the difference in the CO concentration in the jet flames is not significant, which may be due to the slight difference in the flame temperature at increased diluent concentrations. This is because the thermal effect of dilution leads to a lower flame temperature at increased diluent concentrations. The lower the flame temperature, the slower the rate of oxidation of CO to CO_2 as a result of the quenching of the oxidation reaction, (RØkke and Hustad, 2005). This lower temperature leads to the formation of more CO in the diluted cases due to the thermal effect of dilution, where increased diluent concentrations lead to a reduction in the flame temperature, and hence lower CO oxidation rates, which explains the reason for the higher CO concentration at higher diluent concentrations.It has already been established that an increase in the fuel-stream diluent concentration leads to decreased flame temperatures and this reduction in the temperature leads to a reduction in the NO that is produced via the thermal NO (Zeldovich) mechanism. The discussions on the NO formation via the Zeldovich mechanism is presented in Section 2.4.2.1. The NO concentration profile of the jet flames is presented in figure 5.9.

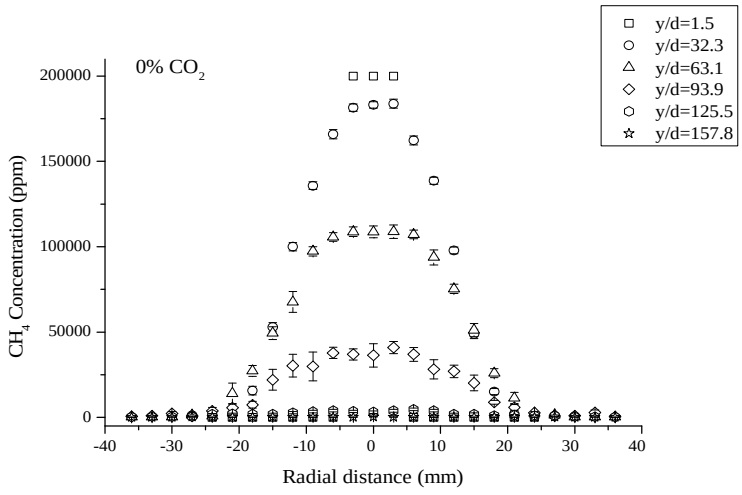

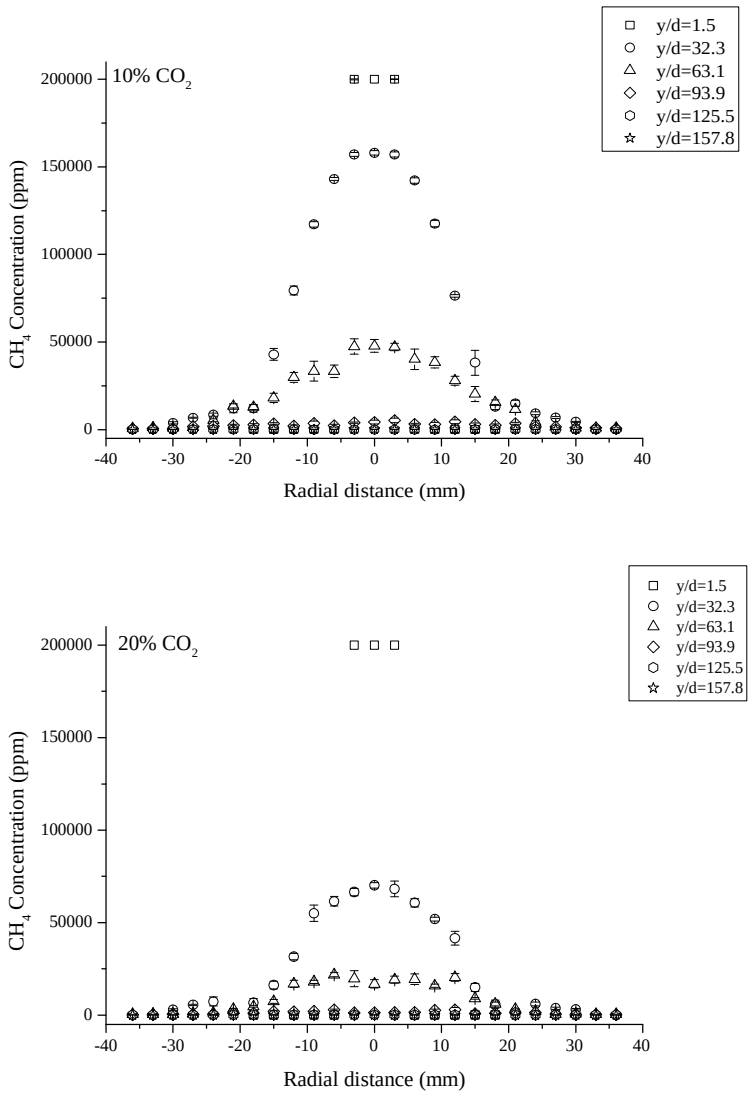

Figure 5.5. The variation of the fuel concentration as a function of the radial distance for the three jet flames investigated.

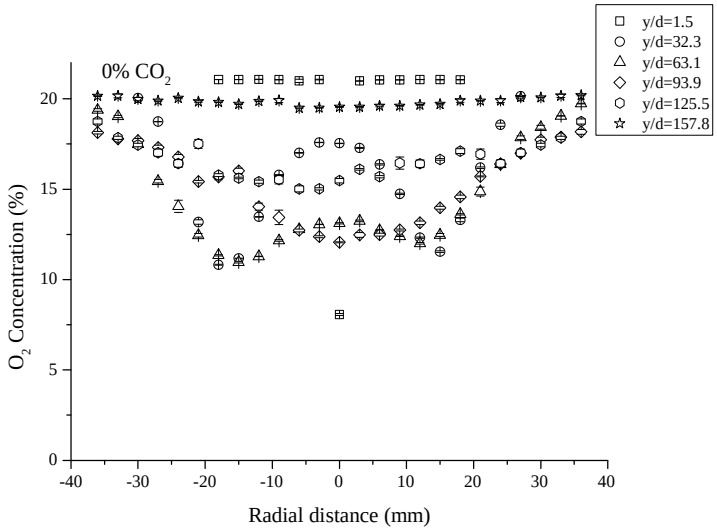

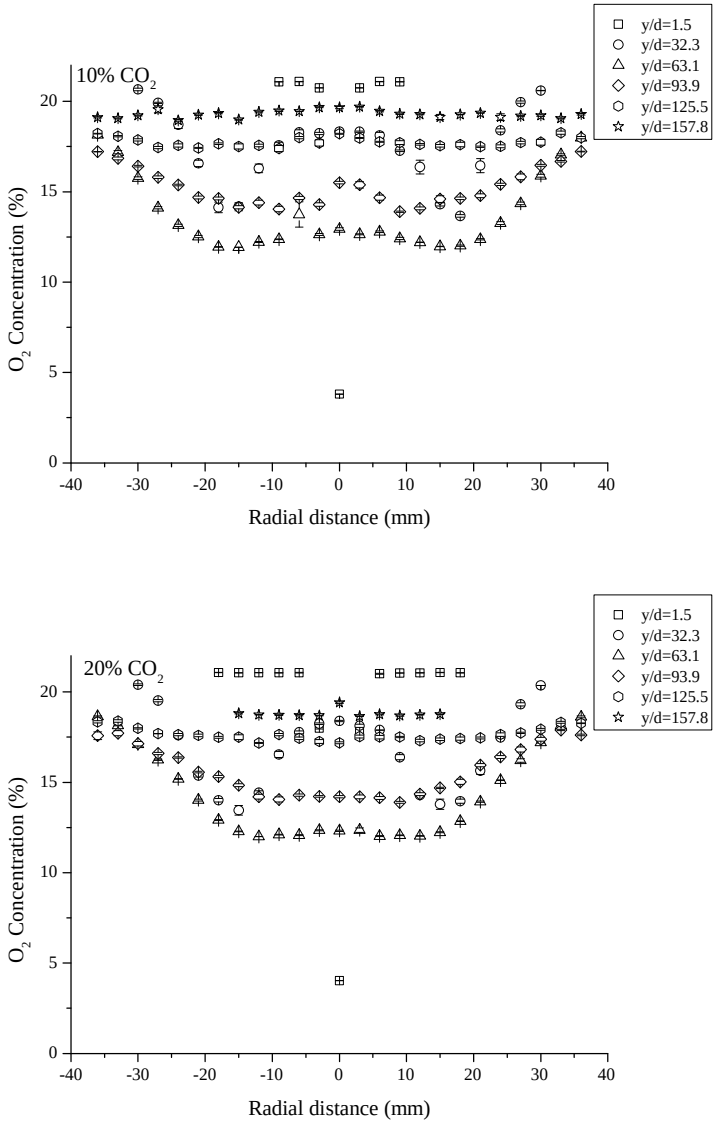

Figure 5.6. The variation of the O_2 concentration as a function of the radial distance for the three jet flames investigated.

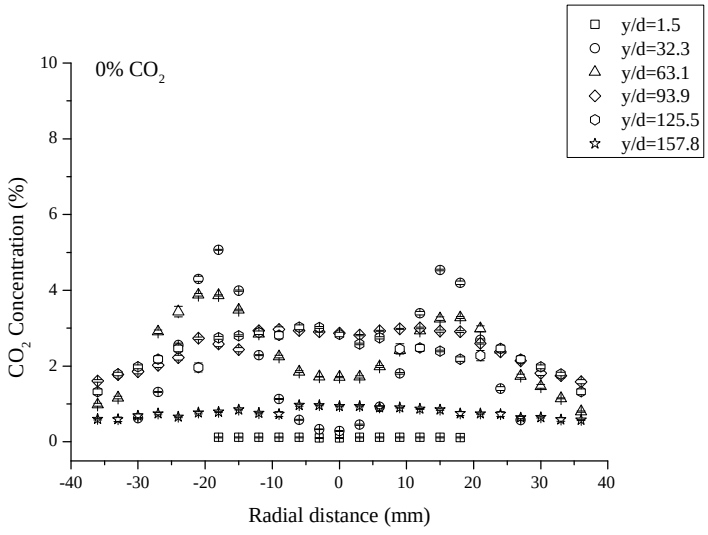

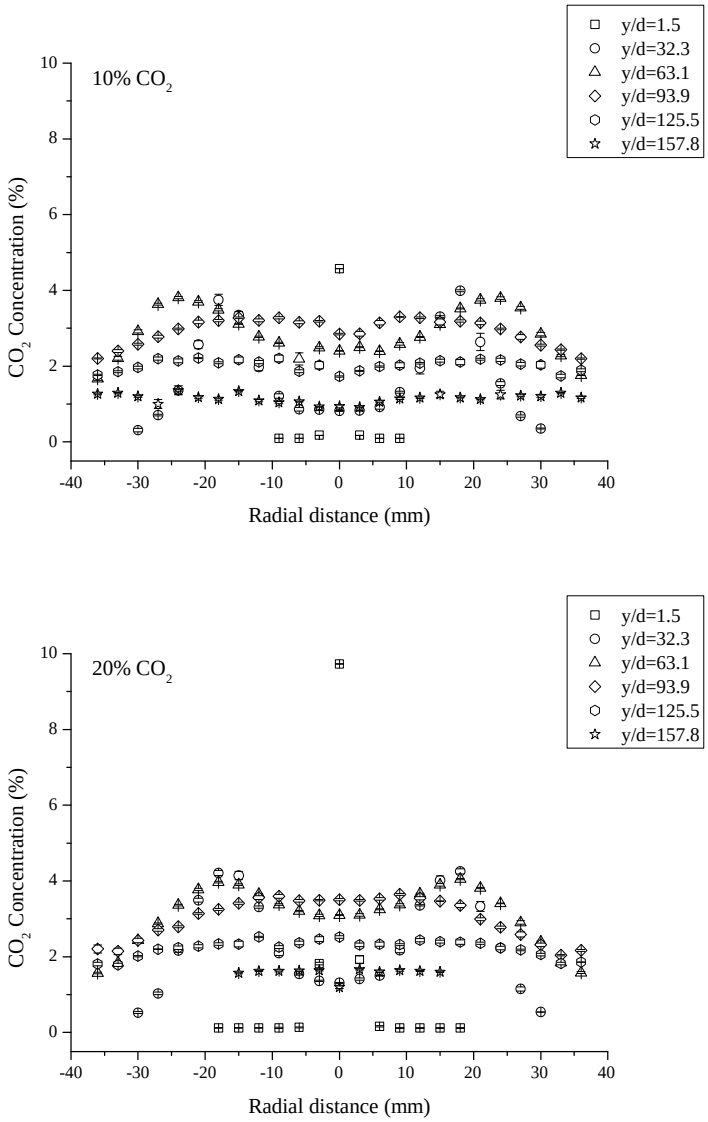

Figure 5.7. The variation of the CO_2 concentration as a function of the radial distance for the three jet flames investigated.

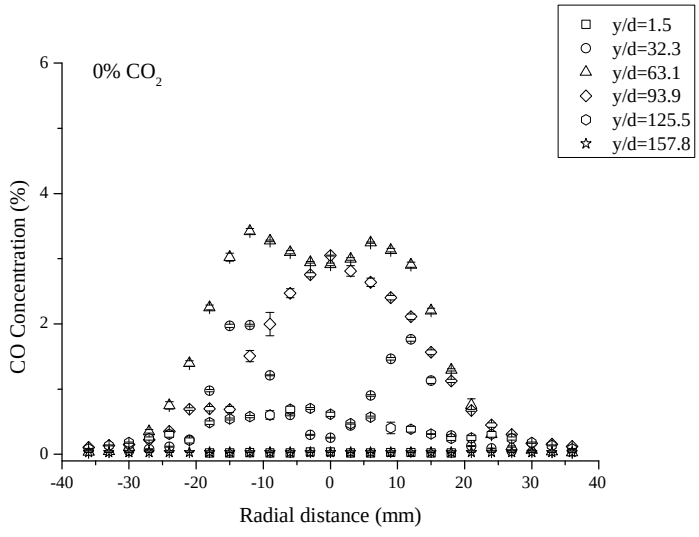

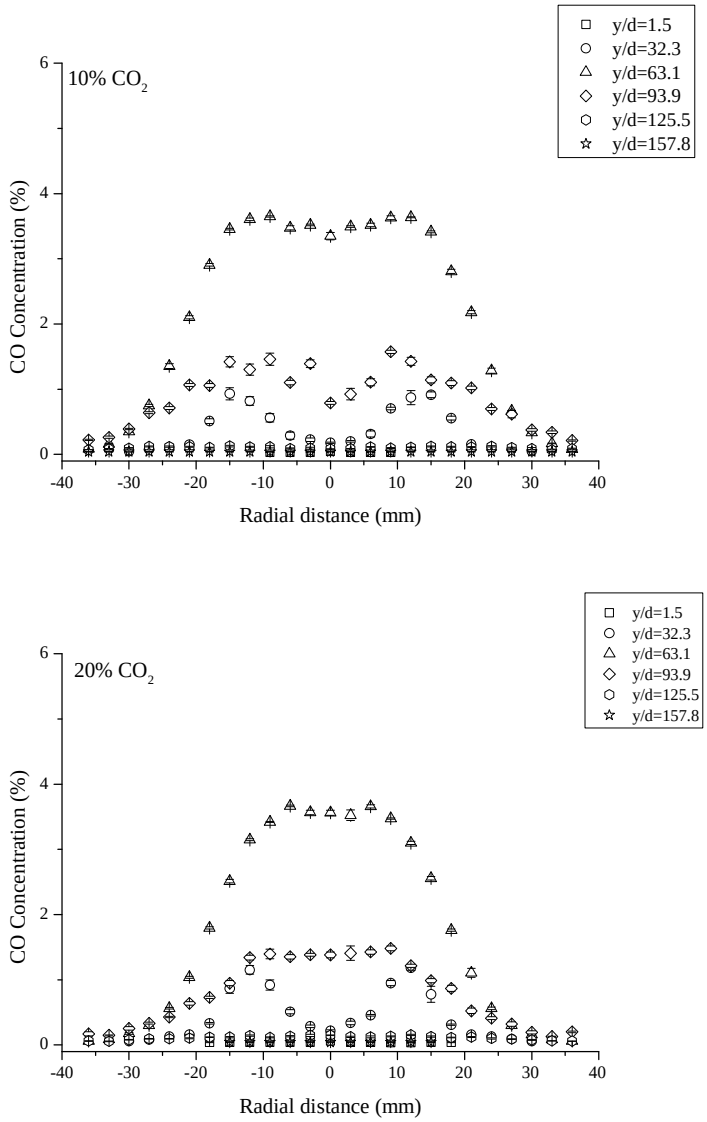

Figure 5.8. The variation of the CO concentration as a function of the radial distance for the three jet flames investigated.

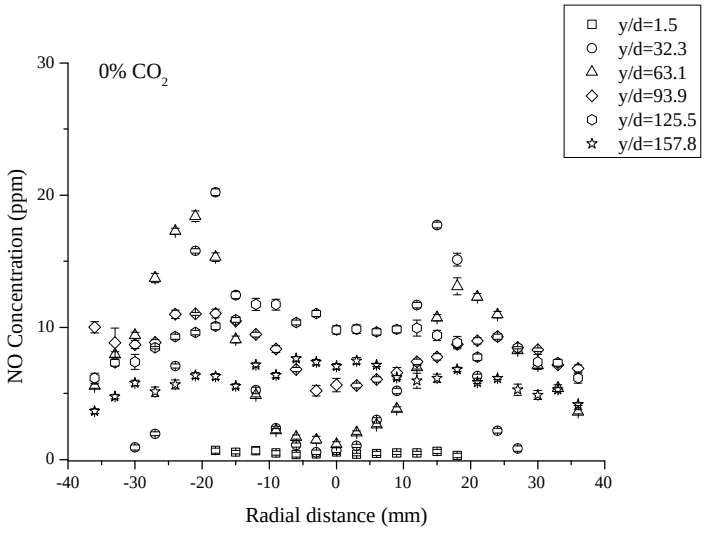

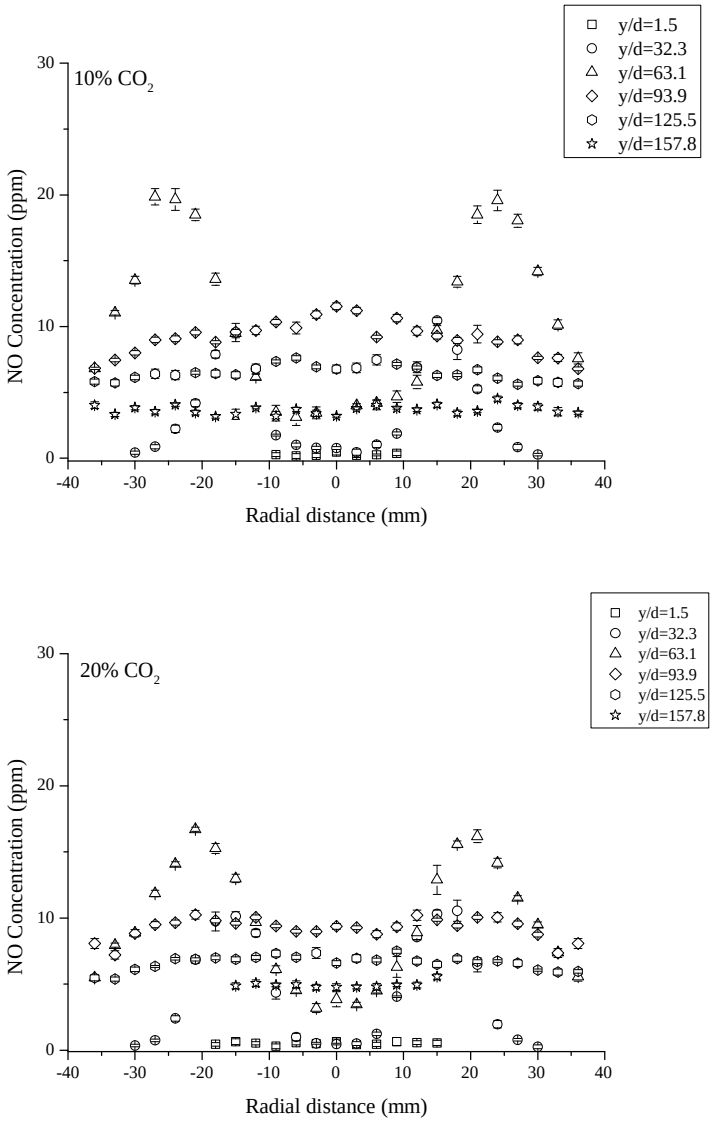

Figure 5.9. The variation of the NO concentration as a function of the radial distance for the three jet flames investigated.

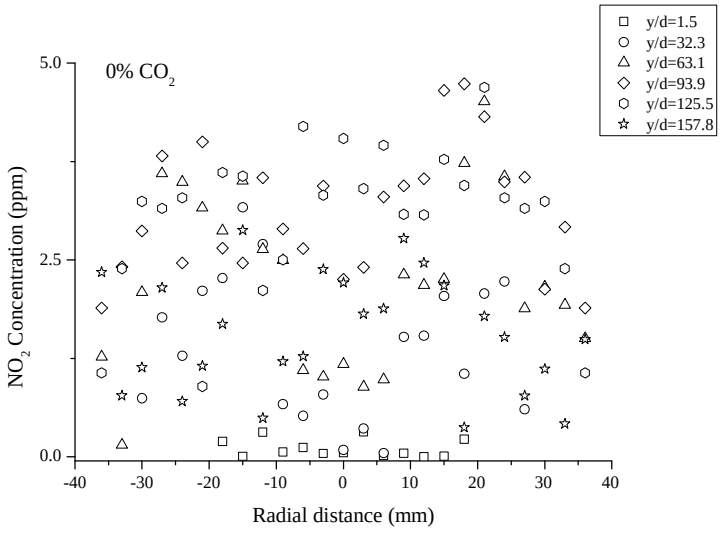

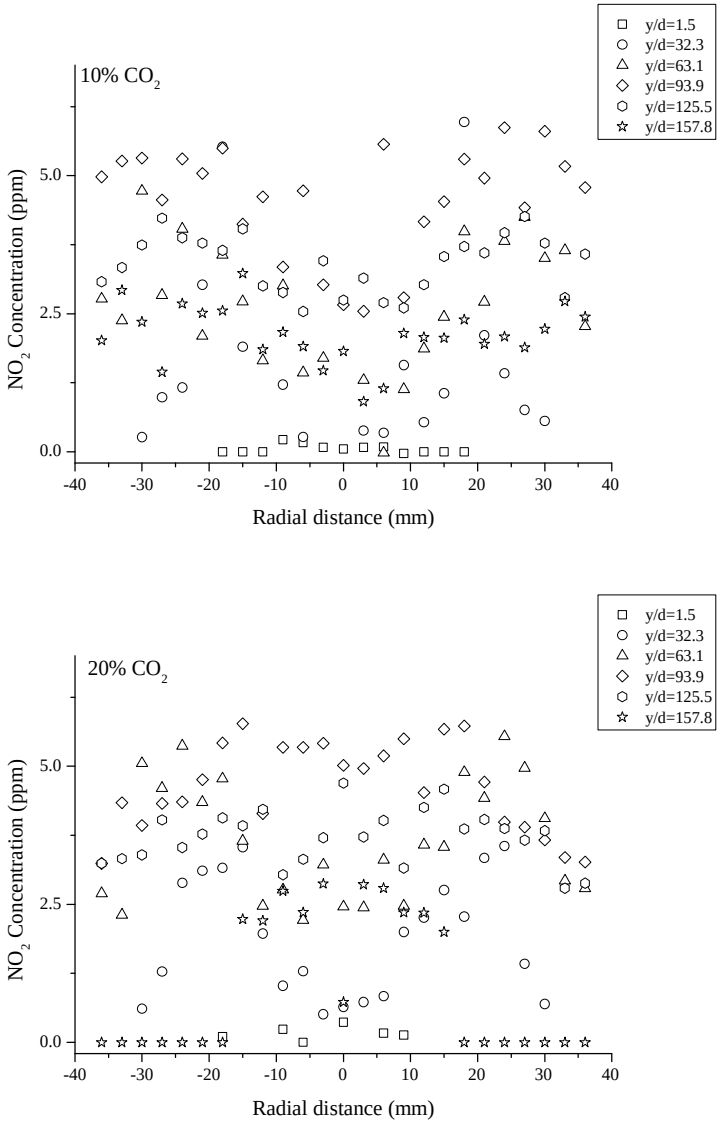

Figure 5.10. The variation of the NO_2 concentration as a function of the radial distance for the three jet flames investigated.

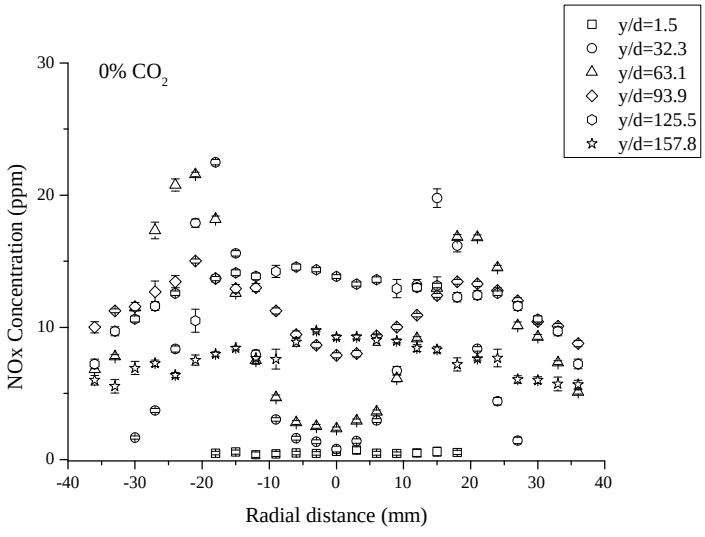

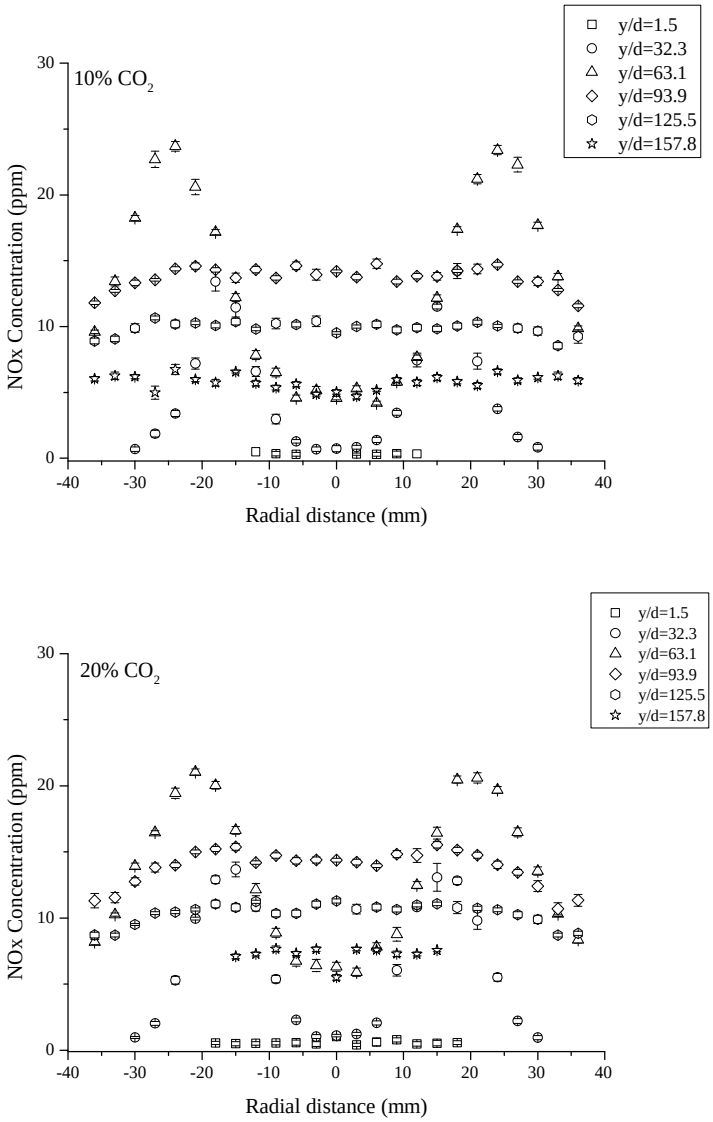

Figure 5.11. The variation of the NOx concentration as a function of the radial distance for the three jet flames investigated.

In the undiluted case (0% CO_2), the peak temperature of the flame, which is 1925 K, is recorded at the location of the peak concentration of NO at a normalised location of y/d=32.3, while for the 10% and 20% CO_2 diluted cases, the peak temperature of the flames are 1890 K and 1858 K, respectively, at y/d=63.1. Similarly, the peak concentration of NO in the 0%, 10% and 20% CO_2 diluted flames were 23.4 ppm, 19.9 ppm, and 16.7 ppm, respectively. The NO formation via the Zeldovich mechanism has been known to be prominent at locations in the flame where the flame temperature exceeds about 1800 K (Turns, 1995). In the flames investigated, the flame temperature exceeds 1800 K, which suggests that the formation of NO is possibly via the thermal formation mechanism. The reduction in the NO concentration at increased diluent concentrations confirm that dilution leads

to a reduction in the flame temperature, and dilution also leads to a reduction in the thermal NO concentration. Similarly, NOx is made up of at least 80% NO, while NO_2 constitutes between 7% - 40% of NOx (Turns and Lovett, 1989), therefore, the NOx profile shown in figure 5.11 has a similar trend with the NO concentration. The NO_2 concentration profile of the jet flames shown in figure 5.10 at 0%, 10% and 20% CO_2 diluent concentrations show that the maximum concentrations of NO_2 were 4.74 ppm, 5.77, and 5.97 ppm, respectively, at a normalised distance of y/d = 93.9.

The peak concentration of NO_2 measured in the flames show that there is not much difference in the NO_2 at different diluent concentrations. Similarly, the peak concentration of NO_2 is found to be at the far-burner downstream locations in the flame, where the radical species which are formed in the maximum flame temperature location in the flames are cooled, and also at locations where there is an occurrence of flame dilution and rapid cooling (Gollahalli, 1977; Homma And Chen, 2000). The formation of NO_2 in methane flames is mainly through the oxidation of NO with the HO_2 radical species in the flame's reaction zone as shown in reaction R2.4.2.1 (Merryman and Levy, 1974; Hori, 1986), although it is possible for NO_2 to be formed through the reaction of NO_2 with other species, such as OH, O, and O_2 (Glarborg and Hadvig, 1991; Hanson and Salimian, 1998). NO_2 is found in small concentrations in some combustion systems (Liu *et al.*, 2001), which is one of the reasons NO_2 is neglected (Zhuang and Leuckel, 1998), but accounted for, generally, as NOx. However, NO_2 has a higher toxicity than NO (Homma and Chen, 2000), and at sufficient conditions of temperature and radical species concentration, NO could be converted to NO_2 (Driscoll, *et al.*, 1992; Turns *et al.*, 1993). Further discussions on the effect of dilution on the species in a mixture fraction space are presented in the next section.

5.5.1 PROFILES OF SPECIES IN MIXTURE FRACTION SPACE

As discussed in Section 4.6, diffusion flames are presented in mixture fraction space, to gain an understanding of the fuel-rich and the fuel-lean regions in the jet flame, and to visualise regions where the flame is stoichiometric. The variation of the mass fraction as a function of the mixture fraction of the reactant (CH_4, O_2, and N_2), the intermediate (CO), and the product (CO_2 and H_2O) species at various downstream locations in the flame are shown in figures 5.12 to 5.17. The calculation

of the mean mixture fraction, $\bar{\xi}$, was performed based on the carbon-atom balance based on the experimental measurements of the total hydrocarbons, CO, and CO_2 by utilising the expression by Masri and Bilger (1986) which is already expressed in equation (4.1). When flames are stabilised above the burner, without the aid of stabilisers, increasing the concentration of the diluent in the fuel-stream, decreases the temperature of the flame, and the greater the concentration of the diluent, the greater the effect of the dilution on the flame, which further leads to a lower temperature until flame blow-out occurs. This increase in the diluent reduces the concentration of the reactive species, resulting in the leanness of the fuel, until the flame extinguishes. This is due to the entrainment of air into the flame which is stabilised above the burner port, in addition to the effect of an increase in the diluent concentration which causes to the flame to be stabilised further away from the near-nozzle region, and an increase in the flame lift-off height. This greater entrainment of air and increased diluent concentrations lead to a reduction in the concentration of the reactive radical species, and a reduction in the rates of reaction due to lower flame temperatures (Namazian *et al.*, 1988).

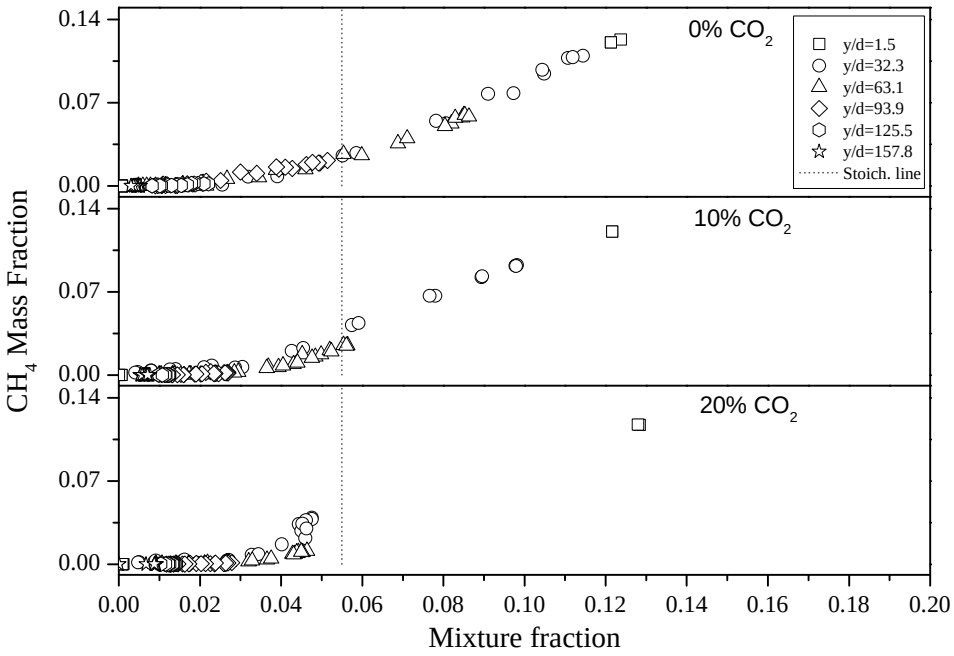

Figure 5.12. CH_4 mass fraction as a function of the mixture fraction plots for flames A, B, and C, corresponding to the CO_2 mole fraction of 0%, 10%, and 20% respective dilution levels.

This leanness may be due to (i) the thermal effect of the diluent, where the high heat capacity of the diluent on the flame leads to lower flame temperatures. Similarly, this leanness may be due to (ii) dilution effects, where the reaction rates are affected, due to the dilution of the fuel which leads to a lesser and / or the deficiency in the concentration of the reactive species in the flame. In addition, this leanness may be due to (iii) chemical effects, where the diluent takes part in chemical reactions, which leads to changes or modifications in the flame's chemistry (Lock *et al*., 2007), and / or a reduction in the fuel concentrations and a reduction in the concentration of soot in the flame.

These effects cause changes in the flame, such as in the in-flame measurement of the mass fraction of the species, the post-flame measurement of the pollutant species, and in the structural modification of the jet flame, due to the various differences in the mixing-rate of the fuel and the air in the stream-wise regions, which leads to geometrical changes in the flame (Masri and Bilger, 1986), and ultimately leads to an increase in both the length and the volume of the flame, and an increase in the flame's lift-off height at increased diluent concentrations until the flame blows out (Gollahalli,1977).

According to Masri and Bilger (1986), the concentration of the species is dependent on the flame's measurement location, due to the differences in the intensity of the mixing and the reaction rates at such locations, where the rate of mixing and reaction increases at locations in the flame with increased air entrainment and high temperatures, which enhance the chemical kinetic effects of the flame at such locations. Similarly, at different diluent concentrations, the mass fraction of the fuel varies depending on the concentration of the diluent and the location in the flame where the measurement is performed, where in mixture fraction space, this varies between 0 and 1, where 0 denotes that the flame is fuel-lean and air-rich, and 1 which is a pure fuel stream, and the flame is fuel-rich or air-lean, while the intermediate values denote streams that are partially mixed (Drake *et al*., 1987). For instance, in figure 5.12, the mass fraction of the fuel at y/d=1.5 is very high, but reduces at increased diluent concentrations. The same trend is observed at other normalised axial locations. The peak mass fraction of the fuel at the location closest to the burner is because this is the location where the fuel issues, which implies that in the mixture fraction space, the flame is fuel-rich at that location. Similarly, the lowest concentration of the fuel is expected at the tip of the

flame, where the fuel has been consumed, and at radial locations away from the jet's centreline. Therefore, in the mixture fraction space, the lowest concentration of the fuel will be observed at the fuel-lean region, and is also applicable in the other diluted cases.

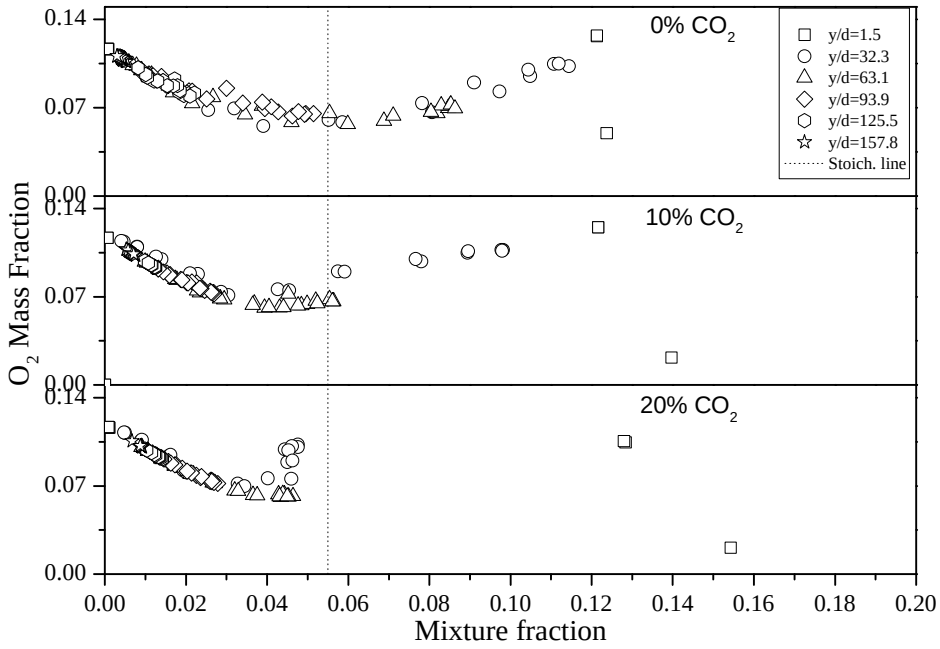

Figure 5.13 O_2 mass fraction as a function of the mixture fraction plots for flames A, B, and C.

In addition, an increase in the diluent concentration reduces the maximum mean concentration of the fuel, which implies that the dilution of the fuel-stream reduces the concentration of the fuel, making the flame fuel-lean at such locations. Similarly, the distribution of the variation of the concentration of the species showed that at increased diluent concentrations, the reactant, intermediate and product species are observed at the fuel-lean side of stoichiometric. This trend starts from the near-burner location at the 10% CO_2-diluted case, and becomes more prominent in the 20% CO_2-diluted case, as the flame approaches its blow-out limit. This trend indicates that just before flame extinction, the flame becomes fuel-lean due to either / or a combination of the thermal, chemical and dilution effects of the CO_2 on the flame, and is also consistent with the investigations of Lock *et al*. (2007). In figure 5.13, the mixture fraction plots of the three cases are shown. In all the cases, the peak mass fraction of oxygen was observed at the non-reacting region between the burner nozzle and the base of the flame stabilised above the burner, the at the tip of

the flame, and at the radial location away from the flame-front, where these locations are favourable for the entrainment of air into the flame.

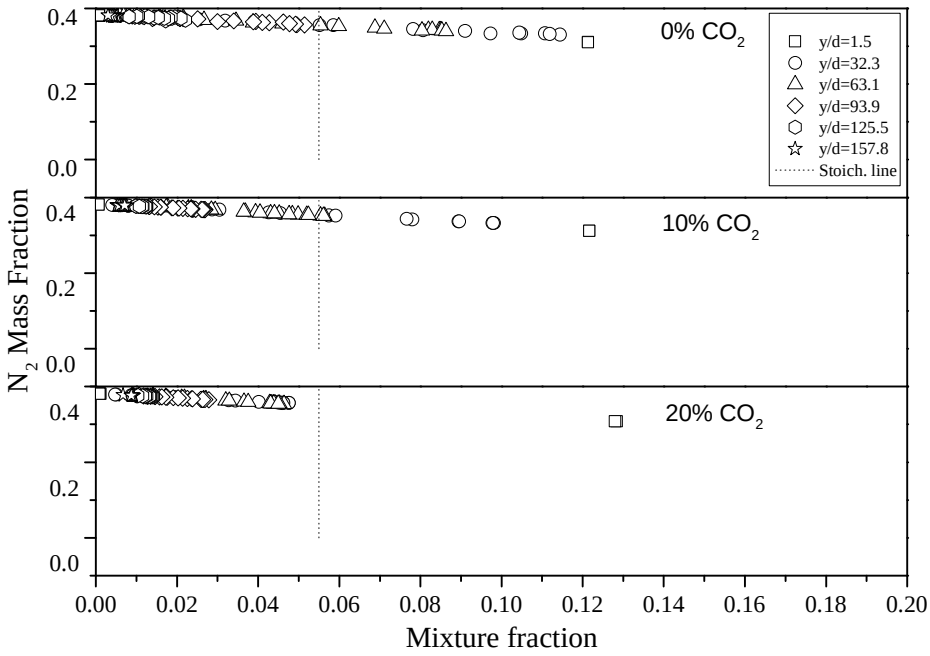

Figure 5.14 N_2 mass fraction as a function of the mixture fraction plots for flames A, B, and C.

Similarly, the profile of the O_2 mass fraction was observed to be lifted above the abscissa of the mean mixture fraction coordinate - an indication that the flame is stabilised above the burner nozzle, as shown in the photographs in figure 5.1. Similarly, in figures 5.15 and 5.16, the mass fraction of the product species have the same trend, and decrease downstream from y/d=32.3 to y/d=157.8 across the flames at different levels of dilution. Figure 5.17 shows the mass fraction of the intermediate species - CO increases downstream between y/d=1.5 and y/d=63.1, where it peaks midstream at y/d=63.1, before decreasing further axially, which suggest a favourable condition for CO formation at that location. The variation of the CO_2 mass fraction as a function of the mixture fraction shows that at 0% CO_2 diluent concentration, the maximum mass fraction of CO was recorded on the fuel-rich side of stoichiometric, while the maximum mass fraction of CO_2 was recorded on the fuel-lean side of stoichiometric.

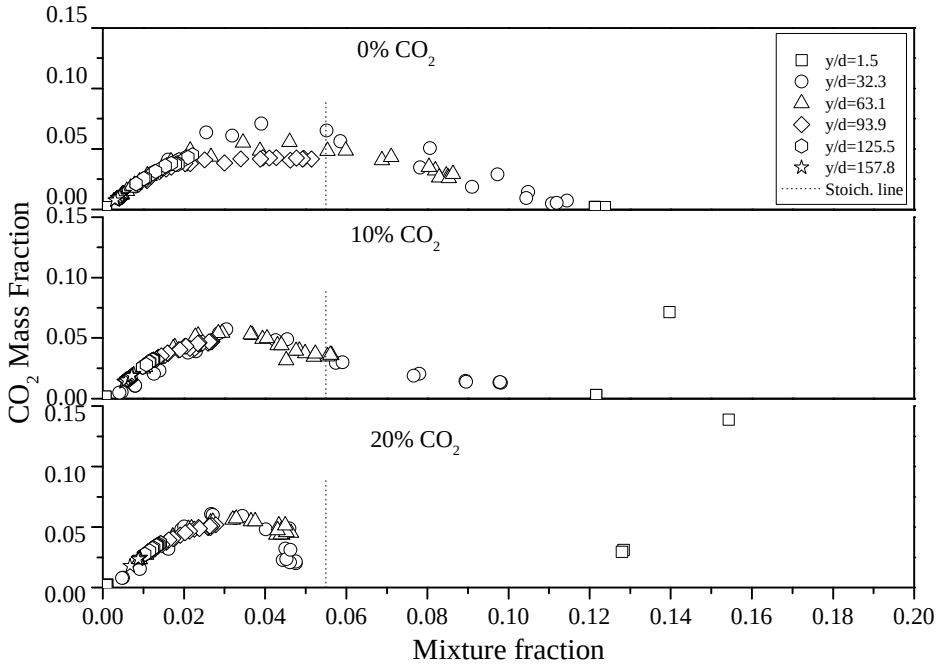

Figure 5.15 CO_2 mass fraction as a function of the mixture fraction plots for flames A, B, and C.

However, in the 10% CO_2 and 20% CO_2 fuel-stream diluted cases, the increase in the concentration of the diluent led to an increase in the CO_2 mass fractions on the fuel-rich side of stoichiometric. This is due to the extra CO_2 content in the flame, which leads to a further decrease in the flame temperature, and a slower oxidation of CO to CO_2, and hence higher CO concentrations. Similarly, in the 0% CO_2 diluent concentration case, the maximum CO mass fraction lies on the fuel-rich side of stoichiometric, while in the 10% CO_2 and the 20% CO_2 fuel-stream diluted cases, the maximum CO mass fraction lies on the lean side of the stoichiometric. This is more prominent in the 20% CO_2 diluted case, where at most of the normalised axial locations, the species lie on the fuel-lean side of stoichiometric. This suggests that the formation of CO may be promoted at locations of low concentrations of air (oxygen and nitrogen, as shown in figures 5.13 and 5.14), high concentration of the fuel (Colorado *et al*., 2009), and at reduced flame temperatures. This is because the lower the flame temperature, the lesser the rate of oxidation of CO to CO_2, due to the quenching of the oxidation reaction (RØkke and Hustad, 2005), which leads to a higher concentration of the CO in the flame. This also implies that the higher the CO_2 diluent concentration in the fuel-stream, the higher the mass fraction of CO in the flame.

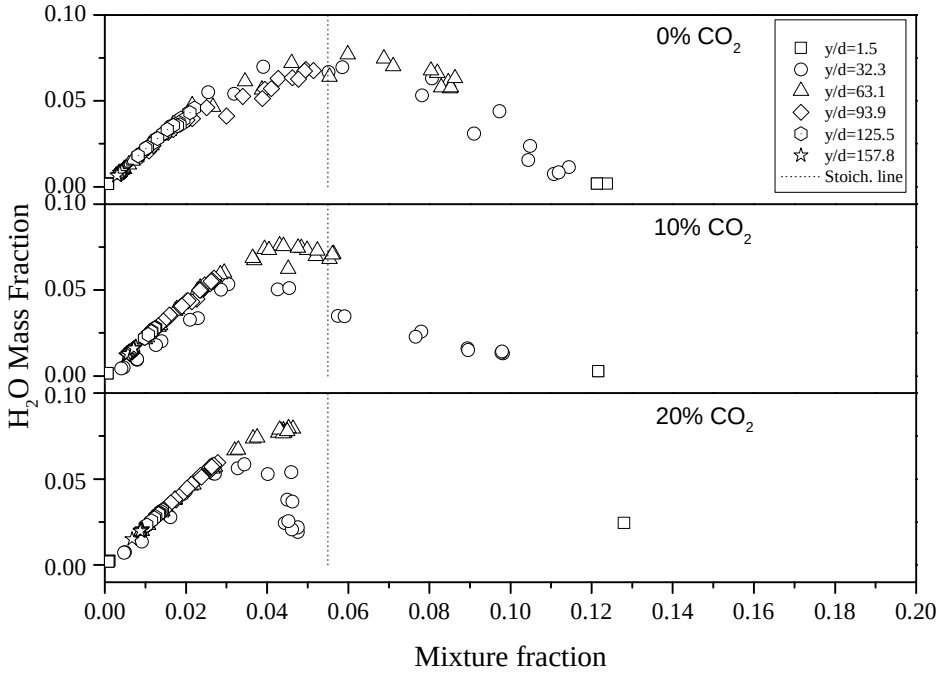

Figure 5.16 H_2O mass fraction as a function of the mixture fraction plots for flames A, B, and C.

This is as anticipated, because when CO_2 and H react to yield CO and OH, this reaction leads to a higher mass fraction of CO and OH due to the chemical effects of CO_2 on the fuel stream (Liu *et al*., 2001). In addition, the dilution of the fuel stream leads to changes in the flame's structure, and in the stoichiometry of the flame, since dilution reduces the concentration of the reactant species, which leads to a lesser concentration of the fuel for combustion. Consequently, this reduction in the concentration leads to a decrease in the flame's local and global residence times, leading to a change in the chemistry of the flame, and a shift in the stoichiometric conditions of the flame (Turns *et al*., 1993). As stated earlier, the oxidation of CO is via the reaction of CO and OH to yield CO_2 and H, as discussed in section 2.4.1.6. Similarly, soot is mainly oxidised via the OH radical (Warnatz, 2006), and this radical is also responsible for oxidising CO, implying that both soot and CO compete for oxidation by the OH radical.

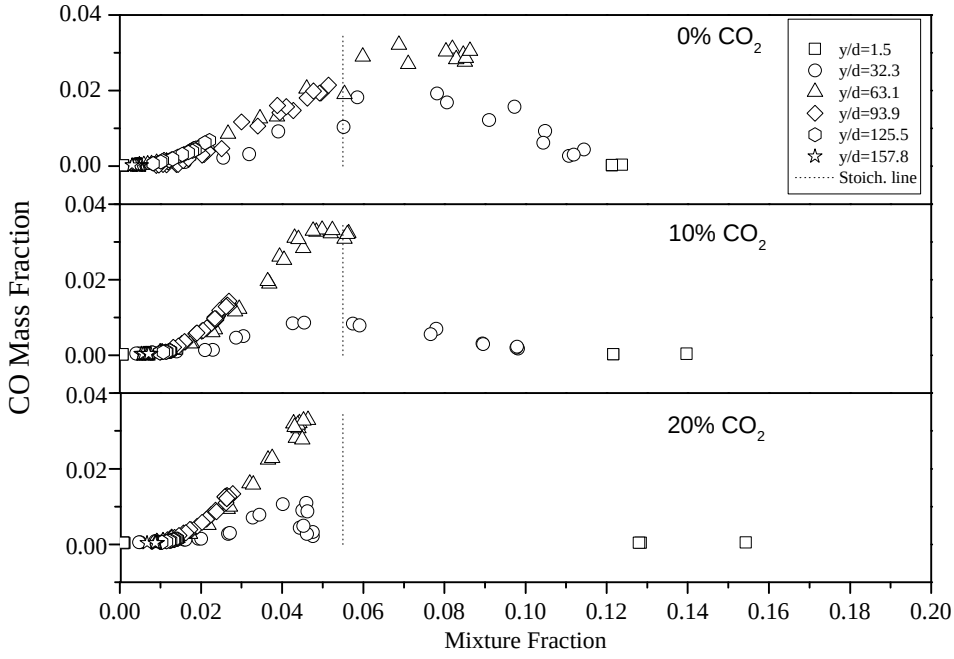

Figure 5.17. CO mass fraction as a function of the mixture fraction plots for flames A, B, and C.

If the concentration of soot in the flame is very high, this high soot concentration may reduce the CO oxidation rate because the amount of OH available in the flame may have been reduced because of the high soot concentration in the flame which consumes the OH, while decreasing the oxidation of CO in the flame, thus making soot and CO to be effectively in competition for the OH radical. Also, although CO is more reactive than soot (Puri *et al.*, 1994), this competition for the OH radical leads to the suppression of the CO oxidation when there is a high soot concentration in the flame. These soot concentrations suppress the oxidation of CO by OH, since the OH will be largely reactive with soot, because of the high concentration of soot in the flame, while the OH will be less reactive with CO because of the lower concentration of CO in the flame. In addition, at lower temperatures, the efficiency of the collision of the OH reaction with the soot particle decreases in flames that have a high soot concentration (Santoro, 1993). Similarly, at higher temperatures, up to about 28% of the collision occurring between the soot particles and the OH lead to a reaction at temperatures between 1575 K-1865 K (Neoh *et al.*, 1984). The CO oxidation reduces mainly because of the competition for OH by soot particles, leading to a reduction in the availability of the OH for CO oxidation at increased soot particle concentration. This OH concentration depends both on the flame's stoichiometry and temperature (Puri *et al.*, 1993), which may be controlled by

thermal or chemical mechanisms in the region of oxidation in the flames. The thermal effects is due to the thermal quenching of the OH as a result of radiative heat losses, while the chemical effects are due to the reaction of OH with soot particles and CO. In methane flames, the competition for OH between CO and soot is very small, which implies that the rate of oxidation of CO by OH is greater than the rate of oxidation of soot by OH. This is because CO is more reactive than soot (on a carbon basis) (Puri *et al*., 1994), and also because the sooting propensity of methane is very low at normal pressures (Brookes and Moss, 1999), where these experiments were performed. The low concentration of soot in methane flames lead to a greater reactivity in the rate of oxidation of CO by OH, than the rate of oxidation of soot by OH. As the soot concentration increases in a flame, the rate of competition between CO and soot for OH also increase. Hence the higher the concentration of soot, the higher the competition for OH, and the higher the rate of suppression of CO oxidation, such that soot becomes more readily oxidised by OH than CO, because of the high concentration of soot in the flame. Similarly, although fuel-stream dilution with CO_2 reduces flame temperatures, these lower temperatures also promote the formation of CO (Bowman, 1992) due to the effect of the quenching of oxidation reaction, thereby leading to higher CO levels in the flame, with the levels increasing with an increase in the FSD. The dilution of fuel with CO_2 has also been known to reduce the concentration of NO, and to increase the concentration of NO_2 (Liu *et al*., 2001). NO is the dominant nitrogen oxide pollutant species that is emitted by hydrocarbon flames. Although these pollutants do not take part in the combustion process, the chemical reactions which involve these pollutant species occur in an established setting of combustion reactions, thereby connecting the chemistry of these pollutants to the combustion process (Bowman, 1975). The discussions of the effect of FSD on the local NOx concentrations and on the post-flame emissions is presented in the next section.

5.5.2 NO AND NO_2 CONCENTRATION PROFILES

In Section 5.4, it was observed that increasing the mole fraction of the diluent in the fuel-stream leads to a decrease in the temperature of the flame, as a result of the high heat capacity of the diluent, which absorbs the flame temperature, thereby lowering the temperature and making the flame cooler due to decreased flame temperatures. This decreased flame temperature further has an advantage of reducing the thermal NOx concentrations in the flame. The NOx is mainly NO,

therefore the reduction in the flame temperature leads to a decrease in the NO concentrations. The effect of the different diluent concentrations on the concentration of NO, NO_2, and NOx as a function of the mixture fraction are shown in figures 5.18 to 5.20, respectively.

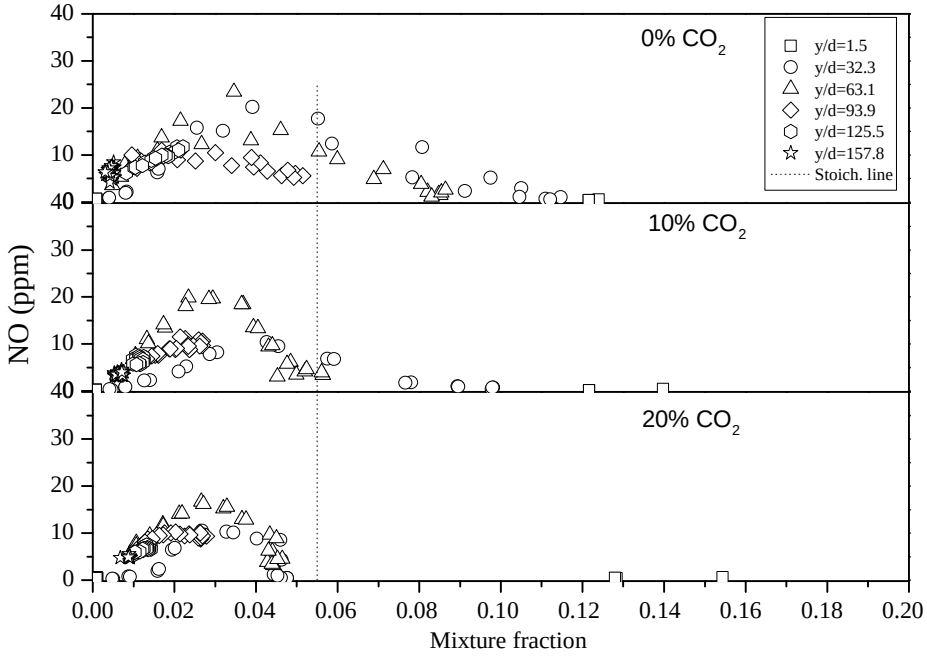

Figure 5.18. NO concentration as a function of the mixture fraction plots for flames A, B, and C.

In the three jet flames investigated, the peak concentration of these pollutant species are observed on the lean side of stoichiometric, and is consistent with the investigations of Hart *et al*. (1975) and Gollahalli (1977). This is because the higher pure fuel concentrations lead to higher flame temperatures, and an increase in the concentration of O_2 and N_2 which are available within the flame zone enhances the NO formation in the flame via the Zeldovich mechanism (Turns and Myhr, 1991). In contrast, the dilution of the fuel-stream with CO_2 leads to a decrease in the concentration of the reactant species at regions of high temperature in the flame (Ivernel, 1973). This ultimately leads to the following: losses of the radical species, slower rates of reaction due to decreased temperatures, and hence decreased NO concentrations via the Zeldovich formation mechanism (Turns, 1995). This is confirmed by the reduction in the mass fraction of the fuel at increased diluent concentrations, as shown in figure 5.12, and also in figure 5.21, where the thermal effect of the diluent decreases the temperature of the flame.

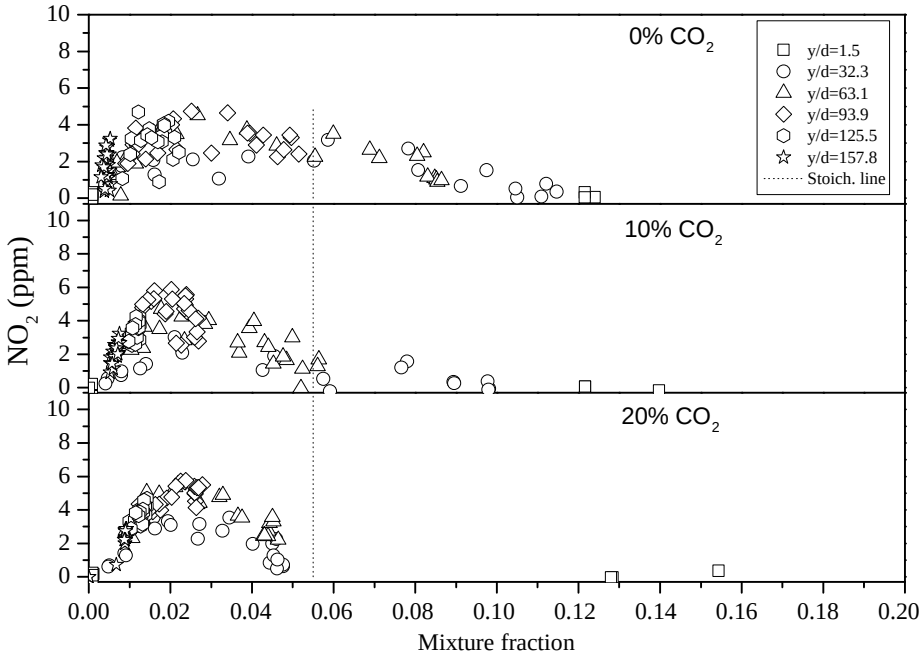

Figure 5.19. NO_2 concentration as a function of the mixture fraction plots for flames A, B, and C.

An increase in the diluent concentration of the inert in the fuel-stream leads to a flame lift-off, as explained in Section 5.3, and also leads to reductions in the fuel mass fraction and in the temperature of the flame, which leads to the flame being stabilised further away from the burner port and the flame's reaction zone moving further downstream. This causes the flame to be fuel-lean and also leads to a reduction in the NOx concentration at increased diluent concentrations. In the three jet flames studied, the maximum concentrations of NO were 23.4 ppm, 19.9 ppm, and 16.7 ppm, while the maximum concentrations of NO_2 were 4.7 ppm, 5.8 ppm, and 5.9 ppm, corresponding to the 0% CO_2, 10% CO_2 and 20% CO_2 diluent concentrations in the jet streams, respectively.

From the profiles of the NO and NO_2 concentrations, the dilution of the fuel-stream with the 10% and the 20% CO_2 diluent concentrations decrease the NO concentration in the flame by 15% and 29%, while the same diluent concentrations increase the NO_2 concentrations in the flame by 23% and 26%, respectively. This demonstrates that increasing the diluent concentration decreases the NO concentrations, while increasing the diluent concentration leads to an increased NO_2 concentrations, and is consistent with the investigations of Marinov *et al*. (1998). Hydrocarbon flames consist of about 90% NO in NOx (Bowman, 1992; Namazian

et al., 1994), while the contribution of NO_2 is about 7-10% (Turns and Lovett, 1989), which suggests that the concentration profile of NO and NOx are similar.

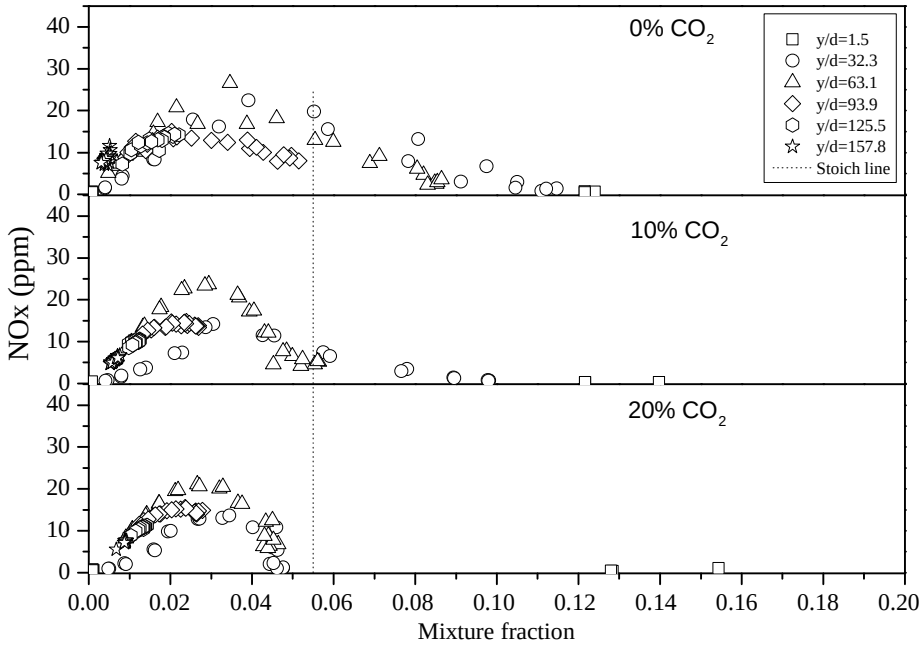

Figure 5.20. NOx concentration as a function of the mixture fraction plots for flames A, B, and C.

In the jet flames studied, the concentration of NO_2 measured in the CH_4 flame was very small. This is due to the slow rate at which NO is converted to NO_2 in CH_4 flames, because of the low propensity of CH_4 to produce the HO_2 radical during the NO to NO_2 oxidation. The effectiveness of the HO_2 radical to oxidise NO to NO_2 is greater at lower flame temperatures. For example, propane flames are the most effective of the C_1-C_3 hydrocarbons in a low temperature ranging from 700K and above, ethylene – 800K and above, while in methane flames, the effectiveness is from 1000K and above (Marinov *et al*., 1998). The effectiveness of the conversion of NO to NO_2 in methane flames is low because of the higher temperature at which the HO_2 radical promotes the conversion of NO to NO_2, thereby leading to low NO_2 concentrations. In figure 5.19, it was found that the NO_2 concentration in the flame increased at increased diluent concentrations.

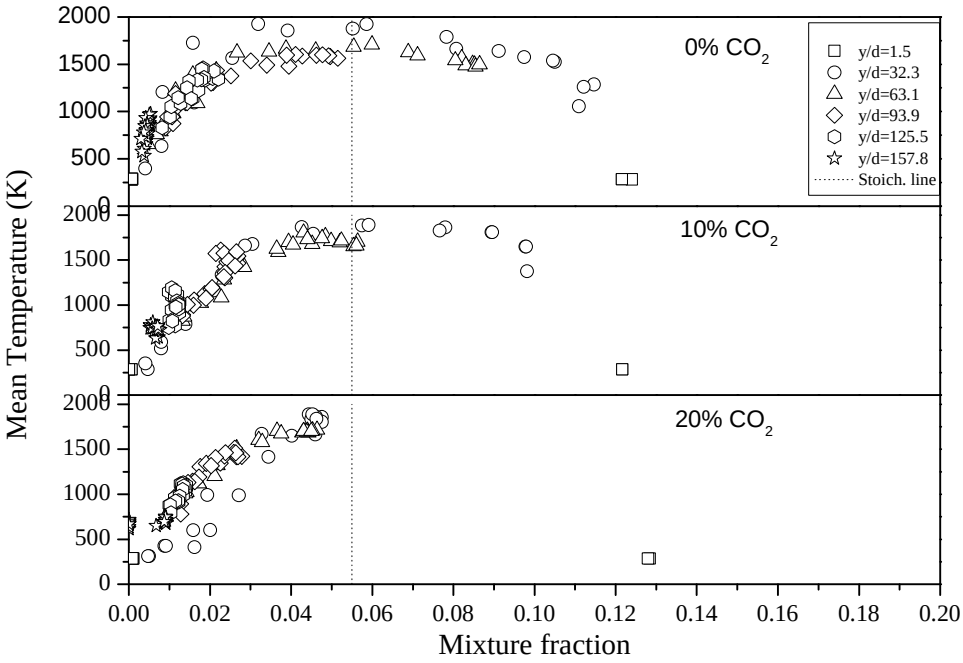

Figure 5.21. Mean temperature as a function of the mixture fraction plots for flames A, B, and C.

This is because, as already stated, between the diluted and the undiluted cases, the rate of production of HO_2 is slow in methane flames, which leads to a lesser conversion of NO to NO_2 in the undiluted case, due to the higher flame temperature in the undiluted case, which leads to a slow rate of production of the HO_2 radical, and hence, a slow NO to NO_2 conversion, leading to a lower NO_2 conversion in the undiluted case, compared to the diluted cases. However, in the 10% CO_2 and 20% CO_2 diluted cases, the dilution of the fuel stream leads to a lower flame temperature due to thermal effects, and this low temperatures promote the conversion of NO to NO_2, due to the low temperature which is effective for the production of the HO_2 radical, and hence a greater concentration of NO_2 in the diluted cases, compared to the undiluted case.

5.6 EFFECT OF FUEL-STREAM DILUTION ON EICO, EINO AND EINO$_2$

The pollutants emitted at the post-flame location in the flame may be controlled by the reactant species composition, the temperature and the structure of the flame, and the chemical reaction which occurs at such locations. These pollutants are measured and reported as an emission index (EI). The EI is the mass of the pollutant emitted (grams) per mass of the fuel that is combusted (kilogram) (Gollahalli, 1977), and is expressed in equation (2.46). The NOx emissions from

fossil fuels is attributed to NO which oxidises to NO_2 in the atmosphere (Pourkashanian *et al*., 1998), therefore the EINOx is normally reported as an NO_2 equivalent, and the molecular weight of NO_2 is used in estimating the EINOx (Driscoll, *et al*., 1992; Turns *et al*., 1993).

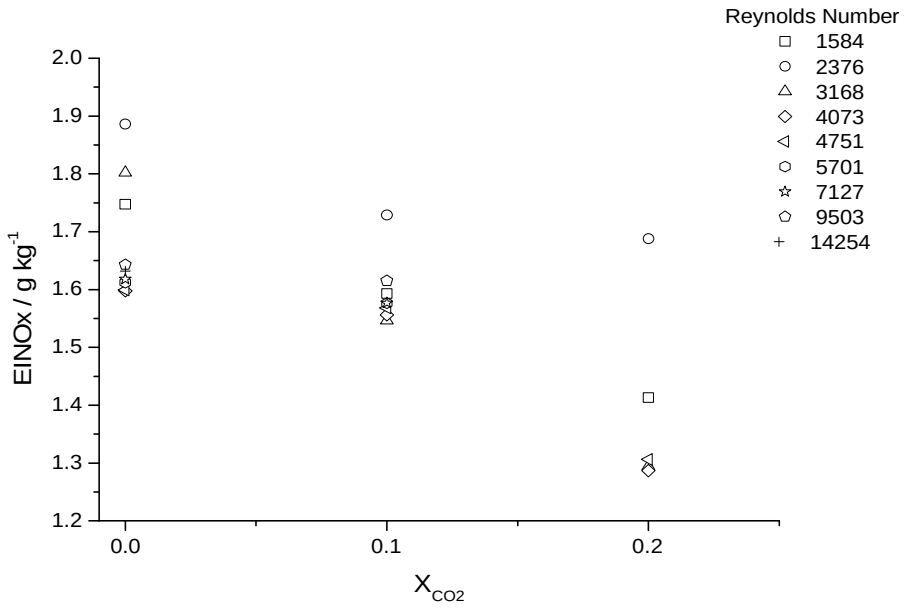

Figure 5.22 EINOx as a function of the CO_2 diluent mole fraction.

Figures 5.22 to 5.24 show the variation of the EI of the pollutant as a function of the diluent mole fraction. Similarly, it was observed that by increasing the concentration of the diluent in the jet stream, the EINOx decreased, while the EICO was increased. The decrease in the EINOx is due to the fuel dilution which leads to the lower concentration of reactant species, and lower flame temperatures because of the thermal effect of the diluent, which leads to a decrease in the formation of NOx via the Zeldovich mechanism. The EINOx profile follows the same trend as the EINO profile, even at Reynolds numbers ranging from 1584-14254, as shown in figure 5.23.

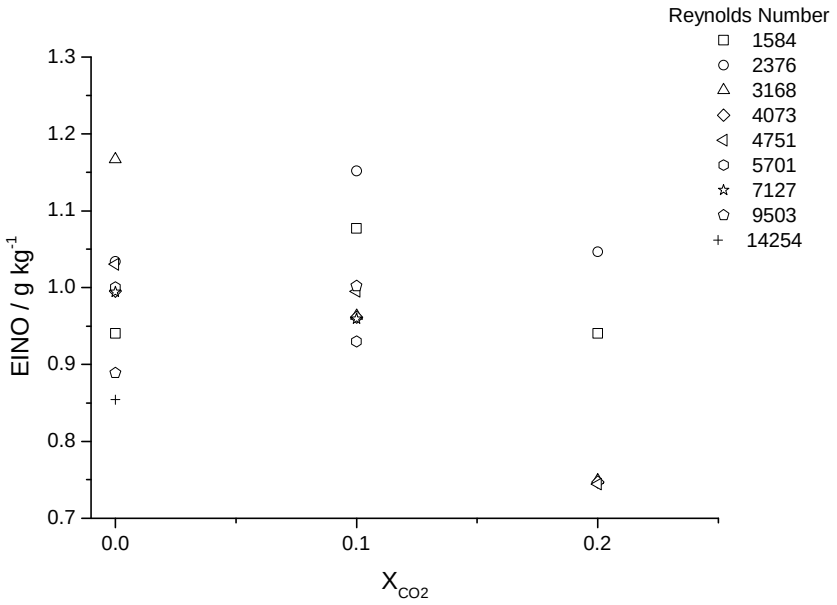

Figure 5.23 EINO as a function of the diluent mole fraction at different Reynolds number.

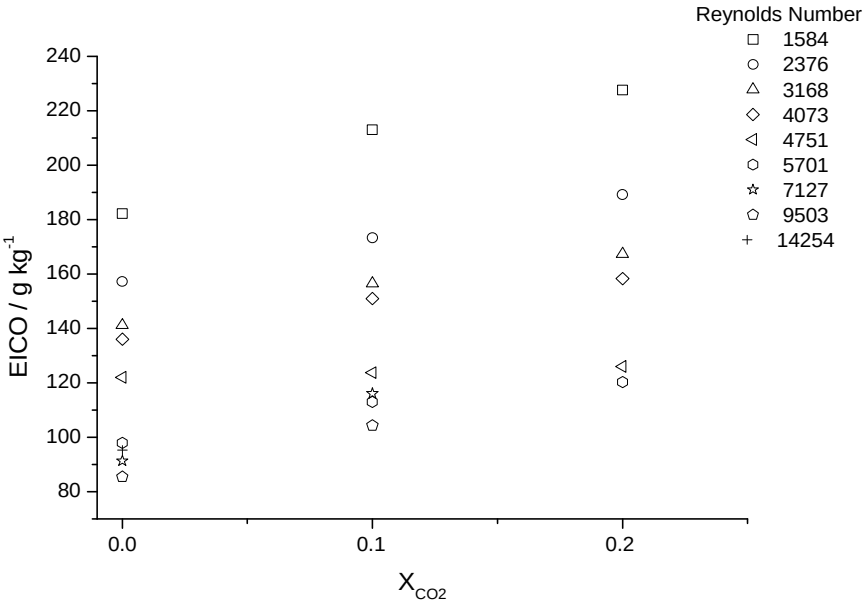

Figure 5.24 EICO as a function of the diluent mole fraction at different Reynolds number.

In figure 5.24, the effect of CO_2 dilution on EICO is presented and it is observed that the EICO increases as the diluent mole fraction increases. This trend may be explained by the thermal effect of the diluent which leads to lower temperatures. This low temperatures slow down the rate of oxidation of CO to CO_2 which inhibits the full oxidation of CO to CO_2 at the post-flame region, through the reaction of CO

with OH, which is slow. This decrease in the temperature due to the dilution of the fuel stream leads to a slower CO burn-out, and hence a greater concentration of CO, and an increase in the EICO when the concentration of the diluent is increased. This trend was also observed at all the range of the Reynolds numbers that were investigated, and is also consistent with the observations of Turns and Bandaru (1993). In figure 5.25, the variation of $EINO_2$ at different diluent mole fractions in the duct is presented. At this post-flame location, there are more NO_2-forming radicals due to the air dilution, and less fuel concentration. The mixing of the combustion product with air, and reduced flame temperatures at this location promote the formation of HO_2 radicals and a faster NO to NO_2 conversion. The slow residence time at the post-flame region due to dilution (Turns and Myhr, 1991), or a reduction in the mixing rate beyond the flame, due to the reduced velocity difference (Hori, 1986), may be responsible for this conversion.

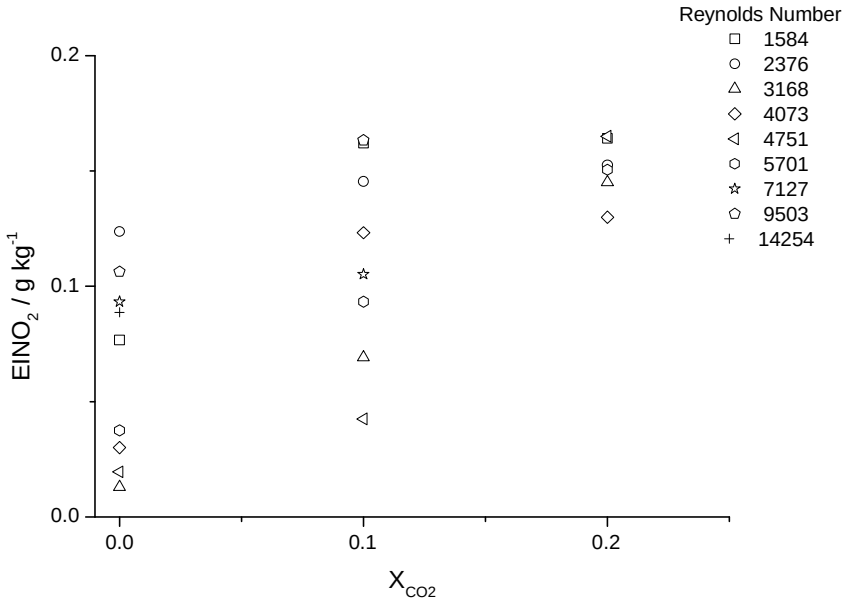

Figure 5.25 $EINO_2$ as a function of the diluent mole fraction at different Reynolds number.

The amount of NO to NO_2 conversion is very small if the rate of mixing of the combustion products with air is very small, but the conversion becomes very significant at higher mixing rates. This is because flame velocities are very low at downstream locations closer to the tip of the flame. As the velocity of the flame product and the air stream approach each other, there is a diminished-mixing, and hence factors such as the low co-flow velocity could impact the mixing rate of combustion products with cold air at the flame tip (Driscoll *et al*.,1992), hence there

is higher NO_2 conversion because of the higher dilution and lower temperature. Methane already has a lower tendency to form HO_2 due to its high effective temperature, and therefore the dilution of methane at the post-flame region leads to a lower flame temperature. This promotes a higher HO_2 radical formation and a higher NO to NO_2 conversion, hence higher $EINO_2$. However, the NO to NO_2 conversion could be reduced in the post-flame region by increasing the temperatures to between 1100 K -1400K (Amano and Hase, 1994).

Chapter 6

COMPARISON OF POLLUTANT EMISSIONS FROM METHANE AND PROPANE FLAMES AND THE EFFECT OF FUEL-STREAM DILUTION ON SOOT EMISSION IN PROPANE DIFFUSION FLAMES

6.1 INTRODUCTION

In the last two chapters, the effects of varying the fuel jet velocity and the diluent mole fraction of CO_2, respectively, on the temperature, flame structure, and on the composition of species in methane / air jet flames were investigated, where the consequences of varying these test conditions on the emission indices of the pollutant species were examined.

Fuel	CH_4	C_3H_8
Flow regime	Buoyancy-controlled	
Reynolds number	5700	
Froude number	21000	1800
Jet velocity (m/s)	27	7.6
Heat Release rate (kW)	8	5
Mixing	Non-premixed and unconfined	
Co-flow air velocity (m/s)	0.3	
Duct suction velocity (m/s)	6.6	
In-flame and post-flame measurements	Emission indices of species, average visible flame length, average lift-off distance, soot emission factor, and soot morphology	

Table 6.1 Test conditions for the present investigation.

In this chapter, a comparison of the emission indices of methane and propane jet flames, and the effect of varying the fuel-stream diluent mole fraction on propane flames on soot morphology is presented. The experimental conditions are shown in Table 6.1. The choice of methane and propane in this investigation was because these fuels were affordable, and also because propane has a higher sooting propensity than methane, and as such, propane was also utilised in the subsequent

investigations on the effect of CO_2 dilution on soot morphology which is reported later in this chapter.

(a) **(b)**

Figure 6.1 Photograhs of (a) methane, and (b) propane flames

These fuels were compared based on equal Reynolds number, and both flames were in the buoyancy-dominated regime. A comparison of the results obtained on the visual observation, flame structure, temperature, in-flame composition of major species, and the EI of the pollutant species for the different fuels are presented in the next section.

6.2 VISUAL OBSERVATION OF THE FLAME

Figures 6.1 (a) and (b) are photographs of the lifted methane and attached propane flames, respectively. The results show that flame A consists of a shorter flame with a wider flame base, added with a bluish edge, and an orange-yellowish colour at the far-burner region, while flame B is longer and slender at the flame base, and has a higher luminosity than flame A. The larger base of flame A compared to flame B is due to the stabilisation of the flame above the rim of the jet nozzle which leads to an enhancement of air entrainment into the flame, due to partial-premixing which is favourable for the mixing of the fuel and oxidiser streams (Namazian *et al.*, 1988), thereby widening the flame base, which increases at higher

strain rates until flame extinction occurs. The luminous orange-yellow colour of the flames, which is due to the incandescence of carbon particles in the flame indicates the presence of soot, while the non-luminous bluish colour of the flame is an indication of CO (Giovanetti *et al*., 1980; Choudhuri and Gollahalli, 2000). The luminosity of the flame increases with the number of carbon atoms in the hydrocarbon, thereby promoting soot, due to the increase in the carbon content in the flame (Haynes and Wagner, 1981), which leads to a higher soot volume fraction in flame B, compared with flame A. Similarly, the mean visible flame length and mean lift-off height of flame A were 51.3±5 cm and 8.5±4 cm, respectively, while the mean visible flame length of flame B was 60.4±5 cm, thus indicating that the mean visible flame length of flame B was higher than flame A. This is expected because in the lifted flame – flame A, increasing the air entrainment into the jet flame causes the flame to be stabilised at a location above the burner, where a lesser mixing of the air is required for complete combustion, therefore the flame becomes shorter. However, in the attached flame –flame B, the flame length is longer because based on the stoichiometric requirement for propane /air combustion, a greater volume of air is required for the combustion of propane than methane, therefore the propane flame extends to a height where the total flux of the air that is entrained into the flame would be sufficient for the complete combustion of propane. Therefore a longer flame length will be required for the combustion of propane than methane, and this suggests the reason for the longer flame length of flame B than flame A, as expected. The measured flame length and the lift-off height matches the linear relationship between the flame's average lift-off height and the jet velocity by Kalghatgi (1984), which has been verified by Chen *et al*. (1992) which are expressed in equations 2.40 and 2.41 for methane and propane flames, respectively.

6.3 TEMPERATURE PROFILES

The radial temperature profiles at three axial locations of the lifted methane flame and the attached propane flame are presented in figures 6.2 (a) and (b). Both flames exhibit an off-axis maximum mean temperature at y/d=32.3 and 63.1, but further downstream at y/d=93.9, only flame A has an off-axis peak as shown in figures 6.2 (a) and (b). In flames A and B, the steepest gradient of the temperature profile is at y/d=32.3 and shows a more rapid decrease in the temperature in the radial direction, while at the far-burner region (y/d=93.9), both flames have the least steep profile. The difference in the steepness of the profile at each axis is an

indication of the level of air entrainment into the flame, leading to different levels of dilution at those locations. Similarly, the highest temperature in flames A and B were 1985 K and 1700K, respectively. The difference between the maximum temperature in both flames is about 285 K, and this maximum temperature depends on factors such as the rate of dilution of the fuel stream, heat release rates, etc. (Gollahalli,1998).

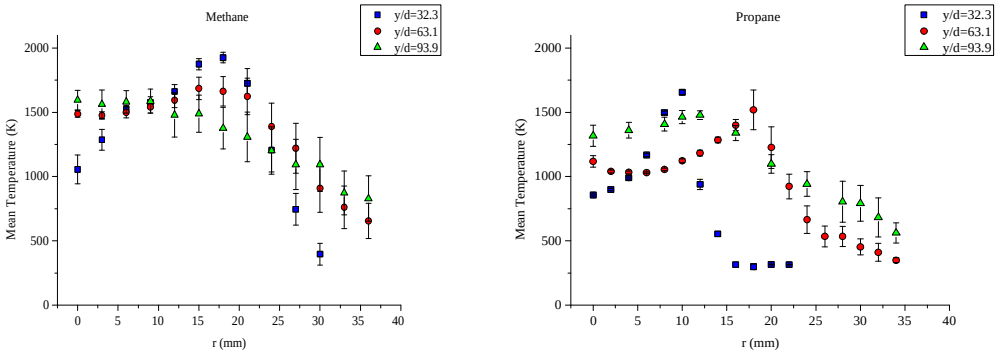

Figure 6.2 Mean temperatures of (a) methane, and (b) propane flames.

This is expected because flame A has a higher jet velocity than flame B, therefore, although the flames are in the buoyancy regime (with a Froude number 21000 and 1800 for flames A and B, respectively), the flames are compared based on equal *Re*, and on the dependency of *Re* on the jet velocity (strain rate), higher strain rates yield higher flame temperatures (Turns and Myhr, 1991). The lower flame temperature of flame B is due to the in-flame soot concentration which leads to a higher radiation, compared to flame A, as expected. This is because according to Turns and Myhr (1991), in the buoyancy-dominated regime, an increase in the sooting propensity of a flame leads to a decrease in the flame temperature for all fuels.

6.4 COMPOSITION PROFILES OF MAJOR SPECIES

Comparisons of the respective radial concentration profiles of the fuels, oxygen, nitrogen, carbon monoxide, carbon dioxide, water, and nitrogen oxide at three different axial locations of flames A and B are shown in figures 6.3 - 6.9.

6.4.1 CH_4 AND C_3H_8 MOLE FRACTIONS

In figures 6.3 (a) and (b), the profiles of the fuels for flames A and B, respectively, are presented. The highest mole fraction of the fuel was at y/d=32.3,

which is the closest location to the burner nozzle where the fuel issued, and where the highest concentration of the fuel is expected.

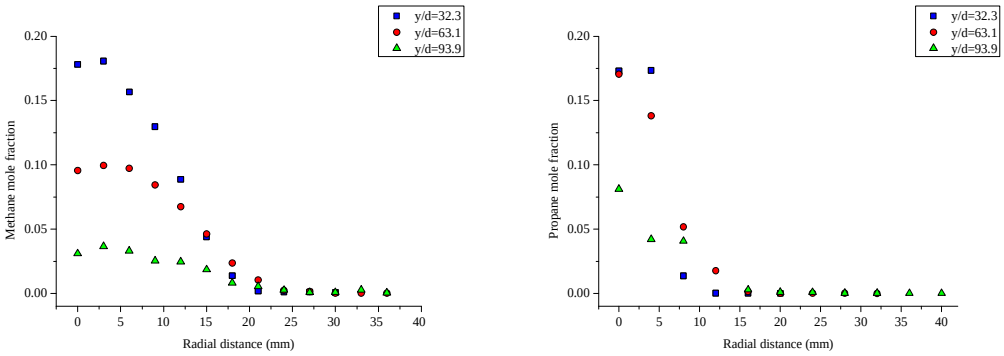

(a) **(b)**

Figure 6.3 Fuel mole fraction as a function of the radial distance for (a) methane, and (b) propane flames, respectively.

In addition, at all the downstream locations, the highest mole fraction of the fuels were at the flame's centreline, and the fuel mole fraction decreased radially outwards away from the burner nozzle. Similarly, at y/d=63.1 and y/d=93.9, the fuel mole fraction of flame B was higher than flame A. This is expected because flame B has a longer flame length than flame A due to the stoichiometric requirement of the fuel and air needed for combustion, which increases the length of flame B, thereby requiring more fuel and air for combustion, than flame A. Similarly, mixing is more enhanced in flame A, because flame A is stabilised above the burner, where air entrainment is favourable, in addition to the higher temperature at y/d=63.1 and y/d=93.9 in flame A, which leads to a more intense consumption of fuel, and hence a less fuel mole fraction in flame A than flame B.

6.4.2 O_2 MOLE FRACTION

The profiles of O_2 for flames A and B are presented in figures 6.4 (a) and (b), respectively. It is seen that the profiles of these flames are different. This is due to the differences in the stability of the flames. Whereas flame A is stabilised above the jet nozzle, flame B is attached to the rim of the nozzle. These differences in the stability leads to differences in the structure of the flame, which are explained as follows: the stabilisation of the jet flame either above the jet rim (lifted flame) or on the jet rim (attached flame) has different consequences on the level of the air which is entrained into the flame. The lift-off in flame A leads to a higher air entrainment, since the flame base is a favourable location of air entrainment, compared with

flame B, where the attachment of the flame on the jet rim leads to a lower entrainment of air into the flame.

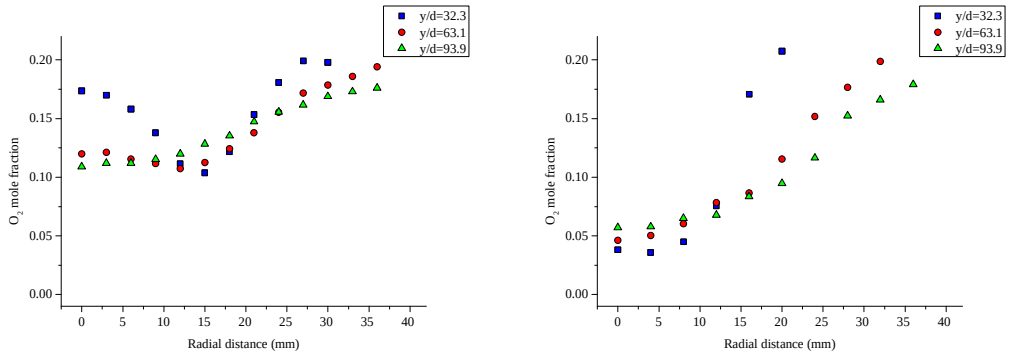

(a) **(b)**

Figure 6.4 O_2 mole fraction as a function of the radial distance for (a) methane,and (b) propane flames, respectively.

The higher mole fraction of O_2 at the centreline at y/d=32.3 in flame A is an indication of the higher entrainment of air into the flame compared to flame B. Similarly, at y/d=32.3, moving radially away from the flame's centreline, the O_2 mole fraction decreases up to a radial location where it starts to increase again. Also, the "V" structure is an indication of the location in the flame where the measurement was made. This is the leading-edge of the flame where the flame is stabilised above the jet nozzle. However in the case of the attached flame - flame B, the mole fraction of O_2 reduces at the flame's centreline and increases radially outwards, as expected. Also, in all the axial locations, the centreline O_2 mole fraction of flame A is higher than flame B because of the lift-off in flame A which enhances higher air entrainment into the flame.

6.4.3 N_2 MOLE FRACTION

In figure 6.5, the N_2 mole fraction profile for both flames are presented. The composition of air is mainly O_2 and N_2, with N_2 having a higher mole fraction than O_2. In both flames, at all the axial locations, the lowest mole fraction of N_2 is at the centreline, where the highest mole fraction of the fuel is recorded, while the N_2 increases radially away from the jet centreline, where the maximum mean mole fraction is observed. In addition, traversing radially away from the jet centreline, the mean mole fraction of N_2 becomes uniform at downstream locations in the flame,

which indicates that there is no fuel to react with the air, and hence this location is far away from the flame zone.

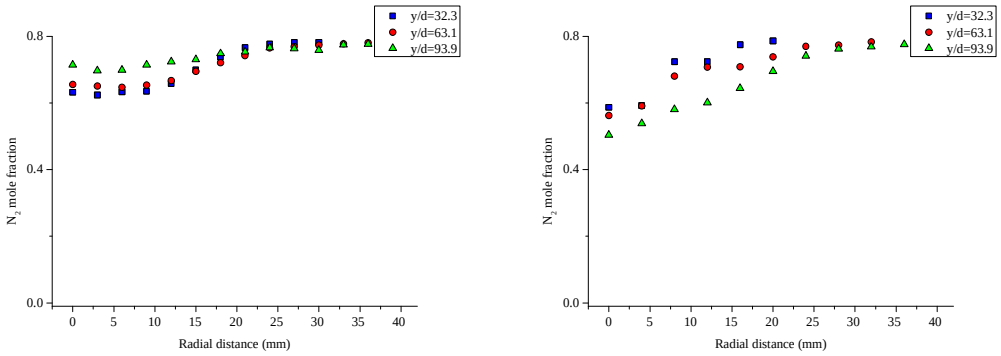

(a) **(b)**

Figure 6.5 N_2 mole fraction as a function of the radial distance for (a) methane, and (b) propane flames, respectively.

Similarly, a comparison between flames A and B show a difference in the concentration profile of N_2 at the different axial locations, especially in flame B, while there is no significant difference in this profile at downstream locations in flame A. This is due to the difference in the entrainment of air into the flame, where there is a lower level of air entrainment into the flame in flame B, compared to flame A. This leads to a better mixing in flame A, since flame A is a lifted flame, which supports a higher air entrainment compared to flame B, as expected. In practical flaring systems, air (O_2 and N_2) is used as the oxidant, not pure oxygen, thereby yielding products such as C, CO, CO_2, N_2O, NO, NO_2, UBHCs, traces of impurities (VOCs, PAHs), etc. Nitrogen reacts with oxygen to form NO, as already discussed in section 2.4.2. The difference in the concentration of NO between flames A and B will be discussed later.

6.4.4 CO and CO_2 MOLE FRACTION

The profiles of the CO for flames A and B are shown in figures 6.6 (a) and (b), respectively, while the profiles of CO_2 for flames A and B are shown in figures 6.7 (a) and (b). The pathways for the formation of CO are shown in Section 2.4.1. CO is an indicator of the degree of incomplete combustion. Comparing the CO profiles of these flames at all axial locations, it is observed that flame B has a higher CO mole fraction than flame A. This is due to incomplete combustion in flame B, since there is insufficient air and lower temperatures which are required to oxidise CO to CO_2, whereas, the higher entrainment of air into flame A, and the higher

temperatures lead to a better mixing, and hence a better combustion, leading to a lower CO mole fraction at y/d=93.9, compared to the mid-flame, at y/d=63.1, and a generally lower CO mole fraction in flame A, since the CO has been rapidly oxidised to CO_2, compared to flame B.

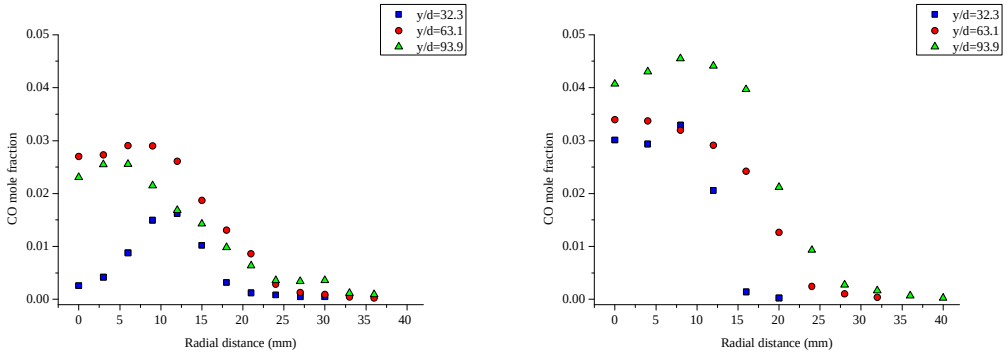

(a) **(b)**

Figure 6.6 CO mole fraction as a function of the radial distance for (a) methane,and (b) propane flames, respectively.

Similarly, the higher CO_2 mole fraction in flame B compared to flame A is due to the increase in the number of carbon atoms in flame B because of the stoichiometric requirement of the fuel and the air for the combustion of flame B, leading to greater products of combustion in flame B than flame A. The temperature and the stoichiometry of the flame affects the rate of formation of CO_2, which explains the similarity in the radial profiles of the temperature and CO_2 in both flames. Similarly, the CO_2 radial profile and the H_2O radial profile shown in figures 6.8 (a) and (b), follow the same trend because they are both products of combustion.

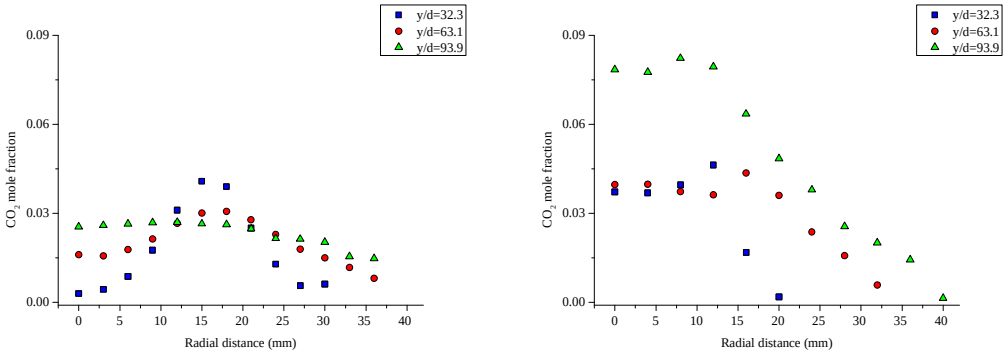

(a) **(b)**

Figure 6.7 CO_2 mole fraction as a function of the radial distance for (a) methane, and (b) propane flames, respectively.

In hydrocarbon flames, the oxidation of CO to CO_2 is primarily via the reaction of CO with OH to yield CO_2 and H, as shown in reaction R2.4.1.6, while other likely routes are via reactions with the HO_2 and O_2 radicals, as shown in reactions R2.4.1.7 and R2.4.1.8, respectively. Hydrocarbons which produce reactive radicals, such as OH or O-atoms, are the most effective in promoting hydrocarbon oxidation which lead to more HO_2 production. This eventually reacts with CO to produce CO_2 and OH. However, this reaction is only significant at temperatures above about 1600K, and the reaction involving O_2 is very slow compared with the reaction involving the OH radical. In addition, the oxidation of CO to CO_2 depends on factors such as the level of mixing, the amount of the air that is entrained into the jet flame, and on the rate of oxidation of CO to CO_2. This oxidation rate is temperature-dependent. At low temperatures, the rate of oxidation of CO to CO_2 is reduced (RØkke and Hustad, 2005), leading to the formation of more CO as a result of the quenching of the oxidation reaction, and the greater number of carbon atoms in flame B, which explains the reason for the greater CO mole fraction in flame B compared to flame A.

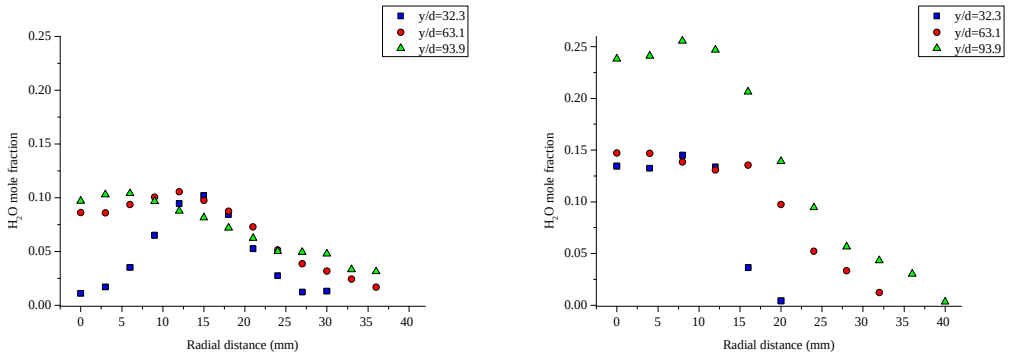

(a) **(b)**

Figure 6.8 H_2O Mole fraction as a function of the radial distance for (a) methane,and (b) propane flames, respectively.

6.4.5 NO CONCENTRATION

The profiles of NO for flames A and B are shown in figures 6.9 (a) and (b), respectively. Flame B has a higher NO concentration than flame A, despite the difference in the fuel jet velocity between both flames. This is because the adiabatic flame temperature for flame B is higher than for flame A, therefore a higher NO production rate would be expected for flame B than flame A. In flame A, the NO concentration profile follows the temperature profile. This is expected because the

maximum temperature in flame A is 1985 K, therefore the Zeldovich NO formation route is likely, since the thermal NO formation is dependent on the temperature in flames where the temperature is above 1800 K, because of the high activation energy requirement for the initiation of the reaction. In flame B, the maximum flame temperature is about 1700 K, therefore, the formation of NO via the Zeldovich mechanism may not be likely, implying that Prompt NO may be significant. Prompt NO are more prominent in fuel-rich than in fuel-lean flames, and are weakly dependent on the flame temperature (Hayhurst and Vince, 1980), contributing between 10 ppm to 30 ppm of the total NO levels in a hydrocarbon flame, while the thermal NO has a contribution of about 100 ppm (Peters and Donnerhack, 1981). NOx is made up of about 90% NO, while the percentage of NOx that is NO_2 varies between 8 - 80%, and NO is converted to NO_2 in the atmosphere (Driscoll *et al*., 1992). The formation of NO_2 is determined by the role of the hydrocarbon to yield radicals such as OH for the oxidation of the fuel, and in the production of the HO_2 radicals which aids in converting NO to NO_2.

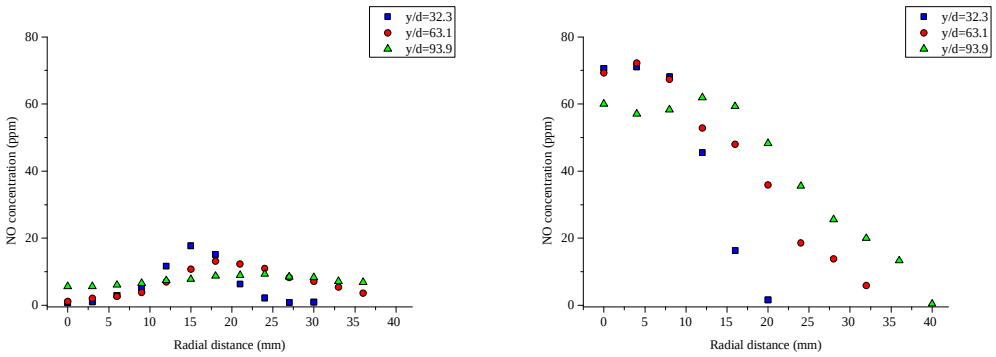

(a) **(b)**

Figure 6.9 NO concentration as a function of the radial distance for (a) methane, and (b) propane flames, respectively.

NO_2 is formed mainly by the oxidation of NO during combustion, in cooler regions of the flame at temperatures of about 700 K. The oxidation of NO to NO_2 is effectively promoted via the reaction of NO with HO_2 to yield NO_2 and OH, although reactions with other radicals exist, such as $HORO_2$ and RO_2, but are not significant. Hydrocarbons, which produce radicals such as OH, O-atom, etc., are more effective in promoting this NO oxidation and producing the HO_2 radical which reacts with NO to yield NO_2. However, hydrocarbons, which produce radicals such as the methyl and allyl radicals, tend to limit the oxidation of the NO to NO_2. This is

because the methyl radical promotes the reduction of NO_2 to NO, at higher reaction temperatures and longer residence times, thereby reducing NO_2 levels in the flame via the reversible reaction: $NO_2 + CH_3=CH_3O + NO$. The reaction of HO_2 with the NO to yield NO_2 and OH, further oxidises methane due to the OH which is produced. At increased temperatures, more NO_2 is formed as methane is oxidised, but the conversion of NO to NO_2 is limited because of the slow rate of production of HO_2 (due to the high temperature in methane), and due to the reduction of NO_2 to NO via the methyl radical. Amongst the $C_1 – C_3$ hydrocarbons, the effectiveness of the conversion of NO to NO_2 via the HO_2 radical is dependent on the type of fuel, and is more effective at low reaction temperatures. Propane is more effective due to its low reaction temperature which promotes the conversion of NO to NO_2 via the HO_2 radical. Methane is less effective because of its high reaction temperature which leads to the production of a small amount of the HO_2 radical, thereby slowing the NO - NO_2 oxidation. The temperature which promotes the NO-NO_2 conversion via the HO_2 radical is about 700K in propane flames, while it is about 1000 K in methane flames. Therefore, the conversion of NO to NO_2 is slower in methane flames, because of the higher reaction temperature for this conversion, compared to the higher conversion which is due to the lower reaction temperature in propane flames.

6.5 MIXTURE FRACTION OF SPECIES

Plots of the major species in mixture fraction space are shown in figures 6.10 to 6.16. As discussed in Section 4.6, the expression by Masri and Bilger (1986) was employed in determining the mixture fraction, which is based on the carbon atom balance of the fuel, CO, and CO_2 that were measured in this experiment. For a methane-air and a propane-air flame, the stoichiometric mass fraction for the completion combustion of these fuels using air as the oxidiser are 0.055 and 0.06 (Kalghatgi, 1981), respectively, and is represented by the vertical dotted lines in the plots, where the left and the right hand sides of the dotted lines are the fuel-lean (oxygen-rich) and the fuel-rich (oxygen-lean) regions of the flames, respectively.

In figures 6.10 (a) and (b), the plots of the mean mass fraction as a function of the mixture fraction for the methane and propane fuels are presented. In both cases, the maximum mass fraction of the fuel was at the fuel-rich side of stoichiometric, y/d=32.3, as expected. This is because this is the downstream location close to the burner where the fuel issues and it is expected that the mass fraction of the fuel be

higher at this location than further downstream. However, at y/d =63.1, the mass fraction of propane is higher than methane at this location. This is because the higher jet velocity and the higher entrainment of air into the lifted methane flame promotes a greater mixing than the propane. Therefore more fuel is consumed at that location in the methane flame than the propane flame, and hence a higher concentration of the propane fuel at that location in the flame.

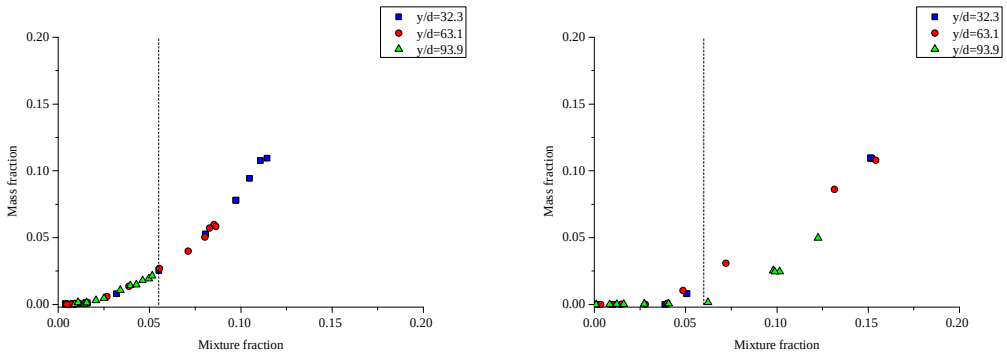

(a) **(b)**

Figure 6.10 Mass fraction as a function of the mixture fraction for (a) methane, and (b) propane fuels, respectively.

Similarly, the maximum mass fraction of propane is higher than that of methane. In addition, at y/d=93.9, the maximum mean mass fraction of the fuel in flame A lies on the fuel-lean side of stoichiometric, while that of flame B lies on the fuel-rich side of stoichiometric.

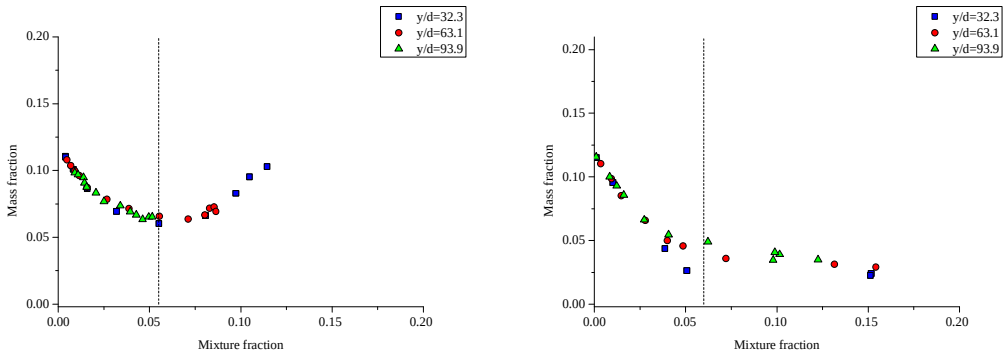

(a) **(b)**

Figure 6.11 O_2 mass fraction as a function of the mixture fraction for (a) methane, and (b) propane fuels, respectively.

The difference in the region of the maximum mean mass fraction in both flames at y/d=93.9 is due to the shorter flame length and the greater mixing due to the higher

air entrainment into flame A which promotes a faster consumption of the fuel leading to a reduction in the mass fraction of flame A than in flame B.

In figure 6.11 (a) and (b), the mass fraction of O_2 in both flames is presented. The difference in the structure of these flames is because flame A is a lifted flame while flame B is an attached flame. Similarly, whereas flame A has a "U" shape, flame B has an "L" shape. The shape of flame A is due to the stabilisation of the flame above the burner rim, which gives the flame the structure it has at the leading-edge of the jet flame. Similarly, in flames A and B, at y/d=32.3 and at y/d=63.1, the mass fraction of O_2 is recorded at both side of the stoichiometric, while at y/d=93.9, in flame A alone, the mass fraction of O_2 is recorded at the fuel-lean side of stoichiometric alone. This is because at this location, most of the fuel has been consumed, while at that same location in flame B, the mass fraction of O_2 is recorded at both sides of stoichiometric. The differences recorded at y/d=93.9 between both flames is due to the different degrees of the entrainment of air into the flame which influences the level of mixing. Overall, the mass fraction of O_2 in flame B is higher than flame A due to the stoichiometric requirement and the higher amount of air required for the entrainment and the complete combustion of flame B than flame A. In summary, this investigation shows that the flame regime, be it attached or lifted, affects the amount of air that is entrained into the flame, which also affects the structure of the flame.

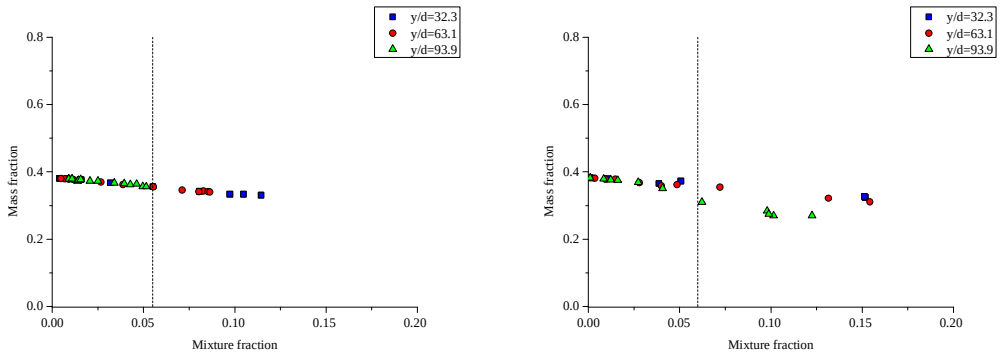

(a) **(b)**

Figure 6.12 N_2 mass fraction as a function of the mixture fraction for (a) methane, and (b) propane fuels, respectively.

The distribution of N_2 in both flames is shown in figures 6.12 (a) and (b). The mass fraction of N_2 is recorded at both sides of stoichiometric in the methane lifted and propane attached flames at y/d=32.3 and at y/d=63.1. However, at y/d=93.9, the

mass fraction of N_2 is at the lean side of stoichiometric, while in flame B, the mass fraction of N_2 is found on both sides of stoichiometric. The major difference between these flames is the mass fraction of N_2 at the fuel-rich side of stoichiometric in both flames. The stoichiometric air requirement for the combustion of propane is higher than the requirement for methane, and since the composition of air is mainly N_2 and O_2, the maximum mean mass fraction of O_2 and N_2 are higher in flame B than in flame A, as expected.

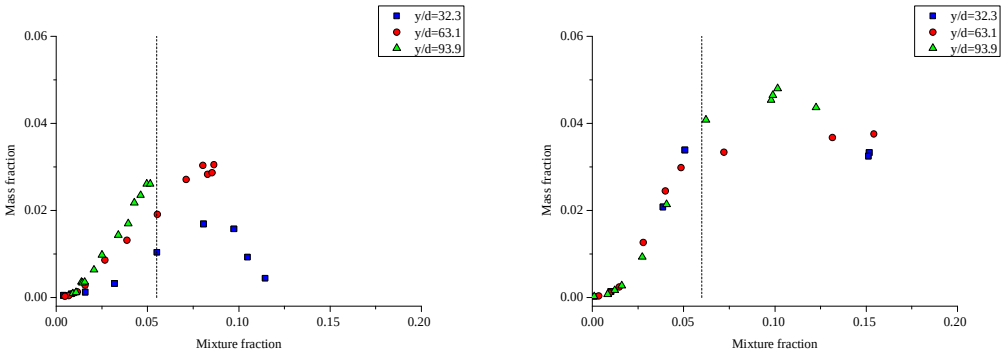

(a) **(b)**

Figure 6.13 CO mass fraction as a function of the mixture fraction for (a) methane, and (b) propane fuels, respectively.

In figures 6.13 (a) and (b), the plots of the mass fraction as a function of the mixture fraction of CO in methane and propane flames are shown, respectively. The maximum mean mass fraction of CO is higher in flame B than in flame A. Similarly, in both flames, the maximum mass fraction of CO lies on the fuel-rich side of stoichiometric as expected. This is because CO is formed at flame locations where there is a high concentration of fuel, but with insufficient air to promote the conversion of CO to CO_2. In addition, CO may be formed at locations of low temperatures in the flame, where these low temperatures inhibit the oxidation of CO to CO_2. For example, at two downstream locations, flame A is at a stoichiometric condition which are at y/d=32.3 and at y/d=63.1. This is due to the sufficient amount of fuel, air, temperature, etc., required for complete combustion, whereas, in flame B, it is only at y/d=93.1 that flame B is near stoichiometric. This suggests that conditions such as the flame temperature, air entrainment, etc., into flame B is insufficient for a complete combustion, except at the mean mixture fraction value where the flame is near stoichiometric, which is at y/d=93.1. Similarly, at all the downstream locations in flame B, the CO mass fraction is higher than in flame A.

This is expected because the stabilisation of the flame above the burner in flame A promotes air entrainment into the flame, than in flame B, and hence a larger conversion of CO to CO_2 is expected in flame A, since the CO is converted to CO_2, leading to a lower CO mass fraction in flame A compared to flame B. The difference in the region of the maximum CO mass fraction in flames A and B is also attributable to the difference in the length of both flames. Flame B is longer than flame A, therefore, the region where combustion occurs varies in both flames. The region of the complete combustion is marked by the region of the formation of the product species, namely CO_2 and H_2O, as shown in figures 6.14 and 6.15, respectively. Similarly, the region of incomplete combustion also varies in both flames, therefore, incomplete combustion occurs at different locations in both flames due to the differences in the length of the flames. CO is an intermediate species and a product of incomplete combustion, but CO could be easily converted to CO_2 when there is sufficient air, temperature and mixing (Bussman and Baukal, 2009). The plots of the mass fraction of CO_2 as a function of the mixture fraction in both flames are shown in figures 6.14 (a) and (b). In comparison, the CO_2 mass fraction is higher in flame B than in flame A. It should be recalled that in propane-air combustion, a greater amount of CO_2 is formed as a product in comparison with methane-air combustion.

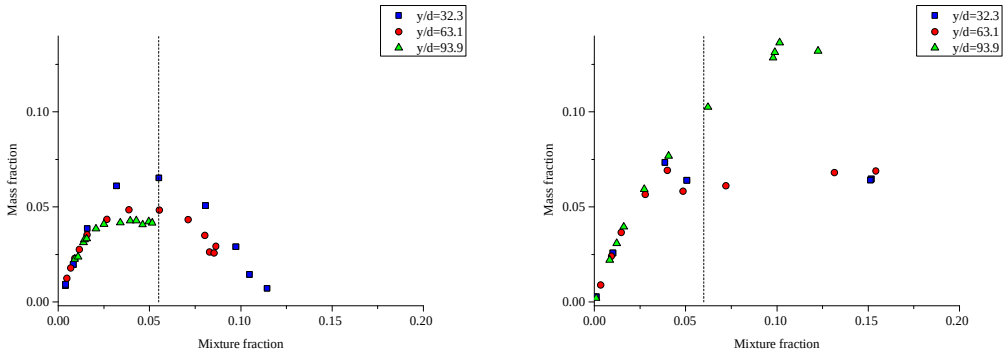

(a) **(b)**

Figure 6.14 CO_2 mass fraction as a function of the mixture fraction for (a) methane, and (b) propane fuels, respectively.

However, in flame A, the maximum mass fraction of CO_2 is at the stoichiometric line. This is due to the sufficient air that is entrained into the flame in addition to the favourable temperature and the mixing, which promotes complete combustion, and hence the combustion is at a stoichiometric condition at y/d=32.3

and at y/d=63.1. However, at y/d=93.9, the maximum mass fraction of CO_2 is at the lean side of stoichiometric, thus indicating that there is more air than fuel at that location. This is expected because this is the downstream location close to the flame tip where most of the fuel has been consumed, and therefore a lesser product of combustion is expected. Similarly, the low temperature at this downstream location reduces the rate of reaction for the oxidation of CO to CO_2, leading to a lower mass fraction of CO_2. In flame B, the maximum CO_2 mass fraction is at the fuel-rich side of stoichiometric, and coincides with the location of less air and a higher CO mass fraction than in flame A. The major products of combustion are CO_2 and H_2O, and H_2O follows the same trend as CO_2, as shown in figures 6.15 (a) and (b).

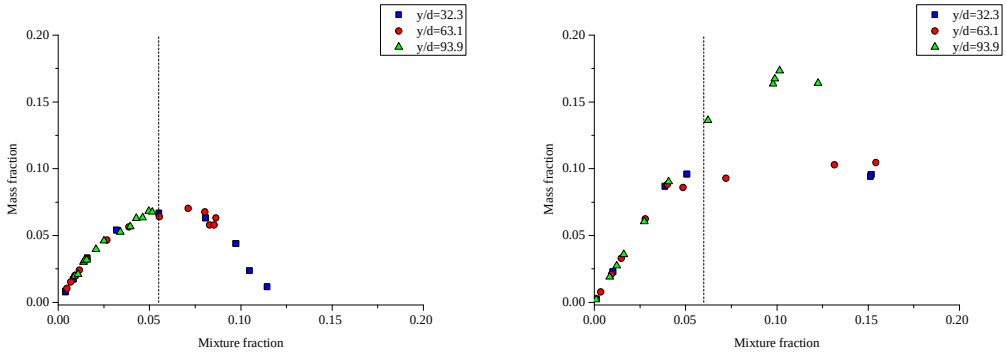

(a) **(b)**

Figure 6.15 H_2O mass fraction as a function of the mixture fraction for (a) methane, and (b) propane fuels, respectively.

This is due to the lesser air entrained into flame B, and the higher flame temperature which promotes the conversion of CO to CO_2. Other possible routes for the formation of CO_2 are via the reaction of CO with OH, HO_2, and O_2 (Bowman, 1975), with the reaction between CO and OH being the primary reaction in hydrocarbon flames.

The plots of the concentration of NO (ppm) as a function of the mixture fraction for flames A and B are shown in figures 6.16 (a) and (b). In flame A, at y/d=32.3, the maximum concentration of NO is 18 ppm and it is at the stoichiometric line, while at y/d=63.1 and y/d=93.9, the maximum NO concentration is at the lean side of stoichiometric. The region of the maximum mean concentration of NO at y/d=32.3 coincides with the region of the highest flame temperature of the jet, which suggests that the Zeldovich mechanism may be the possible route for the formation of the thermal NO. This is because thermal NO has been known to be

prominent in the regions in the flame where temperatures of about 1800 K are recorded (Turns, 1995). In flame B, the highest concentration of NO, which is at y/d=63.1, is about 72 ppm, and according to Caldeira-Pires and Heitor (2000), in the absence of pre-heated air, NO concentrations of less than 100 ppm are expected in laboratory-scale non-premixed propane flames.

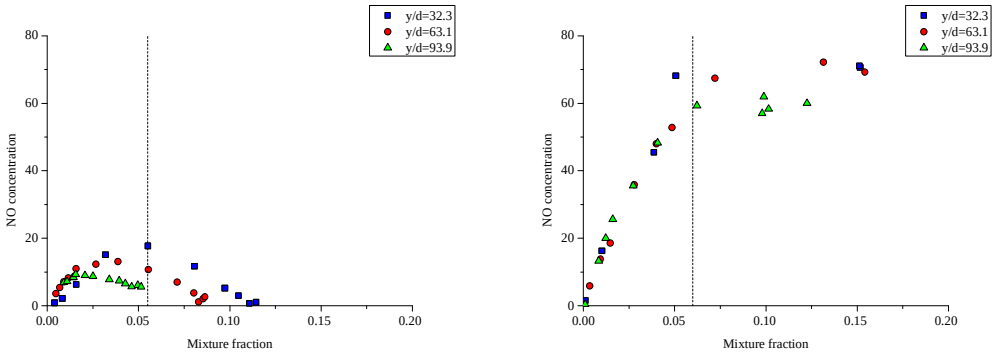

(a) **(b)**

Figure 6.16 NO mass fraction as a function of the mixture fraction for (a) methane, and (b) propane fuels, respectively.

Similarly, at all locations in the propane flame, the peak average NO concentration lies on the fuel-rich side of stoichiometric, as expected, suggesting that the prompt NO formation mechanism may be the prominent route of NO formation, because prompt NO is independent of temperature, and the maximum temperature in flame B is less than 1800, implying that the thermal NO is not likely, and is consistent with the suggestions of Hayhurst and Vince (1980) and Caldeira-Pires and Heitor (2000).

6.6 EMISSION INDICES OF POLLUTANT SPECIES

The post-flame composition of the species were measured at the same axial location for both fuels at a sufficient level of dilution, as explained in Chapter 3, and the EI of the pollutant species were calculated from equation 2.46. A comparison of the EI of these species for the different fuels are tabulated in Table 6.2. Comparing the fuels of the jet flames, the EI of the pollutant species are higher for methane than propane under the same Reynolds number. The soot emission factor, which is used in estimating the unit of the pollutant emitted per fuel consumed, for vertically-oriented laborataory-scale propane flame was derived from the following expression:

$$d_f = \frac{v_a}{v_g} \tag{6.1}$$

$$FS = \left(\frac{m_s}{v_b} \right) \times d_f \tag{6.2}$$

The soot emission factor for propane was 0.09 kg/m^3, while it was 0 for methane. This is because methane produces little or no soot under normal pressures, but produces significant soot under higher pressures (Brookes and Moss, 1999).

Emission Index (g/kg)	**Methane**	**Propane**
EINO	0.63	0.39
EINO$_2$	0.35	0.30
EICO	320.9	230.8
Soot Emission Factor (kg/m^3)	0	0.09

Table 6.2 Emission Indices of pollutant species and soot emission factor from methane and propane flames.

EICO is higher in methane than in propane. This is because based on the test conditions of the fuels examined, methane has a fuel flowrate than propane, and hence a shorter global residence time which inhibits the complete oxidation of CO to CO_2 via the reaction of CO and OH to yield CO_2 and H, which is a relatively slow reaction, hence leading to a higher EICO in methane than in propane. Increased fuel flow rate lead to decreased residence times, and decreased residence times prevent the complete oxidation of CO to CO_2. Similarly, EINO is higher in methane flames than in propane flames, as expected (Wang *et al*., 2002). This is because the flame temperature of flame A is higher than flame B, therefore a greater thermal NO, hence a greater EINO in flame A than flame B is expected. In addition, Turns and Myhr (1991) have shown that increasing the Froude number leads to increased EINO for all fuels. In Table 6.1, the Froude number of flames A and B are 21000 and 1800, respectively, and according to Turns and Myhr (1991), the EINO increases with jet exit velocity / the flame Froude number. Hence, the EINO in flame A is greater than the EINO is flame B because of the higher Froude number in flame A, as expected.

Lastly, $EINO_2$ was higher in methane than in propane. This is due to the higher NO at the post-flame region, which promotes a greater formation of NO_2 than propane. At this post-flame region, there is a greater availability of the OH radical in methane than propane due to the stabilisation of the flame above the burner which leads to a higher air entrainment in the methane flame. This leads to the reaction of oxygen to yield the OH radical, whereas, the high soot concentration in the attached propane flame suppresses the OH radical, thus reducing the OH radical in the flame and a lesser NO_2 concentration. The radicals which are formed at locations of high temperature in a lifted flame, are rapidly cooled at downstream locations in the flame (Gollahalli, 1978), thereby promoting the OH radical in the flame, in addition to the dilution at the post-flame location, which also promotes the OH radical which leads to a greater formation of HO_2 which oxidises NO to NO_2, hence leading to a higher $EINO_2$ in the lifted methane flame than in the attached propane flame, as expected.

6.7 EFFECT OF FUEL STREAM DILUTION ON SOOT AT DIFFERENT AXIAL LOCATIONS IN THE FLAME

In the previous chapter, the effect of varying the diluent concentration on the fuel jet stream was investigated, where it was concluded that dilution leads to a reduction in the flame temperature.

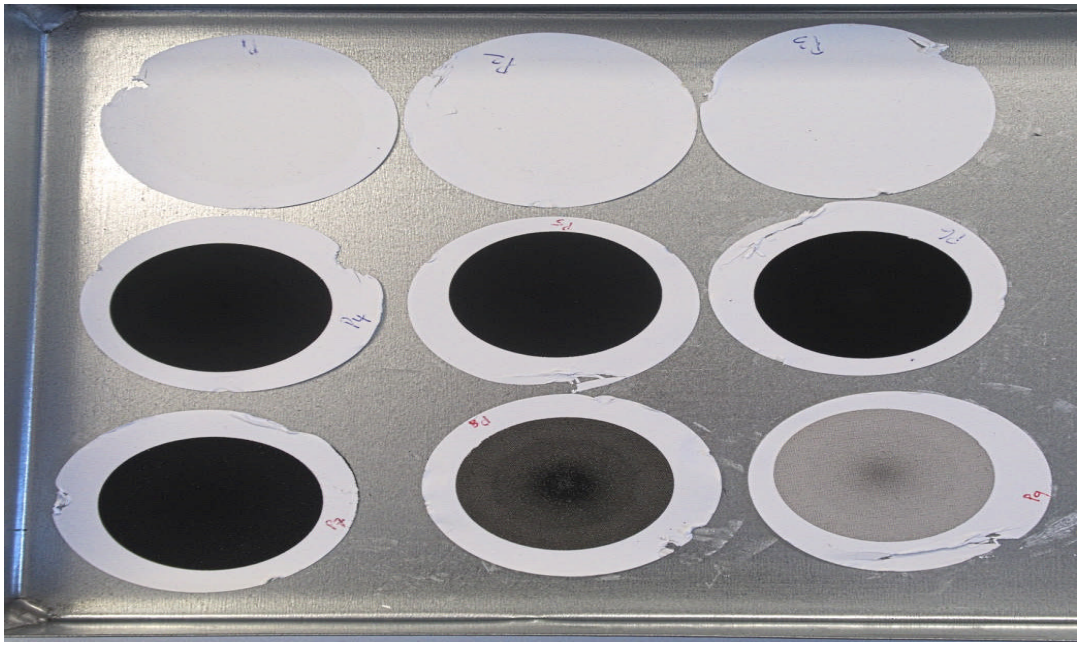

Figure 6.17 Photographs of soot deposition at different diluent mole fractions and at different axial locations in the flame.

Similarly, this reduction in the temperature leads to a reduction in the rate of the fuel pyrolysis, leading to a decrease in the formation of soot precursors, and therefore reduced soot concentrations. This section shows the effect of dilution on soot. Figure 6.17 shows the photographs of soot deposition at different diluent mole fractions and at different axial locations in the flame. The axial locations were chosen at regions where soot inception, growth and oxidation were suspected, and where the greatest amount of soot was expected. However, it was not expected that the locations where the soot was sampled were the definite locations where soot inception, growth, and oxidation occurred. This is because the process of soot formation does not occur in definite steps (Puri, 1993; Stasio, 2001), and the flame in this study is in the turbulent regime (Re = 5700), where the turbulence increases the intermittency of the soot field in the flame (Lee *et al*., 2009).

Similarly, detailed studies of the formation of soot in turbulent non-premixed jet flames are constrained by the short residence times and the intermittency involved in these flames (Bento *et al*., 2006). Intermittency plays a major role in diffusion flames, where a steep gradient in the temperature and concentration of species may be observed (Puri, 1993), and this intermittency leads to an increase in the random spatial distribution of the precursors of soot and their particles. The stages of soot evolution and oxidation are listed as: formation of soot precursors, particle inception, growth (surface and particle coagulation), agglomeration, and oxidation. Soot may be formed at locations in the flame where the temperature is between 1200 K and 1800K (Yee *et al*., 2009), corresponding to y/d =63.1 and y/d=93.8 in the propane flame investigated. The effect of the variation of the diluent mole fraction at the different locations in the flame are discussed in the following subsections.

6.7.1 EFFECT OF CO2 DILUTION ON SOOT AT Y/D=1.5

At the near-burner zone (NBZ) (5 mm above the burner, y/d=1.5), the analyses of the soot particle performed using the Field Emission Scanning Electron Microscopy (FESEM) did not show any evidence of any soot deposition at this location, even at higher magnifications on filter papers PI, P2, and P3, which correspond to diluent mole fraction of 0, 0.1, and 0.2 CO_2, respectively, as shown in figure 6.17. Soot formation occurs in fuel-rich regions in the flame in the presence of an abundant pyrolysis product. Increasing the temperature of the flame increases

the rate of the fuel pyrolysis, which leads to increased formation of soot precursors, and increased soot concentrations (Puri, 1993). Soot formation and growth is determined by the amount of soot precursors (PAH / acetylene – a product of pyrolysis) in the flame, which plays an important role during the pyrolysis, soot inception and growth stages, in the combustion of hydrocarbons (Fairweather *et al*., 1992; Bento *et al*., 2006). Particle inception affects the amount of soot produced (Puri, 1993), by controlling the rate of production of soot, thereby controlling the surface area in the zone of the soot particle inception where reactions occur, and this inception depends on the temperature and the concentration of the reactant species (Du *et al*., 1988). Soot emissions, volume fraction, radiation, etc. have been found to be associated with the soot inception stage (Santoro *et al*., 1983; Kent and Wagner, 1984). It is at this stage that the amount of soot to be produced is determined, even though Kennedy *et al*. (1990) suggests that it is at the surface growth stage that the amount of the soot to be produced is determined. At the particle inception stage, the collision of the reactive species with the surface of the soot particle increases, leading to an increase in the reactivity of the soot particles and hence, a greater particle growth in the flame at the soot growth stage. Flames that form a greater amount of soot have a greater active site and have higher collision efficiency. This increase in the reactivity may be due to the effect of high temperatures in the heavily-sooting flames, which leads to an increase in the active site that is exposed to reaction due to the greater accessibility to the gas species. This increase in reactivity may also be due to the amount of active sites present in the inception zone (where there is a large amount of soot concentration) which may still be present in the oxidation zone and take part in oxidative reactions. Smaller particle sizes yield a greater rate of soot oxidation, even at the same concentration. This is due to an increase in the surface area, which is exposed to an oxidative attack by the OH radical (Puri *et al.,* 1994). Using a thermal degradation mechanism, hydrocarbon fuels rely on the O, H, OH radicals to dissociate the molecules of the fuel to smaller molecules / free radical species (Wu *et al*., 2007), which are more stable. Pyrolysis leads to particle inception that is a rate-limiting process in the formation of soot (Frenklach *et al*., 1984; 1986; Frenklach and Warnatz, 1987), which greatly impacts on the sooting propensity of diffusion flames (Glassman and Yaccarino, 1981; Gomez, 1984). The formation of soot begins at locations where there is an existence of both a chemically-controlled and a kinetically-controlled reaction step, which leads to the precursor species being formed. However, the absence of soot particles

does not necessarily suggest the absence of soot precursors (Du *et al*., 1988). At locations where partial-premixing occurs due to the diffusion of oxygen into the flame, the small concentration of O_2 which diffuses into the flame has been found to actually enhance the rate of fuel pyrolysis in the flame (Smith and Gordon, 1956; Schug *et al*., 1980), by homogeneously catalysing the process of the initial fuel pyrolysis. This increase in fuel pyrolysis due to O_2 diffusion into the fuel stream is feasible only at low concentrations of O_2. At higher O_2 concentrations, the OH radical formed from the reaction of O_2 and H actually suppresses the soot precursors, thereby reducing soot inception. Similarly, it has been suggested that the soot inception zone lies between the location of the maximum OH concentration and high PAH concentration (Smyth *et al*., 1997) in the flame. PAHs are the species which are responsible for fluorescence, and the region of high PAH fluorescence intensity is characterised by the location where there is a sharp increase in the soot particle number density (Santoro *et al*. 1983). However, at y/d= 1.5, where the flame is non-luminous, but bluish due to partial premixing (Chen and Goss, 1989), no particles were observed. Any particle that may have been observed at this bluish region would be so small that the dynamic light scattering (DLS) technique may not be feasible to sample and analyse the particle, since the particles would be smaller than the scattering limit (Kroner *et al*., 2003). The absence of a soot particle at this location suggests that this location is possibly not the inception zone, because at the inception stage, a large number of small primary particles exist, where the soot particles have a spherical shape, and particles of diameter about 10nm are expected at such locations (Du *et al*., 1988), thus suggesting that the inception zone may lie further downstream in the flame.

6.7.2 EFFECT OF CO2 DILUTION ON SOOT AT Y/D=63.1

Particle growth encompasses the surface growth reaction and the growth by coagulation. In particle growth, the size of the particle increases either due to coagulation or surface growth. About 90% of the soot yield occurs at the surface growth stage (Haynes and Wagner, 1981). In surface growth, chemical reactions take place and there is also a bonding of the precursor species on the particles' surface. Through PAH condensation and acetylene addition, these precursor species react on the surface of the particle, causing surface growth (Guo *et al*., 2007), and increasing the mass of the soot particle, because of the reactions occurring at the

soot particles' surface during soot growth. PAH condensation and acetylene addition are always in competition with each other, although the rate of condensation of PAH is shorter than the rate of addition of acetylene, implying that acetylene is the dominant species during surface growth (Harris and Weiner, 1988).

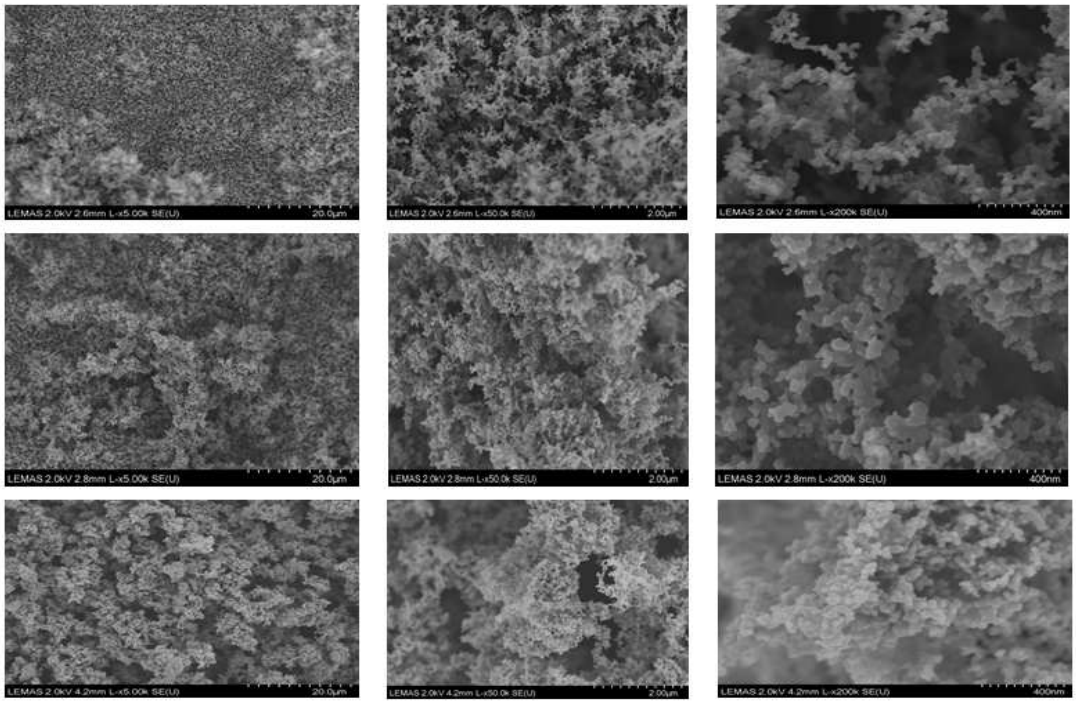

Figure 6.18 FESEM analysis of soot deposition on a filter paper at 20 µm; 2 µm; and 400 nm (from left to right), corresponding to 0, 0.1, and 0.2 (from top to bottom) CO_2 mole fraction at y/d=63.1.

Similarly, during surface growth, the concentration of the soot increases because of the increase in the mass of the precursor species at the surface of the particle, but the number of primary particles do not change, while in growth by coagulation, where the primary particles collide with each other thereby leading to coalescence, the count of the primary particles decrease, while the concentration of the soot is unchanged. This increase in the soot mass at the surface growth stage may be affected by the oxidative action of the OH radical on the soot particles, where oxidation leads to a reduction in the particle size and mass. At y/d=63.1, there is significant soot deposition, as expected, and as shown in the undiluted and diluted cases P4, P5 and P6, corresponding to 0%, 10%, and 20% CO_2 diluent concentrations, respectively, in figure 6.17, and at different particle size magnifications in figure 6.18. This is likely the surface growth zone, which is characterised by the agglomeration of primary particles, with particle sizes ranging from 10 nm to 70 nm in diameter, as shown in the undiluted and diluted cases in

figures 6.19 to 6.21, respectively, and this is consistent with the observations of Köylü *et al*. (1995) and Bockhorn *et al*. (2009).

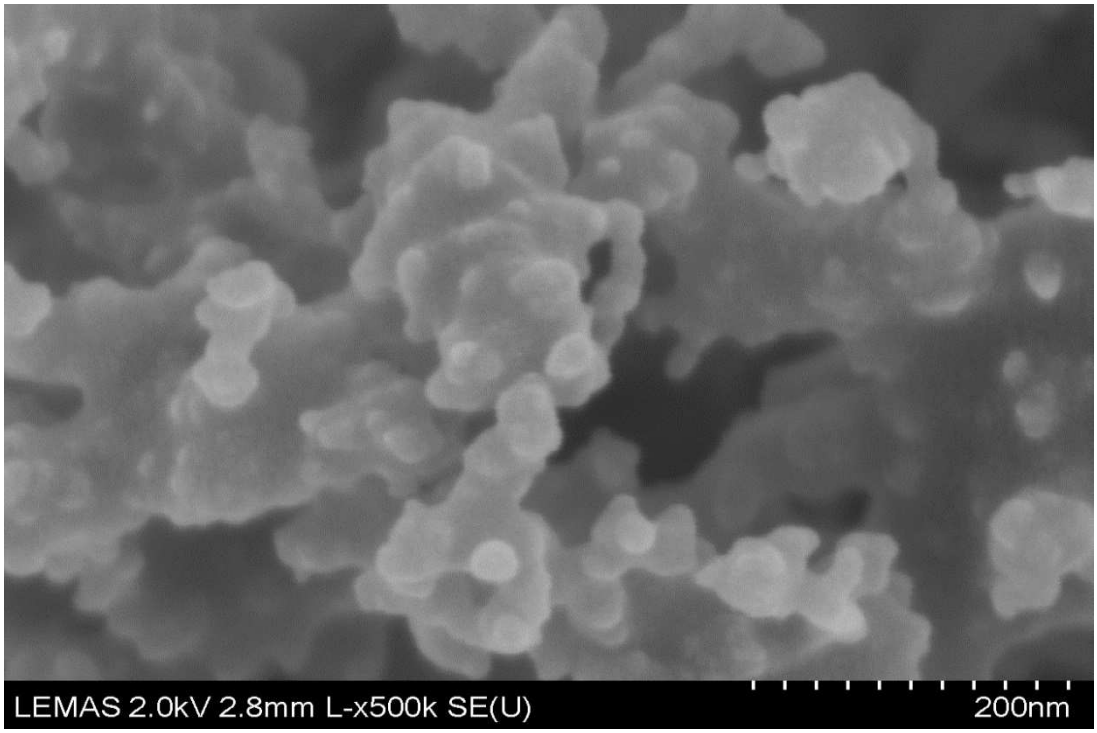

Figure 6.19 Particle size distribution for the undiluted fuel case at y/d=63.1.

In addition, the increase in the soot volume fraction characterises the surface growth stage. This is due to the condensation of the particle growth species, such as acetylene or PAH on the surface of the particles, while the primary particle number density remains unchanged, compared with the inception stage where the number density of the primary particle increases, while the particle size remains unchanged (Oh and Shin, 2006). The greater agglomeration of the primary particles shown in figure 6.19, which is the undiluted case, compared to the diluted cases in figures 6.20 and 6.21, is because in the diluted cases, the effect of dilution on the soot particle, leads to lower temperatures, a reduction in the frequency of the collision of the particles, and hence fewer collisions and lower particle reactivity. This leads to a reduced soot growth by coagulation, and a fewer agglomeration of the primary particles. The fewer agglomerates and the smaller primary particles in the diluted cases therefore have a greater probability of soot oxidation, due to an increase in the surface area which is exposed to an oxidative attack by the OH radical (Puri *et al.*, 1993), hence reducing the soot volume fraction in the diluted cases, compared to the undiluted case. In figures 6.22 (a) to (c), the size distribution of the primary particles are shown for the 0, 0.1 and 0.2 diluent mole fraction, respectively. In both

the undiluted and the diluted cases, the size of the primary particles ranged from 10 nm to 70 nm. In addition, the decrease in the aggregate size leads to an increase in the smaller particles, and hence increased counts of smaller particles at increased diluent concentrations.

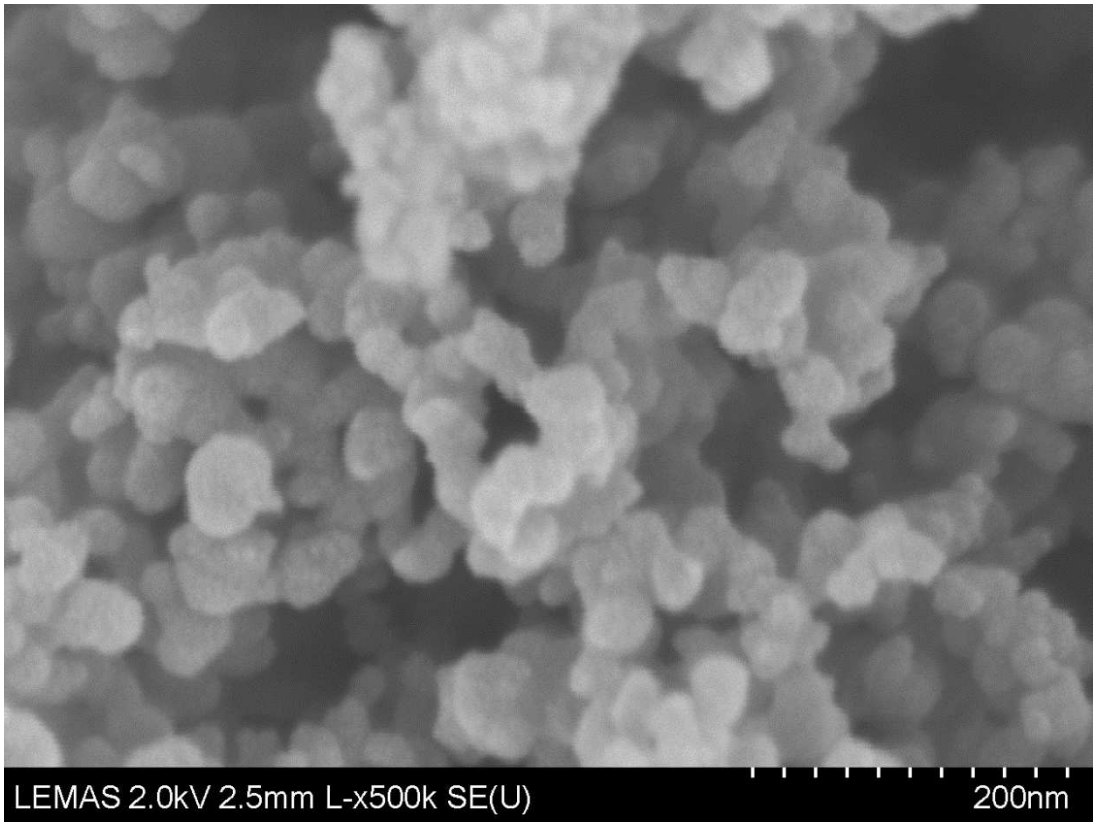

Figure 6.20 Particle size distribution for the 0.1 CO_2 mole fraction at y/d=63.1.

The decrease in the aggregate size at higher diluent mole fraction is expected because during soot growth by coagulation, high temperatures promote a greater particle reactivity, greater collision of the reactive species, and a greater agglomeration leading to larger aggregates, and hence a lesser primary particle mean count since most of the aggregates are agglomerated. However, fuel-stream dilution decreases the temperature which reduces the rate of collision of the reactive species. This reduction in the temperature leads to a higher particle mean count of smaller particles, since the reactivity and the rate of collision decreases, leading to a lesser agglomeration of the aggregates (Puri, 1993).

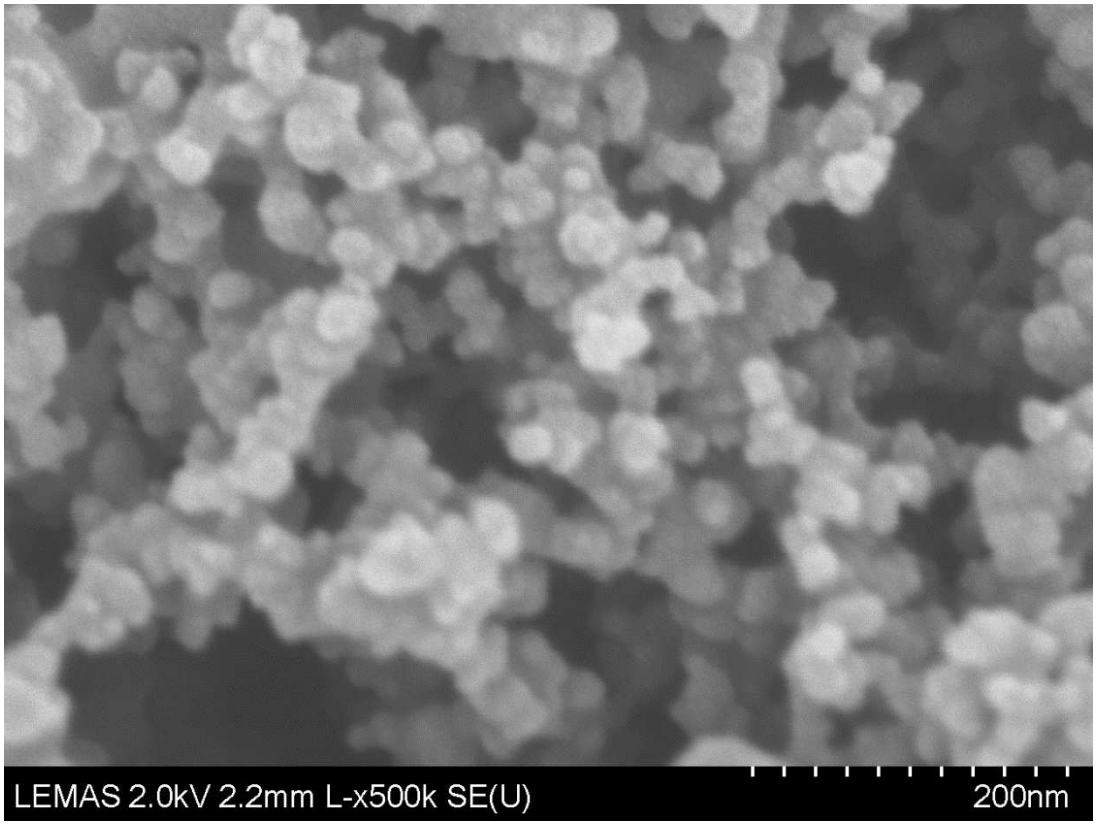

Figure 6.21 Particle size distribution for the 0.2 CO_2 mole fraction at y/d=63.1.

Similarly, in surface growth, the size of the aggregate increases due to the bonding of the precursor species on the particles' surface, thus leading to a greater soot mass, larger aggregate size, and a higher soot concentration. However, the effect of dilution on the surface growth leads to a decrease in the aggregate size, reduced soot mass and reduced soot volume fraction. This reduction in the aggregate size is due to the effect of dilution on the particle which leads to a detachment of the gas-phase species on the surface of the soot particle, thereby reducing the particle size and the surface area available for agglomeration, and hence less soot mass, since the surface growth is suppressed. Therefore, this investigation suggests that using CO_2 as a diluent leads to a decrease in the aggregate size due to the suppressed particle growth. This is because particle growth is dependent on the residence time (Puri, 1993), and dilution leads to reduced residence times (Turns and Bandaru, 1993; Kumar and Mishra, 2008). It should be noted that the residence time of the soot particles is not the same as the residence time of the bulk flow, which depends on the mass flowrate of the fuel (Charest *et al.*, 2014). The residence time of a soot particle is the period of time between the formation of the soot particle which occurs at the particle inception zone near the nozzle exit of the burner, and the destruction

of the soot particle at the oxidation region which is further downstream the jet, near the flame tip (Puri, 1993; Charest *et al*., 2014).

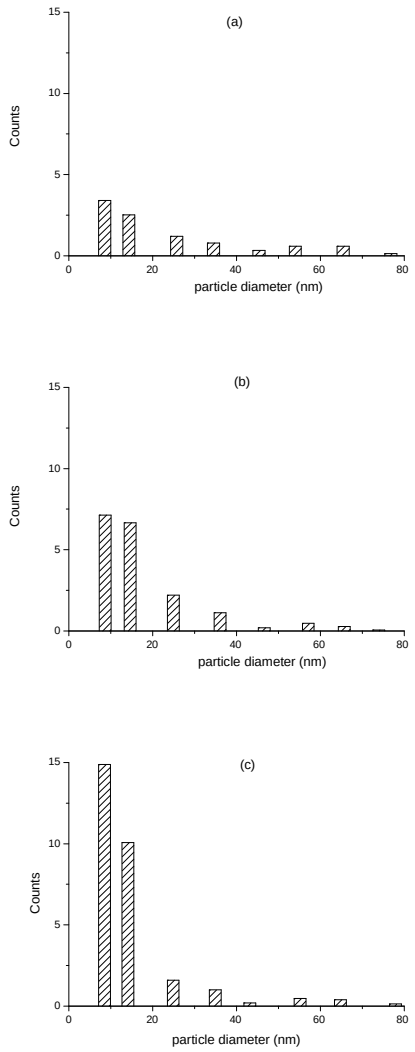

Figure 6.22 Particle size distribution of (a) 0, (b) 0.1, and (c) 0.2 CO_2 diluent mole fraction at y/d=63.1.

At the inception zone, the decrease in the residence time would be expected because the effect of the diluent on the flame leads to a decreased particle inception rate (Guo *et al*., 2007), by promoting the oxidation of the soot precursors in the flame via the OH radical (Gollahalli and Zadeh, 1985), which delays soot nucleation, and a detachment of the gas-phase species on the surface of the soot particle, which decreases the soot particles available for coagulation and surface growth (Vandesburger *et al*., 1984; Koylu *et al*., 1992), thereby suppressing soot growth at the soot growth stage (Oh and Shin, 2006). At the soot growth stage, when the temperature is high, there is a greater reactivity and collision of the particles, which leads to particle growth by coalescence, and this coalescence leads to an

increase in the size of the aggregates, and a decrease in the primary particle count since most of the particles are agglomerated.

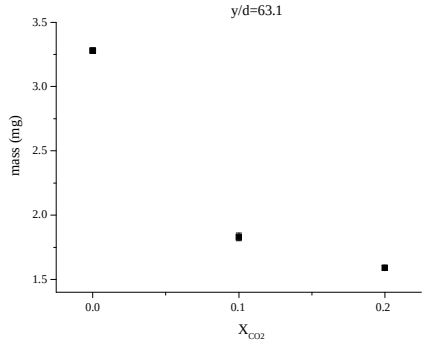

Figure 6.23 Variation of the soot mass as a function of the diluent concentration at y/d=63.1.

Similarly, the soot mass increases due to the reactions of the growth species on the surface of the soot particle. These species are formed at the inception zone and are the rate-controlling step which determines the formation of soot (Puri, 1993). High temperatures promote the growth of these species via coalescence, and high temperatures also lead to a high oxidation rate. However, dilution leads to a reduction in the flame temperature, and hence lesser collision and a lesser reactivity of the particles (Puri, 1993), which leads to a lesser agglomeration of the particles, which implies that the growth by agglomeration is suppressed, leading to a greater count of the primary particles and a decrease in the size of the aggregates as shown in figure 6.24. In addition, the reaction of the inert diluent leads to the formation of OH when the diluent,CO_2, reacts with the H radical to yield OH and CO. Similarly, O_2 and the OH radical are the main species which are responsible for the soot oxidation (Puri, 1993).

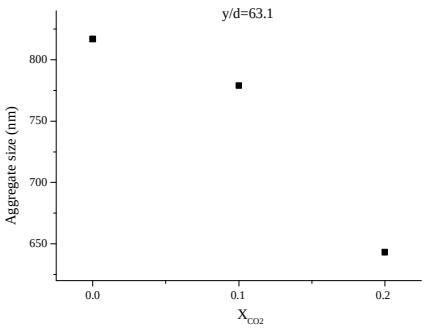

Figure 6.24 Variation of the aggregate size as a function of the diluent mole fraction at y/d=63.1.

Therefore, dilution leads to a reduction in the mass of the particle, due to the oxidative action of the OH radical on the soot particles, and dilution also leads to the reduction in the soot mass because the temperatures of the growth species are reduced, leading to a slower reaction of the growth species on the particle. This is due to the reduction in the fuel pyrolysis, which inhibits the formation of soot precursors, thereby leading to a reduction in the particle mass as shown in figure 6.23. Dilution also leads to reduced particle mass because the bonding of the precursor species is interrupted by the oxidative action of the OH radical, which reduces particle inception. At the inception and surface growth stages, CO_2 dilution leads to a decrease in the temperature of the flame, and a reduction in the concentration of the reactive species, which finally reduces the rate of soot inception and surface growth (Axelbaum *et al*., 1988). Fuel-stream dilution leads to increased losses of radicals in the fuel and decreased particle residence time. Hence, there is a decreased particle mass available for surface growth and this leads to a decrease in the soot volume fraction (Puri, 1993). In addition, increasing the temperature of the flame causes the rate of the pyrolysis of the fuel to be increased, which leads to a higher rate of formation of the soot precursors, and increased soot concentrations (Puri, 1993). Therefore, when the flame temperature is reduced due to fuel-stream dilution, this reduced temperature leads to a greater radiant fraction, less OH radical oxidation reaction rates, fewer collisions of the reactive species due to chemical and dilution effects, and hence less soot growth.

6.7.3 EFFECT OF CO2 DILUTION ON SOOT AT Y/D=188

At the tip of the flame (y/d=188), the photographs of the soot deposition P7, P8, and P9, corresponding to the 0, 0.1, 0.2 diluent mole fraction, respectively, are shown in figure 6.17. Similarly, the photographs of the soot aggregates in both the undiluted and the diluted cases at different magnifications (5000, 50,000, and 200,000) at y/d=188 are shown in figure 6.25, and at a magnification of 500,000 the original size as shown in figures 6.27 to 6.29. Also shown are the images of soot at a post-flame location of y/d=308 at different magnifications (5000, 50,000, and 200,000) in figure 6.26, and at a magnification 500,000 of the original size as shown in figure 6.30 for the undiluted case. Soot oxidation is the most-sensitive to local flame temperatures and this is because high temperatures promote high rates of soot burnout and it requires the greatest activation energy of all the stages in the soot formation (Takahashi and Glassman, 1984). At temperatures less than about 1300K,

the rate of oxidation of the soot particles may be too slow to oxidise the mature soot particles, and thus smoke will be emitted (Kent and Wagner, 1984). The smoking of a flame depends on the time taken for the soot to burn out before the effect of the radiation losses, and the entrainment of fresh air quenches its oxidation. In non-premixed flames, soot may be suppressed at the hot reaction zone where there is a high concentration of OH and a high temperature which promotes the rate of the soot burn-out.

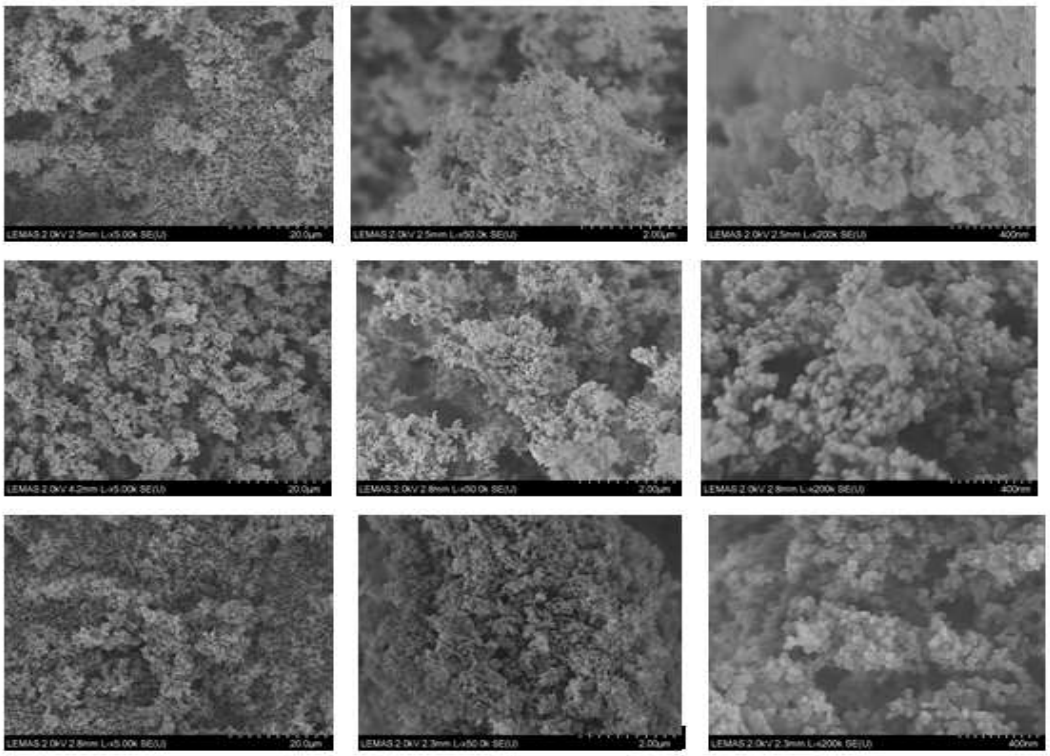

Figure 6.25 FESEM analysis of soot deposition on a filter paper at 20 µm; 2 µm; and 400 nm (from left to right), corresponding to 0, 0.1, and 0.2 (from top to bottom) CO_2 mole fraction at y/d=188.

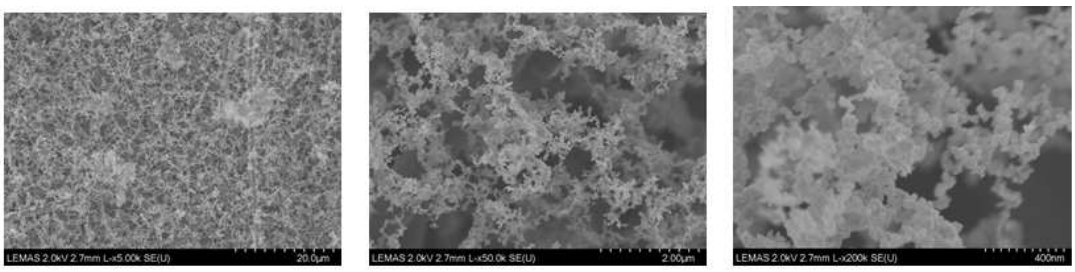

Figure 6.26 FESEM analysis of soot deposition on a filter paper at 20 µm, 2 µm, and 400 nm, at y/d=308 for the undiluted fuel case.

The rate of oxidation is also dependent on the surface area of the soot particles that are exposed to oxidative attack by radicals such as the O_2 and OH radicals (Warnatz, 2006), CO_2 (Garo *et al.*, 1990), etc. However, a decrease in the temperature decreases the rate of oxidation of soot by the OH, thereby increasing the concentration of the soot particles. This is because fewer particles escape from the flame, while at increased temperatures, the rate of oxidation is increased, thereby decreasing the soot volume fraction because more soot escapes from the flame. OH is the dominant radical species for soot oxidation in flames, and OH concentration reduces at the flame tip due to lower flame temperatures at that location, thereby leading to a decrease in the rate of soot burnout and hence higher soot volume fraction (Neoh *et al.*, 1984; Santoro and Miller, 1987; Santoro and Puri, 1991; D'Anna *et al.*, 2007). Although the OH radicals are formed when molecular O_2 reacts with the H atoms, there is a more effective attack of carbon by OH than O_2 (Puri *et al.*, 1993). Similarly, via the reaction of CO_2 and H to yield CO and OH, diluents like CO_2 also lead to the promotion of the OH radical, which leads to soot oxidation. Dilution decreases flame temperature and reactant concentration, leading to a reduction in the chemical reaction rates.

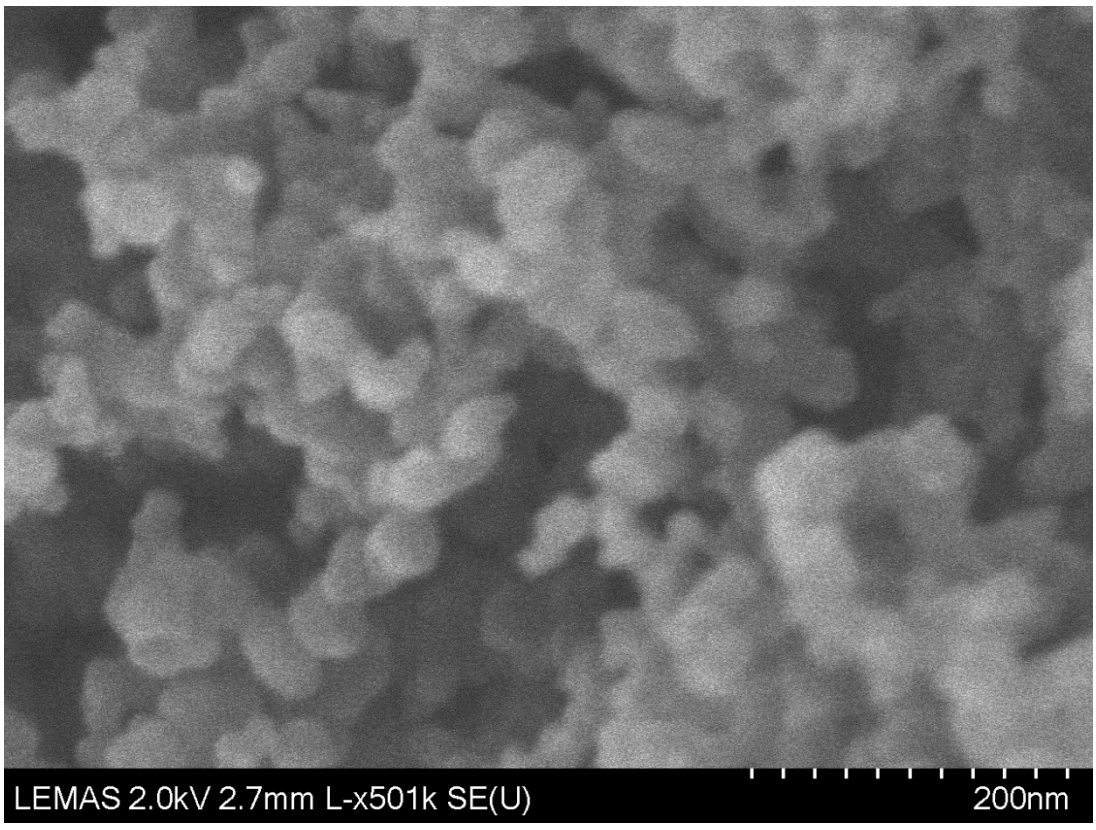

Figure 6.27 Photograph of soot particles for the undiluted case at y/d=188.

It should be noted that in the oxidation zone, not all the aggregates may be completely oxidised. The partial oxidation may be due to the eddies which escape oxidation either via the flame tip, laterally via eddy motion (Puri, 1993), and / or via air entrainment into the flame which essentially reduces the eddies which contain these aggregates (Lee *et al*., 2009). The quenched intermediates emitted from the soot formation process have a different appearance (colours), and may either be condensed products of the heavier hydrocarbons which are formed during combustion, or droplets of fuel which escape the combustion zone without being combusted. In all the cases investigated at the tip of the flame (y/d=188) and at the post flame location (y/d=308), non-spherical and poly-dispersed soot particles were observed, where the soot particles were largely agglomerated, and with little evidence of isolated primary particles.

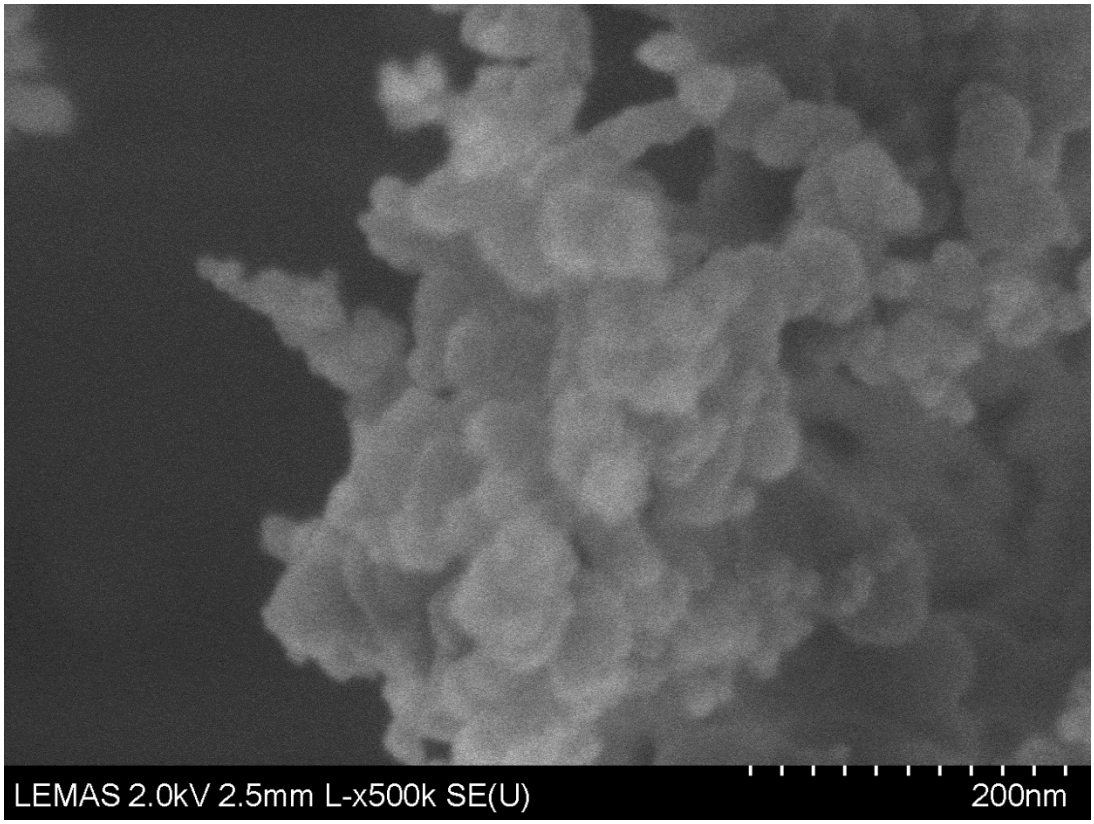

Figure 6.28 Particle size distribution for the 0.1 CO_2 mole fraction at y/d=188.

This is because of the intermittency of the turbulent flame investigated, which leads to an escape of some particles that are not agglomerated from the soot growth zone. However, the particle count of the primary particles in the oxidation zone was very small, and the size of a few primary particles was about 20 nm in all the cases investigated, as shown in figures 6.31 (a) to (c), and in the post-flame region in figure 6.32. In addition, at increased diluent concentrations at the oxidation zone, the

increase in the mean particle count of the primary particles at the oxidation zone is due to the growth by the coagulation of the particle at the growth stage and not by surface growth. This is because in the soot oxidation zone, there is no attachment of the growth species on the particle via surface growth. Therefore the count of the particles do not change. Surface growth has been known to be halted at locations in the flame where there is a depletion of the growth species, suppression of the growth species due to dilution, or a reduction in the reactivity of the particles, which thereafter promotes soot growth (Subramaniasivam, 1992).

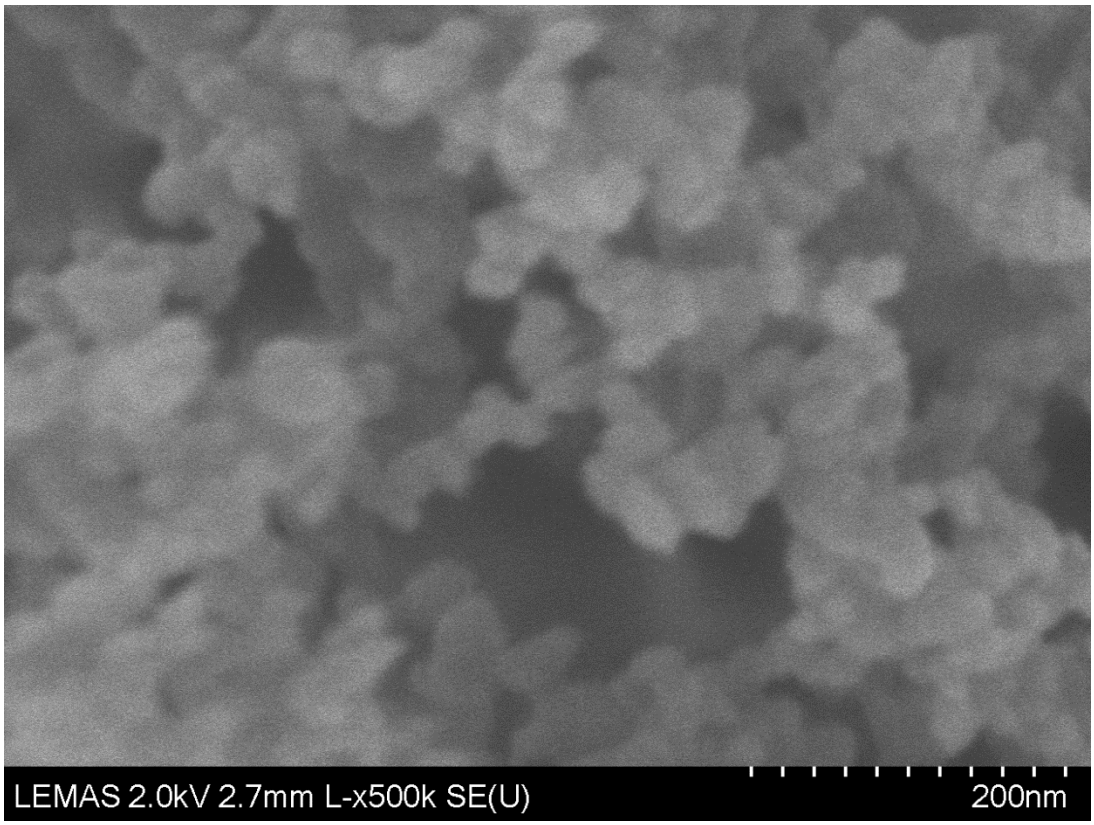

Figure 6.29 Particle size distribution for the 0.2 CO_2 mole fraction at y/d=188.

Therefore, this study suggests that in the oxidation zone, the soot particles which are transported from the growth stage grow mainly via the coagulation of the soot particles, and coagulation leads to a decrease in the particle count due to particle reactivity and collision at high temperatures which leads to coalescence. However, dilution leads to a reduction in the temperature and therefore fewer collisions and coalescence and hence a greater particle count. Therefore, this study suggests that increasing the concentration of the diluent in the fuel-stream leads to a greater particle count due to particle growth by coagulation at the oxidation zone. This is because the particle reactivity and the rate of collision decreases, leading to a lesser agglomeration of the aggregates, and hence a decrease in the aggregate size at higher

diluent mole fractions. Similarly, the variation in the deposition of soot on the filter papers in the undiluted and diluted cases as shown in P7, P8 and P9, corresponding to 0%, 10%, and 20% CO_2 dilution, respectively, is because this is the tip of the flame where intermittency is expected. This leads to variations in the temperature and in the species composition as expected, added with the entrainment of air into the unconfined flame, leading to variation in the soot field. In the oxidation zone, the amount of soot oxidised depends on the flame temperature, the fuel concentration at the oxidation region, and the concentration of the oxidising species, which are mainly O_2, the O- atom and the OH radicals (Puri, 1993).

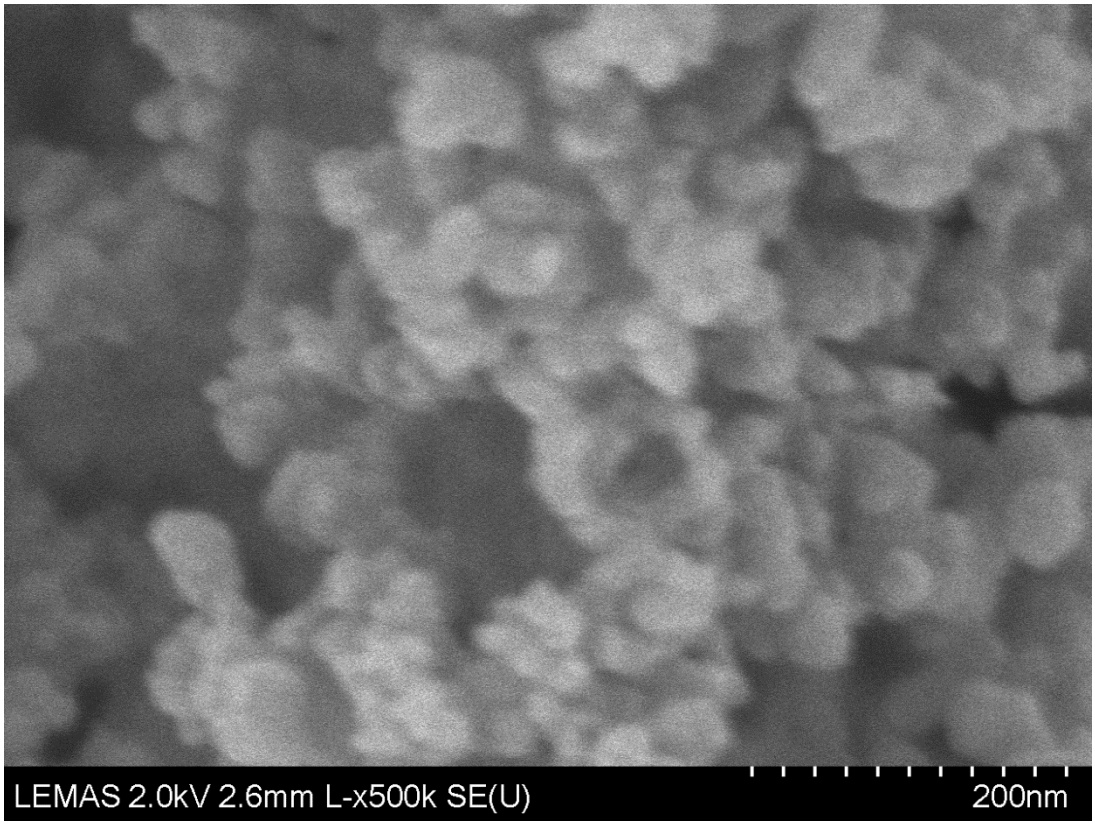

Figure 6.30 Particle size distribution at y/d=308 for the undiluted case.

Soot oxidation is the most-sensitive to the flame temperature than other soot formation stages and this is because of the very high activation energy required for the oxidation of soot (Puri, 1993). If the temperature is high, then the rate of oxidation of the soot particles will also increase and hence more soot is burnt out. Similarly, at low temperatures, such as the dilution of the fuel stream, which leads to a decrease in the flame temperature, these low temperatures lead to fewer particle collisions and reactivity, which leads to an increase in the count of the primary particles at increased diluent concentrations as shown in figure 6.31 and a smaller aggregate size, as shown in figure 6.34. In addition, diluting the fuel-stream with

CO_2 leads to the formation of the OH radical via the reaction of CO_2 and H to yield OH and CO. Since O_2 and the OH radical are the main oxidising species which are responsible for the reduction in the mass of soot and in soot oxidation, and the concentration of the fuel is low at the oxidation region (Teini *et al*., 2012; Puri, 1993), therefore an increase in the diluent concentration leads to lower temperatures and lower soot oxidation rates, and hence a decrease in the soot mass as shown in figure 6.33.

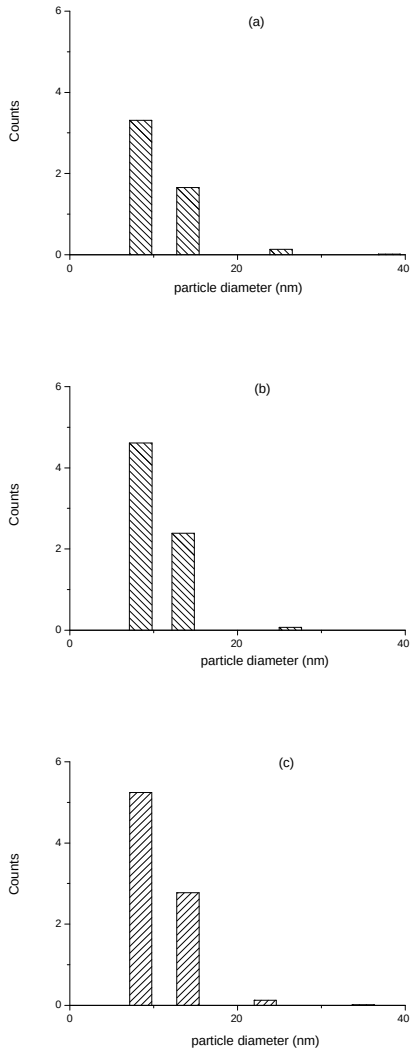

Figure 6.31 Particle size distribution of (a) 0, (b) 0.1, and (c) 0.2 CO_2 diluent mole fraction at y/d=188.

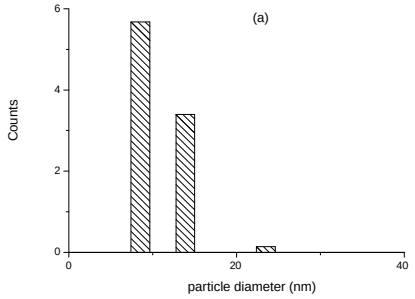

Figure 6.32 Particle size distribution of (a) 0, (b) 0.1, and (c) 0.2 CO_2 diluent mole fraction at y/d=308.

At the flame tip and at the post-flame region, there was no difference between the size of the aggregates and those sampled in the duct. This is because there is sufficient air dilution leading to a lesser deposition of soot in both cases, and the low OH concentration and the low temperature are not sufficient for soot oxidation at those locations. Similarly, the size of the aggregates at the oxidation zone are larger than those at the soot growth stage. This is because at the soot growth stage, there is a greater oxidative attack on the soot by the OH radicals (Oh and Shin, 2006). This attack leads to the smaller particle sizes yielding a greater rate of soot oxidation, due to an increase in the surface area that is available for surface growth (Puri *et al.*, 1993). However, at the oxidation zone, the larger particles take a longer time to be oxidised due to their surface area, which does not promote a fast oxidative attack, and hence a larger size of the aggregates at the oxidation zone.

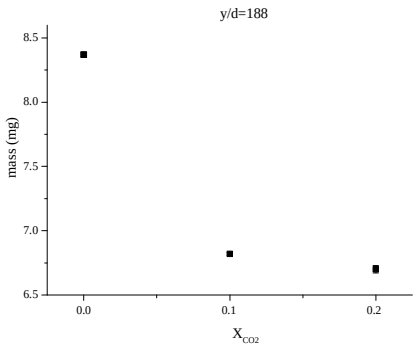

Figure 6.33 Variation of the soot mass as a function of the diluent concentration at y/d=188.

The difference between the maximum aggregate sizes in the soot growth and the oxidation zones suggest that the effect of dilution on the particle size depends on the sampling location in the flame. This has been confirmed in the numerical and

experimental analyses by thermophoretic sampling and TEM analysis of soot aggregates in propane flames in laminar and turbulent conditions conducted by Koylu *et al*. (1995), Stasio (2001), etc. These authors suggest that the fractal properties of soot aggregates do not vary, irrespective of the fuel type or flame condition (be it laminar or turbulent), but the primary particles' average count in an aggregate and the aggregate size varies, depending on the sampling location where measurements are made (Stasio 2001; Oh and Shin, 2006). Similarly, the differences in the type of fuel has been known to affect the particle size in the early stages of the soot formation process, where the particle sizes which are newly formed, vary, based on the fuel-type, but as the particles mature, the size of these particles are independent of the fuel type, and the fuel-type does not affect the chemical characteristics of the soot particle (Puri, 1993).

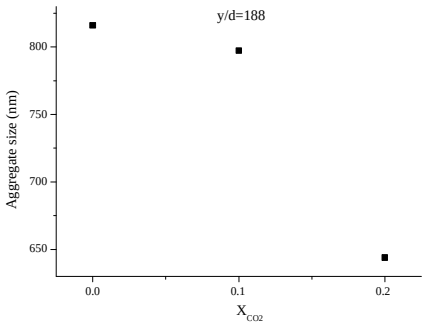

Figure 6.34 Variation of the soot aggregate size as a function of the diluent mole fraction at y/d=188

In addition, Teini *et al*. (2012) suggest that the effect of CO_2 on the soot morphology on acetylene flames is minor, except at the particle inception stage of the flame. Bockhorn *et al*. (1982) and Santoro *et al*. (1983) also suggest that there is no difference in the morphology of soot particles in propane-oxygen, acetylene-oxygen, ethene - air non-premixed flames. CO_2 dilution leads to a delay in the formation of soot at the inception zone and also lowers the flame temperature, thereby decreasing the oxidation rate, and decreasing the concentration of the soot particle (Neoh *et al*., 1984; Santoro and Miller, 1987).

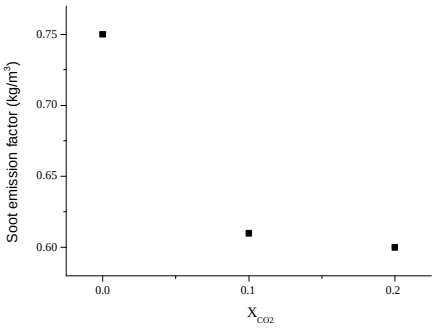

Figure 6.35 Variation of the soot emission factor as a function of the diluent mole fraction at the post-flame location.

The decreased temperature of the flame also causes a reduction in the soot emitted because the concentration of soot reduces at low temperatures due to the effect of dilution which reduces the rate of the fuel pyrolysis at the inception stage. This leads to a decrease in the formation of soot precursors, and therefore reduced soot concentrations, because it is at the inception stage that the concentration of the soot is determined (Santoro *et al*., 1983; Kent and Wagner, 1984; Puri, 1993). This is because particle inception depends on the temperature of the jet flame and on the mass fraction of the reactant species (Du *et al*., 1988). Also, inception controls the rate of the production of the soot, thereby controlling the surface area in the zone of the soot particle inception where the reaction occurs. Therefore, an increase in the concentration of the diluent in the flame slows down the rate of production of the soot precursors. This also leads to a reduction in the growth of the species via surface growth, leading to a slower reaction of the growth species on the particle, and a reduction in the particle mass. This ultimately reduces the concentration of soot in the jet flame, and hence less soot is emitted from the flame, which implies that the soot emission factor is reduced at increased diluent mole fraction as shown in figure 6.35.

In summary, this investigation suggests that CO_2 dilution affects the size of the aggregates and the particle mean count at the soot growth stage**.** The matching of the measurements of the particle size of propane flames without CO_2 dilution with the measurements of Bockhorn *et al*. (2009) is reasonable, and increases the confidence on the accuracy of the present investigation using CO_2 as a diluent at different mole fractions. Further, it is consistent with the observations of Koylu *et al*. (1995) and Stasio (2011). Similarly, the dilution of the fuel stream leads to a decrease in the rate of the particle inception, due to the delay in the particle nucleation and in the

suppression of the soot precursors at the inception stage. At the soot growth stage, dilution reduces the soot mass, since the surface growth is suppressed, due to the detachment of the gas-phase species on the surface of the particle. Dilution also reduces growth by agglomeration since the thermal effect of dilution leads to lower flame temperatures which lead to lesser collision and lesser reactivity, and hence lesser agglomeration. At the post-flame location, the temperatures are low and the soot emission factor decreases at increased diluent concentrations due to the effect of dilution which leads to lower temperatures and a decrease in the soot oxidation rate and hence a low soot burn-out.

Chapter 7

GENERAL CONCLUSIONS AND SUGGESTIONS FOR FUTURE STUDIES

7.1 CONCLUSIONS

For the first time, a detailed side-by-side comparison of methane jet flames at different test conditions has been investigated. Similarly, a comparison of the effect of the changes in the flame structure, flame stability, and in the emissions from non-premixed methane and propane laboratory-scale flares over a wide range of test conditions has been presented. These investigations consist of the simultaneous comparison of the in-flame and the post-flame composition of the major species, varying the fuel jet velocities, varying the concentration of the diluent on the fuel stream, and the effect of dilution on soot.

In Chapter 4, the fuel jet velocity was varied, where the measurements and the discussions on the flame temperature, the in-flame concentration, and the EI of the pollutant species at different jet velocities were presented. The discussions on the temperature presented a comparison of the measured mean and the fluctuating flame temperatures of the flames at the different jet velocities. The measurements of the in-flame concentration of the species showed both the spatial variation of the species and the variation of the species mass fraction in a mixture fraction space, and the EINOx and EICO were compared for the different flames. This study involved flames at Reynolds number ranging from 1584 to 14254 where the vertically-oriented co-flowing flames which were investigated were in the laminar, transitional and turbulent regimes and were either attached to the rim of the jet nozzle or stabilised above the jet nozzle. From these investigations, the following conclusions are made:

- The laminar attached flames are more luminous than the transitional lifted and turbulent lifted flames.
- The mean visible height of the flame increases as the velocity of the jet increases, from the laminar regime, up to a critical point, where a further increase in the velocity of the jet does not cause an increase in the flame height.
- The mean flame lift-off height increases at an increased fuel jet velocity, from the transitional lifted regime to the fully lifted turbulent regime, where in the fully lifted turbulent regime, increasing the jet velocity further, causes the

flame to blow out, indicating that the stability of the flame decreases with an increasing fuel jet velocity.

- Increasing the fuel jet velocity increases the flame's temperature. Also, by increasing the number of axial temperature measurements made at a particular downstream location, the flame can be better characterised, and a better temperature profile can be presented, where the fluctuations in the temperature are better captured.
- CO concentration decreases at increased jet velocities and as the flame is stabilised above the burner. This is due to the higher temperature of the flame at increased jet velocities, and the greater entrainment of air into the lifted flame than in the attached flame, which promotes the oxidation of CO to CO_2, and hence a lower CO concentration in the lifted flame.
- EICO decreases with increasing jet velocity. This is attributed to the stabilisation of the flame above the burner which leads to a higher air entrainment into the flame, and hence a higher OH radical. Increasing the fuel flowrate decreases the sooting propensity because of the greater availability of the OH radical due to the higher air entrainment into the flame which oxidises soot. This increase in the flowrate leads to a higher OH availability due to air entrainment, and this OH oxidises CO to CO_2, hence lesser EICO as the jet velocity is increased.
- In the laminar regime, an increase in the jet velocity leads to an initial increase in the EINOx, before a decrease in the EINOx as the flame approaches the transitional regime. However, beyond the transitional regime, an increase in the jet velocity does not lead to any changes in the EINOx. In the laminar regime, the initial increase in EINOx before the decrease in the EINOx at increased jet velocities is due to an increase in the fuel flowrate which leads to both decreased flame residence times and decreased radiant fractions, and hence higher flame temperatures, leading to a higher EINOx. However, at increased jet velocities and the flame becoming transitional and stabilised above the burner, there is greater mixing, and a greater air dilution, which leads to a lesser concentration of reactive species, shorter flame length, and lower flame temperatures leading to a reduction in the thermal NOx, and hence lower EINOx.

In Chapter 5, the effect of the dilution of the fuel-stream with CO_2 was investigated, where the mole fraction of the diluent was varied from 0 to 0.22 at a fixed fuel flowrate, and the following investigations were made: the effect of the

changes in the visible appearance of the flame, the flame length and lift-off height, the in-flame temperature, the spatial variation of the concentration of the major species, and the variation of the mass fraction of the species as a function of the mixture fraction, and the EICO, EINO and $EINO_2$ of the flame at different diluent mole fractions, due to the dilution of the fuel stream. These results show the significance of varying the mole fraction of the diluent on the fuel jet, and from these investigations, the following conclusions are made:

- An increase in the diluent mole fraction leads to a decrease in the flame's luminosity. This luminosity is due to the chemiluminescence from the hot radical species in the reaction zone. However, when the concentration of the diluent is increased in the jet stream, there is a reduction in the flame temperature and in the reactive species, and hence lower flame luminosity.
- The flame length decreases while the lift-off height increases at increased CO_2 concentrations. The decrease in the flame length is due to the effect of dilution on the flame, which leads to a slower rate of reaction due to a decrease in the flame temperature, and a reduction in the reactant species in the flame, thereby reducing the residence time of the flame, and a reduction in the time scale which is required for the mixing and the burning of the fuel, which decreases the flame speed, and causes the fuel to travel a shorter distance before combusting. Similarly, flame blow-out is sensitive to the concentration of the diluent in the fuel stream, and also, the increase in the flame's lift-off height is due to the effect of dilution which leads to a reduction in the concentration of the reactant and in the length of the heat-release zone and hence a reduction in the flame's reaction rate due to the reduced flame temperature, which leads to the flame being stabilised at downstream locations where a better mixing occurs.
- The dilution of the fuel stream with a 10 vol.% CO_2 and a 20 vol.% CO_2 leads to a 35 K and 67 K decrease, respectively, in the flame temperature due to the high heat capacity of CO_2 which absorbs the heat generated during combustion, thereby reducing the flame temperature via the thermal cooling of the flame.
- An increase in the concentration of the diluent leads to an increase in the CO concentration due to the thermal effect of the diluent which reduces the flame temperature and this lower flame temperature reduces the rate of

oxidation of CO to CO_2, thereby increasing the CO concentration in the flame.

- The dilution of the fuel stream at 0.1 and 0.2 mole fraction of the diluent leads to a 23% and a 26% increase, respectively, in NO_2 concentrations, while leading to a 15% and a 29% decrease in NO concentrations. The decrease in the NO is due to the decrease in the flame temperature due to the thermal effect of dilution which leads to decreased flame temperatures, and hence a decrease in the formation of NO via the Zeldovich mechanism which promotes the formation of thermal NO at high temperatures. Similarly, the increase in the NO_2 concentration at increased diluent concentrations is due to the lower flame temperature due to dilution, which promotes the conversion of NO to NO_2. This low temperature is effective for the production of the HO_2 radical species, and it is this radial species that promotes the conversion of NO to NO_2 in methane flames. Hence, the greater the concentration of the diluent in the fuel stream, the greater the conversion of NO to NO_2, and hence higher NO_2 concentrations. Therefore NO_2 concentrations are higher in the diluted fuel streams than in the undiluted fuel stream.
- Fuel-stream dilution leads to a decrease in the EINOx and an increase in the EICO. The decrease in the EINOx is due to the fuel dilution which leads to the lower concentration of reactant species, and lower flame temperatures because of the thermal effect of the diluent, which leads to a decrease in the formation of NOx via the Zeldovich mechanism. Similarly, the increase in the EICO is due to the thermal effect of the diluent which leads to lower temperatures. This low temperatures slow down the rate of oxidation of CO to CO_2 which inhibits the full oxidation of CO to CO_2 at the post-flame region, through the reaction of CO with OH, which is a slow reaction which leads to a slower CO burn-out, and hence a greater concentration of CO at increased diluent concentrations.

Finally, in Chapter 6, comparisons were made between methane and propane flames at the same Reynolds number where comparisons between the flames' visible appearance, flame stability, in-flame temperature, in-flame concentration of major species and the pollutant emissions from these flames were presented. In addition, this chapter examined the effect of the dilution of propane jets with CO_2, and how

the variation of the diluent mole fraction on the fuel stream affects the soot particle size. Comparing methane and propane flames at the same Reynolds number in the buoyancy-dominated regime, the following conclusions are made:

- Luminosity increases with the number of carbon atoms in the hydrocarbon, therefore propane flames are more luminous than methane flames. Also, the luminous orange-yellow colour is due to the incandescence of carbon particles in the flame which indicates the presence of soot, while the non-luminous bluish colour is an indication of CO.
- The methane flame has a shorter flame length and is stabilised above the jet nozzle, while the propane flames is longer and is stabilised at the rim of the jet nozzle. The shorter length of the methane flame is due to the increase in the entrainment of air into the lifted flame which causes the flame to be stabilised at a location above the burner, where a lesser mixing of the air is required for complete combustion, therefore the flame becomes shorter. Similarly, the propane flame is longer because a greater volume of air is required for the combustion of propane than methane, therefore the propane flame extends to a height where the total flux of the air that is entrained into the flame would be sufficient for the complete combustion of propane, therefore a longer flame length will be required for the combustion of propane than methane, and this suggests the reason for the longer flame length of propane than methane flame.
- The peak mean temperature of the methane flame is higher than that of the propane flame. This is because based on the condition of comparison of both flames, where the flames are compared based on equal Reynolds number, methane has a higher jet velocity than propane, therefore, based on the jet velocity dependency on flame temperatures, higher jet velocities yield higher temperatures. Similarly, the lower temperature of the propane flame is due to the soot concentration in the flame, which leads to a greater radiation, and an increase in the sooting propensity of fuels lead to a decrease in the flame temperature.
- The peak concentration of CO is lower in methane flames than in propane flames due to the stabilisation of the methane flame above the jet nozzle, where there is a sufficient entrainment of air into the flame. In addition, the higher temperature of the methane flame compared to the propane flame

promotes the conversion of CO to CO_2, leading to a lower CO concentration and a higher CO_2 concentration, and hence a better combustion in the methane flame, since CO_2 is an indicator of complete combustion.

- EICO is higher in methane than in propane. This is because based on the test conditions of the fuels examined, methane has a higher strain rate than propane, and hence a shorter global residence time which inhibits the complete oxidation of CO to CO_2 via the reaction of CO and OH to yield CO_2 and H, leading to a higher EICO in methane than in propane. Increased strain rates lead to decreased residence times, and decreased residence times prevent the complete oxidation of CO to CO_2.
- EINO is higher in methane flames than in propane flames. This is because the flame temperature of the methane flame is higher than the propane flame, therefore a greater thermal NO, hence a greater EINO in flame A than flame B is expected. In addition, an increase in the Froude number leads to an increase in the EINO for all fuels. The Froude number of the methane and the propane flames are 21000 and 1800, respectively, and the EINO increases with the jet exit velocity or the flame Froude number. Therefore, the EINO in the methane flame is greater than the EINO in the propane flame because of the higher Froude number for the methane flame at the test condition which was compared with the propane flame.
- During soot growth by coagulation, high temperatures promote a greater particle reactivity, which leads to a greater collision of the reactive species, and hence a greater particle agglomeration, leading to larger aggregates, and hence a lesser primary particle count, since most of the aggregates are agglomerated. However, fuel-stream dilution decreases the flame temperature, which reduces the rate of collision of the reactive species. This reduction in the temperature leads to a higher count of smaller particles, since the particle reactivity and the rate of collision decreases, leading to a lesser agglomeration of the aggregates, hence a decrease in the aggregate size at higher diluent mole fractions.
- In surface growth, the size of the aggregate increases due to the condensation of the particle growth species, on the surface of the particle on the surface of the particle, leading to a greater soot mass, larger aggregate size, and an increase in the soot volume fraction. However, an increase in the

concentration of the diluent in the propane jet stream leads to a decrease in the aggregate size, lesser soot mass and lesser soot volume fraction. This reduction in the aggregate size is due to the thermal effects of dilution which lead to low temperatures, and a lesser particle collision and reactivity, which reduces the probability of the agglomeration of the particle, and hence a reduction in the surface area available for agglomeration and the size of the aggregate. The decrease in the soot mass is due to the effect of dilution, which suppresses the soot precursors due to the effect of the oxidising species which leads to the suppression of the growth species, thereby reducing the attachment of the gas-phase species on the particles which hinders the growth of the particle via surface growth.

- At the post-flame location, the temperatures are low and the soot emission factor decreases at increased diluent concentrations due to the effect of dilution which leads to lower temperatures and a decrease in the soot oxidation rate and hence a low soot burn-out.

7.2 FUTURE WORK

The results in this study were aimed at providing an understanding of how varying different test conditions have an effect on the flame stability and emissions. While these results are revealing, more work has to be done over a wider range of test conditions. This may include characterising the soot and the pollutant emissions, and the structure of the flame, where the effect of crosswinds on the flame at high momentum ratios is investigated. In addition, this research has shown the effect of the dilution of the fuel stream on the emission levels in the flame. Similarly, it is known that natural gas is composed mainly of methane and other hydrocarbons. However, this composition varies from one field to the other, and the fields have a varying amount of CO_2 and H_2S in the reservoir. In addition to other factors, the composition of the fuel also determines the soot and the pollutant emission levels in the flame. To the best of the author's knowledge, there is no simultaneous measurement of the soot and pollutant emission levels in non-premixed flames at turbulent conditions. This is necessary in order to characterise, compare and quantify the overall emissions from a particular fuel type, and will be applicable mainly in industrial-scale flares where there is difficulty in quantifying emissions, and where the application of scaling laws will be useful. In this investigation, CO_2 was used as the inert diluent where the diluent mole fraction was varied, and the

maximum diluent mole fraction used was 0.22. Therefore, future investigations should compare the effect of the fuel-type on the pollutant emissions at higher jet velocities and at higher diluent mole fractions, for a general assessment of the effect of dilution on the soot and pollutant emissions in the flame. It is expected that such investigations would aid in establishing effective and reliable scaling relationships, and in populating and updating the already-existing database of the characteristics of flames, which is useful in validating combustion models.

In addition, this study has looked at the effect of the dilution of the fuel-stream on the soot particle size, where it is has been established that the thermal, chemical and dilution effects of the diluent are responsible for the suppression of soot in flames. Although different investigators agree that these effects are not independent of each other, however, there is no certainity regarding the contributions of each of these effects on soot suppression in non-premixed flames. It is therefore suggested that experimental and analytical methodologies be developed to quantify the individual contributions of the thermal, chemical and dilution effects of the diluent on the soot particle size, and at higher diluent mole fractions.

The experiments reported in this study were performed using the available equipment for the investigations. It is suggested that future investigators use more advanced probing and diagnostic systems to perform the investigations which are suggested in this study.

REFERENCES

Abramoff, M.D., Magalhaes, P.J., and Ram, S.J. (2004) Image Processing with ImageJ, Biophotonics Int., Laurin Publishing Co. Inc., 11,7, 36-42.

Agafonov, G.L., Borisov, A.A., Smirnov ,V.N., Troshin, K.Y., Vlasov, P.A., Warnatz, J. (2008) Soot Formation during Pyrolysis of Methane and Rich Methane / Oxygen Mixtures behind Shock Waves, Combustion Science and Technology, 180, 1876 - 99.

Agafonov, G.L., Smirnov V. N., and Vlasov, P.A. (2011) Shock Tube and Modelling Study of Soot Formation during the Pyrolysis and Oxidation of a number of Aliphatic and Aromatic Hydrocarbons, Proceedings of the Combustion Institute, 33, 625 – 32.

Al-Fawaz, A.D., Dearden, L.M., Hedley, J.T., Missaghi, M., Pourkashanian, M., Williams, A., and Yap, L.T. (1994) NOx Formation in Geometrically Scaled-Gas Fired Industrial Burners, Twenty Fifth Symposium (International) on Combustion, The Combustion Institute, 25, 1, 1027-34.

Annamalai, K., and Puri, I.K. (2007) Combustion Science and Engineering, CRC Press, Taylor and Francis Group, Boca Raton, Florida, 755-66.

Amano, T., and Hase, K., (1994) Cooling Conditions of Hot Exhaust Gas for Low Conversion of NO to NO_2, Journal of the Institute of Energy 67: 473,174–80.

Amato, A., Hudak, B., D'Souza, P., D'Carlo, P., Noble, D., Scarborough, D., Seitzman, J., and Lieuwen, T. (2011) Measurements and Analysis of CO and O_2 Emissions in CH_4 / CO_2 / O_2 Flames, Proceedings of the Combustion Institute 33, 3399-405.

API (1997) Guide for Pressure-Relieving and Depressurising Systems, API Recommended Practice (RP) 521, Fourth Edition, American Petroleum Institute, Washington D.C., 39-54.

API (2014) Pressure-Relieving and Depressurising Systems, API Standard 521, Sixth Edition, American Petroleum Institute, Washington D.C, 102-140.

Apte, V.B. (ed.) (2006) Flammability Testing of Materials used in Construction, Transport and Mining: Fundamental Measurement Techniques, Woodhead Publishing, Cambridge, England, 22-27.

Arctic Council (2011) An Assessment of Emissions and Mitigation Options for

Black Carbon for the Arctic Council, Technical Report of the Arctic Council Task Force on Short-Lived Climate Forcers, Arctic Council.

Arctic Monitoring Assessment Programme (2013) Arctic Ocean Acidification Assessment: Key Findings, Arctic Ocean Acidification International Conference, May 6-8, Bergen, Norway.

Atkins, P. W. (1997) Physical Chemistry, 5th edition, Oxford University Press, Oxford, UK, 29-30.

Axelbaum, R.L., Flower, W.L., and Law, C.K. (1988) Dilution and Temperature Effects of Inert Addition on Soot Formation in Counterflow Diffusion Flames, Combustion Science and Technology, 61, 51-73.

Baron, T. (1954) Reactions in Turbulent Free Jets - The Turbulent Diffusion Flame, Chemical Engineering Progress, 50, 2, 73-6.

Barr, J. (1953) Diffusion Flames, Flames of Fuel Jets, Fourth Symposium (International) on Flame and Explosion Phenomena, The Combustion Institute, Williams and Wilkins, Baltimore, 765-71.

Baukal, C.E. (ed.) (2003) Industrial Burners Handbook, CRC Press, LLC.

Baukal, C.E. (ed.) (2011) Industrial Combustion Testing, CRC Press, Boca Raton, FL.

Baukal, C.E. and Schwartz, R.E. (eds.) (2001) Burner Design, The John Zink Combustion Handbook, CRC Press, Boca Raton, Florida, 353.

Baukal, C.E. and Schwartz, R.E. (eds.) (2001) Pollutant Emissions, The John Zink Combustion Handbook, CRC Press, Boca Raton, Florida, 189.

Baulch, D.L., and Drysdale, D.D. (1974) An Evaluation of the Rate Data for the Reaction $CO + OH \rightarrow CO_2 + H$. Combustion and Flame, 23, 215-25.

Becker, H.A., and Liang, D. (1978) Visible Length of Vertical Free Turbulent Diffusion Flames, Combustion and Flame, 32, 115-37.

Becker, H.A., and Liang, D. (1982) Total Emission of Soot and Thermal Radiation by Free Turbulent Diffusion Flames, Combustion and Flame 44, 305–18.

Becker, H.A., and Yamazaki, S. (1977) Soot Concentration Field of Turbulent /Air Diffusion Flames, Proceedings of the Combustion Institute, 16, 681-91.

Becker, H.A., and Yamazaki, S. (1978) Entrainment, Momentum Flux, and

Temperature in Vertical Free Turbulent Diffusion Flames, Combustion and Flame, 33, 123-149.

Beltrame, A., Porshnev, P., Merchan-Merchan, W., Saveliev, A., Fridman, A., Kennedy, L. A., and Charon, O. (2001) Soot and NO Formation in Methane-Oxygen Enriched Diffusion Flames, Combustion and Flame, 124, 1-2, 295-310.

Bento D.S., Thomson, K.A., and Gülder, Ö.L. (2006) Soot Formation and Temperature Field Structure in Laminar Propane–Air Diffusion Flames at Elevated Pressures, Combustion and Flame, 145, 4, 765-78.

Berhan, S., Atreya, A., Chernovsky, M. and Sacksteder, K. (2001) Effect of Fuel Dilution by CO2 on Spherical Diffusion Flames in Microgravity, AIAA 2001-0622, 1-7.

Bertolo, M., Sayre, A.N., Dugue, J., and Weber, R. (1993) Scaling Characteristics of Aerodynamics and Low-NOx Properties of Industrial Natural Gas Burners, The Scaling 400 Study, Part V: The 4 MW Test Results, International Flame Research Foundation, IFRF Doc. No. F 40/Y/12.

Beychok, M.R. (1987) Observations and Predictions of Jet Diffusion Flame Behaviour, Atmospheric Environment, 1967, 21, 8, 1868.

Beychok, M.R. (1994) Fundamentals of Stack Gas Dispersion, Milton Beychok, Irvine, CA, USA.

Beychok, M.R. (2005) Fundamentals of stack gas dispersion, 4th Edition, Milton R. Beychok Publishers, New Port Beach, California.

Bilger, R.W. (1989) Turbulent Diffusion Flames, Ann. Rev. Fluid Mech.21, 101-35.

Bilger, R.W., and Beck, R.E. (1975) Further Experiments on Turbulent Jet Diffusion Flames, 15th Symposium (International) On Combustion, 15, 1, 541-52.

Bilger, R.W., Starner, S.H., and Kee, R.J. (1990) On Reduced Mechanisms for Methane-Air Combustion in Nonpremixed Flames, Combustion and Flame, 80, 135-49.

Birch, A.D., Brown, D.R., Fairweather, M., and Hargrave, G.K. (1989) An Experimental Study of a Turbulent Natural Gas Jet in a Cross-Flow, Combust. Sci. Technol.,66, 217-32.

Blanquart, G., and Pitsch, H. (2007) Parameter Free Aggregation Model for Soot Formation 5th US Combustion Meeting, Western States Section of the Combustion Institute, USA.

Blanquart, G., and Pitsch, H. (2009) A Joint Volume-Surface-Hydrogen Multi-variate Model for Soot Formation in: Combustion Generated Fine Carbonaceous Particles, Bockhorn, H., D'Anna, A., Sarofim, A.F., and Wang, H. (Eds.), Proceedings of International Workshop, Anacapri, KIT Scientific Publishing, 437-63.

Blinov, V.I., and Khudiakov, G.N. (1957) Diffusion Burning of Liquids, Dokl. Akad. Nauk., S.S.S.R., 113, 1094.

Bockhorn, H. (Ed.) (1994) Soot Formation in Combustion (Mechanisms and Models), Springer Series in ChemicalPhysics 59, Springer-Verlag, Berlin.

Bockhorn, H, Fetting, F., Wannemacher, G., and Wenz, H.W. (1982) Optical Studies of Soot particle Growth in Hydrocarbon Oxygen Flames, 19th Symposium (International) on Combustion, The Combustion Institute, 1413-20.

Bockhorn, H, Fetting, F., Wenz, H.W. (1983) Investigation of the Formation of High Molecular Hydrocarbons and Soot in Premixed Hydrocarbon-Oxygen Flames, Ber. Bunsenges. Phys. Chem.87, 1067 – 73.

Bohm, H., Hesse, D., Jander, H. (1988) The Influence of Pressure and Temperature on Soot Formation in Premixed Flames in 22nd Symposium (International) on Combustion, The Combustion Institute, Pittsburgh, 403-11.

Bond, T.C., Bhardwaj, E., Dong, R., Jogani, R., Jung, S., Roden, C., Streets, D.G., and Trautmann, N.M. (2007) Historical Emissions of Black and Organic Carbon Aerosol from Energy-Related Combustion, 1850–2000. Global Bio-geochemical Cycles 21:1–16.

Bond, T. C., Doherty, S. J., Fahey, D. W., Forster, P.M., Berntsen, DeAngelo, T.B., Flanner, M. G., Ghan, S., Kärcher, B., Koch,D., Kinne, S.,Kondo,Y., Quinn, P. K., Sarofim,M. C., Schultz, M. G., Schulz, M., Venkataraman, C., Zhang, H., Zhang, S., Bellouin, N., Guttikunda, S. K., Hopke, P. K.,

Jacobson, M.Z., Kaiser,J. W., Klimont, Z., Lohmann, U., Schwarz, J.P., Shindell, D., T. Storelvmo, T., Warren,S. G., and Zender, C. S. (2013) Bounding the Role of Black Carbon in the Climate System: A Scientific Assessment, Journal of geophysical Research-Atmospheres, American Geophysical Union.

Bone, W.A. and Townend, T.A. (1927) Flame and Combustion in Gases, Longmans, Green and Co. Ltd, London.

Bott, R. D. (2007) Flaring: Questions and Answers, 2nd edition, Canadian Centre for Energy Information, Canada, 1-24.

Boulanger, J., Vervisch, L., Reveillon, J., and Ghosal S. (2003) Effects of Heat Release in Laminar Diffusion Flames Lifted on Round Jets, Combust Flame., 134, 355–68.

Bowman, C.T. (1975) Kinetics of Pollutant Formation and Destruction in Combustion, Prog. Energy Combust. Sci., Pergamon Press, UK, 1, 33-45.

Bowman, C.T. (1977) Probe Measurements in Flames. Experimental Diagnostics in Gas Phase Combustion Systems, Progress in Astronautics and Aeronautics, 53, Zinn, B.T. (ed.), 3-24.

Bowman, C.T. (1992) Control of Combustion-Generated Nitrogen Oxide Emissions, 24th Symposium on Combustion, The Combustion Institute, Pittsburgh, 24, 1, 1859-78.

BP Statistical Review of World Energy (2015), London, UK.

Briones, A.M., Aggarwal, S.K., and Katta, V.R. (2006) A Numerical Investigation of Flame Liftoff, Stabilization and Blowout, Phys. Fluids, 18, 043603.

Broadwell, J.E., Dahm,W.J.A., and Mungal, M.G. (1984) Blowout of Turbulent Diffusion Flames. In: Twentieth Symposium (International) on Combustion. The Combustion Institute, Pittsburgh, 303–10.

Brookes, S.J. and Moss, J.B. (1999) Measurements of Soot Production and Thermal Radiation from Confined Turbulent Jet Diffusion Flames of Methane, The Combustion Institute, Elsevier Science Inc., 116, 49-61.

Brookes, S.J., and Moss J.B. (1999) Predictions of Soot and Thermal Radiation Properties in Confined Turbulent Jet Diffusion Flames, Combustion and Flame, 116, 486-503.

Brzutowski, T.A. (1973) A New Criterion for Predicting the Length of a Gaseous Turbulent Diffusion Flame, Combust. Sci. Technol., 6, 313-319.

Brzustowski, T.A., and E. C. Sommer, E.C. (1973) Predicting Radiant Heating from Flares, Proceedings–Division of Refining, 53, American Petroleum Institute, Washington, D.C., 865–93.

Brzutowski, T.A. (1975) The Turbulent Diffusion Flame in a Crosswind, in Proceedings of the Fifth Canadian Congress of Applied Mechanics, Fredericton, Canada, 605-606.

Brzustowski, T.A. (1976) Flaring in the Energy Industry, Progress in Energy and Combustion Science, 2, 129-41.

Brzustowski, T.A. (1977) Hydrocarbon Turbulent Diffusion Flame in Subsonic Crossflow, Prog. Astro. Aero., 58, 407-30.

Buckmaster J. (1996) Edge-flames and their Stability. Combustion Science and Technology, 115, 1-3, 41–68.

Buckmaster, J. (2002) Edge-Flames, Progress in Energy and Combustion Science, 28, 435–75.

Burke, S., and Schumann, T. E. W. (1928) Diffusion Flames, Ind. Eng. Chem. 20, 998-1004.

Bussman, W.R., and Baukal, C.E. (2009) Ambient Conditions Impact CO and NOx Emissions: Part I, Petroleum Technology Quarterly, PTQ Q2, 92-9.

Bussman, W.R., and Baukal, C.E. (2009) Ambient Conditions Impact CO and NOx Emissions: Part II, Petroleum Technology Quarterly, PTQ Q3, 36-41.

Byggstoyl, S., and Magnussen, B.F. (1983) A Model for Flame Extinction in Turbulent Flow, Fourth Symposium on Turbulent Shear Flow, Karlsruhe.

Byggstoyl, S. (1984) PhD Thesis, Norwegian Institute of Technology, Trondheim, Norway.

Caldeira-Pires, A., and Heitor, M.V. (2000) Experimental Characterization of Non-Premixed Turbulent Jet Propane Flames, Experimental Thermal and Fluid Science, 23, 115-32.

Cambustion (2009) Particulate Mass Measurement with DMS Series Fast Spectrometers Application Note, DMS01, 5, Cambridge, UK.

Campau, R.M., and Neerman, J.C. (1967) SAE Trans., 75, 582.

Canadian Association of Petroleum Producers (2007) A Recommended Approach to

Completing the National Pollutant Release Inventory (NPRI) for the Upstream Oil and Gas Industry, Calgary, Canada.

Canteenwalla, P.M., Thomson, K.A., Smallwood, G.J., and Johnson, M.R. (2007) Soot Emissions from Turbulent Diffusion Flames Burning Simple Alkane Fuels, 2007 Spring technical Meeting Combustion Institute Canadian Section, Section E-Paper 1, 1-6.

Catalanotti, E. (2011) Theoretical and Experimental Investigation of Alternative Aviation Fuels, PhD Thesis, University of Leeds, UK.

Cha, M. S., and Chung, S. H. (1996) Characteristics of Lifted Flames in Nonpremixed Turbulent Confined Jets, Twenty-Sixth Symposium (International) on Combustion, The Combustion Institute, 121-8.

Charest, M.R.J., Gulder, O.L, Groth, C.P.T. (2014) Numerical and Experimental Study of Soot Formation in Laminar Diffusion Flames Burning Simulated Biogas Fuels at Elevated Pressures, Combustion and Flame, 161, 2678-91.

Chang, T., and Chao, Y. (2011) The Stabilization Characteristics of Turbulent Lifted Diffusion Flames of CH_4 / CO Blended Fuels, Proceedings of the Combustion Institute, 33, 1655-62.

Chen, R-H., and Driscoll, J.F. (1990) Nitric Oxide Levels of Jet Diffusion Flames: Effects of Coaxial Air and Other Mixing Parameters, Twenty-Third Symposium (International) on Combustion, 281-88.

Chen, T. H, and Goss, L. P. (1989) Flame Lifting and Flame/Flow Interactions of Jet Diffusion Flames, AIAA paper, 89-0156, Reno, NV.

Chen, T. H., and Goss, L. P. (1991) Statistical OH-Zone Structures of Turbulent Jet Flames from Lift-off to Near-Blowout, Combustion Science and Technology, 79, 4-6, 311-24.

Chen, T. H., Goss, L.P., Talley, D. G., and Mikolaitis, D. W. (1992) Dynamic Stabilization Zone Structure of Jet Diffusion Flames from Lift-off to Blowout, Journal of Propulsion and Power, 8, 3, 548-52.

Chigier, N. A. (1981)Energy, Combustion, and Environment,McGraw-Hill, New York, USA., 9.

Choudhuri A., Gollahalli, S.R., and Mallinson, R. (1998) Combustion

Characteristics of Hydrogen-Propane Mixtures, Proceedings of the American Chemical Society 215th National Meeting, March 29-April 2, 107-12.

Choudhuri, A.R., and Gollahalli, S.R. (2000) Combustion Characteristics of Hydrogen-Hydrocarbon Hybrid Fuels, International Journal of Hydrogen Energy, 25, 451-62.

Choudhuri, A.R., and Gollahalli, S.R. (2003) Characteristics of Hydrogen–Hydrocarbon Composite Fuel Turbulent Jet Flames, International Journal of Hydrogen Energy, 28, 445-54.

Clague, A.D.H., Donnet, J.B., Wang, T.K., peng, J.C.M. (1999) A Comparison of Diesel Soot with Carbon Black, Carbon, 37, 1553-65.

Coats, C.M. (1996) Coherent Structures in Combustion. Progr Energy Combust Sci. 22:427–509.

Colket, M.B., Chiappetta, L., Guile, R.N., Zabielski, M.F., and Seery, D.J. (1982) Internal Aerodynamics of Gas Sampling Probes, Combustion and Flame, 44, 1-3, 3-14.

Colket, M.B., and Seery, D.J. (1994) Reaction Mechanisms for Toluene Pyrolysis, 25th Symposium (International) on Combustion, 25, 883-91.

Colorado, A.F., Medwell, P.R., and Dally, B.B. (2009) LCV Fuels Emissions of Turbulent Nonpremixed Jet Flames under MILD Combustion Conditions, Proceedings of the Australian Combustion Symposium, December 2-4, 2009, The University of Queensland, Australia.

Cook, D.K., Fairweather, M., Hammonds, J., and Hughes, D.J. (1987) Chem. Eng. Res. Des. 65, 310-17.

Coppalle, A. and Joyeux, D. (1994) Temperature and Soot Volume Fraction in Turbulent Diffusion Flames: Measurements of Mean and Fluctuating Values, Combustion Flame, 96, 275-85.

Council Directive 2001/80/EC of the European Parliament and of the Council (2001) Official Journal of the European Communities, L309/1.

Cox, G., and Chitty, R. (1980) A Study of the Deterministic Properties of Unbounded Fire Plumes, Combustion and Flame, 39, 191-209.

Cumber, P.S., and Spearpoint, M. (2006) A Computational Flame Length

Methodology for Propane Jet Fires, Fire Safety Journal, 41, 3, 215-28.

Dahm, W.J.A., and Dibble, R.W. (1988) Co-flowing Turbulent Jet Diffusion Flame Blowout, Twenty Second Symposium (International) On Combustion, The Combustion Institute, 801-8.

Dahm, W.J.A., and Mayman, A.G. (1990) Blowout Limits of Turbulent Jet Diffusion Flames for Arbitrary Source Conditions, AIAA Journal, 28, 7, 1157-62.

Dalzell, W.H., Williams, G.C., and Hottel, H.C. (1970) A light Scattering Method for Soot Concentration Measurements, Combustion and Flame, 14, 2, 161-169.

D'Alessio, A., D'Anna, A., D'Orsi, A., Minutolo, P., Barbella, R., and Ciajolo, A. (1992)Precursor Formation and Soot Inception in premixed Ethylene Flames, The Combustion Institute, 24, 973 - 80.

D'Alessio, A., Barone, C., Cau, R., D'Anna, A., and Minutolo, P. (2005) Surface Deposition and Coagulation Efficiency of Combustion-Generated Nanoparticles in the Size Range from 1 to 10 nm in Proceedings of the Combustion Institute, 30, 2595-603.

D'Anna, A., Kent, J.H., and Santoro, J.C. (2007) Investigation of Species Concentration and Soot Formation in a Co-Flowing Diffusion Flame of Ethylene, Combustion Science and technology, 179, 1-1, 355-69.

D'Anna, A., Sirignano, M., Commodo, M., Pagliara, R., and Minutolo, P. (2008) An Experimental and Modelling Study of Particulate Formation in Premixed Flames Burning Methane, Combustion Science and Technology, 180, 950 - 58.

Dearden, L. M. (1996) Theoretical and Experimental Investigation of High Temperature Natural Gas Combustion Processes, PhD Thesis, University of Leeds, Leeds, UK.

Decroix, M.E., and Roberts, W. L. (2000) Transient Flow Field Effects on Soot Volume Fraction in Diffusion Flames, Combustion Science and Technology, 160,165-89.

Desgroux, P., Mercier, X., Lefort, B., Lemaire, R., Therssen, E., and Pauwels, J.F. (2008) Soot Volume Fraction Measurement in Low-Pressure Methane Flames by Combining Laser-Induced Incandescence and Cavity Ring-Down

Spectroscopy: Effect of Pressure on Soot Formation, Combustion and Flame, 155, 289-301.

Dobbins, A. R., Fletcher, R. A., and Lu, W. (1995) LaserMicroprobe Analysis of Soot Precursor Particles andCarbonaceous Soot, Combustion and Flame, 100, 301-9.

Dobbins, A.R. and Subramaniasivam, H. (1994) Soot Precursor Particles in Flames. In: Bockron, H. (ed.) Soot Formation in Combustion: Mechanisms and Models, Springer, Berlin/Heildelberg, 290-301.

Dold, J.W. (1988) Flame Propagation in a Non-Uniform Mixture: The Structure of Anchored Triple-Flames. in: Kuhl, A.L., *et al*., (eds.). Eleventh International ` Colloquium on Dynamics of Explosions and Reactive Systems. AIAA., 240–8.

Dombrovsky, L.A. (2010) Radiative Properties of Soot Particles, Thermopedia, A to Z guide to Thermodynamics, Heat and Mass Transfer, and Fluids Engineering.

Donnerhack, S., and Peters, N. (1984) Stabilization Heights in Lifted Methane-Air Jet Diffusion Flames Diluted with Nitrogen, Combustion Science and Technology, 41, 1-2, 101-8.

Drake, M.C., Correa, S.M., Pitz, R. W, Shyy, W., and Fenimore, C.P. (1987) Superequilibirum and Thermal Nitric Oxide Formation in Turbulent Diffusion Flames, Combustion and Flame, Elsevier Science Publishing Co. Inc., New York, 69, 347-65.

Driscoll, J.F., Chen, R-H., and Yoon, Y. (1992) Nitric Oxide Levels of Turbulent Jet Diffusion Flames: Effects of Residence Time and Damköhler Number, Combustion and Flame, 88, 37-49.

Du, D.X., Axelbaum, R.L., and Law, C.K. (1988) Experiments on the Sooting Limits of Aerodynamically-Strained Diffusion Flames, 22nd Symposium (International) on Combustion, The Combustion Institute, 387-94.

Dubnowski, J. J. and Davies, B. C. (1983), Flaring Combustion Efficiency: A Review of the State of Current Knowledge, Proceedings of the Annual Meeting Air

Pollution Control Association, Atlanta, Georgia, 76, 4, APCA, Pittsburgh, Pa, USA 83-52.

Economist: Blending Wall Stands in Way of Ethanol growth. (2008) PHYSorg.com.

Eisner, A. D., and Rosner, D. E. (1985)Experimental Studies of Soot Particle Thermophoresis in Non-Isothermal Combustion gases using Thermocouple Response Techniques, Combustion and Flame, 61, 153-66.

Eickhoff, H., Lenze, B., and Leuckel, W. (1984) Experimental Investigations on the Stabilization Mechanism of Jet Diffusion Flames. In: Twentieth symposium (international) on combustion, The Combustion Institute, Pittsburgh, 311–18.

El-Ghafour, S.A.A., El-Dein, A.H.E., and Aref, A.A.R. (2010) Combustion Characteristics of Natural Gas-Hydrogen Hybrid Fuel Turbulent Diffusion Flame, International Journal of Hydrogen Energy, 35, 2556-65.

Erete, J. I. (2012) Diffusion Flames in Natural Gas Flares, M.Sc. Thesis, University of Leeds, Leeds, UK.

Erete, J. I., Aboje, A. A., Hughes, K. J., Ma, L., Pourkashanian, M., and Williams, A. (2015) An Investigation of Methane and Propane Vertical Flares, Journal of the Energy Institute.

Fairweather, M., Jones, W.P., Lindstedt, R.P. (1992) Predictions of Radiative Transfer from a Turbulent Reacting Jet in Cross-Wind, Combustion and Flame, The Combustion Institute, 89, 45-63.

Fairweather, M., Jones, W.P., Ledin, H.S., and Lindstedt, R.P. (1992) Predictions of Soot Formation in Turbulent, Non-premixed Propane Flames, 24th Symposium (International) on Combustion, The Combustion Institute. 1067-74.

Farina, M.F. (2010) Flare Gas Reduction: Recent Global Trends and Policy Considerations, GE Energy, GEA18592, 10.

Farias, T.L., Carvalho, M.G., and Köylü, Ü. Ö (1998) Radiative Heat Transfer in Soot-containing Combustion Systems with Aggregation, Int.J. Heat Mass Transfer, 41, 17, 2581-87.

Feikema, D., Chen, R-H., and Driscoll, J.F. (1991) Blowout of Nonpremixed Flames: Maximum Coaxial Air velocities Achievable, with and without Swirl, Combustion and Flame, 86, 347-58.

Fells, I., and Rutherford, A.G. (1969) Burning Velocity of Methane-Air Flames, Combustion and Flame, 13, 2, 130-8.

Fenimore, C.P., and Jones, C. W. (1967) Oxidation of Soot by Hydroxyl Radicals,

Journal of Physical Chemistry, 71, 3, 593-97.

Flower, W.L., and Bowman, C.T. (1984) Measurements of the Effect of Elevated Pressure on Soot Formation in laminar Diffusion Flames, Combust. Sci. Technol.37, 93 – 7.

Flower, W.L., and Bowman, C.T. (1988) Soot Production in Axisymmetric Laminar Diffusion Flames at Pressures from One to Ten Atmospheres, Proc. Combust. Inst., 21, 1115-24.

Frenklach, M. (2002) Reaction Mechanism in Soot Formation in Flames, J. Phys. Chem. Chem. Phys., 4, 2027-37.

Frenklach, M., Clary, D.W., Gardiner, W.C., and Stein, S.E. (1984) Detailed Kinetic Modeling of Soot Formation in Shock-tube Pyrolysis of Acetylene, 20th Symposium (International) on Combustion, The Combustion Institute, 887-901.

Frenklach, M., and Warnatz, J. (1987) Detailed Modeling of PAH Profiles in a Sooting Low-Pressure Acetylene Flame, Combustion Science and Technology, 51, 265-83.

Garo, A., Prado, G., and Lahaye, J. (1990) Chemical Aspects of Soot Particles Oxidation in a Laminar Diffusion Flame, Combustion and Flame, 79, 226 – 33.

Gas Flaring in Nigeria: A Human Rights, Environmental and Economic Monstrosity, 2005.

Gaydon, A. and Wolfhard, H. (1970) Flumes. Chapman and Hall, London.

Gerstein, M. (1991) Fossil Fuel Combustion, John Wiley and Sons Inc., 423-525.

Gimenes, T. (2006) Final Project: Characterization of Diesel Sprays in the Eindhoven High pressure Cell, EI3 Energétique & Environment.

Giovanetti, A.J., Hoult, D.P., Keck, J.C. and Sarofim, A.F. (1980) Flame Luminosity and Unburned Hydrocarbon Measurements in Swirling Combustion, Topical Report, US Department of Energy, EX-76-A-01-2295.

Glarborg, P. and Hadvig, S. (1991). Development and Test of a Kinetic Model for Natural Gas Combustion, Nordic Gas Technology Centre, DK, ISBN 87-89309-44-8.

Glassman, I. (1979) Phenomenological Models of Soot Formation in Combustion

Systems, Princeton University Mech. and Aero Eng. Report No. 1450.

Glassman, I. and Yaccarino, P. (1981) The Temperature Effect in Sooting Diffusion Flames, 18th Symposium (International) on Combustion, The Combustion Institute, 1175-83.

Glassman, I. (1988) Soot Formation in Combustion Processes, Twenty Second Symposium (International) on Combustion Proceedings, Pittsburgh,PA, 295-311.

Glassman, I. (1998) Sooting Laminar Diffusion Flames: Effects of Dilution, Additives, Pressure and Microgravity, 27, 1589-96.

Global Gas Flaring Reduction Partnership, Towards a World Free of Flares.

Gollahalli, S.R. (1977) Effects of Diluents on the Flame Structure and Radiation of Propane Jet Flames in a Concentric System, Combustion Science and Technology, 15, 3-4, 147-60.

Gollahalli, S.R. (1978) Aerodynamic and Diluent Effects on the Emission of Nitrogen Oxides from Hydrocarbon Diffusion Flames, The Canadian Journal of Chemical Engineering, 56, 510-14.

Gollahalli, S.R. (1998) Effects of Flame Lift-off on the Differences between the Diffusion Flames from Circular and Elliptic Burners, Journal of Energy Resources Technology, 120, 161-66.

Gollahalli, S. R., Brzustowski, T. A. and Sullivan, H. F. (1975) Characteristics of a Turbulent Propane Diffusion Flame in a Cross-wind, Transactions of the Canadian Society for Mechanical Engineers, 3, 4, 205–14.

Gollahalli, S.R., and Nanjundappa, B. (1995) Burner Wake-Stabilized Gas Jet Flames in Crossflow, Combustion Science and Technology, 109, 327-46.

Gollahalli, S.R., and Puri, R. (1992) Flame Structure and Pollutant Emission Characteristics of a Burning Kerosene Spray with Injection of Diluents, Journal of Energy Resources Technology, 114, 209-15.

Gollahalli, S.R., Savas, O., Huang, R.F., Rodriguez Azara, J.L. (1986) Structure of Attached and Lifted Gas Jet Flames in Hysteresis region. in: Twenty-first Symposium (International) on Combustion, The Combustion Institute, Pittsburgh, 1463–71.

Gollahalli, S.R., and Zadeh, G.K. (1985) Flame Structure of Attached and Lifted Jet Flames of Low-Calorific-Value Gases, Energy Sources, 8, 1, 43-66.

Gomez, A., Sidebotham, G., and Glassman, I. (1984) Sooting Behaviour in Temperature-Controlled Laminar Diffusion Flames, Combustion and Flame, 58, 45-57 .

Goudie, G.O., and Taylor, W.L. (1951) Experiments at University of Glasgow, Scotland, United Kingdom.

Green, R.M. and Witze, P.O. (2000) Laser-Induced Incandescence and Elastic-Scattering Measurements of Particulate-Matter Volume Fraction Changes During Passage Through a Dilution Tunnel, Proc. 10th Int. Symposium. on Application of Laser Tech. to Fluid Mech.

Gunther, R. (1966) Gaswarme, 15, 376.

Guo, H., Min, J., Galizzi, C., Escudie, D., and Baillot, F. (2010) A Numerical Study on the Effects of CO_2 /N_2 / Ar Addition to Air on Lift-off of a Laminar CH_4 / Air Diffusion Flame, Combustion Science and Technology,182: 11-12, 1549-63.

Guide to thermocouple and resistance thermometry (2004) Issue 6.0, TC Ltd., Uxbridge, England, 5-7.

Guidelines to Defra / DECC's GHG Conversion Factors for Company Reporting (2013)Produced by AEA for the Department of Energy and Climate Change (DECC) and the Department for Environment, Food and Rural Affairs (Defra), 12th June.

Guigard, S.E., Kindzierski, W.B., and Harper, N.(2000), Heat Radiation from Flares. Report prepared for Science and Technology Branch, Alberta Environment, ISBN 0-7785-1188-X,Edmonton, Alberta.

Gülder, Ö. L.(1995) Effects of Oxygen on Soot Formation in Methane, Propane, and n-Butane Diffusion Flames,Combust. Flame, 101, 4, 302–10.

Gülder, Ö. L., Intasopa, G., Joo, H.I., Mandatori, P.M., Bento, D.S., and Vaillancourt, M.E. (2011) Unified Behaviour of Maximum Soot Yields of Methane, Ethane and Propane Laminar Diffusion Flames at High Pressures, The Combustion Institute, Combustion and Flame, 158, 2037-2044.

Hammer, J.A. (1990) A Comparison of Several Theories which use Jet Scaling to Predict Liftoff Heights of Turbulent Jet Flames, GALCIT Report FM 90-3, USA, 1-26.

Hanson, R.K., and Salimian, S. (1984) Survey of rate Constants in the N/H/O

System, Combustion Chemistry, Springer-Verlag, 361-421.

Harris, S.J. and Weiner, A.M. (1983) Surface Growth of Soot Particles in Premixed Ethylene / Air Flames, Combustion Science and Technology, 31, 3-4, 685-92.

Harris, S.J. and Weiner, A.M. (1984) Soot Particle Growth in Premixed Toluene / Ethylene Flames, Combustion Science and Technology, 38, 75-87.

Harris, S.J. and Weiner, A.M (1988) A Picture of Soot Particle Inception, 22nd Symposium (International) on Combustion, The Combustion Institute, 333-39.

Harris, S.J., Weiner, A.M., and Ashcraft, C.C. (1986a) Soot Particle Inception Kinetics in a Premixed Ethylene Flame, Comb. Flame, 64, 65.

Hart, R., Nasralla, M., and Williams, A. (1975) The Formation of Oxides of Nitrogen in the Combustion of Droplets and Sprays of some Liquid Fuels, Combustion Science and Technology, 11: 1-2, 57-65.

Hawthorne, W.R., Weddel, D.S., and Hottel, H.C. (1949) Mixing and Combustion in Turbulent Fuel Jets, Third Symposium (International) on Combustion, Williams and Wilkins, Baltimore, 266-88.

Hayhurst, A.N., and McClean, H-A., G. (1974) Mechanism for Producing NO from Nitrogen in Flames, Nature, 251, 303-5.

Hayhurst, A.N., and Vince, I.M. (1980) Nitric Oxide Formation from N_2 in Flames: The Importance of “Prompt” NO, Prog.Energy.Combust.Sci.,6, 35-51.

Haynes, B.S. and Wagner, G.H. (1981) Soot Formation, Progress in Energy and Combustion Science, 7, 4, 229-73.

Heitor, M.V. and Moreira, L.N. (1993) Thermocouples and Sample Probes for Combustion Studies, Progress in Energy and Combustion Science, Pergamon Press, 19, 259-78.

Heskestad, G. (1999) Turbulent Jet Diffusion Flames: Consolidation of Flame Height Data, Combustion and Flame, 118: 51-60.

Homma, R., and Chen, J.-Y. (2000) Combustion Process Optimization by Genetic

Algorithms: Reduction of NO_2 Emission via Optimal Post-flame Process, Proceedings of the Combustion Institute, 28, 2483-9.

Hori, M. (1986) Experimental Study of Nitrogen dioxide Formation in Combustion Systems, The Combustion Institute, Pittsburgh, 1181-88.

Hori, M., Matsunaga, N., Malte, P.C., and Marinov, N.M. (1992) The Effect of Low Concentration Fuels on the Conversion of Nitric Oxide to Nitrogen dioxide, The Combustion Institute, Pittsburgh, 909-16.

Hottel, H.C. (1953) Burning in Laminar and Turbulent Fuel Jets, Fourth Symposium (International) on Combustion Williams and Wilkins, Baltimore, 97.

Hottel, H.C. and Hawthorne, W.R. (1949) Diffusion in Laminar Flame Jets, Third Symposium on Combustion, Flame and Explosion Phenomena, 3, 1,254 - 66.

Homann, K.H. (1984) Formation of Large Molecules, Particulates and Ions in Premixed Hydrocarbon Flames: Progress and Unresolved Questions, 20th Symposium (int.) on Combustion, The Combustion Institute, 857-70.

Hori, M., Matsunaga, N., Malte, P.C., and Marinov, N.M. (1992) The Effect of Low Concentration Fuels on the Conversion of Nitric Oxide to Nitrogen Dioxide, The Combustion Institute, Pittsburgh, 909-16.

Hottel, H. C., and Broughton, F. P. (1932) Determination of True Temperature and Total Radiation from Luminous Gas Flames, Ind. and Eng. Chem. ,4,2, 166-75.

Hottel, H.C., and Hawthorne, W.R. (1949) Diffusion in Laminar Flame Jets, Third Symposium (International) on Combustion, Williams and Wilkins, Baltimore, 254.

Howard, J.B. and Bittner, J.D. (1983) Structure of Sooting Flames: Soot in Combustion Systems and its Toxic Properties, Lahaye, Prado, Plenum Press, New York, 57-93.

Howard, J.B. and Longwell, J.P. (1983) Formation Mechanisms of PAH and Soot in Flames, Polynuclear Aromatic Hydrocarbons Formation, Metabolism and Measurements, Cooke, M. and Dennis, A.J. (eds.) Battelle Press, 57-62.

Howard, L. M. (1998) An Experimental Investigation of Oxygen-Enriched Methane Turbulent Diffusion Flames, Ph.D. Thesis, University of Leeds, UK.

Howell, L. (2004) Flare Stack Diameter Scaling and Wind Tunnel Ceiling and Floor Effects on Model Flares, Thesis, University of Alberta, Canada.

Ibrahim, S.M.A., and El-Mahallawy, F.M. (1985) The Structure of Turbulent Free Diffusion Flames, Combustion and Flame, 60, 141-55.

Idicheria, C.A., Boxx, I.G., and Clemens, N.T. (2004) Characteristics of Turbulent Nonpremixed Jet Flames Under Normal- and Low-Gravity Conditions, Combustion and Flame, 138, 384-400.

International Petroleum Industry Environmental Conservation Association (IPIECA) and American Petroleum Institute (API). (2009) Oil and Natural Gas Industry Guidelines for Greenhouse Gas Reduction Projects, Part III: Flare Reduction Project Family, October 2009.

IGSD (2012) Primer and Short-Lived Climate Pollutants, Slowing the Rate of Global Warming Over the Near Term by Cutting Short-Lived Climate Pollutants to Complement Carbon dioxide for the Long Term, Institute for Governance and Sustainable Development, 1-55.

Intasopa, G. (2011) Soot Measurements in High-Pressure Diffusion Flames of Gaseous and Liquid Fuels, M.Sc. Thesis, University of Toronto, Ontario, Canada.

International Association of Oil and Gas Producers (OGP) (2000) Flaring and Venting in the Oil and Gas Exploration and Production Industry: An Overview of Purpose, Quantities, Issues, practices, and Trends, Report No. 2.79/288

I.P.C.C.(1996) Climate Change 1995: The Science of Climate Change. Contribution of Working Group I to the Second Assessment Report of the Intergovernmental Panel on Climate Change [Houghton, J.T., Meira Filho, L.G., Callander, B.A., Harris, N., Kattenberg, A., and Maskell, K. (eds.)],Cambridge University Press, Cambridge, United Kingdom, New York, NY., USA., and Melbourne, Australia.

I.P.C.C.(2007) Climate Change 2007: Mitigation. Contribution of Working Group III to the Fourth Assessment Report of the Intergovernmental Panel on Climate Change [Metz,B., Davidson, O.R., Bosch,P.R., Dave, R., Meyer, L.A. (eds.)],

Cambridge University Press, Cambridge, United Kingdom and New York, NY, USA.

Ismail, O. S. and Umukoro, G. E. (2014) Modelling Combustion Reactions for Gas Flaring and its Resulting Emissions, Journal of King Saud University – Engineering Sciences.

Ivernel, A. (1973) The Effect of Oxygen-Enrichment or Preheating of the Oxidiser on Nitric Oxide Formation. In Weinberg, F.J. (Ed). Proc. Combust. Inst. European Symposium, 463-68.

Iwata, N. (2006) VA-3000 series multiple gas analyser, Horiba Technical Reports, 10, 1-4.

Iyogun, C.O. and Birouk, M. (2008) Effect of Fuel Nozzle Geometry on the Stability of a Turbulent Jet Methane Flame, Combustion Science and Technology, 180, 12, 2186-2209.

Jacobson, M. (2010) Short-Term Effects of Controlling Fossil-Fuel Soot, Biofuel Soot and Gases, and Methane on Climate, Arctic Ice, and Air Pollution Health,J. Geophys.

Jeng, S-M., Chen, L-D., and Faeth, G.M. (1982) The Structure of Buoyant Methane and Propane Diffusion Flames, Nineteenth Symposium (International) On Combustion, The Combustion Institute, 349-58.

Jeng, S-M., and Faeth, G.M. (1984) Species Concentration and Turbulence Properties in Buoyant Methane Diffusion Flames, Journal of Heat Transfer, 106, 721-27.

Jeng, S.-M., Lai, M.-C, and Faeth, G.M. (1984) Non-luminous Radiation in Turbulent Buoyant Axisymmetric Flames, Combustion Science and Technology, 40, 1-4, 41-53.

Johnson, M.R. and Coderre, A.R. (2011) An Analysis of Flaring and Venting Activity in the Alberta Upstream Oil and Gas Industry, Journal of the Air and Waste Management Association, 61, 2, 190-200.

Johnson, M.R and Coderre, A.R. (2012) Opportunities for CO_2 Equivalent

Emissions Reductions via Flare and Vent Mitigation: A Case Study for Alberta, Canada, International Journal of Greenhouse Gas Control, 8, 121-31.

Johnson, M.R., Devillers, R.W., and Thompson, K.A.(2011) Quantitative field Measurement of Soot Emission from Large Gas Flare using Sky-LOSA. Environmental Science and Technology 45l, 345–50.

Johnson, M.R., and Kostiuk, L.W. (1999) Effects of a Fuel Diluent on the Efficiencies of Jet Diffusion Flames in Crosswind, The Combustion Institute, Canadian Section, Spring Technical Meeting, Alberta, 1-6.

Johnson, M.R., and Kostiuk, L.W. (2000) Efficiencies of Low-Momentum Jet Diffusion Flames in Crosswinds, Combust. Flame 123, 189–200.

Jones, A., Feather, H., McCracken, S., and Sutherlin, T. (2013) To Flare or Not to Flare: Satellite Assessment of Gas Flaring and Climate Relationships, Earthzine.

Joo, H.I.,and Gülder, Ö.L. (2009) Soot Formation and Temperature Field Structure in Co-Flow Laminar Methane-Air Diffusion Flames at Pressures from 10 to 60 atm, Proceedings of The Combustion Institute, 32, 769 – 75.

Joo, H.I., and Gülder,Ö. L. (2010) Soot Formation and Temperature Structures in Small Methane-Oxygen Diffusion Flames at Subcritical and Supercritical Pressures, Combustion and Flame, 167, 1194-1201.

Joo, H.I., and Gülder, Ö.L. (2011) Experimental Study of Soot and Temperature Field Structure of Laminar Co-Flow Ethylene-Air Diffusion Flames with Nitrogen Dilution at Elevated Pressures, Combust. Flame,158, 416-22.

Kalghatgi, G.T. (1981) Blow-Out Stability of Gaseous Jet Diffusion Flames. Part 1: In Still Air, Combustion Science and Technology, 26:5-6, 233-39.

Kalghatgi, G. T. (1983) The Visible Shape and Size of a Turbulent Hydrocarbon Jet Diffusion Flame in a Crosswind, Combustion and Flame 52, 91–106.

Kalghatgi, G.T. (1984) Lift-off Heights and Visible Lengths of Vertical Turbulent Jet Diffusion Flames in Still Air, Combustion Science and Technology 41, 1, 17-29.

Karatas, A.E., and Gülder, Ö.L. (2012) Soot Formation in High Pressure Laminar

Diffusion Flames, Progress in Energy and Combustion Science, 38, 818-45.

Kaskan, W. E. (1957) The Dependence of Flame Temperature on Mass Burning Velocity, Sixth Symposium on Combustion, The Combustion Institute, Elsevier Publishers, New York, 134-43.

Kellerer, H., Koch, R., and Wittig, S. (2000) Measurements of the Growth and Coagulation of Soot Particles in a High Pressure Shock Tube, Combustion and Flame, 120, 188-99.

Kellerer, H., Müller, A., Bauer, H.J., and Wittig, S. (1996) Soot Formation in a Shock Tube under Elevated Pressure Conditions, Combustion Science and Technology, 113 - 4, 67-80.

Kelman, J.B., and Masri, A.R. (1997) Reaction Zone Structure and Scalar Dissipation Rates in Turbulent Diffusion Flames, Combustion Science and Technology, 129, 1-6, 17-55.

Kent, J. H., and Wagner, H. G. (1982) Soot Measurements in Laminar Ethylene Diffusion Flames, Combust. Flame, 47, 53.

Kent, J. H., and Wagner, H. G. (1984) Why do Diffusion Flames Emit Smoke? Combustion Science and Technology, 41, 245-69.

Kennedy, I.M., Kollmann,W., and Chen, J.Y. (1990) A Model for Soot Formation in a Laminar Diffusion Flame, Combustion and Flame, 81, 73-85.

Kiran, D.Y., and Mishra, D.P. (2007) Experimental Studies of Flame Stability and Emission Characteristics of Simple LPG Jet Diffusion Flames, Elsevier Publishers, Kidlington, 86, 10-11, 1545-51.

Konnov, A.A., Zhu, J.N., Bromly, J.H., and Zhang, D. (2005) The Effect of NO and NO_2 on the Partial Oxidation of Methane: Experiments and Modeling, Proceedings of the Combustion Institute, 30, 1, 1093-1100.

Kosdon, F.J., Williams, F.A., and Buman, C. (1969); Combustion of Vertical Cylinders in Air, Twelfth Symposium (International) On Combustion, The Combustion Institute, Pittsburg, 253-264.

Köylü, U. O., Faeth, G. M., Farias, T. L., and M. G. Carvalho, M. G. (1995) Fractal

and Projected Structure Properties of Soot Aggregates, Combustion and Flame, 100, 621-33.

Köylü, Ü. Ö., McEnally, C. S., Rosner, D.E., and Pfefferle,L. D. (1997) Simultaneous Measurements of Soot VolumeFraction and Particle Size / Microstructure in Flames Using a Thermophoretic Sampling Technique, Combustion and Flame 110, 494-507.

Kroner, G., Fuchs, H., Tatschl, R., and Glatter, O. (2003) Determination of Soot Particle Size in a Diffusion Flame: A Dynamic Light Scattering Study, Aerosol Science and Technology 37, 10 818-27.

Lahaye, J. (1990) Mechanisms of Soot Formation, Polymer Degradation and Stability, 30, 111-21.

Leahey, D.M., and Schroeder, M.B. (1987) Observations and Predictions of Jet Diffusion Flame Behaviour, Atmospheric Environment, 21, 4, 777.

Leahey, D.M., and Schroeder, M.B. (1990) Observations and Predictions of Jet Diffusion Flame Behaviour, Atmospheric Environment, Part A, General Topics, 24A, 9, 2527-29.

Lee, B.J., Kim, J.S., Chung, S.H. (1994) Effect of Dilution on the Lift-off of Non-Premixed Jet Flames, in: twenty-fifth Symposium (International) on Combustion, 25, 1175-81.

Lee, K. B., Thring, M. W., and Beer, J. M. (1962) On the Rate of Combustion of Soot in Laminar Soot Flames, Combustion and Flame, 6, 137-45.

Lee, K., Megaridis, C.M., Zelepouga, S., Saveliev, A.V., Kennedy, L.A., Charon, O., and Ammouri, F. (2000)Soot Formation Effects of Oxygen Concentration in the Oxidizer Stream of Laminar Co-annular Non-premixed Methane/Air Flames", Combustion and Flame, 121, 323-33.

Lee, S.Y., Turns, S.R., and Santoro, R.J. (2009) Measurements of Soot, OH and PAH Concentrations in Turbulent Ethylene /Air Jet Flames, Combustion and Flame, 156, 2264-75.

Lee, W., and Na, Y.D. (2000) Soot Study in Laminar Diffusion Flames at Elevated Pressure using Two –Pyrometry and Abel Inversion, JSME Int. J. Ser. B. 43, 550-5.

Lenz, W., and Günther, R. (1980) Measurements of Fluctuating Temperature in a

Free-Jet Diffusion Flame, Combustion and Flame, 37, 63-70.

Leung, K.M., Lindstedt, R.P., and Jones, W.P. (1991) A Simplified Reaction Mechanism for Soot Formation in Nonpremixed Flames, Combustion and Flame, 87, 289-305.

Lewis, B., and Von Elbe, G. (1951) Combustion Flames and Explosion of Gases, Academic Press Inc., 488, 90.

Lewis, B., and Von Elbe, G. (1987) Combustion Flames and Explosion of Gases, Academic Press Inc., 488, 90.

Libby, P.A., and Williams, F.A. (Eds.) (1994) Turbulent Reacting Flows, Academic Press, California, USA.

Liu, F., Guo, H., Smallwood, G.J., and Gulder, O.L. (2001) The Chemical Effects of Carbon Dioxide as an Additive in an Ethylene Diffusion Flame: Implications for Soot and NOx Formation, Combustion and Flame, 125: 778-87.

Liu, F., Thomson, K.A., Guo, H., and Smallwood, G. J. (2006) Numerical and Experimental Study of an Axisymmetric Co-Flow Laminar Methane-Air Diffusion Flame at Pressures between 5 and 40 Atmospheres, Combustion and Flame, 146, 456 – 71.

Livesey, J.B., Roberts, A.L., and Williams, A. (1971) The Formation of Oxides of Nitrogen in some Oxy-Propane Flames, Combustion Science and Technology, 4, 1, 9-15.

Lock, A., Briones, A. M., Aggarwal, S.K., Puri, I.K., and Hegde, U. (2007) Lift-off and Extinction Characteristics of Fuel- and Air-Stream-Diluted Methane-Air Flames, Combustion and Flame, 149, 340-52.

Lock, A., Aggarwal, S.K., Puri, I.K., and Hegde, U. (2008) Suppression of Fuel and Air Stream Diluted Methane-Air Partially Premixed Flames in Normal and Microgravity, Fire Safety Journal, 43, 24-35.

Lock, A., Aggarwal, S.K., and Puri, I.K. (2009) Effect of Fuel Type on the Extinction of Fuel and Air Stream Diluted Partially Premixed Flames, Proceedings of the Combustion Institute, 32, 2583-90.

Lockwood, F.C., and Moneib, H.A. (1982) Fluctuating Temperature Measurements in Turbulent Jet Diffusion Flame, Combustion and Flame, 47, 291-314.

Lohuizen, K. (2008) Gas Flare at Ughelli, Delta State, Nigeria, Science for Human Rights.

Lyle, K.H., Tseng, L. K., Gore, J.P., and Laurendeau, N.M. (1999) A Study of Pollutant Emission Characteristics of Partially Premixed Turbulent Jet Flames, Combustion and Flame, 116: 627-39.

Lyons, K.M. (2007) Toward an Understanding of the Stabilization Mechanisms of Lifted Turbulent Jet Flames; Experiments, Progress in Energy and Combustion Science, 33, 211-31.

Lyons, K.M., Watson, K.A., Carter, C.D., and Donbar, J.M., (2005) On Flame Holes and Local Extinction in Lifted-jet Diffusion Flames, Combust. Flame., 142, 308-13.

Macadam, S., Beer, J.M., Safofim, A.F., and Hoffmann, A.B. (1996) Soot Surface Growth by Polycyclic Aromatic Hydrocarbon and Acetylene Adition, 26th Symposium (International) on Combustion, 26, 2295-2302.

Magnussen, B.F. (1975) An Investigation into the Behaviour of Soot in a Turbulent Free C_2-H_2 Flame, Fifteenth Symposium (International) on Combustion, The Combustion Institute, Pittsburgh, 1415-25.

Majeski, A.J., Wilson, D.J., Kostiuk, L.W. (2004) Predicting the Length of Low-Momentum Jet Diffusion Flames in Crossflow, Combustion Science and Technology, 176, 12, 2001-26.

Mandatori, P.M., and Gülder, O. L. (2011) Soot Formation in Laminar Ethane Diffusion Flames at Pressures from 0.2 to 3.3 MPa, Proc. Combust. Inst., 33, 577-84.

Manning, F.S., and Thompson, R.E. (1995) Oilfield Processing of Petroleum: Crude Oil, PennWell Publishing Company, Tulsa, Oklahoma, USA.

Marinov, N., Pitz, W., Westbrook, C., Hori, M., and Matsunaga, N. (1998) An Experimental and Kinetic Calculation of the Promotion Effect of Hydrocarbons on the NO-NO_2 Conversion in a Flow Reactor, 27th Symposium (International) on Combustion, The Combustion Institute.

Mansurov, Z.A. (2005) Soot Formation in Combustion Processes (Review), Combustion, Explosion, and Shock Waves, 41, 6, 727-44.

Manzello, S.L., and Choi, M.Y. (2002) Morphology of Soot Collected in Microgravity Droplet Flames, Int. J. Heat Mass Transfer, 45, 5, 1109-16.

Masri, A.R. and Bilger, R.W. (1986) Turbulent Non-premixed Flames of Hydrocarbon Fuels near Extinction: Mean Structure from Probe Measurements, 21st Symposium (International) on Combustion, the Combustion Institute, 1511-20.

Matsui, Y., Kamimoto, K., and Matsuoka, S.(1979) A Study on the Time and Space Resolved Measurement of Flame Temperature and Soot Concentration in a D.I. Diesel Engine by the Two-Colour Method, SAE Paper 790491.

Matthews, R.D., Sawyer, R.F. and Schefer, R.W. (1977) Interferences in Chemiluminescent Measurement of NO and NO_2 Emissions from Combustion Systems, Environmental Science and Technology, 11, 1092-96.

Mauss, F., Schafer, T., and Bockhorn, H. (1994a) Inception and Growth of Soot Particles in Dependence on the Surrounding Gas Phase, Comb. Flame, 99, 697.

McCaffrey, B. J. (1979) Purely Buoyant Diffusion Flames: Some Experimental Results, NBSIR 79-1910, National Bureau of Standards, Washington, USA.

McCaffrey, J., and Evans, D. D. (1986) Very Large Methane Jet Diffusion Flames, Twenty-First Symposium (International) on Combustion, The Combustion Institute, 25-31.

McCrain, L.L. and Roberts, W.L. (2005) Measurements of the Soot Volume Field in Laminar Diffusion Flames at Elevated Pressures, Combust. Flame, 140(1–2), 60-9.

McDaniel, M. (1983) Flare Efficiency Study, 133. Research Triangle Park, NC, U.S. Environmental Protection Agency.

McEnally, C. S., and Pfefferle, L. D. (1996) Aromatic and Linear Hydrocarbon Concentration Measurements in a Non-Premixed Flame,Combust. Sci.Technol.116–7, 183-209.

McEnally, C. S., and Pfeffrele, L. D.(1999) Experimental Study of Non-Fuel Hydrocarbon Concentrations in Co-flowing Partially Premixed Methane/Air Flames, Combust. Flame, 118, 4, 619–32.

McEnally, C. S.,Köylü, Ü. ÖPfefferle., L. D., and Rosner, D. E. (1997) Soot Volume Fraction and Temperature Measurements in Laminar Non-Premixed Flames Using Thermocouples, Combustion and Flame,109, 701-20.

McEwen, J. D. N., and Johnson, M. R. (2012) Black Carbon Particulate Matter Emission Factors for Buoyancy-Driven Associated Gas Flares, Journal of the Air and Waste Management Association, 62, 3, 307-21.

Megaridis, C. M., and Dobbins, R.A. (1988) Soot Aerosol Dynamics in a Laminar Ethylene Diffusion Flame, 22nd Symposium (International) on Combustion, The Combustion Institute, Combustion Science and Technology,22, 353-62.

Megaridis, C. M., and Dobbins, R.A. (1989) Comparison of Soot Growth and Oxidation in Smoking and Non-Smoking Ethylene Diffusion Flames, Combustion Science and Technology, 66, 1-16.

Merryman, E.L., and Levy, A. (1974) Nitrogen Oxide Formation in Flames: The Roles of NO_2 and Fuel Nitrogen, 15th Symposium (International) on Combustion, The Combustion Institute, 1073-83.

Meunier, Ph., Costa M., and Carvalho, M.G. (1998) NOx Emissions from Turbulent Propane Diffusion Flames, Combustion and Flame 112, 221-30.

Miake-Lye, R. C., and Hammer, J. A. (1989) Lifted Turbulent Jet Flames: A Stability Criterion Based on the Jet Large-Scale Structure. in: Twenty- second Symposium (International) on Combustion, The Combustion Institute, Pittsburgh, 817–24.

Miller, I.M., and Maahs, H. G. (1977) High-Pressure Flame System for Pollution Studies with results for Methane-Air Diffusion Flames, NASA Technical Note, NASA TN D-8407.

Miller, K.A., Siscovick, D.S., Sheppard, L., Shepherd, K., Sullivan, J.H., Anderson, G.L., and Kaufman, J.D. (2007) Long Term Exposure to Air Pollution and Incidence of Cardiovascular Events in Women, The New England Journal of Medicine, 356, 447-58.

Min, J., and Baillot, F. (2012) Experimental Investigation of the Flame Extinction Processes of Nonpremixed Methane Flames inside an Air Coflow Diluted with CO_2, N_2 or Ar, Combustion and Flame, 159, 3502-17.

Min, J., Baillot, F., Wyzgolik, A., Domingues, E., Talbaut, M., -Rouland, B., and

Galizzi, C. (2009) Experimental Study of Non-Premixed Ch4/Air Flames: Effect of CO_2 Addition and Reactant Preheating, Proceeding of the European Combustion Meeting 2009.

Mishra, D.P. (2014) Experimental Combustion: An Introduction, CRC Press, Taylor and Francis Group, Boca Raton, Florida.

MIT Energy Initiative (2010) The Future of Natural Gas, USA.

Mokhatab, S., and Poe, W.A. (2012) Handbook of Natural Gas Transmission and Processing, 2nd ed. Elsevier Copyright Inc., UK., 627.

Molkov,V, and Saffers, J-B. (2012) Hydrogen Jet Flames, International Journal of Hydrogen Energy.

Müeller, A., and Wittig, S. (1994) Experimental Study on the Influence of Pressure on Soot Formation in a Shock Tube, Springer Series in Chemical Physics, 59, 350 – 70.

Mukherjee, J., Sarofim, A.F., and Longwell, J.P. (1994) Polycyclic Aromatic Hydrocarbons from the High Temperature Pyrolysis of Pyrene, Combustion and Flame, 96, 3, 191-200.

Mungekar, H.P., and Atreya, A. (2006) Flame Radiation and Soot Emission from Partially Pre-Mixed Methane Counter-flow Flames, Journal of Heat Transfer, 128, 4, 361 - 67.

Muniz, L., and Mungal, M.G. (1997) Instantaneous Flame-Stabilization Velocities in Lifted Jet Diffusion Flames, Combustion and Flame, 111, 16-31.

Namazian, M., Kelly, J. T., and Schefer, R.W. (1988) Near-field Instantaneous Flame and Fuel Concentration Structures, 22nd Symposium (International) on Combustion, The Combustion Institute, 627-34.

Namazian, M., Kelly, J.T., and Schefer, R.W. (1994) Simultaneous NO and Temperature Imaging Measurements in Turbulent Non-Premixed Flames, 25th Symposium on Combustion, The Combustion Institute, 25, 1149-57.

National Earth Science Teachers Association (2010) Arctic Weather, Windows to the Universe Team, Boulder, CO: Date of last modification for this page, 28/06/2007 Online. Available: http://www.windows2universe.org. 18/02/2014

Neoh, K.G., Howard, J.B., and Sarofim, A.F. (1984) Effect of Oxidation on the

Physical Structure of Soot, in 20th Symposium (International) on Combustion, 154-64.

Newhall, H.K. and Shahed, S.M. (1971) Kinetics of Nitrogen Oxide Formation in High Pressure Flames, 13th Symposium (International) on Combustion 13, 1, 381-89.

Niger Delta Development Commission (2006) Niger Delta Regional Development Master Plan: Niger Delta Region, Land and People, Printing Development Company Limited, Port Harcourt, Nigeria, 1-53.

Novakov, T. (1984) 2nd International Conference on Carbonaceous Particles in the Atmosphere, The Science of Total Environment, Vol. 36.

Nwaichi, E. O., and Uzazobona, M. A. (2011) Estimation of the CO_2 Level due to Gas Flaring in the Niger Delta, Research Journal of Environmental Sciences 5, 6, 565-72.

Ogiemwonyi, C. (2009) The Uncertainty over Gas Flare Target, West Coast Trader, February / March Edition, 23-24.

Oh, J., and Noh, D. (2014) The Effect of CO_2 Addition on the Flame Behaviour of a Non-Premixed Oxy-Methane Jet in a Lab-scale Furnace, Fuel, 117, 79-86.

Oh, K.C, and Shin, H.D. (2006) The Effect of Oxygen and Carbon dioxide Concentration on Soot Formation in Non-premixed Flames, Fuel, 85, 615-24.

Oliver, J.G.J., Janssens-Maenhout, G., Muntean, M., and Peters, J.A.H.W. (2013) Trends in Global CO_2 Emissions; 2013 Report, The Hague: PBL Netherlands Environmental Assessment Agency; Ispra: Joint Research Centre.

Omega Temperature Measurement Handbook (2007) 6th Edition, MMXi, A18.

Palacios, A., Munoz, M., and Casal, J. (2009) Jet Fires: An Experimental Study of the Main Geometrical Features of the Flame in Subsonic and Sonic Regimes, AIChE Journal, 55, 1, 256-63.

Palmer, H.B., and Cullis, C.F. (1965) The Formation of Carbon from Gases. In: Walker Jr., P.L., Editor, Chemistry and Physics of Carbon, 1, New York, Marcel and Dekker, 265-325.

Park, K., Cao, F., Kittelson, D.B., and McMurry, P.H. (2003) Relationship between Particle Mass and Mobility for Diesel Exhaust Particles, Environ. Sci. Technol. 37, 577 - 83.

Particulate Mass Measurement with DMS Series Fast Spectrometers, Cambustion Application Note, DMS01

Peters, N. (1983) Local Quenching due to Flame Stretch and Non-premixed Turbulent Combustion, Combust Sci Technol., 30,1–17.

Peters, N., and Göttgens, J. (1991) Scaling of Buoyant Turbulent Jet Diffusion Flames, Combustion and Flames, 85, 206 -14.

Peters, N., and Williams, F. A. (1983) Lift-off Characteristics of Turbulent Jet Diffusion Flames. AIAA J. 21,3, 423–9.

Phillips, H. (1965) Flame in a Buoyant Methane Layer. in: Tenth Symposium (International) on Combustion, The Combustion Institute, Pittsburgh, 1277–83.

Pitts, W. M. (1988) Assessment of Theories for the Behavior and Blowout of Lifted Turbulent Jet Diffusion Flames. In: Twenty-second Symposium (International) on Combustion, The Combustion Institute, Pittsburgh, 809–16.

Pohl, J.H., and Soelberg, N. R. (1986) Evaluation of the Efficiency of Industrial Flares: H_2S Gas Mixtures and Pilot Assisted Flares, USEPA-600/2-86/080

Pohl, J. H., Tichenor, B.A., Lee, J., and Payne, R. (1986) Combustion Efficiency of Flares, Combustion Science and Technology, 50, 217-31.

Popovitcheva, O.B., Persiantseva, N.M., Trukhin, M.E., Rulev, G.B. and Shonija, N. (2000) Experimental Characterization of Aircraft Combustor Soot: Microstructure, Surface area, Porosity and Water adsorption," Physical Chemistry, Chemical Physics, 2, 4421-26.

Poudenx, P. (2000) Plume Sampling of a Flare in Crosswind: Structure and Combustion Efficiency, Thesis, University of Alberta, Canada.

Pourkashanian, M., Missaghi, M., Williams, A., and Yap, L. (1990) The Prediction of NO Emissions from an Industrial Burner, Proceedings of the American Flame Research Foundation (AFRF) Conference, San Francisco, California, October 8-10.

Pourkashanian, M., Foster, T.J., Wilson, C.W., and Williams, A. (1998)

Measurement and Prediction of NO and NO_2 Emissions from Aero-engines in: Gas Turbine Engine Combustion, Emissions and Alternative Fuels, RTO-MP14, 19-1 -19-9.

Pourkashanian, M., Yap, L.T., Howard, L., Williams, A., and Yetter, R.A. (1998)

Nitric Oxide Emissions Scaling of Buoyancy-Dominated Oxygen-Enriched and Preheated Methane Turbulent Jet Diffusion Flames, 27th International Symposium on Combustion, The Combustion Institute, 1451-60.

Puri, I. K. (1992) Extinction Criteria for Buoyant Nonpremixed Flames, Combustion Science and Technology, 84: 1-6, 305-21.

Puri, I.K. (Ed.) (1993) Environmental Implications of Combustion Processes, CRC Press Inc., Boca Raton, FL., 71-95.

Puri, R., Richardson, T. F., Santoro, R. J., and Dobbins, R. A. (1993) Aerosol Dynamic Processes of Soot Aggregatesin a Laminar Ethene Diffusion Flame, Combustion and Flame, 92, 320-33.

Puri, R., and Santoro, R.J. (1991) The Role of Soot Particle Formation on the Production of Carbon Monoxide in Fires, 3rd Symposium (International) on Fire Safety Science, 595-604.

Puri, R., Santoro, R.J., and Smyth, K.C. (1994) The Oxidation of Soot and Carbon Monoxide in Hydrocarbon Diffusion Flames, Combustion and Flame 97, 124-44.

Putnam, A.A. and Gringerg, J.M. (1965) Axial Temperature Variation in a Turbulent Buoyant-Controlled Diffusion Flame, Combustion and Flame, 9, 418.

Putnam, A.A. and Speich, C.F. (1963) A Model Study of the Interaction of Multiple Turbulent Diffusion Flames, Ninth Symposium (International) on Combustion, 867-77.

Qamar, N.H., Alwahabi, Z.T., Chan, Q.N., Nathan, G.J., Roekaerts, D., and King, K.D. (2009)Soot Volume Fraction in a Piloted Turbulent Jet Non-Premixed Flame of Natural Gas, Combustion and Flame, 156, 1339 – 47.

Rao, R.S. and Krishna, K.M. (2012) Environment Management: Particulate Matter from Refinery Flares and Health Effects of Soot, International Journal of Information Technology and Business Mangement, Vol.6:1., 81-2.

Richter, H. and Howard, J.B. (2000) Formation of Polycyclic Aromatic Hydrocarbons and their Growth to Soot—AReview of Chemical Reaction Pathways," Progress in Energy and Combustion Science, 26, 565–608.

Richter, H., Granata, S., Green, W.H., and Howard, J.B. (2004) Detailed Modeling of PAH and Soot Formation in Laminar Preliminary Mixture Benzene / Oxygen / Argon at Low Pressure Flame, Proc. Combust. Inst., 30, 1397 - 1405.

Rissler, J., Swietlicki, E., Bengtsson, A., Boman, C., Pagels, J., Sandström, T., Blomberg, A., and Löndahl, J. (2012) Experimental Determination of Deposition of Diesel Exhaust Particles in the Human Respiratory Tract, Journal of Aerosol Science, 48, 18-33.

RØkke, P.E., and Hustad, J.E. (2005) Exhaust Gas Recirculation in Gas Turbines for Reduction of CO_2 Emissions: Combustion Testing with Focus on Stability and Emissions, Int. J. of Thermodynamics, 8, 4, 167-73.

RØkke, N.A., Hustad, J.E., and SØnju, O.K., (1994) A Study of Partially Premixed Unconfined Propane Flames, Combustion and Flame, 97, 88-106.

Roper, F.G. (1984) Soot Escape from Diffusion Flames: A Comparison of Recent Work in this Field, Combustion Science and Technology, 40, 5-6, 323-29.

Rosen, H., Hansen, A.D.A., Dod, R.L., and Novakov T. (1980) Soot in Urban Atmospheres: Determination by an Optical Absorption Technique, Science, 208, 741-44.

Rosen, H. and Novakov. T. (1977) Raman Scattering and the Characterization of Atmospheric Aerosol Particles, Nature 266, 708-10.

Ruetsch, G.R., Vervisch, L., Linan, A. (1995) Effects of Heat Release on Triple Flames. Phys. Fluids 7, 1447–54.

Rummel, K. and Veh, P.-O. (1941) Die Strahlung Leuchtender Flammen, 1 Teil Archiv f.d. Eisenhuttenwesen 14, Jhrg., Heft 10.

Sabine, L.C., Feely, R.A., Gruber, N., Key, R.M., Lee, K., Bullister, J.L., Wanninkhof, R., Wong, C.S., Wallace, D.W.R., Tilbrook, B., Millero, F.J., Peng, T-H.,Kozyr, A., Ono, T., and Rios, A.F. (2004) The Oceanic Sink for Anthropogenic CO_2, Science, 305, 367-71.

Saito, K., Williams, F. A., and Gordon, A. S. (1986) Effects of Oxygen on Soot Formation in Methane Diffusion Flames, Combust. Sci. Technol., 47, 117–38.

Samanta, A., Ganguly, R., and Datta, A. (2010) Effect of CO_2 Dilution on Flame Structure and Soot and NO Formations in CH_4-Air Non-premixed Flames, Journal of Engineering for Gas Turbines and Power, 132, 124501-1 – 124501-5.

Santoro, R.J., Semerjian, H.G., and Dobbins, R.A. (1983) Soot Particle Measurement in Diffusion Flames, Combustion and Flame 51, 203-18.

Santoro, R.J., Yeh, T.T., Horvath, J.J., and Semerjian, H.G. (1987) The Transport and Growth of Soot Particles in Laminar Diffusion Flames, Combustion Science and Technology, 53, 2-3, 89-115.

Santoro, R.J., and Miller, J.H. (1987) Soot Particle Formation in Laminar Diffusion Flames Langmuir, 3, 244-54.

Santos, A., and Costa, M. (2005) Re-examination of the Scaling Laws for NOx

Emissions from Hydrocarbon Turbulent jet Diffusion Flames, Combustion and Flame, 142, 1-2, 160-9.

Santos, A. A. B., Torres, E. A., and Pereira, P. A. (2011) Experimental Investigation of the Natural Gas Confined Flames Using the OEC, Energy, 36, 1527-34.

Schittkowski, T., Mewes, B., Brüggemann, D. (2002) Laser-Induced Incandescence and Raman Measurements in Sooting Methane and Ethylene Flames, Physical Chemistry Chemical Physics, 4, 11, 2063 - 71.

Scholefield, D.A., and Garside, J.E. (1949) The Structure and Stability of Diffusion Flames. in: Third Symposium (International) on combustion, 102–10.

Schuetz, C.A., and Frenklach, M. (2002) Nucleation of Soot: Molecular Dynamics, Simulations of Pyrene Dimerization, Proc. Combust. Inst., 29, 2307 – 14.

Schug, K. P., Manheimer-Timnat, Y., Yaccarino, P., and Glassman I. (1980) Sooting Behavior of Gaseous Hydrocarbon Diffusion Flames and the Influence of Additives, Combustion Science and Technology, 22, 5-6, 235-50.

Seeger, T., Egermann, J., Dankers, S., Beyrau, F., Leipertz, A. (2004) Comprehensive Characterization of a Sooting Laminar Methane-Diffusion Flame Using Different Laser Techniques, Chemical Engineering and Technology, 27, 11, 1150 – 56.

Seinfeld, J, H. and Pandis, S. N. Atmospheric Chemistry and Physics - From Air Pollution to Climate Change (2nd Edition). John Wiley & Sons.

Shaddix, C.R. and Smyth, K.C. (1996) Elusive History of m = 1.57 – 0.56i for the Refractive Index of Soot: Brief Communication, Combustion and Flame, 107, 3, 314-20.

Shaddix, C.R., and Smyth, K. C. (1996) Laser-Induced Incandescence Measurements of Soot Production in Steady and Flickering Methane, Propane, and Ethylene Diffusion Flames, Combustion and Flame, 107, 418-52.

Shore, D. (2006) A Proposed Comprehensive Model for Elevated Flare Flames and Plumes, AICHE Paper, XXXX, X, 1-39.

Shukla, B., Susa, A., Miyoshi, A., and Koshi, M. (2007) In Situ Direct Sampling Mass Spectrometric Study on Formation of Polycyclic Aromatic Hydrocarbons in Toluene Pyrolysis, J. Phys. Chem. A. 111, 8308 – 24.

Siegel, K.D. (1980) Degree of Conversion of Flare Gas in Refinery High Flares, 192, PhD Dissertation, Fridericiana University Karlsruhe, Karlsruhe, Germany.

Sivathanu, Y.R., and Faeth, G.M. (1990) Soot Volume Fractions in the Overfire Region of Turbulent Diffusion Flames. Combustion and Flame 81, 133–49.

Skjøth-Rasmussen, M.S., Glarborg, P., Østberg, M., Johannessen, J.T., Livbjerg, H., Jensen, A.D., and Christensen, T.S. (2004) Formation of Polycyclic Aromatic Hydrocarbons and Soot in Fuel-Rich Oxidation of Methane in a Laminar Flow Reactor, Combustion and Flame, 136, 91 – 128.

Smallwood, G.J. (2008) A Critique of Laser-Induced Incandescence for the Measurement of Soot, PhD Thesis, Cranfield University.

Smith, E.C.W. (1940) The Emission Spectrum of Hydrocarbon Flames, Proc. R. Soc. Lond.174, 110-25.

Smith, S.R., and Gordon, A.S. (1956) Studies of Diffusion Flames. I. The Methane Diffusion Flame, J.Phys. Chem. 60, 759-63.

Smooke, M.D., Mcenally, C.S., and Pfefferle, L.D. (1999) Computational and Experimental Study of Soot Formation in a Co-Flow, Laminar Diffusion Flame, Combustion and Flame,117, 117-39.

Smoot, L. D., Smith, J.D., and Jackson, R. E. (2009) Technical Foundations to Establish New Criteria for Efficient Operation of Industrial Steam-Assisted Gas Flares, IFRF, 16th International Members' Conference, MA, USA.

Smyth, K.C., Miller, J.H., Dorfman, R.C., Mallard, W.G., and Santoro, R.J. (1985) Soot Inception in a Methane / Air Flame as Characterised by Detailed Species Profiles, Combustion and Flame, 62, 157-81.

Smyth, K.C., Shaddix, C.R., and Everest, D.A. (1997) Aspects of Soot Dynamics as

Revealed by Measurements of Broadband Fluorescence and Flame Luminosity in Flickering Diffusion Flames. Combustion and Flame 111: 185-207.

Sobiesiak, A., and Brzustowski, T.A. (1984) Some Characteristics of the Stabilization Region of Lifted Turbulent Jet Diffusion Flames. Abstract for Paper Presented at the 1984 Fall Technical Meeting, Eastern Section, The Combustion Institute, Clearwater beach, FL.

Sobiesiak, A., and Brzustowski, T.A. (1986) On the Structure of the Stabilization Region of Lifted Turbulent Jet Diffusion Flames. Abstract for Paper Presented at the 1986 Spring Meeting, Western States Section, The Combustion Institute, Banff, Canada.

SØnju, O. K., and Hustad, J. (1984) An Experimental Study of Turbulent Jet Diffusion Flames, Progress in Astronautic and Aeronautic Series, 95, 320-39.

Sonibare, J.A., and Akeredolu, F.A. (2004) A Theoretical Prediction of Non-Methane Gaseous Emissions from Natural Gas Combustion, Energy Policy, 32, 1653-65.

Stanmore, B. R., Brilhac, J. F., and Gilot, P. (2001) The Oxidation of Soot: A Review of Experiments, Mechanisms and Models, Carbon, 39, 2247-68.

Stasio, S. (2001) Electron Microscopy Evidence of Aggregation under Three Different Size Scales for Soot Nanoparticles in Flame, Carbon, 39, 109-18.

Steward, F.R. (1970) Prediction of the Height of Turbulent Diffusion Buoyant Flames, Combustion Science and Technology, 2, 203-12.

Stohl, A. (2006) Characteristics of Atmospheric Transport into the Arctic Troposhere, Journal of Geophysical Research, 111

Stohl, A., Klimont, Z., Eckhardt, S., Kupiainen, K., Shevchenko, V.P., Kpoeikin, V. M., and Novigatsky, A. N. (2013) Black Carbon in the Arctic: The Underestimated Role of Gas Flaring and Residential Combustion Emissions, Atmos. Chem. Phys., 13, 8833-55.

Strosher, M. T. (2000) Characterization of Emissions from Diffusion Flare Systems,

J. Air & Waste Management. Assoc., 50, 1723-33.

Subramaniasivam, H. (1992) Soot Formation in the Buoyancy-Dominated Ethene Diffusion Flame, United States Department of Commerce Technology Administration, National Institute of Standards and Technology, NIST-GCR-92-609.

Takahashi, F, and Glassman, I. (1984) Sooting Correlations for Premixed Flames, Combustion Science and Technology, 37, 1-19.

Takahashi, F., Linteris, G.T., and Katta, V.R. (2008) Extinguishment of Methane Diffusion Flames by Carbon dioxide in Co-flow Air and Oxygen-Enriched Microgravity Environments, Combustion and Flame, 155, 37-53.

Takahashi, F., Mizomoto, M, and Ikai, S. (1982) Transition from Laminar to Turbulent Free Jet Diffusion Flames, Combustion and Flame, 48, 85-95.

Teini, P.D., Karwat, D.M.A., Atreya, A. (2012) The Effect of CO_2/H_2O on the Formation of Soot Particles in the Homogeneous Environment of a Rapid Compression Facility, Combustion and Flame, 159, 1090-99.

Thomas, A. (1962) Carbon Formation in Flames, Combustion and Flame, Elsevier Inc. 6, 46-62.

Thomas, P.H. (1963) The Size of Flames from Natural Fires, Ninth Symposium (International) on Combustion, 844-59.

Thomas, P.H., Webster, C.T., and Raftery, M.M. (1961) Some Experiments on Buoyant Diffusion Flames, Combustion and Flame, 5, 359-67.

Thomson,K.A., Gülder Ö.L., Weckman E.J., Roydon A. Fraser , Greg J. Smallwood G.J. and Snelling D.R.. (2005) Soot Concentration and Temperature Measurements in Co-Annular, Non-Premixed CH4/Air Laminar Flames at Pressures up to 4 MPa, Combustion and Flame, 140, 222-232.

Thomson, K.A., Johnson, M.R., Snelling, D.R and Smallwood, G.J. (2008) Diffuse-Light- Two-Dimensional Line-of-Sight Attenuation of Soot Concentration Measurements, Applied Optics, 47, 5, 694-703.

Turns, S.R. (1995) Understanding NOx Formation in Nonpremixed Flames, Experiments and Modeling, Progress in Energy and Combustion Science, 21, 5, 361-85.

Turns, S.R. (1996) An Introduction to Combustion – Concepts and Applications, McGraw-Hill Int. Editions, Singapore.

Turns, S.R., and Bandaru, R.V. (1993) Carbon Monoxide Emissions from Turbulent Non-premixed Jet Flames, Combustion and Flame, 94: 462-8.

Turns, S. R. and Lovett, J. A. (1989) Measurements of Oxides of Nitrogen Emissions from Turbulent Propane Jet Diffusion Flames, Combustion Science and Technology, 66, 4, 233 - 49.

Turns, S.R., and Myhr, F.H. (1991) Oxides of Nitrogen Emissions from Turbulent Jet Flames; Part I – Fuel Effects and Flame Radiation, Combustion and Flame 87: 319-35.

Turns, S.R., Myhr, F.H., Bandaru, R.V., and Maund, E.R. (1993) Oxides of Nitrogen Emissions from Turbulent Jet Flames: Part II – Fuel Dilution and Partial Premixing Effects, Combustion and Flame, The Combustion Institute, 93, 255-69.

Upatnieks, A., Driscoll, J.F., Rasmussen, C.C., Ceccio, S.L. (2004) Lift-off on Turbulent Jet Flames-Assessment of Edge Flame and other Concepts using Cinema-PIV. Combust Flame, 138, 259–72.

U.S. Environmental Protection Agency. 1995. AP-42 Compilation of Air Pollutant Emission Factors, Volume I, 5th ed.—Section 13.5.

US Environmental Protection Agency (2009) WebFIRE (Factor Information Retrieval System) v.6.25.

US Environmental Protection Agency (2012) Parameters for the Properly Designed and Operated Flares, Report for Flare Review Panel, US EPA Office of Air Quality Planning and Standards (OAQPS).

US Environmental Protection Agency (2012) Report to Congress on Black carbon,

Department of the Interior, Environment, and Related Agencies Appropriations Act, 2010, EPA-450/R-12-001.

Vanquickenborne L., and Van Tiggelen, A. (1966) The Stabilization Mechanism of Lifted Diffusion Flames. Combust Flame, 10, 59–69.

Vandsburger, U., Kennedy, I. M., and Glassman, I. (1984) Sooting Counter-flow Diffusion Flames with Varying Oxygen Index, Comb. Sci. Tech., 39, 263-85.

Versteeg, H.K., and Malalasekera, W. (1995) An Introduction to Computational Fluid Dynamics: The Finite Volume method, Pearson Education Limited, Essex, England.

Veynante, D., Vervisch, L., Poinsot, T., Linan A., Ruetsch, G.R. (1994) Triple Flame Structure and Diffusion Flame Stabilization. in: Proceedings of the Summer Program. Center for Turbulence Research, NASA Ames/Stanford University, 55–65.

Vieneau, H. (1964) Mixing Controlled Flame Heights for Circular Jets, Thesis, Chemical Engineering, University of Brunswick, Fredericton, N.B.

Vincitore, A.M., and Senkan, S.M. (1997) Experimental Studies of the Micro-Structures of Opposed Flow Diffusion Flames: Methane, Combustion Science and Technology, 130, 233 – 46.

Wagner, H. (1979) Soot Formation in Combustion, 17th International Symposium on Combustion, Pittsburgh, Pennsylvania, The Combustion Institute, 3-19.

Warnatz, J., Mass, U. and Dibble, R.W. (2006) Combustion: Physical and Chemical Fundamentals, Modelling and Simulation, Experiments, Pollutant Formation, Springer– verlag Berlin, Heidelberg, New York, 20-25.

Walls, J.R., and Strickland-Constable, R.F. (1964) Oxidation of Carbon between 1000 - 2000°C, Carbon, 1, 3, 333-38.

Wang, L., Endrud, N.E., Turns, S.R., D'Agostini, M.D., Slavejkov, A.G. (2002) A Study of the Influence of Oxygen Index on Soot, Radiation, and Emission Characteristics of Turbulent Jet Flames, Combust. Sci. Technol., 174, 8, 45-72.

Warnatz, J., Maas, U., and Dibble, R.W. (2006) Combustion: Physical and Chemical

Fundamentals, Modeling and Simulation, Experiments, Pollutant Formation, 4thed., Springer-Verlag, Berlin Heidelberg, Germany.

Weber, R., Sayre, A.N., Dugue, J., and Horsman, H. (1993) Scaling Characteristics of Aerodynamics and Low-NOx Properties of Industrial Natural Gas Burners, The Scaling 400 Study, Part II: The 12 MW Test Results, International Flame Research Foundation, IFRF Doc. No. F 40/Y/9.

Wen, Z., Yun, S., Thomson, M.J., and Lightstone, M.F. (2003) Modeling Soot Formation in Turbulent Kerosene /Air Jet Diffusion Flames, Combustion and Flame, 135, 323-40.

Westenberg, A. A., and deHaas, N.J. (1972) Steady-state Intermediate Concentrations and Rate Constants: Some HO_2 Results, J. Phys.Chem., 76, 1586-93.

Wey, C., Powell, E. A., Jagoda, J. I. (1984) The Effect of Temperature on the Sooting Behaviour of Laminar Diffusion Flames, Combustion Science and Technology, 41, 173-90.

Williams, F.A. (1985) Combustion Theory, Addison-Wesley.

Wohl, K., Gazley, C., and Kapp, N. (1949) Diffusion Flames, Third Symposium (International) on Combustion and Flame and Explosion Phenomena, Williams and Wilkins, Baltimore, MD, 288.

Wohl, K., Kapp, N.M., Gazley, G. (1949) The Stability of Open Flames. in: Third Symposium (International) on Combustion, The Combustion Institute, Pittsburgh, 3–21.

Wu, Y., Al-Rahbi, I.S., Lu, Y., and Kalghatgi, G.T. (2007) The Stability of Turbulent Hydrogen Jet Flames with Carbon dioxide and Propane Dilution, Fuel, 86, 1840-48.

Wu, Y., Lu, Y., Al-Rahbi, I.S., and Kalghatgi, G.T. (2009) Prediction of the Lift-off, Blowout and Blowoff Stability Limits of Pure Hydrogen/Hydrocarbon Mixture Jet Flames, International Journal of Hydrogen Energy, 34, 5940-45.

Wyzgolik, A., and Baillot, F. (2007) Response of the Non-premixed Lifted Flame to

Coaxial Jet Mixing Layers, Proceedings of the Combustion Institute, 31, 1583-90.

Xin, Y., and Gore, J. P. (2005) Two-Dimensional Soot Distributions in Buoyant Turbulent Fires, Proceedings of the Combustion Institute, 30,1, 719 - 26.

Xu, F., and Faeth, G. M.(2000) Structure of the Soot Growth Region of Laminar Premixed Methane/ Oxygen Flames,Combustion and Flame, 121, 4, 640 - 50.

Xu, F., Lin, KC., and Faeth, G. M. (1998) Soot Formation in Laminar Premixed Methane/ Oxygen Flames at Atmospheric Pressure, Combustion and Flame, 115, 195-209.

Xu, F., Sunderland, P.B., and Faeth, G.M. (1997) Soot Formation in Laminar Premixed Ethylene / Air Flames at Atmospheric Pressure, Combustion and Flame, The Combustion Institute, 108, 471-93.

Yagi, S.J. (1943) Soc. Chem. Ind. Japan, 46, 608, 821, 873.

Yagi, S., and Saji, K. (1953) Problems of Turbulent Diffusion and Flame Jet, Fourth Symposium (International) on Combustion, Williams and Wilkins, Baltimore, 771-81.

Yap, L.T., Pourkashanian, M.,., Howard, L., Williams, A., and Yetter, R.A. (1998) Nitric Oxide Emissions Scaling of Buoyancy-Dominated Oxygen-Enriched and Preheated Methane Turbulent Jet Diffusion Flames, 27th International Symposium on Combustion, The Combustion Institute, 1451-60.

Yang, P. and Seitzman, J.M. (2003) Soot Concentration and Velocity Measurement in an Acoustic Burner, American Institute of Aeronautics and Astronautics, AIAA-2003-1014.

Yasa, Z., Amer, N.M., Rosen, H., Hansen, A.D.A., and Novakov, T. (1979) Photoacoustic Investigations of Urban Aerosol Particles, Appl. Opt. 18, 2528-30.

Yilmaz, N., Gill, W., Donaldson, A.B., Lucero, R.E. (2008) Problems Encountered in Fluctuating Flame Temperature Measurements by Thermocouple, Sensors, 8, 7882-93.

Zelepouga, S.A., Saveliev, A.V., Kennedy, L.A., Fridman, A.A. (2000) Relative Effect of Acetylene and PAHs Addition on Soot Formation in Laminar Diffusion Flames of Methane in Oxygen and Oxygen-Enriched Air, Combust. Flame, 122, 76-89.

Zhang, C., Atreya, A., and Lee, K. (1992) Sooting Structure of Methane Counter-flow Diffusion Flames with Preheated Reactants and Dilution by Products of Combustion, 24th Symposium (International) on Combustion , The Combustion Institute), 1049 - 57.

Zhuang, J., and Leuckel, W. (1998) Formation of Nitrogen dioxide in Combustion Processes, International Gas Research Conference, Industrial Utilization and Power Generation, 5, 349-60.

Appendix A

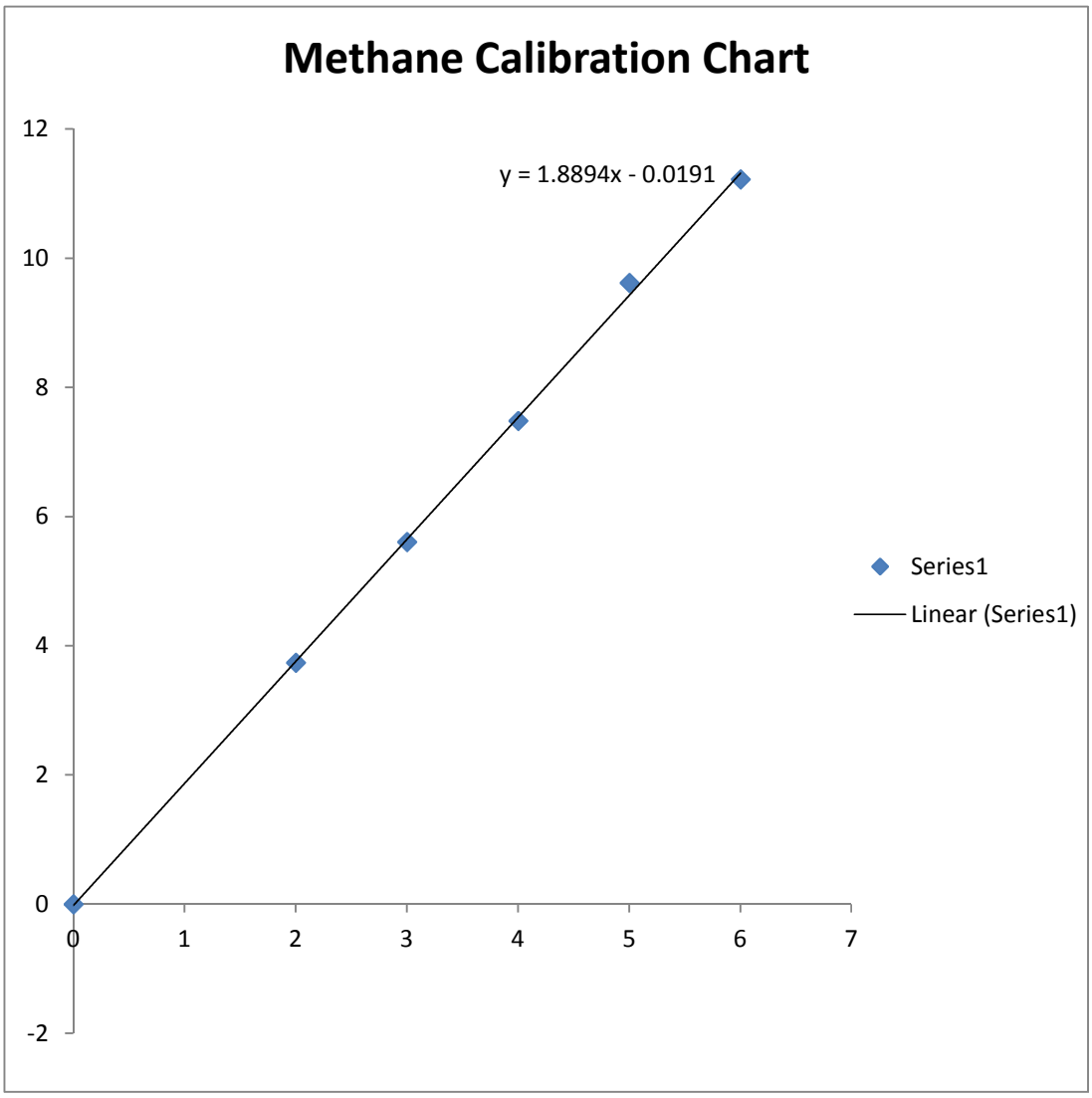
Methane Calibration Chart
y = 1.8894x - 0.0191
12
10
8
6
4
2
0
-2
0
1
2
3
4
5
6
7
Series1
Linear (Series1)

Appendix B

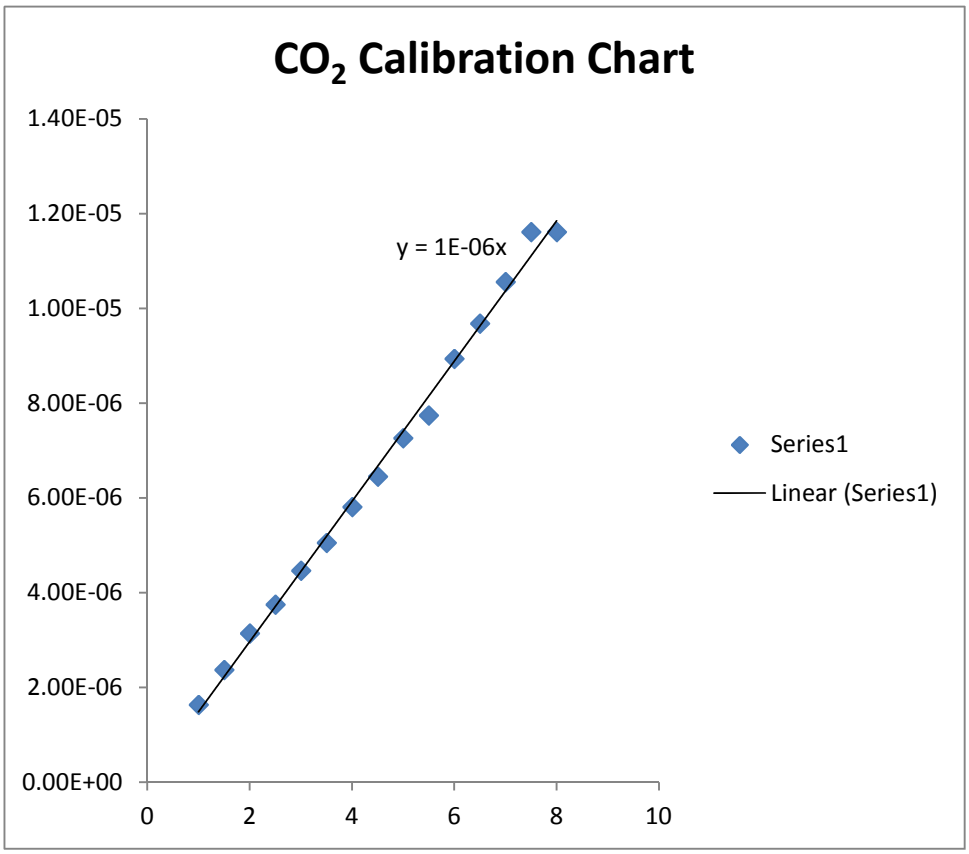
CO2 Calibration Chart
1.40E-05
1.20E-05
1.00E-05
8.00E-06
6.00E-06
4.00E-06
2.00E-06
0.00E+00
0
2
4
6
8
10
y = 1E-06x
Series1
Linear (Series1)

Appendix C

API 521 FLAME LENGTH VERSUS HEAT RELEASE

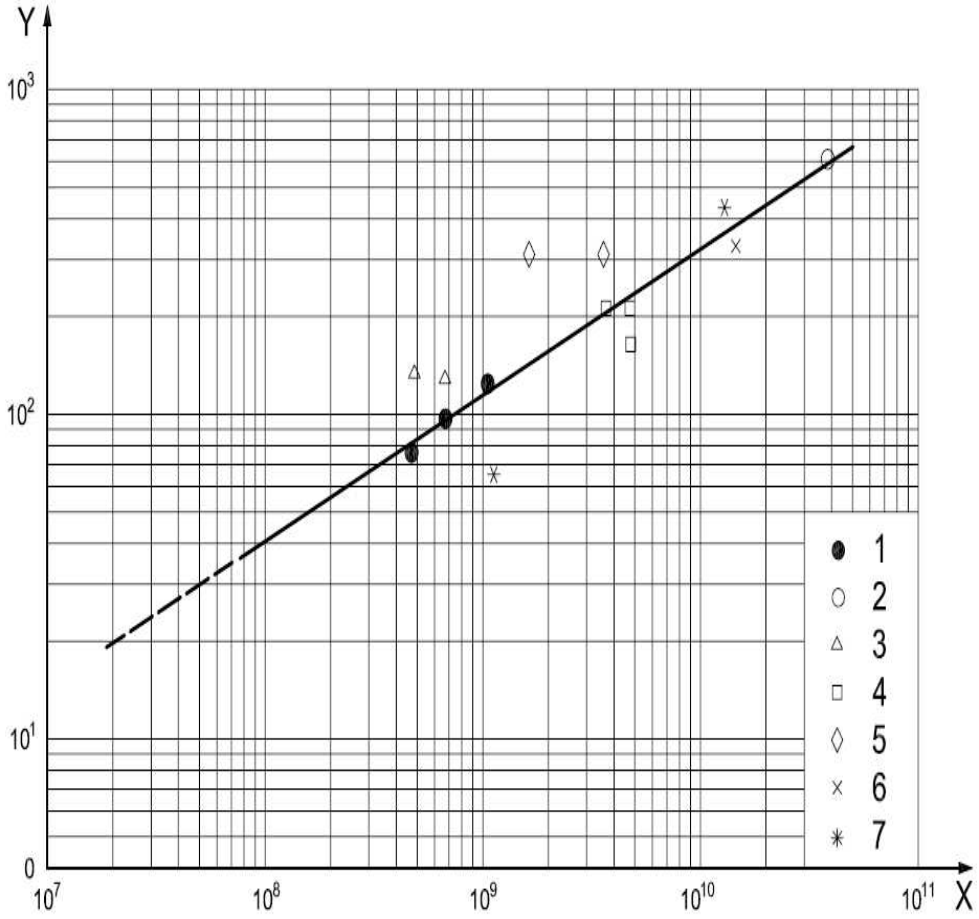

Key

X heat release, expressed in Btu/h
Y flame length (including any lift-off), expressed in ft
1 fuel gas (20-inch stack)
2 Algerian gas well
3 catalytic reformer — recycle gas (24-inch stack)
4 catalytic reformer — reactor effluent gas (24-inch stack)
5 dehydrogenation unit (12-inch stack)
6 hydrogen (31-inch stack)
7 hydrogen (30-inch stack)

Appendix D

REVIEW OF THE LITERATURE ON THE EXPERIMENTAL MEASUREMENTS OF SOOT IN METHANE FLAMES.

Investigator(s)	Pressure Range	Fuel and Oxidiser	Test Configuration	Type of Measurement
Miller and Maahs (1977)	0.1 – 5 MPa	CH_4 - air	Laminar Co-flow Non-premixed	NOx emissions, temperature, flame height, carbon formation, mass concentration
Jeng *et al*. (1984)	0.25 MPa	CH_4 - air	Laminar and Turbulent Co-flow Non-premixed	Mean temperature, radiation, concentration of species
Smyth *et al*.(1985)	0.1 MPa	CH_4 - air	Turbulent Co-flow Non-premixed	Soot particles, concentration of gas species, PAHs, velocity profiles,
Garo *et al*. (1990)	0.1 MPa	CH_4 - air	Laminar Co-flow Premixed	Mean diameter, soot volume fraction, number density
Zhang *et al*. (1992)	0.1 MPa	CH_4 in various oxidiser and dilution streams.	Laminar Counter-flow Non-premixed	Soot precursors, temperature, concentration of gas species, particle number density, volume

				fraction
Müeller and Wittig (1994)	3 – 10 MPa	CH_4 - diluted Ar	Shock tube	Time-resolved particle size, number concentration, volume fraction
Kellerer *et al*. (1996)	1.5-10.5 MPa	CH_4 - diluted Ar	Shock tube Fuel rich	Particle diameter, number density
Shaddix and Smyth (1996)	0.1MPa	CH_4 – air	Laminar Co-flow Non-premixed	Profiles of soot volume fraction,
Vincitore and Senkan (1997)	0.1MPa	75% CH_4, 25% Ar – (20% O_2, 80% Ar)	Laminar Counter-flow Premixed	Soot volume fraction, soot particle size, number density, gas temperature, gas chromatography, concentration of gas species
Xu *et al*. (1998)	0.1 MPa	CH_4 – O_2	Laminar Co-flow Premixed	Soot volume fraction, soot residence time, particle diameter, soot temperature, gas temperature, concentration of gas species, gas chromatography,

				gas velocity
Brookes and Moss (1999)	0.1 and 0.3 MPa	CH_4 – air	Turbulent Co-flow Non-premixed	Prediction of soot temperature, mean mixture fraction, mean soot volume fraction, radiation intensity
Smooke *et al*. (1999)	0.1 MPa	CH_4 / Ar – air	Laminar Co-flow Non-premixed	Gas temperature, concentration of gas species, soot volume fraction
Decroix and Roberts(2000)	0.1 MPa	CH_4 – air	Laminar Counter-flow Non-premixed	Soot volume fraction
Kellerer *et al*. (2000)	1 – 6 MPa	CH_4 - Ar	Shock tube	Soot volume fraction, number density, particle size
Lee *et al*. (2000)	0.1 MPa	CH_4 – air, O_2 (50% and 100%) and 50% N_2	Laminar Co-flow Non-premixed	Soot volume fraction, particle size
Xu and Faeth (2000)	0.1 MPa	CH_4 – O_2	Laminar Co-flow Premixed	Soot temperature, volume fraction, velocities, gas temperature, concentration of gas species, gas

				chromatography, Hydrogen atom concentration
Zelepouga *et al*. (2000)	0.1 MPa	CH_4 – $O_2$and O_2 (21%, 35%, 50% and 100% enriched)	Laminar Co-flow Non-premixed	Soot volume fraction
Beltrame *et al*. (2001)	0.1 MPa	CH_4 – Air,and O_2 (21% to 100% enriched	Laminar Counter-flow Non-premixed	Soot volume fraction as a function of oxygen content at constant and at varying strain rates, concentration of gas species
Schittkowski *et al*. (2002)	0.1 MPa	CH_4 – Air	Laminar Co-flow Non-premixed	Soot particle radius, particle number density, concentration of gas species, gas temperature
Wang *et al*. (2002)	0.1 MPa	Natural gas (94%) CH_4 – Air, and O_2 (21% to 100%)	Turbulent Co-flow Non-premixed	Soot volume fraction, flame radiant heat flux, NOx and CO emission indices
Seeger *et al*. (2004)	0.1 MPa	CH_4 – Air	Laminar Co-flow Non-premixed	Soot volume fraction, particle size, concentration of gas species

Thomson *et al*. (2005)	0.5 – 4 MPa	CH_4 – Air	Laminar Co-flow Non-premixed	Soot volume fraction, soot temperature
McCrain and Roberts (2005)	0.1, 0.4, and 2.5MPa	CH_4 – Air	Laminar Co-flow Non-premixed	Soot volume fraction
Liu *et al*. (2006)	0.5 and 4 MPa	CH_4 – Air	Laminar Co-flow Non-premixed	Soot volume fraction, flame length, flame radius
Mungekar and Atreya (2006)	0.1 MPa	CH_4 – Air	Laminar Counter-flow Partially pre-mixed	Soot volume fraction, soot radiant heat flux, , concentration of gas species
Agafonov *et al*. (2008), (2011)	0.5 and 5.5 MPa	CH_4 – Ar, CH_4 – O_2 / Ar	Shock tube	Soot yield, soot temperature
D'Anna *et al*. (2008)	0.1 MPa	CH_4 – O_2	Laminar Premixed	Soot and organic carbon concentration profile, particle mean size
Desgroux *et al*. (2008)	0.02 – 0.028 MPa	CH_4 – $O_2$and N_2	Laminar Premixed	Spatially resolved soot volume fraction profiles
Thomson *et al*. (2008)	0.98 MPa	CH_4 – Air	Laminar Co-flow Non-premixed	Soot Concentration

Joo and Gülder (2009)	0.1 – 0.6 MPa	CH_4 – Air	Laminar Co-flow Non-premixed	Soot volume fraction, axial and radial soot temperature profiles
Qamar *et al*. (2009)	0.1 MPa	Natural gas (81.3%) CH_4 – Air	Turbulent Co-flow Non-premixed	Axial and radial soot volume fraction
Joo and Gülder (2010)	0.98 - 8.83 Mpa	CH_4 – O_2	Laminar Co-flow Non-premixed	Soot volume fraction, soot temperature
Gülder *et al*. (2011)	0.5- 2, and 1.5 - 5.9MPa	CH_4 – Air	Laminar Co-flow Non-premixed	Soot concentration, temperature profile
Santos *et al*. (2011)	0.1 MPa	Natural gas (89%) CH_4 – Air and O_2 (21%, 23%, 25% enriched)	Turbulent Co-flow Non-premixed	Radiation, concentration of soot, concentration of NOx